The roles of Fibroblast Growth Factor 22 in development, tissue repair and homeostasis, and the associated role of FGF signalling in skin cancer.

Monika Jarosz

This thesis is submitted in fulfilment of the requirements for the degree of

Doctor of Philosophy

University of London

February 2010

Centre for Tumour Biology, Institute of Cancer,
Barts and The London School of Medicine and Dentistry,
Queen Mary University of London,
John Vane Science Centre, Charterhouse Square,
London EC1M 6BQ, UK

DECLARATION OF AUTHORSHIP

I hereby declare that the material presented in this thesis is the result of original work done by the author, Monika Jarosz, at the Department of Tumour Biology, Barts and The London School of Medicine and Dentistry, Queen Mary University of London. All external sources have been properly acknowledged.

Abstract

Fibroblast Growth Factors (FGFs) play critical roles during development, tissue homeostasis and repair and in controlling cell proliferation, survival, migration and differentiation. Of the 22 mammalian FGFs, FGF22, a member of the FGF7/10/22 subfamily, is relatively understudied.

I have investigated the *in vivo* functions of FGF22 in mice engineered to lack *Fgf22*. *Fgf22* null animals were viable, fertile and did not display any obvious abnormalities. No differences in skin histology and pelage hair were observed, demonstrating that FGF22 is dispensable during embryogenesis and in unchallenged adult skin. Mice lacking FGF22 were able to heal acute wounds just as efficiently as wild type mice. However, classical two-step skin carcinogenesis challenge revealed that *Fgf22* null mice developed considerably less papillomas than wild type mice.

Interestingly, *Fgf22* knockout mice displayed a significant reduction in body weight and I identified several novel sites of *Fgf22* expression in the gastrointestinal tract. However, the morphology and function of various tested tissues of the digestive system were not affected by *Fgf22* deletion and the mechanism underlying metabolic differences between *Fgf22* wild type and knockout mice remains unknown.

FGF22 signals through FGFR2b, a receptor tyrosine kinase that we recently have shown plays a tumour-suppressive role in the mouse skin. Another aspect of my project was to verify whether FGFR2 plays a similar role in human skin, by investigating squamous cell carcinoma (SCC) sections and cell lines isolated from patient SCCs. I observed differences in the pattern of anti-FGFR2

immunostaining of normal skin and tumours. Also, since it is well documented that mutations in FGFR2 arise in patients with different types of cancer, I screened DNA isolated from the cell lines and identified eleven different mutations in *FGFR2*.

This study contributes towards a better understanding of the wide spectrum of FGF/FGFR activities and distinct regulatory functions in the biology of physiological and pathological processes.

All truths are easy to understand
once they are discovered;
the point is to discover them.

Galileo Galilei

Science never solves a problem
without creating ten more.

George Bernard Shaw

Acknowledgements

I would like to gratefully acknowledge the enthusiastic supervision of Dr Richard Grose during this work. I am deeply thankful for his wise guidance, great support and encouragement.

I want to express heart-felt gratitude to my dearest friends Magdalena Nowak-Musial, Sabari Vallath and Marcus Pearce for being there for me. I am additionally indebted to Magda for her work and expertise on the retinal aspect of my project.

I would also like to thank Prof Ian Hart and all my colleagues from the lab, especially Maria, Bernardo, Silvia, Fieke, Mike, Antonio, Sally, Monica, Carine, Louise, Katie and Ireny. It has been a great pleasure and fun working with you.

Several people have played a decisive role in saving me from leaving FGFs forever. Richard, Sabari, Mum and Dad - without your support, care and consideration this PhD thesis would not have been written. I am very thankful to you all.

I would also like to thank Barbara, Rob and Jenny for all their hard work in the animal unit at Clare Hall Laboratories, CRUK.

Lastly, I would like to thank St Bartholomew's and the Royal London Charitable Foundation for the funding provided which allowed me to complete this work and fulfil my dreams.

Dedication

I would like to dedicate this thesis to my family, my mother Alicja, my father Jozef and my sister Kasia to whom I owe my deepest gratitude for their endless love and constant encouragement in pursuing my goals.

TABLE OF CONTENTS

LIST OF FIGURES

Chapter 1: Introduction

Chapter 2: Materials and methods

Chapter 3: Fibroblast growth factor 22

Chapter 4: Fibroblast growth factor receptor 2.

LIST OF TABLES

CHAPTER 1

INTRODUCTION

1.1.1 The fibroblast growth factor family

Fibroblast growth factors (FGFs) comprise a large family of widely expressed intercellular signalling molecules (Fig 1.1). The name 'fibroblast growth factors', nonetheless, is a limiting description for this group of cytokines, as FGF functions are not restricted to cell growth. FGFs are responsible for regulating a range of processes, including cell proliferation, survival, migration, differentiation and response to injury (Ornitz and Itoh, 2001). Many are essential for patterning during embryogenesis, controlling complex processes of organ formation and limb development, maintenance of tissue homeostasis in adulthood (Coumoul and Deng, 2003) and management of metabolism (Berndt et al., 2007). The first FGF - FGF1 or acidic FGF - was discovered in 1974 by Gospodarowicz, in cow pituitary gland and brain extract, as a growth factor for fibroblasts (Gospodarowicz, 1974). The FGF family has been growing ever since (the mammalian FGF family now numbers 22 members) just as the range of processes in which they have been described to be engaged has grown. For instance, FGFs play a major role during wound healing stimulating proliferation of endothelial cells, fibroblasts and keratinocytes (with particular focus on FGF1, FGF2 and FGF7 signalling) (Ornitz and Itoh, 2001). FGFs are important for the adult vasculature, as they can promote angiogenesis (FGF1 and FGF2), but their inappropriate signalling may play a role in tumour formation (Grose and Dickson, 2005). They are responsible for formation of the central nervous system and emerging evidence links the FGFs to psychiatric disorders (Riva and Molteni 2005).

FGFs can be grouped into seven subfamilies (Fig 1.1), each containing two to four members, based on their sequence similarities, functional properties and evolutionary relatedness. Members of each subfamily share increased similarities in sequence, as well as in biochemical and developmental properties (Ornitz and Itoh, 2001). There is a certain inconsistency concerning one of the subfamilies – the FGF11 subfamily, members of which are FGF11-FGF14 (Fig 1.1). Called fibroblast homologous factors, they have high sequence and structural homology with FGFs, they bind heparin with high affinity, but lack signal peptides, remain intracellular and function within cells in a receptor-independent manner (Itoh and Ornitz, 2004). Therefore there is some hesitation whether they should be included into the FGF family structure.

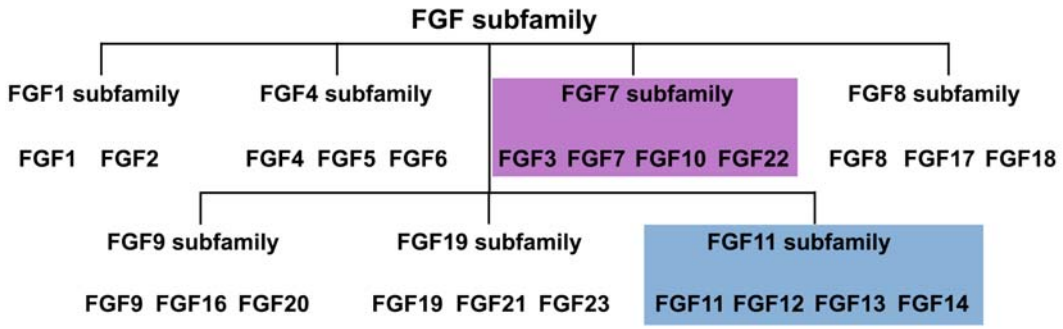

Figure 1.1 Fibroblast growth factor family. Highlighted in blue are FGF homologous factors, which have high sequence identity with the FGF family but do not activate its receptors. Highlighted in purple is the FGF7 subfamily of particular interest to my studies (adapted from Ornitz and Itoh, 2004).

Most human *FGF* genes are scattered throughout the genome, indicating that they were generated by gene duplications and translocations during evolution (Itoh and Ornitz, 2004). They encode a family of proteins ranging in molecular weight from 17 to 34 kDa and sharing a 13 – 71% amino acid homology.

1.1.2 FGF7 subfamily

The main research interests of our lab lie in members of the FGF7 subfamily, consisting of four members: FGF3, FGF7, FGF10 and FGF22, and their cognate receptors. Phylogenetic analyses of the gene loci of the *FGF7* subfamily members in the human genome show that *FGFs 7, 10* and *22*, but not *FGF3*, are closely linked to the hyperpolarisation-activated, cyclic nucleotide-gated potassium channel genes (*HCNs4, 1* and *2*), indicating that those three *FGFs* might have arisen from a common ancestral gene by two successive genome duplications. The *FGF3* genomic locus indicates that it might have arisen from *FGF4* by local gene duplication followed by divergent evolution or, alternatively, it could have derived from an ancestor of the *FGF7* subfamily by gene duplication and chance insertion near *FGF4* (Itoh and Ornitz, 2004).

When comparing sequence similarities, FGFs 7, 10 and 22 are more closely related to each other by sequence than to any other FGFs, with FGF22 sharing ~46% amino acid similarity with FGF10 and ~40% with FGF7 (Nakatake et al., 2001). FGF7 was discovered as a lung fibroblast derived mitogen for murine keratinocytes (Rubin et al., 1989). Unlike other FGFs that act on a wide spectrum of cell types, FGF7 is a secreted glycoprotein acting as a specific mitogen for epithelial cells. It is produced by various types of mesenchymal cells *in vitro* and *in vivo* as well as by γδT cells in inflamed tissues (Werner, 1998) and it serves as a paracrine mediator of mesenchymal-epithelial cross-talk. A very similar expression

pattern of FGF7 and FGF10 was observed in adult mouse tissues, with both growth factors expressed at particularly high levels in mesenchymal cells of the lung and the skin. FGF7, FGF10 and FGF22 act predominately on cells of epithelial origin but, notably, FGF22 is expressed by epithelial cells themselves (Beyer et al., 2003). The biological activities of FGFs are mediated by cell-surface high affinity receptors that belong to the receptor tyrosine kinase family. FGF7 subfamily members activate two receptors: FGFR2b and FGFR1b, although they signal preferentially via FGFR2b (Ornitz et al., 1996, Zhang et al., 2006). FGF7 and FGF10 bind FGFR2b with similar high affinity and compete with each other for this binding (Igarashi and Finch 1998; Lu and Luo 1999). However, striking phenotypic similarities between *Fgf10* and *Fgfr2b* knockout mice have established FGF10 as the predominant ligand for this receptor in development and organogenesis (described in more detail later) (Min et al., 1998). Although FGFR2b remains the only receptor for FGF7, FGF10 and FGF22 can signal through both FGFR2b and FGFR1b (Zhang et al., 2006).

1.2 Fibroblast growth factor receptors – structure and specificity

The FGFs mediate their cellular responses by binding to and activating fibroblast growth factor receptors (FGFRs). The FGFRs share a number of common structural features. They all have an extracellular region composed of three immunoglobulin (Ig)-like domains (D1-D3), a transmembrane sequence, a juxtamembrane domain containing an FRS2 docking site and an intracellular split tyrosine kinase domain (Fig 1.3) (Schlessinger, 2000). The D1 and the linker region between the D1 and D2 sections have much sequence variability, and multiple splice variants, but are considered not necessary for ligand binding – FGF can bind to its receptor even in the absence of domain D1. A hallmark of FGFRs is the presence of an acidic, serine-rich sequence in the D1-D2 linker region, termed

the acid box (Fig 1.3). This region of the protein is thought to have a role in receptor autoinhibition (Olsen et al., 2004), as it can mimic the negative surface potential of acidic glycosaminoglycans and heparan sulphate proteoglycan (HSPG) and thus, bind at the heparin-binding sites located on the surface of the D2 region of the FGFR without initiating a biological response. The D2–D3 fragment of the FGFR ectodomain is necessary and sufficient for ligand binding and specificity.

There are four major tyrosine kinase FGFRs designated as FGFR1, FGFR2, FGFR3 and FGFR4, but a range of splice variants adds to the complexity of the ligand-receptor binding repertoire. Multiple FGFR isoforms are generated by alternative mRNA splicing, so that seven signalling FGFR proteins (FGFRs 1b, 1c, 2b, 2c, 3b, 3c, and 4) with different ligand-binding specificities are created from four *FGFR* genes (Ornitz et al., 1996). Alternative splicing is especially frequent in the D3 domain of the receptors or Ig-loop III. Ig-loop III is encoded by three potential exons: IIIa, IIIb, and IIIc, and gene splicing events lead to the mature mRNA sequence encoding the D3 domain being formed from the invariant IIIa exon followed by either IIIb or IIIc (Fig 1.2). Alternative splicing events are regulated in a tissue-specific manner, in general with exon IIIb expressed in epithelial lineages and exon IIIc in mesenchymal lineages (De Moerlooze et al., 2000). The IIIa splice isoform encodes a secreted extracellular FGF-binding protein with no known signalling capability (Duan et al., 1992).

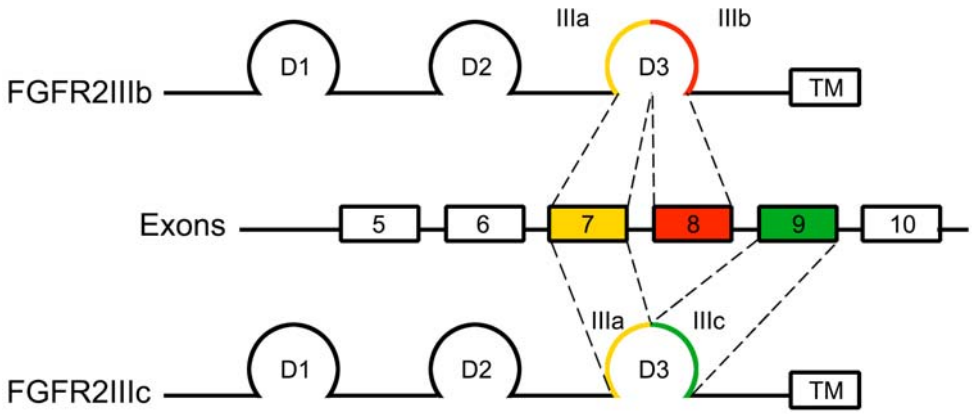

Figure 1.2 Schematic structure of FGFR2IIIb and FGFR2IIIc. The third Ig like loop is involved in alternative FGFR2IIIb or FGFR2IIIc splicing incorporating, exon 8 or exon 9, respectively, in the mature receptor mRNA.

A split intracellular domain containing tyrosine kinase activity is typical of FGF receptors. This kinase region is split in two by a short non-catalytic insert of approximately 15 amino acids (Feng et al., 1997) and contains two phosphorylatable tyrosine residues in FGFR1 and R2, one in FGFR3, and none in FGFR4 (Szebenyi and Fallon, 1999) .

For the most part, there is no one-to-one correspondence between FGF ligands and receptors - for example FGF1 (acidic FGF) is a universal ligand, recognised by all FGF receptors (Ornitz et al., 1996) and FGF5 signals through FGFR1c, FGFR2c, FGFR3c and FGFR4.

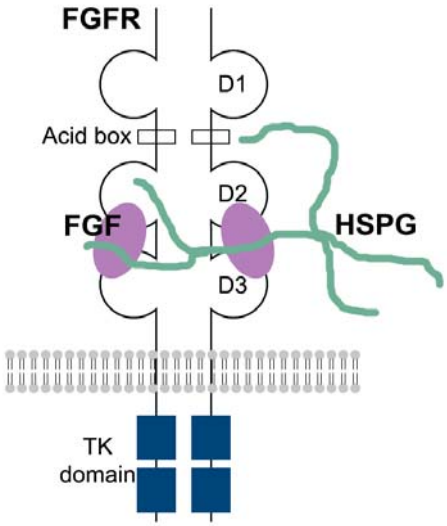

Figure 1.3 Schematic structure of the FGF – FGFR complex, comprising two receptor molecules, two FGFs and two heparan sulphate proteoglycan (HSPG). FGFs (purple) bind with low affinity to cell surface heparan sulphate proteoglycans (HSPG; blue) and, with high affinity, to specific FGFRs. The FGF receptors consist of three extracellular immunoglobulin-like domains (D1-D3), a single transmembrane helix, and an intracellular split tyrosine kinase domain (navy blue).

1.3 FGF signalling

In the presence of heparan sulphate proteoglycans (HSPGs), upon ligand binding, FGF receptor dimers are formed leading to the arrangement of 2:2:2 FGF-FGFR-HSPG complex (Fig 1.3) (Mohammadi et al., 2005), or possibly 2:2:1 complex (Pellegrini et al., 2000). FGF-HSPG interactions stabilise FGFs against thermal denaturation and proteolysis (Gospodarowicz and Cheng, 1986), limit the diffusion and release of FGFs into interstitial spaces and increase the affinity and half-life of the FGF-FGFR dimer (Saksela and Rifkin, 1990). Receptor dimerisation enables the cytoplasmic kinase domains to transphosphorylate on A loop tyrosines and become activated. A loop phosphorylation is followed by

phosphorylation of tyrosines in the C terminal tail, kinase insert and juxtamembrane regions (Mohammadi et al., 1996). Activated multiple tyrosine residues then serve as docking sites for the recruitment of adaptors, docking proteins or signalling enzymes. FGF binding to the FGFRs activates multiple signal transduction pathways that are often inter-dependent (Fig 1.4). When signalling complexes are assembled and recruited to the active receptors, a cascade of phosphorylation events commences. The two main intracellular substrates of FGFR are phospholipase C (PLC)gamma1 (also known as FRS1) and FGFR substrate 2 (FRS2). Phosphorylation of FRS2 is essential for activation of the Ras-mitogen-activated protein kinase (MAPK) and phosphoinositide 3-kinase-Akt signalling pathways (PI3K). The third signalling pathway activated by FGF - PLCγ pathway, is FRS2 independent (Fig 1.4). FGFs are also known to function in the cytosol and nucleus of cells, both through endocytosis of activated FGF-FGFR complexes and through endogenous sources of ligand (Beenken and Mohammadi, 2009).

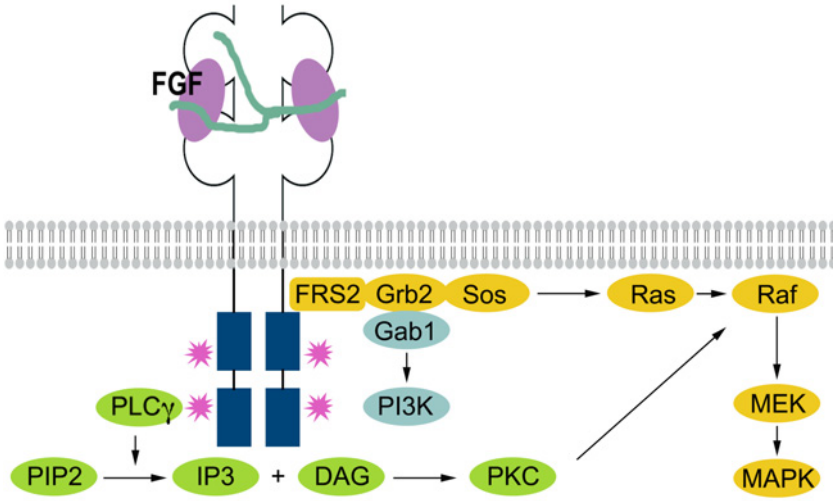

Figure 1.4 Schematic representation of the three principal pathways of FGFR intracellular signalling. Upon FGF binding, activated MAP kinase, PI3 kinase and PLCγ signalling

pathways cause changes in nuclear gene expression profile and/or rearrangement of cell cytoskeleton.

The best understood FGF signalling pathway is the RAS-MAP kinase pathway. It includes ERK1/2, p38, and JNK kinases and activation of the first two, in response to FGF, has been seen in all cell types (Dailey et al., 2005). FRS2 is a very important element in transducing the signal downstream upon FGF activation. It acts as an essential core upon which a signalling complex, consisting of the tyrosine phosphatase Shp2, the adaptor Grb2, and the docking protein Gab1, is formed, leading to the activation of the RAS-MAP kinase and PI3 kinase pathways (Eswarakumar et al., 2005). The FRS2 signalling complex recruits the guanine nucleotide exchange factor Sos, via binding through Grb2, which activates Ras and the downstream effectors of MAP kinase (Fig 1.4). The MAP kinases are a family of proteins that regulate the activity of downstream kinases or transcription factors. FGF signals also activate phosphatidyl inositol hydrolysis, release of intracellular calcium and activation of PKC via recruitment of the SH2 domain of PLCγ to the FGFR. Activated PLCγ hydrolyses PIP2 to form diacylglygerol (Tekin et al., 2007) and IP3 which stimulates calcium release and activation of calcium/calmodulin dependent protein kinases (Dailey et al., 2005).

FGF signalling plays a major role during early vertebrate development. Induction and patterning of mesoderm is one of the earliest events during vertebrate body axis formation and FGF involvement is critical for regulation of target genes [e.g. *brachyury* (Smith et al., 1991)]. Moreover, control of morphogenetic movements (Nutt et al., 2001) and neural patterning (Holowacz and Sokol, 1999) are processes FGF dependent. The wide spectrum of FGF roles in developmental processes is well documented in model organisms, such as *Drosophila melanogaster* and *Caenorhabditis elegans* (described in more detail in

Chapter 5, p.222). FGF signalling regulates expression of target genes, such as *Tbx2, Erm, Pea3,* and *Pax3* (Firnberg and Neubuser, 2002).

FGF signalling itself can be regulated at many levels in the extracellular space and within the cell. Regulation of the extracellular environment is modulated by the presence of HSPGs, as well as by Sef (a negative regulator so named due to Similar Expression Pattern to FGF) considered to regulate FGF signalling at the transmembrane region (Tsang et al., 2002) by either inhibiting FGFR or binding to activated forms of MEK and inhibiting the dissociation of the MEK-ERK complexes. By this means, nuclear translocation of ERK is blocked without inhibiting its activity in the cytoplasm (Torii et al., 2004). At the intracellular level FGF signalling is regulated by PTP MAPK phosphatase 3 (MKP3, also called Pyst1), which antagonises the MAPK pathway via ERK1/2 inactivation. Sprouty proteins (Spry1–4 in mammals) also interfere with FGF signalling through several mechanisms exhibiting different activities and having different interaction partners, including Grb2 and Raf1 (Bottcher and Niehrs, 2005).

1.4 FGF mutations in human birth defects

The fibroblast growth factor family constitutes one of the most critical groups of paracrine factors that act during development. The importance of the proper spatial and temporal regulation of FGF signals is evident from human and mouse genetic studies, which show that mutations leading to the deregulation of FGF signals cause a variety of developmental disorders, including dominant skeletal diseases and cancer (Table 1 and 2). Accurate FGF signalling is responsible for determining certain cells to become mesoderm, for the production of blood vessels, bronchial branching in lung development, limb outgrowth, neural

cell differentiation and survival, growth of metanephric mesenchymal cells in kidney organogenesis and much more (Langman, 2006).

As mentioned above, imbalances in FGF levels and/or mutation of the genes encoding for FGFs or their receptors have been associated with numerous diseases, cancers and other pathological states: FGFs transform fibroblasts and are aberrantly expressed in human tumours, they prevent apoptosis and support tumour growth and angiogenesis (Moon, 2006). For example, homozygous deletions in *FGF3* were identified to cause hereditary deafness, leading to total inner ear agenesis (Tekin et al., 2007). Loss-of-function mutations in *FGF8* lead to Kallmann's syndrome, a developmental disorder characterised by the failure of sexual maturation and infertility, hypogonadism and anosmia (Falardeau et al., 2008). Likewise, loss-of-function mutations in *FGF10* cause Lacrimo-auriculo-dento-digital syndrome. LADD is an autosomal-dominant, multiple congenital anomaly disorder characterised by aplasia, atresia or hypoplasia of the lacrimal and salivary systems, cup-shaped ears, hearing loss, and dental and digital anomalies (Milunsky et al., 2006).

It is clear that FGF receptors play very important roles in human limb and craniofacial development as it has been shown that missense mutations of *FGFR1-3* in humans result in at least 14 congential bone diseases that are broadly classified into two groups: chondrodysplasia syndromes and craniosynostosis syndromes (Yin et al., 2008). Chondrodysplasia affects primarily the skeleton formed through endochondral ossification, resulting in short-limbed dwarfism, while craniosynostosis affects mainly bones formed through intramembraneous ossification, leading to premature fusion of the craniofacial sutures (Chen and Deng, 2005).

Mutations in *FGFR1* can cause Pfeiffer syndrome, a malformation syndrome characterised by limb defects and by the premature fusion of the cranial sutures (craniosynostosis) that results in abnormal skull and facial shape (Muenke et al., 1994).

Mutations in *FGFR2* can give a variety of syndromes and give rise to several conditions like Pfeiffer syndrome, Crouzon syndrome (craniosynostosis, but normal limbs), Jackson-Weiss syndrome (craniofacial malformation and foot abnormalities) and Apert syndrome (craniosynostosis and severe fusion of digits). Mutations in *FGFR2* are explained in more detail in Chapter 4.

Mutations of *FGFR3* cause achondroplasia. Roughly 95% of achondroplastic dwarfs have the same mutation of *FGFR3*, a base pair substitution in the exon encoding the transmembrane region of the protein. In addition, mutations in the extracellular part of the FGFR3 protein or in the tyrosine kinase domain result in thanatophoric dysplasia, a lethal form of dwarfism that resembles homozygous achondroplasia (Bellus et al., 1995). The mutations of fibroblast growth factor receptors that give rise to dwarfism and craniosynostoses are gain-of-function mutations that enable the FGF receptor to become active without binding its ligand.

Interestingly, so far no germline mutations have been identified in FGFR4 (Wilkie, 2005).

As described above, germ-line alterations in *FGFRs* are associated with many congenital skeletal disorders. Interestingly identical mutations of somatic character are found in many types of cancers. Understanding the roles of FGFRs mutations in deregulation of signalling pathways may provide insights into the

mechanism of developmental pathologies and cancer progression.

1.5 *Fgf* knockout mice phenotypes

Significant progress in understanding the mechanisms of normal and abnormal development has come through the joined forces of embryology and molecular biology. Thanks to advanced techniques in mouse genetics allowing generation of transgenic and gene knockout animals, the roles of various molecules whose disruption leads to serious developmental abnormalities and/or embryonic lethality have been elucidated. Phenotypes of *Fgf* knockout mice range from early embryonic lethality to subtle changes in adult physiology, to no identifiable phenotype (see table below).

Fgf	**Phenotype of knockout mouse**	**Physiological role**
Fgf1	Normal (Miller et al., 2000)	Not established
Fgf2	Loss of vascular tone Slight loss of cortex neurons (Zhou et al., 1998) (Dono et al., 1998)	Not established
Fgf3	Inner ear agenesis (Tekin et al., 2007)	Inner ear development (Tekin et al., 2007)
Fgf4	Embryonic lethal (Feldman et al., 1995)	Cardiac valve leaflet formation Limb development (Sugi et al., 2003) (Sun et al., 2002) (Feldman et al., 1995)
Fgf5	Abnormally long hair (Hebert et al., 1994)	Hair growth cycle regulation (Hebert et al., 1994) (Drogemuller et al., 2007) (Housley and Venta, 2006)
Fgf6	Defective muscle regeneration (Floss et al., 1997)	Myogenesis (Armand et al., 2006) (Floss et al., 1997)
Fgf7	Matted hair Reduced nephron branching in kidney (Guo et al., 1996) (Qiao et al., 1999)	Branching morphogenesis (Qiao et al., 1999)
Fgf8	Embryonic lethal (Meyers et al., 1998)	Brain, eye, ear and limb development (Liu and Joyner, 2001) (O'Leary et al., 2007)
Fgf9	Postnatal death Gender reversal Lung hypoplasia (Colvin et al., 2001a)	Gonadal development Organogenesis (Colvin et al., 2001a) (Colvin et al., 2001b)
Fgf10	Failed limb and lung development (Kato and Sekine, 1999)	Branching morphogenesis Multiple organogenesis defects (Kato and Sekine, 1999)
Fgf16	Embryonic lethal (Lu et al., 2008)	Heart development (Lu et al., 2008)
Fgf17	Abnormal brain development (Xu et al., 2000)	Cerebral and cerebellar development (Xu et al., 2000)

Fgf18	Delayed long-bone ossification (Liu et al., 2002) (Ohbayashi et al., 2002)	Bone development (Liu et al., 2002) (Ohbayashi et al., 2002)
Fgf19	Increased bile acid pool (Inagaki et al., 2005)	Bile acid homeostasis Lipolysis Gall bladder filling (Fu et al., 2004) (Tomlinson et al., 2002) (Nishimura et al., 1999)
Fgf20	No knockout model	Neurotrophic factor (Ohmachi et al., 2003)
Fgf21	Late-onset adiposity (Badman et al., 2009)	Fasting response Glucose homeostasis Lipolysis and lipogenesis (Kharitonenkov et al., 2005) (Nishimura et al., 2000)
Fgf22	No knockout model	Presynaptic neural organiser (Umemori et al., 2004)
Fgf23	Hyperphosphataemia Hypoglycaemia Immature sexual organs (Shimada et al., 2004) (Sitara et al., 2004)	Phosphate homeostasis Vitamin D homeostasis (Yamashita et al., 2000) (Saito et al., 2003)

Table 1 Phenotypes of *Fgf* knockout mice (Beenken and Mohammadi, 2009).

Fgfr	**Phenotype of knockout mouse**	**Physiological role**
Fgfr1	Embryonic lethal (Deng et al., 1994)	Mesoderm formation Neural patterning
Fgfr1b	Normal (Partanen et al., 1996)	Not established
Fgfr1c	Embryonic lethal (Partanen et al., 1996)	Mesoderm formation
Fgfr2	Embryonic lethal (Xu et al., 1998)	Impairment in placental development

Fgfr2b	Failed limb and lung development (De Moerlooze et al., 2000)	Branching morphogenesis Multiple organogenesis defects (De Moerlooze et al., 2000) (Revest et al., 2001)
Fgfr2c	Delayed long-bone ossification (Eswarakumar et al., 2002)	Bone development
Fgfr3	Bone overgrowth Deafness (Deng et al., 1996) (Colvin et al., 1996)	Bone development
Fgfr3b	Normal (Eswarakumar and Schlessinger, 2007)	Not established
Fgfr3c	Overgrowth of endochondral bones (Eswarakumar and Schlessinger, 2007)	Bone development
Fgfr4	Normal (Yu et al., 2000)	Liver function

Table 2 Phenotypes of *Fgfr* knockout mice.

Knockout studies have shown that *Fgf10* null mice die shortly after birth, since this growth factor is critical for epithelial-mesenchymal interactions necessary for the development of epithelial components of multiple organs and tissues, including the limbs, lungs, and white adipose tissue (Sekine et al., 1999). *Fgf7* knockout mice on the other hand, are viable with a subtle muscle regeneration phenotype and, surprisingly, no impairment in wound healing (Guo et al., 1996). *Fgfr2b* knockout mice die at birth from multiple developmental defects, phenocopying *Fgf10* knockout mice (Min et al., 1998). *Fgfr2b* null mice fail to develop limbs or lungs due to loss of the progenitor cells by apoptosis, which suggests that FGFR2b is essential for organogenesis and that FGF10 is its key ligand (De Moerlooze et al., 2000). FGFR2b ligands are also essential for wound

healing in a variety of tissues including skin, intestine and liver (Chen et al., 2002) (explained in more detail in 1.6.2).

1.6 FGFs in skin development and homeostasis

1.6.1 Skin structure

Figure 1.5 Transverse H&E stained section of mouse back skin; epidermis (EP), dermis (DE), hair follicle (HF), sebaceous gland (SG), adipose layer (AP), *panniculus carnosus* muscle (PCM).

The skin is a dynamic, regenerating organ. In the human it comprises about 15% of the total body weight and forms the largest organ in the human body. The skin represents the interface with the external world so it serves also as the body's primary defence structure. Skin performs very specific functions, such as providing a permeability barrier, mechanical integrity, maintenance of body temperature, sensation, ultraviolet protection, recognition and defence against infections as well as wound repair and regeneration. In the anatomy of the

skin the epidermis, dermis, and the subcutaneous fat layer can readily be distinguished (Fig 1.5) (Freinkel, 2001).

The epidermis is a multilayered, stratified, continually renewing epithelium that forms the barrier between the organism and its environment (Fig 1.6). In humans the epithelium thickness ranges from 0.4 to 1.5 mm while the full-thickness skin is 1.5 to 4.0 mm. The primary cell in the epidermis is the keratinocyte, with its role being to provide the aforementioned barrier and to effect repair and regeneration of the tissue following injury. Additional cells include melanocytes (cells of neural crest origin that produce pigment to absorb ultraviolet light), Langerhans cells (mobile, dendritic antigen-presenting cells), and Merkel cells (cells with both neuroendocrine and epithelial features) that synapse with the dermal sensory axons and adjacent epithelial cells and are sensitive to mechanical stimuli (especially pressure). The non-keratinocyte population accounts for less than 20% of the epidermal cells in normal adult human skin. There are three epidermal appendages: the sweat glands, the pilosebaceous follicles that produce the hair and sebaceous excretions, and the nails that cover the distal phalanges. The normal turnover rate for the epidermis is about 28 days in a human (Fore, 2006).

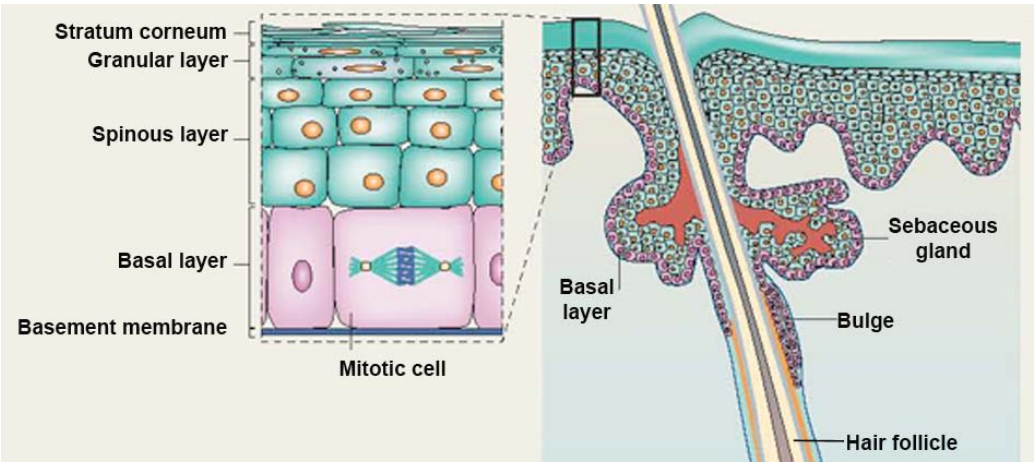

Figure 1.6 Architecture of the epidermis. Epidermis is organized into layers of keratinocytes, which comprise the interfollicular epidermis, interspersed with hair follicles. Proliferating cells (pink) are confined to the basal layer whereas differentiated cells occupy the suprabasal layers (green). As cells differentiate, they leave the basal layer and migrate towards the epidermal surface, changing shape until they enter the outermost cell layer as flattened cornified cells. Finally, these cells are shed from the epidermal surface. In the mouse, the outermost cornified cell layers are arranged in stacks of large hexagonal cells, but in human epidermis the cornified layer is less clearly organized (Jones and Simons, 2008).

The epidermis is separated into layers anatomically as the skin develops and matures from the basal layer (*stratum basale*) adjoining the basement membrane to the outer layer, the *stratum corneum* (Fig 1.6). The epidermal regenerative layer contains the basal keratinocytes, which undergo mitosis. The developing keratinocytes mature and undergo terminal differentiation forming the spinous layer (*stratum spinosum*), the granular layer (*stratum granulosum*) and, finally, the *stratum corneum*. The *stratum corneum* is responsible for the skin barrier that protects the skin, preventing water loss, maintaining satisfactory

hydration of the skin, and preventing over-hydration in addition to many other protective functions (Fore, 2006).

The dermis is located between the subcutaneous fat and dermal-epidermal junction. It is the connective tissue component of the skin and it provides its elasticity and tensile strength. The dermis also protects the body from mechanical injury, binds water and contains sensory stimuli receptors. Moreover the dermis and its blood supply are responsible for delivering nutrients and circulatory support, as the epidermis has no blood supply of its own. In human skin, two main regions of the dermis can be distinguished - the uppermost papillary dermis and the lower reticular dermis. The highest concentration of cells is found within the papillary dermis and around the blood vessels. The cellular components include the fibroblast, monocyte, histiocyte, Langerhans cells, lymphocytes, and eosinophils, along with the vascular- and lymphatic-associated cells. These comprise approximately 10% of the dermal content. The dermis is primarily a connective tissue matrix made up of approximately 90% collagen (mostly Type I) which provides both tensile strength and elasticity to the skin, along with elastin fibres, blood vessels, and lymph vessels, with some muscle fibres and pilosebaceous and sweat glands - structures that originate in the deep dermis and subcutaneous layer (Fore, 2006).

It is important to recognise and bear in mind in biological research the significant differences between mouse and human skin. Aside from the obvious size difference between mice and humans, the epithelium in fur-covered mouse skin is composed of densely distributed hair follicles, whereas epithelium in human skin contains much fewer hair follicles. That is important as in human epidermis there are differences in protein expression in the outer root sheath of the follicles compared with the interfollicular areas (Schon et al., 1995). Mouse epidermis

generally comprises only 2–3 keratinocyte layers and is only one quarter the thickness of human epidermis (Fig 1.6) plus it has a faster epidermal turnover with terminal differentiation of keratinocytes taking only two weeks (Berking et al., 2002). Moreover, mouse dermis is substantially thinner than human dermis and, interestingly, wounding is noticeably different as the major mechanism of wound closure in mouse skin is contraction, whereas in humans re-epithelialisation and granulation tissue formation are the major mechanisms involved (Galiano et al., 2004). Finally, mice have an entire cutaneous muscle layer (*panniculus carnosus)* (Fig 1.5) that is only present in an undeveloped form in humans as the platysma and other small muscles of the face and neck.

1.6.2 FGFs and wound healing

Wound healing is a complex process that starts at the moment of injury and continues until well after the epidermis has healed over. Wound healing is complete when the strength and continuation of damaged tissues are regenerated, underpinned by the formation of new connective tissue and the re-growth of epithelium. The whole process involves proliferation of the epithelial cells, formation of granulation tissue, and recruitment of inflammatory cells (Schafer and Werner, 2007). A variety of different cell types are involved in this process, but I will focus on the important roles of fibroblasts, keratinocytes and dendritic epidermal T cells (DETCs or γδT cells) in wound repair.

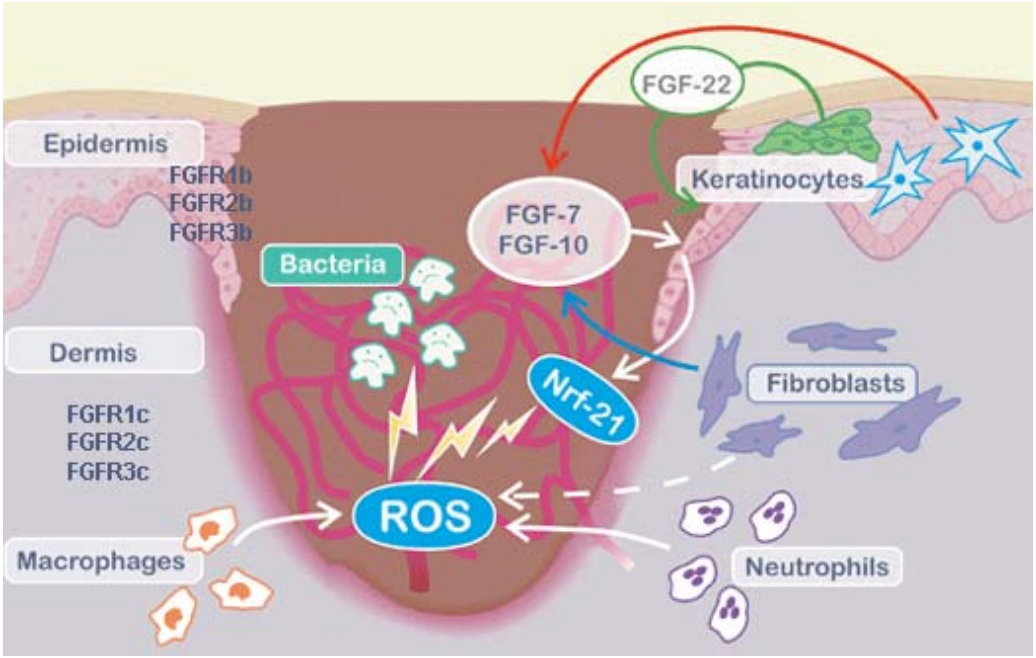

Figure 1.7 A diagrammatical cross-section through wounded skin. Upon injury, dermal fibroblasts (blue) and γδT cells (red) secrete FGF7 and FGF10, and keratinocytes (green) express FGF22. FGFs activate FGFR1-3b expressing keratinocytes at the wound edge and stimulate re-epithelialisation by inducing proliferation, migration and differentiation (adapted from Braun *et al*. 2004).

In the wound healing process (Fig 1.7), a number of stages can be distinguished. First is the formation of a blood clot, which is vital for rapid termination of blood loss and maintenance of the skin's protective function. This clot provides a scaffold for migrating keratinocytes and hence reconstitution of the epidermis. In parallel, the clot provides the primary scaffold for dermal reconstitution as it progresses through granulation tissue formation and final scar tissue maturation. Soon after blood clot formation the inflammatory phase commences, with activation of antibacterial protection pathways and recruitment of key cells into the wound site. Early on the scene are neutrophils, which release free radicals in an oxidative burst to kill bacteria. Soon after macrophages appear,

phagocytosing dead tissue and producing growth factors that stimulate new tissue formation and proliferation of fibroblasts (Schafer and Werner, 2007). The haemostatic clot is lysed by proteases derived from invading cells and replaced by early granulation tissue (days 4-6) composed primarily of hyaluronate but also of newly synthesised cell-derived fibronectin. In the proliferation phase that follows, cells proliferate at the wound site to make new tissue and capillaries (part of the granulation tissue). The keratinocytes of the epidermis migrate over the surface of this tissue to seal the wound, while fibroblasts migrate into the wound bed and differentiate into myofibroblasts, allowing them to drive connective tissue contraction. In the final stage of the process, that in humans can take up to two years, tissue maturation occurs, involving remodelling of the tissues, new collagen formation and scarring reduction. During that time most of the endothelial cells, macrophages and myofibroblasts undergo apoptosis or exit from the wound. A mature scar is never as strong as the original intact skin (Schafer and Werner, 2007).

As mentioned above, major cell types, including keratinocytes, fibroblasts, dendritic epidermal T cells (DETCs or γδT cells) and macrophages, are essential for efficient wound healing (Fig 1.7). All of these cells have been identified as expressing a variety of FGFs and their receptors. In order to study the involvement of FGFs in wound repair, genetically engineered mouse models have been established. Since my primary interest is in the FGF7 subfamily of growth factors, I will focus on the role of FGF7, FGF10, FGF22 and their receptors in the wound healing process. It has been discovered that FGF7 and FGF10 predominantly were expressed by fibroblasts and γδT cells, but what exactly is their role during wound closure? In 1992, Werner et al. established that, in response to injury, within 24 h after wounding *Fgf7* mRNA was up-regulated dramatically (more than 100-fold). *Fgf7* mRNA was detected in dermal fibroblasts adjacent to the wound

and in fibroblasts of the granulation tissue (Werner et al., 1992). In addition, γδT cells are a major source of FGF7 and FGF10 in skin wounds (Jameson et al., 2002).

Accessory to the ligands, all FGFR1-3 are expressed in normal and wounded mouse skin. FGFR2b is expressed in keratinocytes of the normal and wounded epidermis, as well as in hair follicles adjacent to wounds. FGFR1 was found in the regenerating epidermis as well as in wounded blood vessels. The strong upregulation of FGF7 in fibroblasts and γδT cells after skin injury, coupled with the expression of its receptor in keratinocytes, suggested that FGF7 might stimulate wound re-epithelialisation in a paracrine manner (Werner and Grose, 2003).

The first transgenic mice generated to investigate the role of FGFs in wound healing expressed a dominant-negative *Fgfr2b* mutant (lacking a tyrosine kinase domain) in the epidermis, under the control of a *Keratin 14* promoter (Werner et al., 1994). The mutant receptor blocked the signal transduction normally downstream of stimulation with FGFs 1, 3, 7 and 10. The skin phenotype of the transgenic animals was characterised by epidermal atrophy, hair follicle abnormalities and dermal hyperthickening. However, perhaps the most interesting fact was that mice suffered a severe delay in wound re-epithelialisation after injury, when compared with wild-type littermates. At day 5 after injury, the number of proliferating keratinocytes in the hyperproliferative epithelium was 80–90% reduced compared with control mice (Werner et al., 1994). These results demonstrated an important role for FGF receptor signalling in wound repair, although the exact FGF responsible for this defect could not be defined by this study.

FGF7 seemed to be a strong candidate because of its up-regulation in response to injury. Surprisingly, *Fgf7* knockout mice not only lacked any obvious phenotypic abnormalities (Table 1), but also the wound healing process in these mice appeared to be completely normal, suggesting that FGF7 is not required for wound healing (Guo et al., 1996). The most likely explanation for this is redundancy in ligand signalling. Although FGF7 might normally be the most important ligand of FGFR2b in the skin, the lack of the protein in *Fgf7* knockout mice could be compensated for by other known ligands for this receptor, like FGF10, which shows a similar pattern of expression in normal and wounded skin (Werner and Grose, 2003). Unfortunately, the importance of FGF10 in wound healing cannot be studied in *Fgf10* knockout mice as they die shortly after birth (Table 1) due to, among other defects, a failure in lung development (Min et al., 1998, Sekine et al., 1999). Nevertheless, examination of *Fgf10* knockout newborn mouse skin revealed that the granular layer of the epidermis was thinner than that of control mice. The expression of the epidermal differentiation marker loricrin, also was reduced dramatically but transglutaminase 1 (TGase 1), another marker of late terminal differentiation, was expressed normally in the upper spinous and granular layers of both the control and *Fgf10* knockout skin. Similarly, Keratin 14 was expressed normally in the basal layer and hair follicles of *Fgf10* knockout newborns (Suzuki et al., 2000). Furthermore full-thickness *Fgf10* knockout skin grafts transplanted onto nude mice revealed that *Fgf10* knockout skin grafts generated abundant pigmented hairs, comparable to controls, without any differences in morphology of hair follicles and no major abnormalities on the surface or inner structure of the examined hairs (Suzuki et al., 2000).

Interestingly, one phenotype shared by both *Fgf10* and *Fgfr2b* null mice is that their eyes remain open at birth. This is due to a failure of the eyelid epidermis to cover the eye during late embryogenesis, in the equivalent of a developmental

wound healing model. *In vitro* scratch assays, looking at cell migration of primary keratinocytes isolated from the eyelid epidermis of wild type and *Fgf10* knockout foetuses, revealed no difference in cell migration in wild type compared to knockout keratinocytes, although in the mutant cultures the lamellipodia of the cells were not oriented toward the gap and the filopodia appeared to be thinner (Tao et al., 2005).

γδT cells seem to be a key source of FGFR2b ligands in the wounded epidermis two days after wounding. Mice lacking γδT cells show a significant delay in wound healing and impaired epidermal cell proliferation, most likely due to the lack of γδT cell - derived FGF7 and FGF10 in the healing wound (Jameson et al., 2002).

FGF7 and FGF10 signalling is transduced mainly via FGFR2b. Total *FgfR2b* knockout mice do not survive beyond birth. However, at term, the skin of these mice is clearly abnormal with a semi-transparent appearance (Revest et al., 2001). Epidermal specific deletion of *Fgfr2b* under the control of *Keratin 5 Cre* transgene gives no such dramatic phenotype, though the epidermis shows hyperthickening with age. Interestingly 10% of mutant mice develop spontaneous papillomas (Grose et al., 2007).

FGFR1b on the other hand, expressed in normal and wounded mouse skin, has been reported to be down-regulated in wounds of healing-impaired genetically diabetic mice (Zhang et al., 2004). That suggested FGFR1b down-regulation is associated with wound healing defects, but mutant mice lacking *Fgfr1b* did not reveal any obvious abnormalities, neither in the skin, nor in the wound healing process. FGFR1b thus seems to be dispensable for skin development and wound repair (Zhang et al., 2004).

Interestingly, epidermal specific *Fgfr1/2* double knockout mice are characterised by the same phenotypical changes as the dominant-negative *Fgfr2b* mutant mice (Sabine Werner – personal communication) thus emphasising further the importance of FGFR signalling in the process of maintaining skin homeostasis.

Understanding the role of FGFR in the process of wound repair was possible thanks to introduction of the Cre-Lox system, which has proven both useful and efficient. Unfortunately, it is not an adequately useful tool in investigating the role of individual ligands in the healing process, as there are no Cre lines specific for the key ligand-producing cell types - fibroblasts and γδT cells.

What emerges from the above picture is that there is a clear role for FGF signalling in the wound healing process and that this role is protected by redundancy at the level of both ligand and receptor. However, there is at least one more FGF not to have been investigated so far in the wound healing process. FGF22 is expressed towards the end of the repair process and it has been suggested to play a role in differentiation of wound keratinocytes (Beyer et al., 2003).

1.6.3 FGFs and skin carcinogenesis

Cancer is a term used for diseases in which abnormal cells divide without control and are able to invade other tissues. The origin of the word cancer is more than 2,300 years old and it is credited to the Greek physician Hippocrates (460-370 B.C.). Hippocrates used the terms *karkinoma*, which refer to a crab, most likely because the finger-like spreading projections from a cancer reminding the shape of an animal. The world's oldest documented case of cancer was found in Egypt and dates back to 1500 b.c.

There are more than 100 distinct types of cancer and subtypes of tumours can be found within specific organs (Hanahan and Weinberg, 2000). Several lines of evidence indicate that tumourgenesis in humans is a multi-step process and that these steps reflect genetic alterations that drive the progressive transformation of normal human cells into highly malignant derivatives. The immense number of cancer cell genotypes is a manifestation of six essential alterations in cell physiology that collectively dictate malignant growth: self-sufficiency in growth signals, insensitivity to growth-inhibitory (antigrowth) signals, evasion of programmed cell death (apoptosis), limitless replicative potential, sustained angiogenesis, and tissue invasion and metastasis. The genomes of tumour cells must acquire increased mutability in human lifetime in order for the process of tumour progression to reach completion in several decades time. Malfunction of specific tumour suppressor genes, like p53, has been invoked to explain this increased mutability (Hanahan and Weinberg, 2000). That combined with mutated oncogenes, such as Ras, mimicking normal growth signalling contributes to uncontrolled cancer progression.

As a consequence of the insults it receives in the course of its protective duties, the skin is a clear target for cancer-causing genetic damage. Cancer of the skin arises predominantly from cells positioned within the epidermis. The main neoplasms of cutaneous epithelial cells are basal cell carcinoma (BCC) and squamous cell carcinoma (SCC). A distinct type of skin cancer arises from melanocytes, giving rise to malignant melanoma (Green and Khavari, 2004).

Non-melanoma skin cancers like BCC and SCC are the most commonly diagnosed cancer in white populations worldwide, with about 100,000 people diagnosed each year in the UK alone. At the same time around 8,000 people are diagnosed with malignant melanoma. Incidence of this type of cancer quadrupled

in British males between 1975 and 2001, tripled in British females and is increasing in most white populations worldwide (Cancer Research UK, 2005).

Skin SCC is a malignant tumour of keratinising cells of the epidermis or its appendages. It is the second most common malignant tumour of the skin. SCC may occur anywhere on the skin as well as on mucous membranes with squamous epithelium. The occurrence of SCC is usually related to UV light exposure (especially UVB radiation), therefore people with fair skin are at increased risk. Also, exposure to ionising radiation, arsenic or other chemical agents may increase the chances of developing cutaneous SCC. SCC may also develop in chronic inflammatory or degenerative conditions including scars, ulcers, sinus tracts and other pre-existing dermatologic conditions. Moreover patients with decreased immunologic competence are at increased risk of developing this tumour (Drake et al., 1992).

SCCs have the ability to infiltrate locally and cause tissue destruction. Initially developing as carcinoma *in situ*, tumours later become invasive, involving dermis, subcutis, musculature, cartilage and, unlike BCC, may metastasise to regional lymph nodes and subsequently spread to the lung, liver or brain (Johnson et al., 1992).

1.7 FGFs and their receptors in cancer

Human genetic studies have identified numerous activating *FGFR* mutations that are responsible for autosomal dominant bone morphogenetic disorders (Chen and Deng, 2005). Such mutant FGFR2 would be expressed in many other tissues besides the bones, yet individuals carrying these mutations have not been reported to have a high incidence of cancer. Interestingly though,

many FGFR mutations responsible for conditions like craniosynostosis and dwarfism through somatic mutations, contribute to the development of cancer. The underlying mechanism of FGF signalling activation is largely tumour specific, although in general the mechanisms fall into three main groups; 1) Genomic alteration of *FGFR* leading to ligand independent activation, 2) Ectopic expression, or splicing, of FGFR leading to aberrant ligand dependent signalling, 3) Increased FGF expression from the cancer cell acting in an autocrine fashion, or in a paracrine fashion from stromal tissue (Turner and Grose, 2010).

Pathological FGF signalling is a characteristic of various malignancies. For example, modifications to FGF expression are known to cause salivary gland aplasia (FGF10) and autosomal dominant hypophosphatemic rickets (FGF23). Glioblastoma brain tumours exhibit *FGFR1* kinase domain gain-of-function mutations (Rand et al., 2005), and *FGFR1* is activated abnormally in malignant prostate cells (Giri et al., 1999). On the other hand, kinase domain loss-of-function mutations are observed in *FGFR2* in melanoma (Gartside et al., 2009) and overexpression and gain-of-function mutations in *FGFR3* occur in multiple myeloma, an incurable B-cell malignancy (Chesi et al., 1997). Gain-of-function FGFR3 mutations are also the most commonly observed mutations in bladder cancer (Cappellen et al., 1999), and activating *FGFR3* mutations are observed in benign skin tumours (Hafner et al., 2006). *FGFR4* mutations promote metastasis of prostate cancer by increasing cellular motility and invasiveness, nonetheless FGFR4 has potential value as a prognostic marker since Arg388 is associated with increased aggressiveness of prostate cancer (Wang et al., 2004). Moreover, this same allele in *FGFR4* is a predictor of poor clinical prognosis in head and neck squamous cell carcinoma (Streit et al., 2004).

1.8 Therapeutic approaches

Despite major advancements, pharmaceutical companies still face challenges in the development of successful, highly specific therapeutic approaches to the key FGF signalling dependent forms of human cancer. Direct inhibition of FGFRs appears to be of great clinical value and a number of FGFR tyrosine kinase inhibitors have already been developed. Some of them are in early phase clinical trials. All of those inhibitors were designed originally as VEGFR2 ATP competitors, but as the VEGFR2 and FGFR kinase domains have high structural similarity, a number of the VEGFR inhibitory compounds also inhibit the FGFRs (Turner and Grose, 2010). Since the kinase domains of FGFR1-3 are highly similar it might not be possible to develop more selective inhibitors. Sunitinib, a receptor tyrosine kinase inhibitor that has some activity against FGFRs, already has been approved by the Food and Drug Administration (FDA) for treatment of patients with renal cell carcinoma and gastrointestinal stromal tumours (Chow and Eckhardt, 2007). Other developed compounds are listed in the table below.

Small molecular tyrosine kinase inhibitors			
Drug name	**Company**	**Spectrum of activity**	**Clinical development**
SU5402	*In vitro* reagent	Selective FGFR inhibitor (now superseded)	N/A
AZD2171	AstraZeneca	FGFR, VEGFR inhibitor	Phase II
Ki23057	Kirin Brewery	FGFR, PDGFR, VEGFR, c-kit inhibitor	N/A
PD173074	*In vitro* reagent	Selective FGFR inhibitor	N/A
TKI258	Novartis	FGFR, PDGFR, VEGFR inhibitor	Phase II
BIBF 1120	Boehringer Ingelheim	FGFR, PDGFR, VEGFR inhibitor	Phase III
BMS-582664 (Brivanib)	Bristol-Myers Squibb	FGFR, VEGFR inhibitor	Phase II
E7080	Eisai	FGFR, PDGFR, VEGFR inhibitor	Phase I
TSU-68	Taiho Pharmaceutical	FGFR, PDGFR, VEGFR inhibitor	Phase I/II
PKC412	Novartis	FGFR, PDGFR, VEGFR, FLT3, PKC, c-KIT inhibitor	Phase II (as FLT3 inhibitor)

FGFR antibodies and FGF ligand traps			
Name	**Company**	**Target**	
IMC-A1	ImClone	FGFR1c blocking antibody	N/A
PRO-001	ProChon Biotech	FGFR3 blocking antibody	N/A
R3Mab	Genentech	FGFR3 blocking antibody	N/A
1A6	Genentech	FGF19 blocking abtibody	N/A
FP-1039	Five Prime Therapeutics	FGF ligand trap (multiple FGFs)	Phase I

FGF ligand for mucosal chemoprotection			
Palifermin (Kepivance)	Biovitrum AB	recombinant FGF-7 (activates FGFR2b)	Licensed

(Turner and Grose, 2010)

Table 3 FGF therapeutics

Aims

To understand the biological role of Fgf-22 through the generation and characterisation of a *Fgf22* knockout mouse model.

To further investigate the role of FGFR2b in cancer development and progression.

To provide a greater understanding into the role of FGF and FGFR interactions involved in normal and pathological conditions, especially cancer.

Hypothesis

FGF22 is involved in skin development, homeostasis and repair.

FGFR2, a putative tumour suppressor gene in mouse skin, is mutated in human squamous cell carcinoma.

CHAPTER 2

MATERIALS AND METHODS

CHAPTER 2: Materials and methods

2.1 Materials

2.1.1 Chemicals and other consumables

[α-^{32}P] dCTP	Perkin Elmer, USA
β-mercaptoethanol	Sigma, Dorset, UK
Adenine	Sigma, Dorset, UK
Agarose	Invitrogen, Paisley, UK
Alcian Blue 8GX	Sigma, Dorset, UK
Alizarin Red	Sigma, Dorset, UK
Ampicillin	Boehringer, Mannheim, Germany
AvaI restriction enzyme	New England BioLabs, Hitchin, UK
Avidin/Biotin block	Vector Labs, Peterborough, UK
BigDye Terminator v3.1 Cycle Sequencing Kit	AB, Warrington, UK
Bovine serum albumin (BSA)	Sigma, Dorset, UK
Cell strainers 100 µM	Marathon Laboratory Supplies, London, UK
Chelex-100 resin	BioRad, Hemel Hempstead, UK
Chloroform	BDH, Poole, UK
Cholera toxin	Sigma, Dorset, UK
Chromatography paper (3MM)	Whatman, Maidstone, UK
Collagen I	Upstate Scientific, USA

Collagen I coated 60cm culture dishes	VWR, Lutterworth, UK
DAPI mounting medium	Vector Labs, Peterborough, UK
Defined keratinocyte-SFM medium	Gibco, Paisley, UK
Diethylpyrocarbonate (DEPC)	Sigma, Dorset, UK
Diaminobenzidine (DAB substrate)	Dako, Denmark
Dimethylformamide (DMF)	BDH, Poole, UK
Dispase I	Roche, Welwyn Garden City, UK
Dimethylsulphoxide (DMSO)	Sigma, Dorset, UK
ECL reagent	Amersham Biosciences, UK
Ethylenediaminetetraacetic acid (EDTA)	BDH, Poole, UK
Epidermal growth factor (EGF)	Sigma, Dorset, UK
Ethanol	Fisher Scientific, Loughborough, UK
Ethidium bromide	Sigma, Dorset, UK
Fetal calf serum (FCS)	Biosera, Ringmer, UK
Formamide	Sigma, Dorset, UK
Full Range Rainbow Molecular Weight Marker	Amersham, Biosciences, UK
Gel extraction kit QIAquick	Qiagen, Crawley, UK
GelPilot DNA Loading Dye	Qiagen, Crawley, UK
Gentamycin	Gibco, Paisley, UK
Glycine	Sigma, Dorset, UK
HincII restriction enzyme	New England BioLabs, Hitchin, UK
HindIII restriction enzyme	New England BioLabs, Hitchin, UK
Hydrocortisone	Sigma, Dorset, UK

Hydrogen peroxide	Fisher Scientific, Loughborough, UK
Hyperladder I	Bioline, London, UK
In situ Hybridisation Kit	BioChain, USA
Insulin	Sigma, Dorset, UK
Iodine solution	Sigma, Dorset, UK
Isopropanol	Fisher Scientific, Loughborough, UK
Liothyronine	Sigma, Dorset, UK
Mayer's haematoxylin	BDH, Poole, UK
MegaMix	Cambio, Cambridge, UK
Methanol	Fisher Scientific, Loughborough, UK
Microspin G-25 Column	GE Healthcare, Amersham, UK
Milk dried, skimmed	Marvel, UK
M.O.M. Block	Vector Labs, Peterborough, UK
Mouse Leptin ELISA kit	Millipore, Watford, UK
Sodium phosphate (Na_3PO_4)	Sigma, Dorset, UK
Sodium chloride (NaCl)	BDH, Poole, UK
Sodium fluoride (NaF)	Sigma, Dorset, UK
NuPAGE 4-12 % Bis-Tris polyacrylamide gel	Invitrogen, Paisley, UK
NuPAGE MES SDS 20x Running Buffer	Invitrogen, Paisley, UK
NuPAGE LDS sample loading buffer	Invitrogen, Paisley, UK
Nytran SuPerCharge membrane	Schleicher&Schuell, Germany

PAP pen	Zymed, Invitrogen, Paisley, UK
PCT Epidermal Keratinocyte Medium calcium free (CnT-07CF)	Millipore, Watford, UK
PCR purification kit	Qiagen, Crawley, UK
Pepsin Digest ALL-3 solution	Zymed, Invitrogen, Paisley, UK
Permount Mounting Medium	Fisher Scientific, Loughborough, UK
Phenol	Fluka Chemie, Switzerland
Phenylmethanesulphonylfluoride (PMSF)	Sigma, Dorset, UK
Ponceau S Solution	Sigma, Dorset, UK
Porcelain spot plate (6, 12 well)	VWR, Lutterworth, UK
Protease inhibitor cocktail	Calbiochem, Nottingham, UK
Proteinase K	Sigma, Dorset, UK
Protran nitrocellulose transfer membrane	Schleicher&Schuell, Germany
QIAprep Spin Miniprep Kit 250	Qiagen, Crawley, UK
Ready-To-Go DNA Labelling Beads (dCTP)	GE Healthcare, Amersham, UK
Re-Blot Plus Mild Solution (10x)	Invitrogen, Paisley, UK
RIPA Lysis 10x buffer	Upstate Scientific, USA
Sodium dodecyl sulfate (SDS)	National Diagnostics, Hessle, UK
Sodium acetate	BDH, Poole, UK
Sodium orthovanadate	Sigma, Dorset, UK
StreptABComplex/HRP	Dako, Denmark
SuperScript™ II RT	Invitrogen, Paisley, UK
SYBR Green PCR Kit	Qiagen, Crawley, UK

TRI reagent	Sigma, Dorset, UK
Tris-base	Sigma, Dorset, UK
Trypsin (2.5%)	Gibco, Paisley, UK
Tween 20	Sigma, Dorset, UK
Vectashield mounting media with DAPI	Vector Labs, Peterborough, UK
X-gal (5-bromo-4-chloro-3-indolyl-b-D-galactopyranoside)	Melford Laboratories, Suffolk, UK
X-Ray film	FUJIFILM, Japan
Xylene	Fisher Scientific, Loughborough, UK

2.1.2 Antibodies

Primary Antibody	Incubation	Dilution	Supplier
α-BrdU antibody (rat monoclonal)	1 hour room temperature	1:500 in 1 % BSA in PBS	Abcam, Cambridge, UK
α-hFGFR2 (rabbit polyclonal)	overnight at 4°C	1:2000 in 3 % BSA in PBS-T	Abcam, Cambridge, UK
α-Loricrin (rabbit polyclonal)	1 hour room temperature	1:500 in 5 % BSA in PBS	Abcam, Cambridge, UK
α-mKeratin 14 (rabbit polyclonal)	overnight at 4°C	1:1000 in 5 % BSA in PBS	Covance, USA
α-p63 (mouse monoclonal)	overnight at 4°C	1:50 in M.O.M. Diluent	Abcam, Cambridge, UK
α-Phospho-ERK (rabbit polyclonal)	1 hour room temperature	1:1000 in 3 % BSA in PBS-T	Cell Signaling, USA
α-hTubulin (mouse monoclonal)	1 hour room temperature	1:2000 in 3 % BSA in PBS-T	Sigma, Dorset, UK
α-mVimentin (mouse monoclonal)	overnight at 4°C	1:1000 in 3 % BSA in PBS-T	Sigma, Dorset, UK

Table 4 Primary antibodies.

Secondary antibody	Dilution	Supplier
polyclonal goat α-mouse HRP conjugated	1:1000 in 3 % BSA in PBS-T	Dako, Denmark
polyclonal goat α-rabbit HRP conjugated	1:1000 in 3 % BSA in PBS-T	Dako, Denmark
polyclonal goat α-rat HRP conjugated	1:100 in 1% BSA in PBS	Dako, Denmark
goat α-rabbit rhodamine conjugated	1:100 in 5% BSA in PBS	Millipore, Watford, UK

Table 5 Secondary antibodies.

2.1.3 Primers

2.1.3.1 Primers for genotyping

Fgf22

Fgf22 wt_F	5'-TTGTGAACCAAGATGGCAGG-3'
Fgf22 wt_R	5'-CCAGCTTTGGACTTCATCTG-3'
Fgf22 ko_F	5'-TCGACTAGAGGATCAGCTTG-3'
Fgf22 ko_R	5'-CAGGCCAGCATAGTCTACTT-3'

The *Fgf22* wt primers amplify a 286bp fragment and the *Fgf22* ko primers amplify a 133bp fragment from the targeted allele.

Cre/Fgfr2

Cre_F	5'-TCGCTGCCAGGATATACGTA-3'
Cre_R	5'-CTGACCAGAGTCATCCTTAG-3'

This pair of primers is specific for the *CRE* cDNA. The *Cre* primers amplify a 384bp fragment in a positive sample.

Fgfr2 5'Flox IIIb	5'-CTGCCTGGCTCACTGTCC-3'
Fgfr2 3'Flox IIIb	5'-GGCATGCAAATGCAAGGTC-3'

These primers allow the amplification and identification of the *Fgfr2* wild type and floxed alleles. If the mouse is $Fgfr2^{+/+}$, the primers amplify a 400bp fragment. Since

the primers flank one of the engineered loxP sites, the floxed allele contains an additional 90bp between the primer sites. Thus the *Fgfr2* primers amplify a 490bp fragment from the floxed allele.

2.1.3.2 Primers for RT-PCR

Fgf22

Fgf22_F	5'-ATTCTAGAATGCGCAGCCGCCTCTGG-3'
Fgf22_R	5'-ATGGGCCCTCAAGACGAGACCAAGAC-3'

The pair of primers amplifies a 482bp fragment from the targeted allele in a wild type mouse. If the mouse is Fgf22 knockout then no product is obtained.

Fgfr2b

FGFR2IIIa_F	5'-AAGGTTTACAGCGATGCCCA-3'
FGFR2TM836_R	5'-TCTGGGGAAGCTGTAATCTC-3'

The pair of primers amplifies a 290bp fragment or 287bp fragment for the *FGFR2b* and *FGFR2c* respectively.

2.1.3.3 Primers for Real-Time RT-PCR

Fgf7

Fgf7_F	5'-GAACAAAAGTCAAGGAGCAACC-3'
Fgf7_R	5'-GTCATGGGCCTCCTCCTATT-3'

The pair of primers amplifies a 202bp fragment.

Fgf10

Fgf10_F	5’-GAGAAGAACGGCAAGGTCAG-3’
Fgf10_R	5’-CTCTCCTGGGAGCTCCTTTT-3’

The pair of primers amplifies a 289bp fragment.

Fgf22

Fgf22_F	5’-ATTCTAGAATGCGCAGCCGCCTCTGG-3’
Fgf22_R	5’-ATGGGCCCTCAAGACGAGACCAAGAC-3’

The pair of primers amplifies a 482bp fragment in a wild type mouse.

Fgfr1IIIb

FGFR1IIIb_F	5’-TTAATAGCTCGGATGCGGAG-3’
FGFR1IIIb_R	5’-ACGCAGACTGGTTAGCTTCA-3’

The pair of primers amplifies a 110bp fragment.

Fgfr2IIIb

FGFR2IIIa_F	5’-AAGGTTTACAGCGATGCCCA-3’
FGFR2IIIb_R	5’-AGAGCCAGCACTTCTGCATT-3’

The pair of primers amplifies a 145bp fragment.

2.1.3.4 Primers for sequencing

M13_F	5'-GTAAAACGACGGCCAG-3'
M13_R	5'-CAGGAAACAGCTATGAC-3'

2.1.3.5 Mycoplasma screening primers

FWD 1	5'-ACTCCTACGGGAGGCAGCAGTA-3'
FWD 2	5'-CTTAAAGGAATTGACGGGAACCCG-3'
Common REV	5'-TGCACCATCTGTCACTCTGTTAACCTC-3'

2.1.3.6 Loading control primers

HPRT (Hypoxanthine-guanine Phosphoribosyl Transferase)

FWD	5'-CCTGCTGGATTACATTAAAGCGCTG-3'
REV	5'-GTCAAGGGCATATCCAACAACAAAC-3'

The pair of primers amplifies a 351bp fragment.

GAPDH (Glyceraldehyde 3-phosphate dehydrogenase)

mGAPDH419'	5'-TGATGGGTGTGAACCACGAGA-3'
mGAPDH716'	5'-ATGCCAGTGAGCTTCCCGTT-3'

The pair of primers amplifies a 297bp fragment.

2.2 Mice

2.2.1 Conditional knockout mice (K5-R2b null)

Conditional knockout mice, lacking *Fgfr2b* in the epidermis (K5-R2b null), were generated as follows: female mice were bred to homozygosity for a floxed allele (*Fgfr2b*$^{flox/flox}$), with loxP sites inserted into the introns flanking the IIIb exon of the *Fgfr2* gene (De Moerlooze et al., 2000). These were crossed with male mice carrying one copy of the *Cre* recombinase transgene under the control of the *Keratin 5* promoter (Ramirez et al., 2004) in addition to the homozygous *Fgfr2b*$^{flox/flox}$ allele. Provided that the *Cre* allele is transmitted paternally, only epithelia derived from Keratin 5 - expressing cells are targeted for deletion. Maternal transmission results in ubiquitous excision of the floxed sequence caused by *Cre* expression in the maternal germ line (Ramirez et al., 2004). Mice were maintained on a mixed C57Bl6/J×129ola background for *in vitro* primary keratinocyte studies. In the meantime male *K5Cre*$^{+ve}$*; Fgfr2b*$^{flox/+}$ mice were backcrossed with female FVB*/*N mice to generate *Fgfr2b*$^{flox/+}$ mice. The male *K5Cre*$^{+ve}$*; Fgfr2b*$^{flox/flox}$ F1 mice were then backcrossed again with female FVB*/*N mice for a total of 6 generations to obtain *K5-R2b* null mice on an FVB/N background, as FVB/N mice show a high frequency of conversion from papillomas to carcinomas (Woodworth et al., 2004). These mice will be used for future skin carcinogenesis studies.

Littermate controls (*Fgfr2b*$^{flox/flox}$ *Cre* negative) were maintained alongside *K5-R2b* null mice under identical husbandry conditions. Newborn litters were used for preparation of primary keratinocytes or were left with the parents until weaning at the age of 21 days. Adult female *Fgfr2b*$^{flox/flox}$ mice, 6 weeks to 6 months old,

were used for breeding together with *K5Cre*$^{+ve}$*; Fgfr2b*$^{flox/flox}$ males, such that the litters generated were 50% skin specific knockout of *Fgfr2b* and 50% control.

2.2.2 Creation of *Fgf22* knockout mice

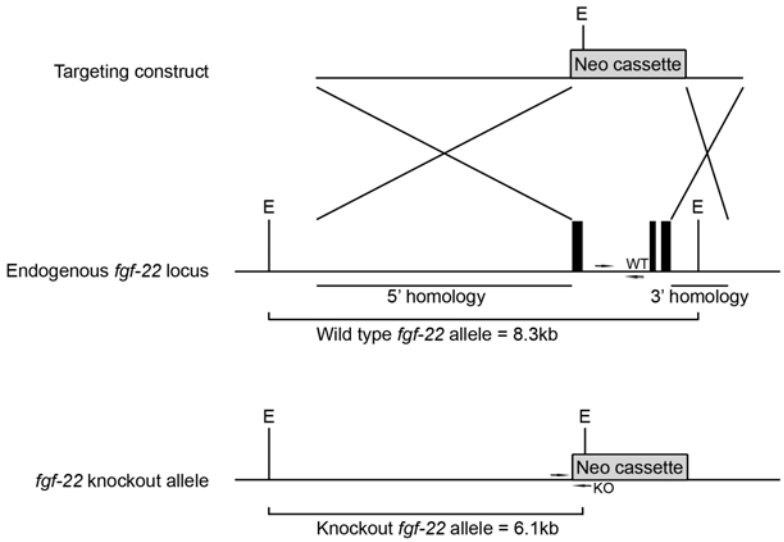

Figure 2.1 *Fgf22* knockout gene construct.

The targeted gene construct above had already been prepared by Dr Richard Grose. As for all 22 members of the FGF family, the *Fgf22* gene consists of three exons. It has been shown previously for *Fgf7* that sequences of exon 1 are essential for its association with heparin and for subsequent binding to FGFR2 (Ron et al., 1993). Since the first intron of *Fgf22* is small (1275 bp), all three exons were targeted for deletion. A targeting vector for the *Fgf22* coding exons was constructed in pBluescript SK^{+} plasmid, using isogenic mouse embryonic stem cells as a source of genomic DNA. Two *Fgf22* genomic fragments were used as 5' (5 kb) and 3' (1.2 kb) arms. The vector was designed to eliminate the entire coding region of exon 1 and the whole of exon 2 and 3 (Fig 2.1). This region was replaced by a neomycin resistance gene flanked with loxP sites. The targeting vector DNA

was transfected into ES cells, and the transfectants were subjected to positive (G418) selection. ES cell clones were picked and grown in a 96 well plate format, on irradiated fibroblast feeder cells. Up to this point, all experiments were performed by the Transgenic Service unit at CR-UK Clare Hall Labs. DNA from surviving colonies was isolated and screened for the desired homologous recombination by Southern blot analysis (as described below). Of a total of 192 ES clones analysed, 2 scored positive for homologous recombination and displayed identical hybridisation patterns. The two mutant clones were injected separately into C57Bl6/J blastocysts. Since ES cells are derived from male embryos, high-percentage male chimaeric animals, as judged by having more than 50% brown coat colour, were mated with C57Bl6/J females. Heterozygous offspring were then mated to produce homozygous mutants, which occurred at the expected Mendelian frequency of 25%. To confirm that the targeted homologous recombination resulted in abrogation of *Fgf22* mRNA expression, reverse transcriptase PCR analysis was conducted on RNA extracted from tissues of wild type, heterozygous and knockout mice (as described below).

2.3 Genotyping, PCR and DNA gel electrophoresis

2.3.1 DNA isolation

To determine the genotype of a mouse, three to five week old mice were ear-snipped or, in case of newborn pups used for keratinocyte isolation, 3 mm of tail tip was cut, for the isolation of genomic DNA. Tissue was digested overnight in a 1.5 ml Eppendorf tube at 55°C in 40 µl of tissue digestion buffer (0.025% SDS, 125 mM Tris-base [pH 8], 0.5 mM NaCl) containing 1 µl Proteinase K (50 µg/µl), added to lysis buffer immediately prior to incubation.

The following day, 16 µl of 5 M NaCl solution was added to the tubes. The samples were mixed by vortexing and incubated at 55°C for another 10 min to allow any precipitate to dissolve. The samples were mixed by vortexing and centrifuged for 15 min at 13,000 rpm and room temperature. 40 µl of the supernatant was transferred into a fresh 1.5 ml Eppendorf tube and 24 µl of Isopropanol was added. The samples were mixed and centrifuged for 10 min with the same conditions as above to precipitate the DNA pellet.

The supernatant was aspirated off and the pellet was washed with 100 µl of 70% Ethanol by vortexing briefly and centrifuging for 10 min at 13,000 rpm, room temperature. The Ethanol was aspirated off, the pellet was air-dried prior to resuspension in 40 µl of EB buffer at 55°C for one hour.

The samples were stored at 4°C until genotype was confirmed. 1 µl of each sample was used for PCR.

2.3.2 Polymerase chain reaction (PCR)

The polymerase chain reaction allows the amplification of any DNA fragment from template DNA using suitable oligodeoxynucleotide primers and enables identification of mutant or wild-type alleles of a gene. All PCR reactions were carried out using MegaMix in 20 µl reaction volume in thin-walled PCR plates. A negative control was always performed with all the mix components except the DNA sample.

Reaction mix:	18.8 µl	MegaMix
	0.1 µl	3'primer (100mM stock)
	0.1 µl	5'primer (100mM stock)
	1 µl	sample

The reaction was performed in a (Techne Flexigene) DNA thermal cycler (Krackeler Scientific, USA) with the following programme:

PCR-programme:	Initial Denaturation	3 min	94°C	
	Denaturation	30 sec	94°C	35 cycles
	Annealing	30 sec	60°C	
	Extension	1 min	72°C	
	Final Extension	10 min	72°C	

2.3.3 Electrophoresis

PCR products were separated on a 2% Agarose/TBE gel. A 100 ml Agarose gel was made by mixing 2 g Agarose with 100 ml of 1x TBE, microwaving it at high power for 3 minutes until the Agarose was dissolved then cooling it down to 56°C. Afterwards, 10 µl of 5 mg/ml Ethidium bromide solution was added. The solution was poured in a medium horizontal gel electrophoresis system gel tank tray (Horizon, USA) and two 20-well combs were immersed in the Agarose to create wells.

10 µl of PCR mix was loaded into the gel and separated at 100 V (PowerEase 500, Invitrogen, Paisley, UK) for 1 hour. Bands were visualised under UV light and photographed using an AutoChemi System (UVP BioImaging Systems, Cambridge, UK).

2.4 RNA isolation

For all the RNA experiments, sterile, RNase-free plastic tubes and pipette tips were used. Water and PBS used were pre-treated with diethylpyrocarbonate (DEPC) to block RNases. 0.1% DEPC was added, solutions were shaken and then left for at least 16 hours, before autoclaving to destroy the DEPC.

Isolation of total RNA from tissues and cell monolayers was performed using TRI reagent. TRI reagent is an improved version of the single-step total RNA isolation reagent developed by Chomczynski and Sacchi (Chomczynski and Sacchi, 1987). It is a mixture of guanidine isothiocyanate and phenol in a mono-phase solution that effectively dissolves DNA, RNA, and protein.

Tissue samples used for RNA extraction were snap-frozen in liquid nitrogen and stored in liquid nitrogen. Just before RNA extraction, samples were transferred into a suitable container and immediately homogenised in TRI reagent (1 ml per 50-100 mg of tissue) using an Ultra-Turrax T25 homogeniser (IKA Labortechnik, Germany). Cell monolayers were lysed directly on the culture dish using 1 ml of the TRI reagent per 10 cm^2 of culture plate surface area. After addition of the reagent, the cell lysate was homogenised by passing through a 1000 µl pipette (several times). To ensure complete dissociation of nucleoprotein complexes, samples were allowed to stand for 5 minutes at room temperature. Then 0.2 ml of Chloroform per ml of TRI reagent used was added. The sample was covered tightly and shaken vigorously for 15 seconds, then allowed to stand for 2-15 minutes at room temperature. The resulting mixture was centrifuged at 13,000 rpm for 15 minutes at 4°C (Sorvall fresco, Thermo Fisher Scientific, USA). Centrifugation separated the mixture into 3 phases: a red organic phase

(containing protein), an interphase (containing DNA), and a colourless upper aqueous phase (containing RNA).

The aqueous phase was transferred to a fresh tube and 0.5 ml of Isopropanol per ml of TRI reagent used in sample preparation was added. The sample was mixed and allowed to stand for 5-10 minutes at room temperature, before centrifugation at 13,000 rpm for 10 minutes at 4°C. This precipitated the RNA to form a pellet on the side and bottom of the tube. The supernatant was removed and the RNA pellet was washed by adding 1 ml (minimum) of 75% Ethanol per 1 ml of TRI reagent used for sample preparation. The sample was vortexed and then centrifuged at 10,000 rpm for 5 minutes at 4°C. The RNA pellet was air-dried for 5-10 minutes.

An appropriate volume of DEPC treated water was added to the RNA pellet (100-500 µl). To facilitate dissolution, it was mixed by repeated pipetting and then incubated at 55-60°C for 10-15 minutes.

2.5 cDNA synthesis

cDNA was generated by reverse transcription from RNAs isolated from tissues or cell lines. Random hexamer primers were used to prime the reverse transcriptase reaction and ensure the efficient amplification of all mRNAs in a sample. Random hexamers are mixtures of 6 base-pair primers with varying sequences that bind to complementary RNA sequences. This results in a very high probability that all transcripts will be reverse transcribed at near 100% RT efficiency and avoid the bias towards 3'end of messages seen when using oligo dT primers (Bookout and Mangelsdorf, 2003). For cDNA synthesis, the SuperScript™ II RT enzyme was used.

A 20 µl reaction volume was used for 1 ng – 5 µg of total RNA. The following components were added to a nuclease-free 500 µl Eppendorf tube.

Reaction mix:	1 µl	random hexamers (50 ng/µl)
	1 ng - 5 µg	total RNA
	1 µl	dNTP Mix (10 mM each)
	the volume was made up to 12 µl with sterile, distilled water	

The mixture was heated to 65°C for 5 minutes and then quickly chilled on ice. The contents of the tube were collected by brief centrifugation and the following were added:

4 µl	5X First-Strand Buffer
2 µl	0.1 M DTT
1 µl	RNaseOUT (40 units / µl)
	(required if using <50 ng starting RNA)

The contents of the tube were mixed gently and incubated at 25°C for 2 minutes. Then the enzyme was added:

1 µl (200 units) of SuperScript™ II RT

The contents of the tube were mixed by pipetting gently up and down and the reaction was incubated at 25°C for 10 minutes to allow primer binding. Incubation at 42°C for 50 minutes allowed reverse transcription to occur, prior to the reaction being inactivated by heating to 70°C for 15 minutes. cDNA samples were used immediately for PCR whenever possible, and the remainder was stored at -20°C.

2.6 PCR product digestion

The ligand binding domain of FGFR2 undergoes alternative splicing to give two isoforms, IIIb or IIIc (see cartoon below). RT-PCR was performed on RNA isolated from a range of cell lines. Primers targeted to the exons flanking the alternatively spliced region yielded similarly sized PCR products.

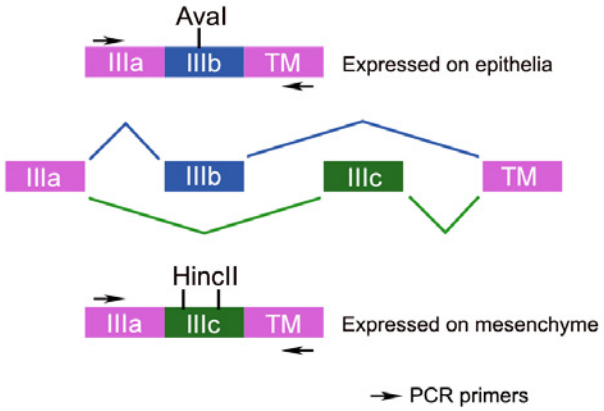

Figure 2.2 FGFR2 splicing isoforms.

Since exon IIIb contains an AvaI site not present in exon IIIc and exon IIIc contains two HincII sites not present in exon IIIb, digestion of PCR products with the restriction endonucleases, HincII and AvaI, revealed which isoform of the receptor was expressed (Fig 2.2).

All PCRs were carried out using MegaMix in a reaction volume of 20 µl in PCR plates. A negative control was always performed with all the mix components except the cDNA sample.

Reaction mix:	18.8 µl	MegaMix
	0.1 µl	FGFR2IIIa F primer (100mM stock)
	0.1 µl	FGFR2TM836 R primer (100mM stock)
	1 µl	cDNA sample

The reaction was performed in a (Techne Flexigene) DNA thermal cycler with the following programme:

PCR-programme:	Initial denaturation	3 min	94°C	
	Denaturation	30 sec	94°C	35 cycles
	Annealing	30 sec	60°C	
	Extension	45 sec	72°C	
	Final extension	10 min	72°C	

10 µl of each PCR product was analysed on a 2% Agarose/TBE gel. The pair of primers amplifies a 290bp fragment from the targeted allele. The remainder of the reactions were restriction digested with AvaI or HincII enzymes in a digest mix as described below.

Digest mix:	10 µl	PCR product
	2 µl	10x buffer 3 (NEB)
	0.2 µl	BSA (100x)
	1 µl	HincII enzyme (10 units/µl)
	the volume was made up to 20 µl with sterile, distilled water	

Or alternatively:

Digest mix:	10 µl	PCR product
	2 µl	10x buffer 4
	1 µl	AvaI enzyme (10 units/µl)
	the volume was made up to 20 µl with sterile, distilled water	

Samples were incubated at 37°C for a minimum of 2 hours. Digestion products were analysed on a 2% Agarose/TBE gel. AvaI enzyme digestion produces 182 and 108bp bands, where HincII enzyme digestion produces three bands of 119, 115 and 53bp.

2.7 Real-time Polymerase Chain Reaction (PCR)

Real-time PCR gives the possibility of monitoring the progress of the PCR amplification as it occurs. Data therefore are collected throughout the PCR process, rather than at the end of the reaction. In real-time PCR, reactions are characterised by the point in time during cycling when amplification of a target is first detected, rather than determining the amount of target accumulated after a fixed number of cycles. The higher the starting copy number of the nucleic acid target, the sooner a significant increase in fluorescence is observed (www.protocol-online.org).

SYBR Green dye was used in all the Real-Time PCR reactions. SYBR Green dye has the ability to bind to double-stranded DNA formed during PCR. As soon as it is added to a sample it binds to all double-stranded DNA present in the sample. Then, during the PCR, DNA Polymerase amplifies the target sequence creating the PCR products. The dye immediately binds to each new copy of

double-stranded DNA and upon excitation emits light. As the PCR progresses, more amplicons are created and, since the SYBR Green dye binds to all double-stranded DNA, it results in an increase in fluorescence intensity proportionate to the amount of PCR product produced (Essentials of Real Time PCR, Applied Biosystems).

In brief, 265 ng RNA from each wound sample was used for reverse transcription into 20 µl cDNA as described earlier (2.5). All the Real-Time PCR reactions were carried out in a 20 µl reaction volume in 96 well PCR plates, always in triplicate. A negative control was performed with all the mix components except the cDNA sample.

Reaction mix:	1 µl	cDNA
	0.1 µl	forward primer
		(0.5 µM working concentration)
	0.1 µl	reverse primer
		(0.5 µM working concentration)
	10 µl	SYBR GREEN PCR Master Mix
	8.8 µl	RNase-free H2O

Serial dilutions (1, 0.75, 0.5, 0.25, 0.1, 0.01, 0.001) of one of the samples were used to establish a standard curve for each of the primer sets used in the Real-Time PCR reaction. The reaction was performed in a StepOne Plus Real-Time PCR System (Applied Biosystems) thermal cycler with the following programme:

PCR-programme:	Incubation	2 min 50°C	
	Taq activation	15 min 95°C	
	Denaturation	15 sec 95°C	40 cycles
	Annealing	30 sec 60°C	
	Extension	30 sec 72°C	
	Final melt curve (dissociation step) from 60°C to 95°C.		

GAPDH primers were used as internal control. The results were evaluated using the $2^{-\Delta\Delta ct}$ method (Livak and Schmittgen, 2001).

2.8 TOPO cloning

TOPO Cloning kit (Invitrogen, UK) was used for quick, routine PCR product cloning. The key ingredient of the TOPO Cloning system is the enzyme, DNA topoisomerase I, which functions both as a restriction enzyme and as a ligase (Fig 2.3). *In vivo* it is essential during replication as it cleaves and rejoins DNA. *Vaccinia* virus topoisomerase I recognises specific sequence and cleaves one DNA strand, enabling the DNA to unwind. The enzyme then religates the ends of the cleaved strand and releases itself from the DNA. TOPO vectors are linearised with this enzyme covalently bound to each 3´ phosphate. This enables the vectors to readily ligate DNA sequences with compatible ends.

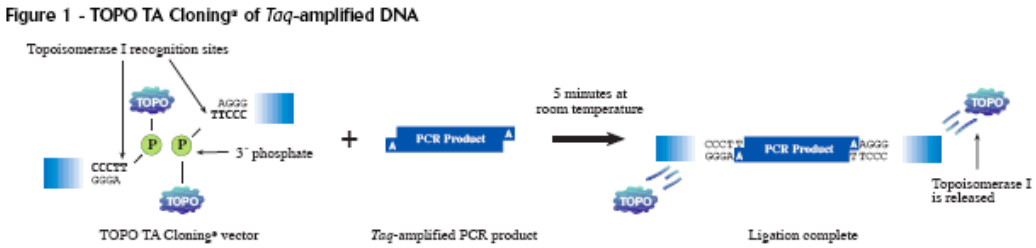

Figure 2.3 TOPO® Cloning Technology, Invitrogen

2.8.1 TOPO TA cloning reaction

Because of the TOPO vector properties mentioned above, fresh PCR product was always used for cloning reactions. The following components were added to a nuclease-free 500 µl Eppendorf tube.

Cloning reaction mix:	4 µl	fresh PCR product
	1µl	salt solution
	1 µl	TOPO vector

The contents of the tube were mixed gently, incubated for 5 minutes at room temperature before placing on ice.

2.8.2 Transforming One Shot TOP10 competent cells

TOP10 competent *E.coli* cells were thawed on ice using one vial per transformation. 2 µl of cloning reaction mix was added into one vial of cells and mixed gently without pipetting up and down. The vial was left on ice for 30 minutes. Afterwards the cells were heat shocked for 30 seconds in a water bath equilibrated to 42°C and then transferred immediately to ice. 250 µl of room

temperature SOC medium was added to the tubes and, after closing tightly, they were shaken horizontally (200 rpm) for 1 hour at 37°C in a shaking incubator.

2.8.3 Plating bacteria

Antibiotic selection plates were prepared in advance. A 400 ml bottle of LB (Luria-Bertani) broth [1% (w/v) tryptone, 0.5% (w/v) yeast extract and 1% (w/v) sodium chloride] with 1.5% (w/v) agar was microwaved at low power until the agar melted. After cooling to approximately 60°C, 400 µl of 100 mg/ml Ampicillin was added. The solution was poured into 10 cm Petri dishes (10 ml/dish) within a sterile area close to a bunsen flame and was left to set. The plates were stored at 4°C.

For blue/white colony screening, 40 µl of 40 mg/ml X-gal in dimethylformamide (DMF) was spread on the top of the selective agar plate 30 minutes before plating the bacteria. 50 µl of transformed cells were plated on pre-warmed selective plates and incubated upside down overnight at 37°C.

2.8.4 DNA Miniprep

The following day 10 white colonies per plate were picked using separate pipette tips, which were then ejected into universal tubes containing 5 ml of LB broth supplemented with 100 µg/ml of Ampicillin. The cap on the universal tube was closed loosely, taped shut and the tubes were shaken (200 rpm) at 37°C overnight. Clare Hall Media Production Services (CRUK) supplied the bacterial medium.

2.8.5 PCR identification of positive clones

To confirm that the transformation was successful, a diagnostic PCR reaction was performed using MegaMix in 20 µl reaction volume with 1 µl of miniprep culture. To ensure DNA release, bacteria were lysed in a first step by heating the reaction mix to 94°C for 10 minutes.

Reaction mix:	18.8 µl	MegaMix
	0.1 µl	3'primer (100mM stock)
	0.1 µl	5'primer (100mM stock)
	1 µl	miniprep sample

The reaction was performed with the following programme:

PCR-programme:	Initial Denaturation	10 min	94°C	
	Denaturation	30 sec	94°C	35 cycles
	Annealing	30 sec	60°C	
	Extension	45 sec	72°C	
	Final Extension	10 min	72°C	

2.8.6 Plasmid extraction

The bacterial cultures from identified positive miniprep clones were harvested by centrifugation at 10,000 rpm for 10 minutes at room temperature, and the plasmid DNA was isolated using the QIAprep Spin Miniprep Kit 250 (Qiagen). The QIAprep miniprep procedure is based on alkaline lysis of bacterial cells followed by adsorption of DNA onto silica in the presence of high salt. The procedure consists of three steps: preparation and clearing of a bacterial lysate, adsorption of DNA onto the membrane, followed by washing and elution of

plasmid DNA. Bacteria are lysed under alkaline conditions in NaOH/SDS (Buffer P2) in the presence of RNase A. SDS solubilises the phospholipid and protein components of the cell membrane, leading to lysis and release of the cell contents, while the alkaline conditions denature the chromosomal and plasmid DNAs, as well as proteins. The lysate is neutralised and adjusted to high-salt binding conditions by the addition of Buffer N3. The high salt concentration causes denatured proteins, chromosomal DNA, cellular debris, and SDS to precipitate, while the smaller plasmid DNA renatures and stays in solution. Such prepared samples are ready for purification on the silica membrane by selective adsorption of plasmid DNA in high-salt buffer and elution in low-salt buffer. Only DNA is adsorbed on the membrane, while RNA, cellular proteins, and metabolites are found in the flow-through. Then, endonucleases are removed by a brief wash with Buffer PB and salts are removed by a wash with Buffer PE. High-quality plasmid DNA is then eluted from the column with 50 - 100 µl of Buffer EB or water.

DNA concentration was determined by using a NanoDrop ND-1000 photospectrometer (NanoDrop Technologies, USA). Samples were measured at 260 nm and EB Buffer was used as a blank control. Samples were stored at -20°C.

2.9 Sequencing

2.9.1 Routine sequencing

For routine sequencing of TOPO constructs, in order to confirm both sequence and orientation, samples (400 - 800 ng of template plasmid DNA per reaction) were sent to the Genome Centre (QMUL).

2.9.2 Mutation screening sequencing

Genomic DNA extracted from SCC cell lines was sequenced in a search for point mutations within *FGFR2*. Primers were designed within introns, approximately 50 bp up- and downstream from the exons of interest. These were amplified by PCR (conditions as described above), and the PCR products cloned into TOPO vector as described. Purified plasmid DNA was sequenced using Cancer Research UK, London Research Institute sequencing services.

2.9.2.1 Labelling

BigDye Terminator v3.1 Cycle Sequencing Kit was used for DNA labelling.

Reaction mix:	3.7 µl	5× buffer
	0.5 µl	BigDye Terminator Mix
	1 µl	3.3 µM Forward or Reverse Primer
	1 µl	200 ng plasmid DNA
	13.8 µl	sterile water

The reaction was performed with the following programme:

PCR-programme:	Denaturation	1 min	96°C	
	Denaturation	30 sec	96°C	25 cycles
	Annealing	15 sec	50°C	
	Extension	4 min	60°C	

2.9.2.2 Precipitation of labelled products

After the labelling reaction, 2 µl of Sodium acetate (3 M pH 5.2), 2 µl of EDTA (125 mM stock concentration) and 50 µl of 100% Ethanol were added to each sample. This was mixed and incubated at room temperature for 30 minutes prior to centrifugation for 20 minutes at 14,000 rpm at room temperature. Afterwards the supernatant was discarded and the pellet was washed in 1 ml of 70% Ethanol. Samples were centrifuged for another 15 minutes, the supernatant was discarded and the pellet was air-dried.

2.10 Cell lysis and Western blotting

2.10.1 Cell Lysis

Cultured cell monolayers were grown to 65-80% confluence. The media from the cells was aspirated off and the culture dishes were placed on ice. The monolayer was washed twice with ice cold PBS and lysed with radio immunoprecipitation assay (RIPA) Lysis buffer supplemented with 2 mM Sodium orthovanadate, 10 mM NaF, 1mM PMSF and 1:100 dilution of protease inhibitor cocktail for 2 minutes on ice.

After lysis, cells were scraped, transferred to Eppendorf tubes and passed through a 25G gauge needle 20 times with a 1 ml syringe. Lysed cells were incubated on ice for a further 10 minutes and then centrifuged at 10,000 rpm for 10 minutes at 4°C. The supernatant was then stored at –20°C.

2.10.2 Determination of protein concentration

Protein concentration for each sample was determined using the Bio-Rad D_C Protein Assay Kit (Bio-Rad Laboratories, Hercules, CA, USA), as follows: 5 µl of each sample was mixed in a 96-well microtitre plate with 200 µl of Bio-Rad reagent B and with 25 µl of a solution obtained by mixing 1 ml of reagent A with 20 µl of reagent S. Protein standards were prepared by diluting a 5 mg/ml solution of BSA in lysis buffer to obtain solutions of a concentration of 2, 1.6, 1.2, 0.8, 0.4, 0.2, 0.1 and 0 mg/ml. 5 µl of each standard in duplicate was incubated with Bio-Rad reagents as described above. After 15 minutes incubation at room temperature, protein concentrations were read using an Anthos 2001 plate reader (Anthos Labtec Instruments, Austria) 96-well microtitre plate spectrophotometer set at a 650 nm wavelength.

2.10.3 Gel electrophoresis

1mm thick NuPAGE 4-12% Bis-Tris polyacrylamide gels were used for Western blot analysis of FGFR2 and p-ERK1/2 proteins. Gels were run in an X Cell SureLock gel tank (Invitrogen, Paisley, UK) using 1x NuPAGE MES SDS Running Buffer. Equal amounts of protein from all the tested cell lysates were mixed with 4x NuPAGE LDS sample buffer, supplemented with 50 mM DTT, that breaks disulphide bonds creating reducing conditions, boiled for 3 minutes at 100ºC and centrifuged at 10,000 rpm for 3 minutes. The sample supernatants and Full Range Rainbow Molecular Weight Marker were then loaded onto the gel and run at 130 V for 1.5-2 hours, after which the gel was prepared for Western blotting.

2.10.4 Western blotting

Western blotting is a technique that separates proteins according to their molecular weight, and is used to analyse the expression levels of proteins, which are recognised via the binding of specific antibodies. For the detection of specific proteins, electrophoretically separated proteins were transferred onto a nitrocellulose membrane. After blocking of non-specific binding sites, the membrane was incubated with the primary antibody and the corresponding secondary antibody, coupled to an enzyme that catalyses the detection reaction.

The resolved gel, after cutting off the wells and the bottom of it, was laid on a Protran nitrocellulose transfer membrane of equal dimensions to the gel and sandwiched between 2 pieces of 3MM Whatman Chromatography paper. Air bubbles were removed by rolling a glass tube over the “sandwich”, which was then assembled in an X Cell II Blot Module transfer apparatus following the manufacturer’s instructions. The gel was immersed in transfer buffer (0.72 g Tris-base, 3.6 g Glycine, 100 ml Methanol brought to 500 ml with distilled water). Proteins ranging in size from 30-90 kDa were transferred at 12 V overnight. Afterwards, membranes were stained with Ponceau S Solution to check the quality of the transfer. The dye was washed away in distilled water.

2.10.5 FGFR2 Western blot

40 µg of total protein from normal human keratinocytes and SCC cell line lysates were loaded onto 1 mm thick NuPAGE 4-12% Bis-Tris polyacrylamide gels. After transfer the membrane was blocked in 5% milk in 0.01% Tween in PBS (PBS-T) for 1 hour, washed three times x10 minutes in PBS-T and then incubated overnight at 4°C with a rabbit polyclonal anti-FGFR2 antibody, diluted 1:2000 in

3% BSA in PBS-T solution. The following day the blot was washed three times in PBS-T and incubated for 1 hour at room temperature with an HRP conjugated polyclonal goat anti-rabbit antibody diluted 1:1000 in 3% BSA in PBS-T. Following three washes in PBS-T, the blot was incubated with ECL reagent. Chemiluminescence was detected by exposure to Fuji medical X-Ray film. Afterwards, the membranes were stripped by incubating in Re-Blot Plus Mild Solution for 20 minutes at room temperature.

After stripping previous antibody, membranes were blocked again in 5% milk solution, washed as previously described and then incubated with different antibodies. Mouse monoclonal α-Tubulin antibody was used to determine protein loading.

2.11 Genomic DNA extraction from cell monolayers

Cultured cell monolayers were grown to 80% confluency. The media from the cells was aspirated off and the cells trypsinised as described below. The cell suspension was transferred into a 15 ml falcon tube and centrifuged 5 min at 5,000 rpm. The supernatant was removed, the cell pellet resuspended in PBS and washed twice with 10 ml PBS, centrifuging between washes. Afterwards, the pellet was resuspended in 800 µl of tissue digestion buffer (as described above) and 5 µl of Proteinase K (50 µg/µl) was added. The sample was incubated overnight at 37°C in a shaking incubator. The following day the sample was transferred into a 2 ml Eppendorf tube and 960 µl of Phenol was added. It was vortexed and left to stand for 5 minutes and vortexed again followed by centrifugation for 10 min at maximum speed. The upper aqueous phase was transferred into a fresh tube and the volume was measured. Phenol/Chloroform equal to the volume of the aqueous phase was added and the sample mixed and centrifuged as above. The aqueous

phase was transferred into a fresh tube and 1/10 the volume 3 M Sodium acetate (pH 5.2) and 3 times the volume 100% Ethanol was added. The sample was shaken gently until the DNA precipitated out and then was centrifuged as above. The DNA pellet was washed in 70% Ethanol, centrifuged and after the supernatant was removed it was air-dried, dissolved in EB buffer and placed in a shaking stage incubator for a two hours at 37°C. Finally the DNA concentration was measured as described previously.

2.12 Southern Blotting

Southern blotting is a technique, developed by Edwin M. Southern in the 1970s, to determine the presence of a particular sequence of DNA within a DNA sample (Southern, 1975). It involves electrophoresing digested DNA fragments on an Agarose gel and then transferring them to a nylon membrane by capillary action. Once immobilised, the DNA can then be allowed to hybridise with a radioactive probe corresponding to the region of interest.

Firstly, 10 µg genomic DNA was digested with an appropriate restriction enzyme in 50 µl reaction volume.

Digest mix:	10 µg	DNA
	5 µl	10x buffer 2
	2 µl	HindIII enzyme (20 units/µl)
	1 µl	sample
	0.125 µl	Spermidine (1M stock)
	0.5 µl	BSA
	6 µl	RNase A (1mg/ml stock)
	the volume was made up to 50 µl with sterile, distilled water	

The samples were incubated at 37°C, vortexing three times per hour. After two hours another 2 µl of restriction enzyme was added and the samples were left at 37°C overnight.

The following day, samples were prepared for electrophoresis by adding 10 µl of x5 GelPilot DNA Loading Dye and run on 0.8% Agarose/TBE gel (as described above) at 70 V for seven hours. Molecular weight ladder (Hyperladder I) was loaded alongside as a reference.

The gel with the separated genomic DNA fragments was photographed with a ruler next to it, in order to measure the distance from the wells to bands of interest. The gel was depurinated in 0.25 N HCl for 15 minutes with gentle rocking. The acid was neutralised by rinsing the gel in 0.4 M NaOH briefly for 5 minutes.

The gel containing the denatured DNA was assembled in a blot to transfer DNA to a positively charged nylon membrane. A gel tray was placed upside-down in a buffer chamber filled with 0.4 M NaOH. A piece of Whatman 3MM paper was placed on top of the tray with its edges immersed in the transfer buffer, thus forming a wick. The Agarose gel was placed upside-down on top of this platform, followed by nylon membrane (Nytran SuPerCharge) pre-soaked in water and marked in the top right-hand corner. Saran wrap was used to seal the edges of the membrane. Three layers of wet Whatman 3MM paper cut to the gel size were laid on top of the membrane. Each time a new layer was added a glass tube was rolled on top of it to remove any trapped air bubbles. A stack of paper towels and a glass plate were assembled with a 200 g weight on top and the DNA was left to transfer overnight by capillary action.

The next day, the transfer setup was disassembled and the nylon membrane removed and rinsed twice in 2x SSC for 5 minutes. The membrane was put between two new sheets of 3MM paper and left to air dry for 2 hours. If it was not used immediately it was stored between filter papers.

2.12.1 ES cells screening probe preparation

The 5'Fgf22 (400-bp) and 3'Fgf22 (600-bp) probes were isolated from Fgf22pBluescript SK^+ plasmid construct by digesting with BamHI, HindIII, and EcoRI enzymes respectively.

5' Construct Digest mix:	4 µg	DNA
	5 µl	10x BamHI buffer
	0.5 µl	BSA (100x)
	4 µl	BamHI enzyme (20 units/µl)
	the volume was made up to 50 µl with sterile, distilled water	

3' Construct Digest mix:	4 µg	DNA
	5 µl	10x EcoRI buffer
	2.5 µl	HindIII enzyme (20 units/µl)
	2.5 µl	EcoRI enzyme (20 units/µl)
	the volume was made up to 50 µl with sterile, distilled water	

The samples were incubated at 37°C for 2 hours. The digested products were separated using gel electrophoresis and photographed (as described earlier). The desired bands were cut out and eluted from the gel by using a QIAquick gel extraction kit (Qiagen) as described in the protocol. The gel slice was melted in the provided solution and subsequent steps were performed as

described above. Dependent on the concentration of the fragment, the product was eluted in 20-50 µl EB buffer.

2.12.2 Probe Labelling

Ready-To-Go DNA Labelling Beads (dCTP) were used to prepare the radio- labelled probe for the Southern Blot analysis. The beads contain buffer, dATP, dGTP, dTTP, FPLCpure Klenow Fragment and random oligodeoxyribonucleotides. 50 ng of the purified DNA probe was diluted to a volume of 45 µl with distilled water. This was heated to 95°C for 3 minutes to denature the DNA, and then quickly moved to ice for 2 minutes. The sample was centrifuged briefly and then transferred into the labelling bead mixture in an Eppendorf tube where 5 µl of [α-^{32}P] dCTP was added. The whole mixture was incubated for 30 minutes at 37°C.

The ^{32}P-labelled probe was purified using a MicroSpin G-25 Column. First, the resin in the column was resuspended by vortexing, then the bottom tab of the column was snapped off, the column placed in a 1.5 ml Eppendorf and centrifuged for 1 minute at 3,000 rpm. The labelled probe was added and the column was centrifuged again for 2 minutes at 3,000 rpm, collecting the flow through containing the purified, labelled probe. This was boiled for 3 minutes and transferred to ice immediately. The contents of the tube were collected by brief centrifugation.

2.12.3 Hybridisation

To block non-specific binding, the membrane was pre-hybridised for 30 minutes at 55°C in 5 ml of the pre-warmed hybridisation buffer (15% HYB or

Church Buffer: 0.2 M Sodium phosphate mix [pH 7.2], 1 mM EDTA [pH 8], 1% BSA, 7% SDS, 15% Formamide in water) in a glass tube in a Micro-4 hybridisation oven (Hybaid, Teddington, UK). 40 µl of the ^{32}P-labelled probe was added to the solution and hybridisation allowed to proceed at 60°C overnight.

The membrane was washed three times for 30 minutes at 65°C in wash buffer (40 mM sodium phosphate mix pH 7.2, 1 mM EDTA pH 8, 1% SDS in water). While still wet, the membrane was covered in Saran wrap and exposed to a storage phosphor screen (Molecular Dynamics, USA). After overnight exposure the screen was read by a phosphor image scanner (Storm 860 – Molecular Dynamics, USA).

2.13 Tissue fixation and wax embedding

Tissue fixation and subsequent wax embedding are routine histological techniques for morphological studies. The fixation has the purpose of preserving the structure and components of the tissue. This is the first and critical step of a protocol before the sections for microscopy could be obtained.

2.13.1 Eye dissection

Mice were killed by cervical dislocation and the eyes were carefully removed with the help of fine watchmaker forceps. The optic nerve was preserved together with the eye, for orientation, and the complete tissue was placed in cold PBS. After eyeball dissection, tissues were fixed in a solution of 4% of Paraformaldehyde (PFA), pH 7.4 for 24 hours at 4^{o}C, then the tissues were washed twice in PBS for 30 min. Tissues were put in a new tube with PBS and left overnight at 4^{o}C.

2.13.2 Oesophagus and stomach dissection

Maximal length of the oesophagus, reaching from trachea to stomach, was dissected out and rinsed in cold sterile PBS pH 7.4. The tissue was then fixed in 99% Ethanol plus 1% Glacial Acetic Acid overnight at 4^{o}C. The next day tissue was washed twice in 70% Ethanol and then stored in Ethanol until further processing.

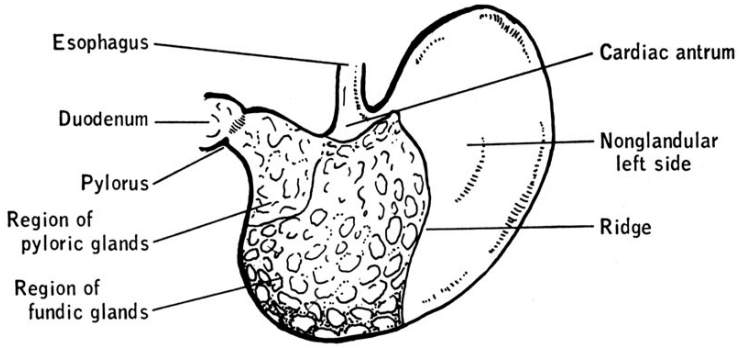

Figure 2.4 Drawing of the stomach, ventral aspect (Biology of the Laboratory Mouse, The Jackson Laboratory).

Stomach and 5 mm proximal duodenum were cut open along the greater curvature (Fig 2.4) and flushed gently with cold, sterile PBS pH 7.4. The tissue was gently stretched, pinned and immersed in 10% Neutral Buffered Formalin (NBF) overnight (Figure 2.5). The tissue was rinsed in 70% Ethanol, and three longitudinal vertical strips were cut as illustrated in Figure 2.5. The Experimental Pathology Department, Cancer Research UK provided support with tissue sectioning.

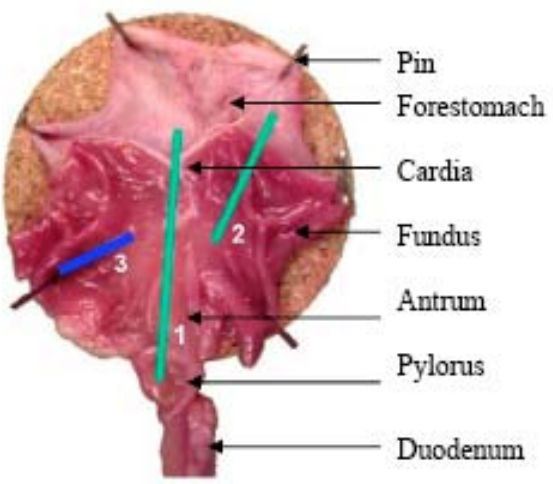

Figure 2.5 Stomach and proximal duodenum were cut and pinned open prior to fixation (Ruehl-Fehlert et al., 2003). Three strips were taken as indicated by the numbers on the picture.

2.14 Tail epidermis whole-mounts

To prepare whole-mounts of mouse tail epidermis, a scalpel was used to slit the tail lengthways. Skin was peeled from the tail, cut into pieces (0.5x0.5 cm^2) and incubated in 5 mM EDTA in PBS at 37°C for four hours. Forceps were used to gently peel the intact sheet of epidermis away from the dermis and the epidermal tissue was fixed in 1% Acetic Acid and 95% Ethanol overnight at 4°C. After rinsing in 100% Ethanol, they were rehydrated through a graded alcohol series to water and transferred to PBS. Then the specimens were counterstained for 10 seconds in a 1:4 dilution of Mayer's haemalum/water and mounted in 30% Glycerol in PBS.

2.15 Immunohistochemistry

Immunohistochemical staining was performed on formalin-fixed paraffin embedded (FFPE) sections to determine the localisation of specific proteins in tissue sections. Negative controls were always performed, where sections were incubated with just secondary antibody.

2.15.1 α-FGFR-2 antibody

Paraffin-embedded human skin and tumour sections (4 μm) were subjected to immunostaining using the streptavidin-peroxidase technique. All the incubation steps were performed in an humidified chamber.

Formalin-fixed paraffin embedded (FFPE) sections were deparaffinized by soaking slides in Xylene twice, each time for 15 minutes. Sections then were rehydrated through incubation for 5 minutes at each concentration of an Ethanol gradient: 100% I, 100% II, 95%, 90%, 80%, 70%, 50% and twice in distilled water. Next, endogenous peroxidase activity was blocked by incubation for 30 minutes with 0.3% Hydrogen peroxide in Methanol. Slides were washed in PBS twice, 2 minutes each time. Afterwards individual sections on slides were circled with a PAP pen.

For antigen retrieval, slides were incubated with pre-warmed Pepsin Digest ALL-3 solution for 5 minutes at 37°C in an humidified chamber. Slides were washed twice in PBS, 2 minutes each time, and Avidin solution was applied for 10 minutes at room temperature. Slides were washed as above, then Biotin solution was applied for 10 minutes at room temperature. Slides were washed and incubated for 15 minutes with 10% normal goat serum in PBS at room

temperature to block non-specific antibody binding. Tissue sections were incubated for 16 hours at 4°C with polyclonal α-FGFR-2 antibody diluted 1:1000 in 1% BSA in PBS. Negative controls were also performed where sections were incubated with rabbit α-IgG antibody, 1:1000 dilution or just secondary antibody.

The following day, slides were washed in PBS, and in the meantime streptavidin-peroxidase complex mix (StreptABComplex/HRP), [1 ml TBS + 1 µl reagent A +1 µl reagent 2] was prepared, mixed and left on ice for 30 minutes prior to use.

Bound antibodies were detected with biotinylated goat anti-rabbit IgG secondary antibody (1:500 dilution in 1% BSA in PBS). Tissue sections were incubated for 30 minutes at room temperature and then washed in PBS. Sections were then treated with streptavidin-peroxidase complex for 30 minutes. Afterwards, slides were washed and Diaminobenzidine (DAB substrate) [1 drop of chromogen in 1 ml of substrate buffer] was applied for 5 minutes. The slides were washed in running water for 2 minutes and then stained in Mayer's haematoxylin for 90 seconds in order to counter stain the nuclei. The slides were washed in running tap water for 1 minute, then in PBS for 1 minute and finally in filtered water. Afterwards slides were dehydrated through an Ethanol series into Xylene (as above but in reverse order). The stained slides were mounted on coverslips using Permount mounting medium.

2.15.2 α-BrdU antibody

Paraffin sections were de-waxed as described earlier (2.15.1).

To block endogenous peroxidase activity, the slides were immersed in 1.5% Hydrogen peroxide in Methanol for 15 minutes. After washing in PBS slides were

incubated in 1N HCl at 60°C for 8 minutes to allow DNA denaturation. Next, slides were incubated twice for 10 minutes in 70% Ethanol/0.1M Tris pH 7.5 and washed twice in 70% Ethanol for 5 minutes. Slides were rinsed briefly in dH_2O and washed in PBS twice for 10 minutes. Individual sections on slides were circled with a PAP pen and anti-BrdU antibody solution (1:500 dilution in 1% BSA/PBS) was applied. Samples were incubated with the antibody for 1 hour at room temperature in an humid chamber.

Afterwards, slides were washed in PBS twice for 10 minutes and incubated with secondary goat anti rat antibody solution (1:100 dilution in 1% BSA/PBS) for 45 minutes at room temperature. Slides were washed in PBS twice for 10 minutes. Streptavidin-peroxidase complex mix was prepared as described previously and left for 30 minutes on ice before use. Sections were then incubated for 45 minutes at room temperature with the ABC solution. Afterwards, slides were washed in PBS twice for 10 minutes, rinsed in tap water for 5 minutes and DAB substrate was applied for 3 minutes. From then on slides were treated as described previously (2.15.1).

2.15.3 α-p63 antibody

Paraffin sections were de-waxed as described earlier (2.15.1).
Endogenous peroxidase activity was blocked by 40 minutes incubation in 1.5% Hydrogen peroxide in Methanol. After washing in PBS twice for 2 minutes slides were microwaved (900W; medium setting) for 20 minutes in 10 mM Sodium citrate buffer solution [pH 6] to allow antigen retrieval. Slides were left at room temperature to cool, then washed in PBS for 3 minutes. Individual samples on slides were circled with a PAP pen and Avidin/Biotin block was applied as described previously. After washing in PBS twice for 2 minutes non-specific

binding was blocked by applying M.O.M. Mouse Ig Blocking Reagent for 1 hour at room temperature. Later, slides were washed in PBS twice for 2 minutes and incubated in prepared M.O.M. Diluent for 5 minutes. Excess solution was tipped off and 1:50 dilution of the mouse primary monoclonal anti-p63 antibody was applied.

The next day, streptavidin-peroxidase complex mix was prepared and left on ice for 30 minutes prior to use. Slides were washed in PBS twice for 2 minutes and then working solution of M.O.M. Biotinylated Anti-Mouse IgG Reagent was applied for 10 minutes. Slides were washed in PBS twice for 2 minutes then incubated in ABC solution for 45 min at room temperature. After another three 5 minute washes in PBS, DAB substrate was applied for 8 minutes. From then on slides were treated as described previously (2.15.1).

2.15.4 α-Loricrin antibody

Paraffin sections were de-waxed as described earlier (2.15.1).
To allow antigen retrieval slides were microwaved (900W; medium setting) for 20 minutes in 10 mM Sodium citrate buffer solution [pH 6]. Afterwards slides were left to cool to room temperature (about 15 minutes) and then rinsed twice in PBS. Non-specific binding was blocked by incubating sections with 5% BSA/PBS at room temperature for 1 hour. Then primary rabbit anti-Loricrin antibody solution (1:500 in 5% BSA/PBS) was applied overnight at 4°C. The next day, three 10 minute PBS washes were performed and secondary goat anti-rabbit rhodamine conjugated antibody solution (1:100 in 5% BSA/PBS) was applied and incubated for 1 hour in the dark at room temperature. After another three 10 minutes PBS washes, also in the dark, and a quick rinse in dH_20, slides were mounted with Vectashield mounting media with DAPI (Vector Laboratories).

2.15.5 α-Keratin14 antibody

Paraffin sections were de-waxed as described earlier (2.15.1). Endogenous peroxidase activity was blocked by 40 minutes incubation in 1.5% Hydrogen peroxide in Methanol. Slides were then washed twice for 2 minutes in PBS and individual sections were circled with a PAP pen. Avidin solution was then applied for 10 minutes at room temperature. Slides were washed as above and Biotin solution was applied for 10 minutes at room temperature. Slides were washed and incubated for 1 hour with 5% BSA/PBS at room temperature to block non-specific antibody binding. Meanwhile, primary antibody solution was prepared (1:1000 in 5% BSA/PBS) and centrifuged for 5 minutes at 13,000 rpm at 4°C. Tissue sections were incubated overnight at 4°C with polyclonal rabbit anti-mouse K14 antibody.

The next day, slides were washed three times for 5 minutes in PBS and 1:100 dilution of a secondary goat anti-rabbit antibody in blocking solution was applied. Sections were incubated for 45 minutes at room temperature. From then on slides were treated as described previously (2.15.1).

2.16 Alcian Blue and Alizarin Red skeletal staining

The combination of Alcian Blue and Alizarin Red allows a differential staining of cartilage and bone (Green, 1952). In the process of staining cartilage becomes blue while the bone gains red colour. Treatment with Potassium hydroxide (KOH) and Glycerol dissolves muscle and connective tissue but spares stained tissues resulting in a clear picture of skeletal structure.

Whole mice, including the tails, were skinned and all their internal organs were removed. Any excess fat, especially behind the neck and between clavicles, also was removed. The carcasses were then left to fix in 95% Ethanol for 3 days at room temperature. Afterwards the skeletons were placed in Alcian Blue staining solution (below) for 14 days on a shaker to ensure even staining. Staining solution was replaced with 95% Ethanol for 1-2 days. The tissue on skeletons was then cleared in 1% KOH for several days. Afterwards the skeletons were put into fresh 1% KOH with Alizarin Red staining solution (below) on a shaker for 1-3 days. When evenly stained, the skeletons were drained and put into 100% Glycerol. Glycerol was replaced twice before staining was completed.

Alcian Blue staining solution	Alizarin Red staining solution
4 volumes of 95% Ethanol	Make 1% KOH in water
1 volume of Acetic acid	Add alizarin red powder to
0.015% Alcian Blue 8GX	1% final concentration.
Stir for 30 minutes, do not filter.	Dissolve well, do not filter.

2.17 Sirius red staining

In bright-field microscopy, Sirius red stains collagen fibres in red on a pale yellow background. Nuclei, if stained, are black, grey or brown. The same slides, when examined through a microscope with cross-polarised light show that the larger collagen fibres (Collagen type I) are bright yellow or orange, and the thinner ones, including reticular fibres and collagen type III, are green. The birefringence is considered to be highly specific for collagen fibres. Keratohyaline granules and some types of mucus, for example, also stain red but do not display any birefringence. The principle of the method is that collagen forms the ground substance of connective tissue and it is composed of three amino acids. It stains

strongly with acid red dyes due to the affinity of the cationic groups of the proteins for the anionic reactive groups of the acid dyes.

Paraffin sections were de-waxed and hydrated as described earlier (2.7.1.). Sections were stained in Picro-sirius red (below) for one hour, then washed in two changes of acidified water (below). Most of the water from the slides was removed by vigorous shaking, sections were dehydrated in three changes of 100% Ethanol, cleared in Xylene and mounted.

Picro-sirius red	Acidified water
0.5 g Sirius Red F3B	5 ml Glacial Acetic Acid
500 ml of saturated aqueous solution of Picric Acid	995 ml of water
Add a little solid picric acid to ensure saturation.	

2.18 ELISA

The type of ELISA performed was a Sandwich ELISA. It is based, sequentially, on binding of leptin in the sample by a pre-titred antiserum and immobilisation of the resulting complexes in the wells of a microtitre plate. After washing, purified biotinylated detection antibody is allowed to bind to the immobilised leptin followed by binding of streptavidin conjugated horseradish peroxidase (HRP) to the immobilised biotinylated antibodies. Quantification of immobilised antibody enzyme conjugates takes place by monitoring (HRP) activity in the presence of the substrate 3,3',5,5'-tetramethylbenzidine (TMB). The enzyme activity is measured spectrophotometrically by the increased absorbancy at 450 nm, corrected from the absorbancy at 590 nm, after acidification of formed

products. Since the increase in absorbency is directly proportional to the amount of captured leptin in the unknown sample, the latter can be derived by interpolation from a reference curve generated in the same assay with reference standards of known concentrations of mouse leptin.

2.18.1 Sample collection and storage

To prepare serum samples, whole mouse blood was directly drawn into a centrifuge tube that contained no anti-coagulant. Blood was left to clot at room temperature for 30 minutes and then samples were centrifuged at 7,000 rpm for 15 minutes at 4°C. Serum supernatant was removed, aliquoted and stored at -20°C for later use.

2.18.2 Assay procedure

All the reagents were pre-warmed to room temperature immediately before use. The 10x concentrated HRP wash buffer was diluted 10 fold by mixing the entire contents of both buffer bottles with 900 ml distilled water. Each well of the assembled microtitre assay plate was washed 3 times – each time with 300 µl of diluted wash buffer. Wash buffer was then decanted and the residual amount from all wells was removed by inverting the plate and tapping it onto absorbent towels. 30 µl of Assay Buffer was added to background wells, standard wells, and QC1 and QC2 wells, while 40 µl of assay buffer was added to sample wells. Then, 10 µl of matrix solution was added to the background wells, standard wells, and QC1 and QC2 wells. Next 10 µl of assay buffer was added to the background wells and 10 µl of mouse leptin standards was added, in duplicates, in the order of ascending concentration to the appropriate wells. Next, 10 µl of QC1 and 10 µl of QC2 was added to the appropriate wells. Finally 10 µl of the unknown samples

were added sequentially in duplicate to the remaining wells, followed by 50 µl of antiserum solution, added to each well used in the assay. The plate was covered with a plate sealer and incubated at room temperature for 2 hours on an orbital plate shaker set to rotate at moderate speed. Following this incubation, the seal was removed, solutions decanted from the plate as described before, and wells were washed 3 times with diluted wash buffer (300 µl per well per wash). Next, 100 µl of detection antibody was added to each well and the plate was sealed and incubated with moderate shaking at room temperature for 1 hour. As before, the seal was removed, solutions decanted and wells were washed 3 times with diluted wash buffer (300 µl per well per wash). Then, 100 µl of enzyme solution was added to each well. The covered plate was incubated with moderate shaking at room temperature for 30 minutes. After 6 washes were performed as described above, 100 µl of substrate solution was added to each well and the covered plate was left for approximately 10 to 15 minutes, upon which a blue colour developed in the wells of leptin standards (with intensity proportional to increasing concentrations of leptin). Colour development was monitored by using 370 nm filter on the spectrophotometer. When the absorbance was between 1.2 and 1.8 at 370 nm, the stop solution was added to terminate the colour development. 100 µl of stop solution was added and the plate was shaken by hand to ensure complete mixing of solution in all wells. This resulted in change of blue colour into yellow after acidification. The absorbance was read at 450 nm and 590 nm in a plate reader within 5 minutes and the difference of absorbance units was recorded.

2.19 Basic cell culture

Routine tissue culture provides a core facility for the development, maintenance and provision of cultured cells. Cultured cells must be provided with an appropriate surface for attachment, promoting cell seeding and spreading,

presence of exogenous serum containing the necessary nutrients, and culture conditions that enable an adequate mass transfer of nutrients and oxygen along with waste removal.

2.19.1 General principles

Cell culture treatments were carried out in a laminar flow hood which provided a sterile environment. The hood was decontaminated with 70% Ethanol before and after each work session. All tissue culture reagents were filter-sterilised using a 0.22 µm syringe-driven or vacuum driven filters (Millipore, Watford, UK) and stored in a sterile container at 4°C. Upon use, media was pre-warmed in a 37°C water bath. Cells were grown in an humidified atmosphere, appropriate CO_2 levels and temperature was maintained in incubators.

2.19.2 Tissue culture media and solutions

2.19.2.1 CR-UK stock media

Cancer Research UK Central Services supplied many of the buffers and media that were used. These included PBS, Trypsin-Versene, E4, normal DMEM, Hams-F12, Pen/Strep, L-Glutamine.

2.19.2.2 Human SCC keratinocyte medium

E4 and Hams-F12 3:1 volume supplemented with 10% Foetal calf serum, L-Glutamine and 0.4 µg/ml Hydrocortisone, 10^{-10} M Cholera toxin, 5 µg/ml Transferrin, $2x10^{-11}$ M Liothyronine, $1.8x10^{-4}$ M Adenine, 5 µg/ml Insulin and 10 ng/ml hEGF. All of the above mentioned are final concentrations.

2.19.2.3 Early passage HaCaT keratinocyte medium

E4 supplemented with 10% Foetal calf serum and Pen/Strep (100 µg/ml).

2.19.2.4 Primary murine keratinocyte media

PCT Epidermal Keratinocyte Medium calcium free (CnT-07CF) including provided supplements together with 8% calcium free Foetal calf serum (South American Origin) and Pen/Strep (100 µg/ml). Additionally, calcium concentration in low calcium media was 0.05 mM and 1.3 mM in high calcium media.

2.19.2.4.1 Preparation of calcium free FBS

100 g of Chelex-100 resin was mixed with 400 ml of dH_20 using a magnetic stirrer. Next the solution was adjusted to pH 7.4 with 4 M HCl and the liquid was carefully decanted without disturbing the pellet. The resin slurry was transferred into 500 ml of FBS and stirred at room temperature for 3 hours. Afterwards, FBS was carefully decanted, filtered through 0.22 µm pore size filter, aliquoted and stored at -20°C.

2.19.3 Mycoplasma screening

As a precaution, routine mycoplasma PCR-based screening was performed for all cell lines. This PCR detects mycoplasma by amplification of 16S – 23S spacer region in rRNA operons. Sequences of primers included are common to 14 different species of mycoplasma.

After a minimum of two days culturing, growth medium was collected into a 50 ml falcon tube and centrifuged for 5 minutes at 4500 rpm. Most of the supernatant was removed, leaving only 500 µl. The pellet was resuspended by repeated pipetting up and down and 1 µl was added to the PCR mix. Nested PCRs were carried out using MegaMix in a reaction volume of 20 µl. A positive control of medium known to be contaminated with mycoplasma was always performed alongside with a negative control with all the mix components except the supernatant sample.

Reaction mix:	17.7 µl	MegaMix
	0.5 µl	FWD 1 primer (100 pmol/µl)
	0.5 µl	Common REV primer (100 pmol/µl)
	0.3 µl	Formamide
	1 µl	sample

The following programme was used:

PCR-programme:	Denaturation	3 min	94°C	
	Denaturation	30 sec	94°C	35 cycles
	Annealing	30 sec	55°C	
	Extension	1 min	72°C	
	Final Extension	10 min	72°C	

1 µl of the PCR product was used for sequential PCR with exactly the same conditions as described above apart from different forward primer used in the reaction mix.

The first round of PCR amplified a 720 bp fragment. The second nested PCR reaction primers amplified a 145 bp fragment.

2.19.4 Early passage HaCaT keratinocyte cell culture

Early passage HaCaT keratinocytes were a gift from Petra Boukamp, DKFZ, Germany. To avoid rapid loss of cells via differentiation, they were neither passaged too often nor split at too high a ratio. At confluence (or postconfluence, optimum 3 to 4 days past confluence), cells were pretreated with 0.05% EDTA in PBS to disassemble desmosomes. The cells were incubated at 37°C until wide intercellular spaces were visible microscopically (up to 20 minutes). EDTA was aspirated off and 3 ml of a 1:1 mixture of EDTA and Trypsin solution was added (final concentrations 0.025% and 0.05%, respectively). Cells were incubated at 37°C for 2 to 5 minutes until they came off the plastic culture dish upon shaking. Complete culture medium with 10% FCS was added to stop Trypsin activity and the cell solution was transferred to a 15 ml falcon tube and centrifuged for 3 minutes at 1,200 rpm. Afterwards the supernatant was aspirated off and the cells were resuspended in complete culture medium with 10% FCS and plated at maximal split ratio of 1 in 10. The medium was changed every 2 days and the optimal time between passages (7 to 10 days) was maintained.

2.19.5 Primary murine keratinocyte cell culture

Primary keratinocytes were isolated from dorsal skin and tails of adult mice. The skin area chosen to obtain keratinocytes should be in the resting phase (telogen) of the hair cycle, meaning that shaven hair reveals pink skin without dark patches, if the mice are on an agouti background.

Mice aged one to three months were killed by cervical dislocation. The hair from the dorsal skin of the mouse was removed with clippers and depilatory cream (Nair) was applied onto hair-free surface for approximately 3 minutes. Afterwards,

excess depilatory cream was removed with cotton gauze and the mice were washed under running water with gentle rubbing. The mice were transferred into the tissue culture hood, where they were washed twice for 2 minutes in Iodine solution, rinsed in sterile water and finally in 70% Ethanol. Mice were placed in Petri dishes, their skin was cut from torso to tail and peeled off using scissors and forceps. Skin was also removed from tails. Removed skin was placed, epidermis side down, on a sterile surface (rough underside of an autoclaved porcelain spot plate) and the hypodermis was carefully scraped off using a scalpel blade. Next the skin was stretched flat and a piece of autoclaved Whatman no. 1 filter paper was applied onto the exposed surface of the dermis. The skin, including the attached paper, was cut into 1 cm wide strips using sterile scissors and placed dermis side down on the surface of recently thawed 1% Trypsin in PBS (back skin) or 0.25% Trypsin in PBS (tail skin). Back skin was incubated with the Trypsin for 2 hours at 37^{o}C and tail skin was left in the solution overnight at 4^{o}C. The epidermis was easily peeled off using curved forceps and placed into ice cold PCT Epidermal Keratinocyte Medium containing high calcium concentration. Collected epidermis was then cut and minced in the medium with sterile scissors, until pieces were small enough to enter the tip of a 10 ml pipette. The resulting suspension was then triturated by pipetting up and down about 30 times. Afterwards it was transferred into a 50 ml conical tube, also kept on ice, leaving most of the *stratum corneum* squames behind. The cell suspension was then centrifuged at 1,450 rpm for 5 minutes. The cell pellet was resuspended in high calcium medium and filtered through a 100 µm cell strainer into a new 50 ml conical tube. The cell strainer was rinsed with additional dose of high calcium medium to release cells entrapped by remaining *stratum corneum* pieces. Another centrifugation step was performed at 1,450 rpm for 5 minutes and the cell pellet was resuspended in 10 ml of high calcium medium. The cells were counted, then centrifuged again and resuspended in the desired volume of low calcium medium

to obtain cell concentration of 1 to 1.25 million cells/ml. Next, the cells were plated in Collagen I coated 60 mm dishes (3 ml of cell suspension containing approximately 3 million cells).

Primary keratinocytes were incubated at 36°C and 7% CO_2 overnight. The next day, the medium containing unattached cells was aspirated off, the dish was rinsed with calcium/magnesium free PBS and fresh low calcium media was added. Thereafter cells were fed every other day.

2.19.5.1 Coating flasks for keratinocyte cell culture

Flask-coating Collagen I solution was prepared by combining 2.76 ml rat tail Collagen (3.6 mg/ml stock) with 0.23 ml Glacial Acetic Acid and 197.47 ml sterile dH_2O. Routinely, a 3 cm dish was coated with 1 ml of coating solution and incubated for 30 minutes at 37°C. Afterwards, excess coating solution was aspirated off and the dish was washed twice with calcium/magnesium free PBS immediately prior to seeding cells.

2.19.5.2 Passaging primary keratinocytes

Primary keratinocytes were passaged when cells reached 70-80% confluence. Medium was removed and the cell monolayer was washed twice with calcium/magnesium free PBS. Then, 1% Trypsin was added and cells were incubated for 30 min at 36°C, 7% CO_2. Once the cells detached, 5 ml of PCT Epidermal Keratinocyte low calcium medium containing 8% calcium free FCS was added to quench the trypsinisation. Cells were carefully resuspended, transferred to a 50 ml conical tube and centrifuged at 1,450 rpm for 5 minutes. Afterwards, the

cell pellet was resuspended in fresh medium and the cells were plated onto pre-coated dishes at a 1:2 split ratio.

2.19.6 Storage and recovery of liquid nitrogen stocks

2.19.6.1 Cryopreservation of cultured cells

Cultures can be preserved effectively in the presence of a cryoprotectant, such as dimethylsulphoxide (DMSO), which reduces the damage from ice crystals. Cells to be stored were harvested in log phase growth. Following trypsinisation, cells were washed in complete medium and resuspended in medium containing 10% DMSO at 1-2x10^6 cells per ml. One ml of cell suspension was placed in a Nunc cryotube in an insulated container and placed at -80°C for 8 hours, before transferring vials to -196°C liquid nitrogen for long-term storage.

2.19.6.2 Thawing cell stocks

Cryopreserved cells are fragile and require quick thawing and immediate retrieval into complete medium. Vials to be recovered from liquid nitrogen were placed in a water bath at 37°C to thaw rapidly. As soon as the vial contents were thawed the cell suspension was transferred to 15 ml Falcon tubes containing 10 ml of pre-warmed complete medium and centrifuged at 1,200 rpm for 3 minutes. The supernatant was removed to get rid of cryoprotectant and cells were resuspended in fresh full medium and transferred to culture dish or flask.

2.20 *In vitro* wound closure assay- Scratch assay

Primary keratinocytes derived from *Fgf22* wild type and knockout mice were seeded at a density of 3 million cells per well in pre-coated 6-well plates. Cells were allowed to grow until the correct confluency was achieved, when the culture medium was aspirated off and the monolayer was washed with calcium/magnesium free PBS. Next, the cells were starved in low serum media (1% FBS) for 2 hours. Then, using a plastic 200 µm pipette tip, scratches were made across and along each well forming a cross. The medium was aspirated off and replaced with normal PCT Epidermal Keratinocyte low calcium medium containing 8% calcium free FCS. To determine the rate of cell migration, a picture of each well at exactly the same point was taken at 0, 6, 12, 18 and 32 hours post-wounding using Time-lapse microscope set up (Zeiss, Hertfordshire, UK). Time-lapse microscopy allows to monitor changes in the amount and speed of cell migration in real-time. Scratch widths were measured at 20 points along their length using ImageJ software (National Institutes of Health, Bethesda, MD). The percentage of migration was determined relative to the scratch width at 0 hours. Experiments were performed in triplicate.

2.21 Organotypic co-culture

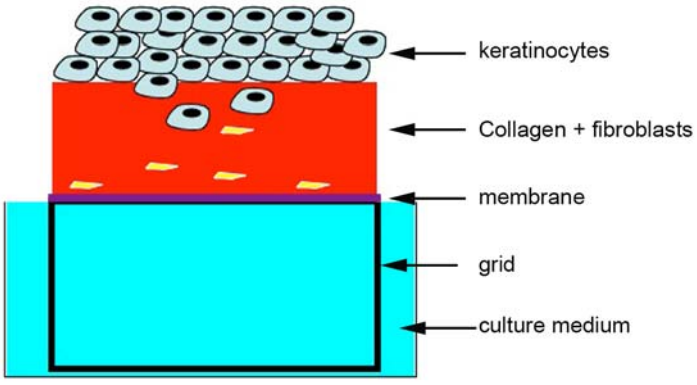

Figure 2.6 Schematic representation of a skin organotypic.

Human foreskin fibroblasts (HFF), immortalised human skin keratinocytes (HaCaT) and human SCC keratinocytes cell lines were used for organotypic co-culture (Fig 2.6). Protocol for co-culture was adapted from (Stark et al., 2004). Collagen type I (3.49 mg/ml, Upstate) was mixed with 0.1% Acetic acid and kept at 4°C. The ice cold Collagen solution (80% of total volume, 4 mg/ml) was then mixed with 10x Hank's salt with phenol red (10% of total volume) and adjusted to pH 7.4 by adding about 40 µl of 2 M NaOH per 6 ml collagen mixture while gently stirring on ice to avoid air bubbles and premature gelation. The fibroblast number necessary for the desired concentration in the gel ($3x10^5$ per ml) was resuspended in FCS (10% of total volume) and added to the gel solution on ice under cautious stirring. With cooled pipettes aliquots of the collagen gel mixture were poured into a 24 well plate (1 ml per well). For gelation, plates were incubated for 1 hour at 37°C in an humidified incubator. Afterwards, the gels were equilibrated by complete immersion in human SCC keratinocyte culture medium for 24 hours.

The next day medium was removed and keratinocytes, at a density of $1x10^6$ in 1 ml of human SCC keratinocyte medium, were plated on top of the collagen structure. The keratinocytes usually attached within 12-24 hours and formed a nearly confluent layer on top of the collagen gel.

The day after, co-cultures were raised to the air-liquid interface thus restricting nourishment to diffusion from below (Fig 2.6). This air-lift procedure was defined as the start of the culture time of organotypic co-cultures. Firstly, membrane discs coated with Collagen were prepared by cutting 100 µm pore size membrane (Tetko Inc., USA) and autoclaving it. Sterile membrane pieces were coated with a Collagen mixture (7 volumes of Collagen I, 1 volume 10x Hanks salt, 1 volume FBS, 1 volume medium) in a Petri dish and incubated for 15 minutes at 37°C in an humidified incubator. Next, 1% Glutaraldehyde in PBS was added so

that the membranes were submerged in the solution. They were then incubated at 4°C for 1 hour and washed 4 times in PBS. In the mean time autoclaved metal grids were placed in wells of a 6-well plate, followed by Collagen coated membranes. Carefully transferred collagen gels were placed on top of each construction and about 4.5 ml of culture medium was added so it just contacted with the lower part of the gel. Medium was changed every 2-3 days. Organotypic co-cultures were grown for 6 days. On the day of harvesting co-culture gels together with the membranes were washed twice in PBS and then fixed in 4% PFA overnight at 4°C. The next day gels were washed twice in PBS, transferred to labelled bijous containing 70% Ethanol and stored at 4°C ready for processing.

2.22 Mouse growth curves

Timed matings of 8 pairs of wild type and 8 pairs of knockout mice were set up. Starting from birth, male and female pups were weighed individually twice a week. After weaning, at 2.5-3 weeks, pups were ear marked and a weight record was kept for each individual pup, weighed twice a week throughout the experiment. Control and experimental animals were housed separately. Measurements were taken up to 5 months of age, and mice were fed normal mouse chow *ad libidum* throughout the experiment.

2.23 *In vivo* wound healing

The purpose of this experiment was to determine whether or not mice lacking FGF22 were able to heal cutaneous wounds. 4 week old female and male mice were used for the purpose of the experiment. Mice were housed in isolator cages of up to 3 mice. Control and knockout animals were housed separately.

All mice were anaesthetised using inhaled Halothane, prior to having their backs shaved with clippers. The dorsal skin was wiped clean with alcohol, and the mice given an injection (*s.c*) of Rimadyl analgesic (25 µl per 25 g mouse). A fold of back skin was laid on a firm cushion of dental wax or cardboard and a clean 3 mm punch biopsy was used to make two full thickness skin wounds. Analgesic was re-administered as above post-operatively. Mice were observed regularly. If at any stage the mice appeared in distress they were killed humanely. For 24 hours after the initial wounding, cages were lined with paper to avoid dust getting into the wound. For the remainder of the experiment, sawdust was used as bedding.

At 0, 1, 5, 14 and 21 days after wounding, the wound healing process was examined. For each time point, 3 female and 3 male mice, both for wild type and knockout animals, were used. At the appropriate time point, mice were killed by anaesthetic overdose and cervical dislocation and the tissue was removed for histological analysis. One hour prior to sacrifice, mice were injected with BrdU. After termination, wounds were removed together with 2 mm of surrounding tissue and one wound per mouse was fixed in acetic ethanol fixative for pathological analysis. The other wound was snap-frozen in liquid nitrogen to allow RNA expression analysis.

2.24 Topical administration of DMBA / PMA to mice

The purpose of this experiment was to determine whether or not mice lacking FGF22 were more susceptible to developing skin tumours than wild type littermates, following treatment with the carcinogen DMBA and the tumour promoter TPA.

Female mice used for the purpose of the experiment were divided into four cohorts, 10 mice in each, at seven weeks of age. Within two groups of wild type mice, one was treated with Acetone (vehicle only control) and the other with DMBA in the initiation step. The same experiment set up was used for knockout animals. All the mice were treated with TPA in the promotion step. Mice were housed in isolator cages of up to 5 mice. Control and experimental animals were housed separately. For 48 hours after the initial DMBA treatment, cages were lined with paper to avoid the production of contaminated dust.

Prior to the experiment, all mice had their backs shaved using clippers. After 8 days, 1 mg of DMBA (25 µg x 20 mice plus 500 µg extra) in the labelled, sealed container was supplied to the animal house facility. It was then diluted in 8 ml acetone (200 µl acetone per 25 µg of DMBA). Then it was checked whether the hair had not re-grown on mice thus confirming that their hair follicles were in the resting phase of the hair cycle (telogen). Afterwards, 200 µl working strength DMBA per mouse was applied for two mice groups - one wild type and one knockout. As a control, other two mice groups (wild type and knockout) had just 200 µl Acetone administered. These treatments, and the subsequent TPA treatments, were done under yellow light. At day fifteen (one week after initial painting), aliquots of TPA stock solution (100x stock = 6 mg dissolved in 1620 µl DMSO) were supplied as 100 µl aliquots in a screw cap tube (enough for 50 x 200 µl applications, after adding to 10 ml Acetone). Mice in all the groups were given a 7.4 µg dose of TPA dissolved in 200 µl Acetone and applied to their back with a dedicated syringe. These procedures were performed by Robert Rudling in the Clare Hall Laboratories Animal Facility.

From day 15 onwards, all the mice were given weekly doses of TPA, as described above. Throughout the experiment animals were monitored for the

appearance of papillomas and tumours. If possible, one hour prior to killing, mice were injected with BrdU. After death, tissues of interest (papillomas / tumours / lymph nodes) were removed and either fixed in NBF or frozen and embedded in optimal cutting temperature compound (OCT).

2.25 Micro CT

Animals, killed by anaesthetic overdose, were imaged on a NanoSPECT/CT scanner (Bioscan, Paris, France). The scanner uses an X-ray source and a detector system, which are mounted on a gantry that rotates around a bed holding the animal. The animals were scanned with an X-ray tube voltage of 45 kVa. Data were acquired at 1° angular increment over 360°, producing 360 views. Each frame was exposed for 1,500 ms with ultra fine frame resolution. This protocol gave a total scan time of 49 minutes. CT images were reconstructed using InVivoScope 1.39 program.

2.26 Ethical regulations

All animals were used in accord with United Kingdom Home Office regulations. Human skin tissue was obtained from people undergoing surgery, following informed consent and approval of the study (obtained by Dr Catherine Harwood, ICMS, QMUL).

CHAPTER 3

FIBROBLAST GROWTH FACTOR 22

CHAPTER 3: Fibroblast growth factor 22

3.1 Introduction

3.1.1 *Fgf22* expression profile

Fgf22 is a relatively recently identified, and understudied, member of the FGF family of growth factors. Its cDNA was isolated for the first time in 2001 by Nakatake *et al.* from human placenta and mouse skin (Nakatake et al., 2001).

In mouse embryonic development, expression of *Fgf22* was not detected until quite late in gestation – embryonic day 16.5 (E16.5 – with full term being 20 days) (Beyer et al., 2003), but the authors did not look for expression earlier than E9.5. Another group, looking at earlier stages of embryonic development, reported that *Fgf22* mRNA transcripts were found in the unfertilised mouse egg, morula and early blastocyst (E3.5) as well as in mouse trophoblast stem cells (TSCs) (Zhong et al., 2006). Furthermore, *Fgf7* mRNA transcripts were absent in pre-implantation embryos (Taniguchi et al., 1998) and *Fgf10* mRNA was detected in mouse eggs and pre-implantation embryos, but not in mouse TSCs or human trophoblast placental cells, suggesting that the embryonic mRNA might be from maternal transcripts, still present in the inner cell mass cells, or produced by differentiated trophectoderm (Zhong et al., 2006).

In the adult mouse, *Fgf22* expression, examined by Northern blot analysis, was detected in the skin and brain, but not various other organs including heart, kidney, spleen, thymus, liver, stomach, intestine, lung and testis (Nakatake et al., 2001). A different group, using RNase protection assay for expression analysis, reported *Fgf22* expression in the epidermis, tongue, and brain, but again not in

heart, kidney, spleen, liver, stomach, intestine, uterus, skeletal muscle or lung (Beyer et al., 2003).

3.1.2 FGF signalling in hair follicle morphogenesis

By *in situ* hybridisation, *Fgf22* mRNA in the skin was found to be expressed preferentially in the inner root sheath (IRS) of the hair follicle (Nakatake et al., 2001). Therefore, *Fgf22* was predicted to play a role in hair development. As discussed later, all FGF7 subfamily members have been reported to affect this process. During hair development, signals from the dermal papilla to the bulge follicular stem cells induce epidermal cell differentiation during anagen to produce a keratinised hair fibre (Fig 3.1). The dermal papilla is a specialised cluster of mesenchymal cells within the dermis and its signalling stimulates stem cells to proliferate and differentiate into IRS, medulla and cortex cells, which together with the cuticle cells terminally differentiate into the mature hair fibre (Schlake, 2005). The IRS can be divided into three layers: the cuticle, Huxley layer and Henle layer, based on structure, patterns of keratinisation and incorporation of trichohyalin. The IRS stops at the level of the sebaceous gland to leave only the hair cortex and surrounding cuticle to protrude above the epidermis (Fig 3.1).

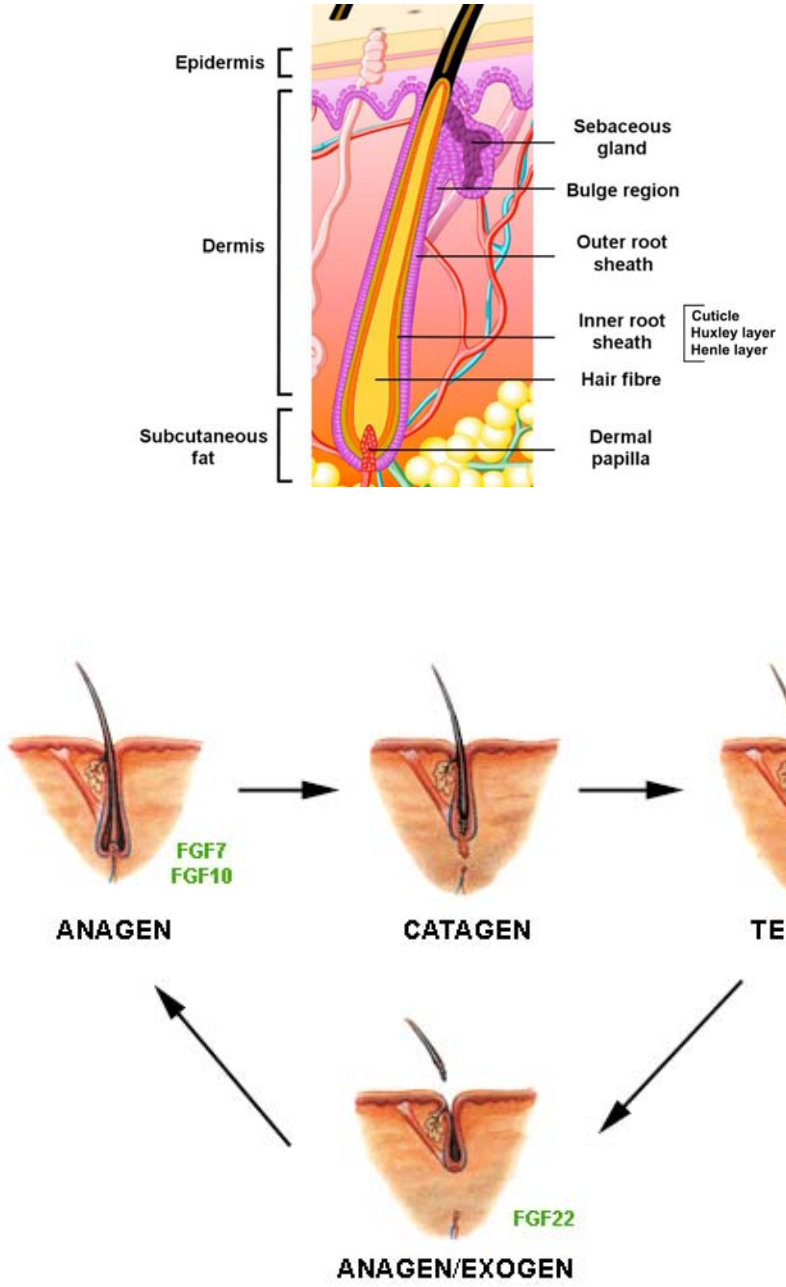

Figure 3.1 Diagram of the structure of a hair and its growth cycle (adapted from www.keratin.com and www.face2facemk.co.uk).

A single hair follicle undergoes successive growth cycles. The hair growth cycle describes the changing morphology of the shaft, grossly, and the follicle, histologically, over time. The four major stages of the cycle are: anagen (the period of active growth), catagen (the period of cessation of the growth and

regression), telogen (the period of relative inactivity) and exogen (the event of the old hair fiber shedding) (Fig 3.1) (Plikus and Chuong, 2008).

FGF7 and FGF10 are expressed in the dermal papilla of the hair follicle (Rosenquist and Martin, 1996) and, as mentioned previously, FGF22 is expressed in the inner root sheath of the hair follicle (Nakatake et al., 2001). Interestingly, *Fgf7* knockout mice display an abnormal hair phenotype – greasy, matted hair of unkempt appearance in older male mice (Guo et al., 1996). Also, transgenic mice that overexpress *Fgf7* in the epidermis demonstrate abnormal patterns of hair growth (Guo et al., 1993), and subcutaneous or intraperitoneal injections of recombinant FGF7 into nude mice stimulate hair growth by extending the anagen phase of the hair cycle (Danilenko et al., 1995). Furthermore, treatment with FGF7 significantly stimulates hair fibre elongation in human scalp hair follicle organ cultures (Iino et al., 2007). Since both *Fgf10* and *Fgfr2b* knockout mice die at birth, their hair phenotype is harder to study (Suzuki et al., 2000). Nevertheless, examination of late stage *Fgfr2IIIb* knockout embryos revealed a reduction in hair follicle development, producing significantly fewer hair follicles which were developmentally retarded (Revest et al., 2001). Given the neonatal lethal phenotype of these mice, Petiot et al. examined full-thickness skin grafts from late-stage *Fgfr2IIIb* null and wild type foetuses, grown on the back of nude mice, and showed that FGFR2b signalling was crucial for normal epidermal growth and development as well as for subsequent hair follicle morphogenesis (Petiot et al., 2003). Transgenic mice expressing dominant-negative *Fgfr2IIIb* in differentiating hair keratinocytes developed abnormally thin, but otherwise normal, hairs characterised by single columns of medulla cells in all hair types (Schlake, 2005). Mice lacking *Fgfr2b* only in the epidermis developed similarly thin and silky pelage hair (Grose et al., 2007). Taken together, these studies show a clear requirement for FGFR2b in normal hair follicle morphogenesis.

Of the other members of the FGF family, FGF5 is expressed in the outer root sheath (ORS) of the hair follicle (Hebert et al., 1994). *Fgf5* knockout mice grew significantly longer hair due to prolonged anagen and delayed catagen during the hair cycle, displaying an angora phenotype (Hebert et al., 1994).

Interestingly, there is a large variation in *Fgf7*, *10* and *22* mRNA expression throughout the hair cycle (which lasts about 21 days in mice) with both *Fgf7* and *Fgf10* expressed at highest levels at anagen V (day 8), when hair grows vigorously, and *Fgf22* strong expression at anagen VI (day 18), when hair follicle length reaches its maximum and is eventually shed (Komi-Kuramochi et al., 2005). This pattern of expression resembles, to some extent, the one found during the wound healing process (Beyer et al., 2003).

3.1.3 FGFs in wound healing

FGFs 7, 10 and 22 have been implicated in the wound healing process. FGF7 is produced by various types of mesenchymal cells and acts specifically on epithelial cells expressing the only known high-affinity receptor for the ligand - FGFR2IIIb. FGF7 is weakly expressed in normal murine and human skin, but upon injury the expression is hugely up-regulated (Werner et al., 1992). FGF10 levels also are increased rapidly following wounding (Tagashira et al., 1997) and levels of both growth factors decline once re-epithelialisation is complete.

In contrast, FGF22 expression declines during the first days after wounding and remains low until day 5 after injury. Subsequently, the expression increases above basal levels at day 7 after wounding and remains elevated until day 13, being localised to the hyperthickened epidermis of fully healed wounds (Beyer et al., 2003). These findings have been confirmed by another group, who reported

that *Fgfs 7, 10* and *22* were all strongly expressed in the skin of young mice. However, following wounding, only *Fgf7* and *Fgf10* mRNA expression increased, while expression of *Fgf22* mRNA declined to approximately half its level in healthy skin (Komi-Kuramochi et al., 2005). Somewhat surprisingly, considering the above findings, the healing process of full-thickness incisional wounds in *Fgf7* knockout mice was not obviously affected and the proliferation rate of the keratinocytes at the wound edge was not impaired (Guo et al., 1996). This was unexpected, since transgenic animals expressing a kinase-deficient, dominant-negative FGFR2b revealed a severe delay in wound re-epithelialisation of full-thickness excisional wounds, when at day 5 after injury, the number of proliferating keratinocytes in the hyperproliferative epithelium was 80–90% reduced compared with control mice (Werner et al., 1994). The mutant receptor blocked signal transduction upon ligand stimulation by forming non-functional heterodimers between mutated receptors lacking functional tyrosine kinase domain and full-length wild type receptors. The truncated FGFR2b thus inhibited actions of FGF7, FGF10, FGF1 and FGF3. The most likely explanation for impaired wound healing in these mice was a blockade of the redundancy in ligand signalling and FGF10 compensation effect. Supporting this hypothesis, a significant delay in wound re-epithelialisation was seen in mice lacking dendritic epidermal T cells (DETC) – an important source of FGF7 and FGF10 in the healing wound (Jameson et al., 2002). Moreover, *Fgf10* and *Fgfr2b* null mice, among many others, share a notable phenotype of eyes remaining open at birth. This is due to a failure of the eyelid epidermis to cover the eye during late embryogenesis, in the equivalent of a developmental wound healing model (Tao et al., 2005). Interestingly, epidermal specific *Fgfr1/2* double knockout mice are characterised by the same phenotypic changes as the dominant-negative *Fgfr2b* mutant mice (Sabine Werner – personal communication) thus emphasising further the importance of FGFR signalling in skin homeostasis.

Treatment of injured epithelia with FGF7 results in an improved wound healing response (Werner, 1998) and recombinant FGF7 already is in use in the clinic for the treatment of chemoradiation-induced oral mucositis. Palifermin, an N-terminally truncated form of FGF7 with increased stability, is an approved drug for the treatment of chemoradiation-induced oral mucositis in patients undergoing bone marrow transplantation (Spielberger et al., 2004). When administered on 3 consecutive days before high-dose chemotherapy, as well as for 3 days following haematopoietic stem cell transplantation, Palifermin reduced the median duration of mucositis from 9 to 6 days, and reduced the incidence of grade 4 mucositis from 62% to 20%. This corresponds with a significant improvement in patient quality of life (Spielberger et al., 2004).

3.1.4 FGFs in the brain

FGF signalling is also known to be essential for brain development. It has been shown that at least 14 FGFs and all four FGF receptors are expressed in the developing or mature nervous system. Members of the FGF7 subfamily are involved in the process of brain development as well. FGF22, along with FGF7 and FGF10, is a presynaptic organiser with roles in vesicle clustering and neurite branching (Umemori et al., 2004). In the developing brain, *Fgf22* transcripts are present in both the external and internal granule cell layer of the cerebellum at postnatal day 7 (Yaguchi et al., 2009). *Fgf22* expression is not found at other developmental stages. FGF7 is expressed at high levels by Purkinje cells, while both FGF7 and FGF10 are expressed at very low levels by granule cells from post-natal day 8. All three members of the FGF7 subfamily exhibit presynaptic organising activity, with FGF22 reportedly expressed by specific neuronal populations during the period when they develop synapses. FGF22 is thought to affect synaptic development of mossy fibres and presynaptic differentiation in the

cerebellar granule layer of the brain. Inactivating FGF22 or its receptor FGFR2 markedly reduced synapse formation between pontine axons and cerebellar granule cells, both in culture and in developing mice, indicating that FGF22 is a crucial presynaptic organiser in the cerebellum (Umemori et al., 2004). Secreted from cerebellar granule cells, it recruits axons projected from pontine and vestibular neurons expressing FGFR2b. In other words, FGF22-FGFR2b signalling organises synapse formation by inducing axon projection toward FGF22 secreting cells.

Unexpectedly, during the process of Fgf22 knockout mouse characterisation, I discovered that the gene plays a role in metabolism and can affect body weight. Not much is known about FGFs contribution to control of metabolism and up till recently only FGF21 seemed to be involved in the process. In fact, pharmacologic studies show that FGF21 has broad metabolic actions in obese rodents and primates that include enhancing insulin sensitivity, decreasing triglyceride concentrations, and causing weight loss (Kliewer and Mangelsdorf, 2010). What makes FGF21 different from FGF22 is the fact that it can diffuse away from its tissues of origin and function as hormone, whereas FGF22 is thought to act in autocrine manner, not to mention that the pattern of tissue expression between those two FGFs is utterly different. Interestingly though, latest findings on FGF7 suggest that this well-established paracrine growth factor can stimulate adipogenesis in autocrine fashion (Zhang et al., 2010). Additionally, due to its spatialtemploral expression in the hypothalamus, FGF5 is thought to be involved in regulation of feeding behavior (Li et al., 1999).

3.1.5 Other sites of *Fgf22* expression

Recently, *Fgf22* expression was reported in bone. Together with *Fgfs 2, 7* and *18, Fgf22* mRNA was detected in the perichondrium and growth plate of rat long bones. Moreover, levels of *Fgf22* expression increased with age and decreasing growth velocity when assayed by quantitative real-time RT-PCR (Lazarus et al., 2007).

Fgf22 expression was also detected in the retina of the eye by cDNA microarray analysis (Takeuchi et al., 2008). The group investigated the effect of nilvadipine, a calcium channel blocker, upon the retina of the retinal degeneration slow mouse (peripherin 2 mutant) and found increased expression of FGF22 after treatment. The retinal degeneration slow mouse is a model of retinitis pigmentosa - a group of heterogeneous diseases of inherited retinal degeneration characterised by night blindness, constricted visual field or ring scotoma, and bonespicule like pigmentation of the retina (Jansen and Sanyal, 1984). Interestingly, strong expression of fibroblast growth factor binding protein 1 (mentioned in more detail later) was also detectable by immunohistochemical analysis in the eye, particularly in the retina, outer plexiform layer, ciliary body, rods, and cones (Aigner et al., 2000).

Tissue	Age	Author
embryo	E0 – E3 E16.5	(Zhong et al., 2006) (Beyer et al., 2003)
skin epidermis inner root sheath of the hair follicle hyperthickened epidermis of healed wounds	7 weeks P1 8 weeks	(Komi-Kuramochi et al., 2005) (Nakatake et al., 2001) (Beyer et al., 2003)
tongue	unspecified	(Beyer et al., 2003)
brain cerebellum	unspecified P7 P8	(Nakatake et al., 2001) (Yaguchi et al., 2009) (Umemori et al., 2004)
retina of the eye	14 weeks	(Takeuchi et al., 2008)
bone	P7	(Lazarus et al., 2007)

Table 6 Fgf22 expression profile.

3.1.6 Properties of FGF22 protein

Murine FGF22, which shows 87% amino acid identity to the human sequence, consists of 486 nucleotides that encode a protein of 162 amino acids with a calculated molecular mass of 19 kDa (Beyer et al., 2003) (Fig 3.2). It shares 46% amino acid identity with FGF10 and 40% identity with FGF7 (Nakatake et al., 2001).

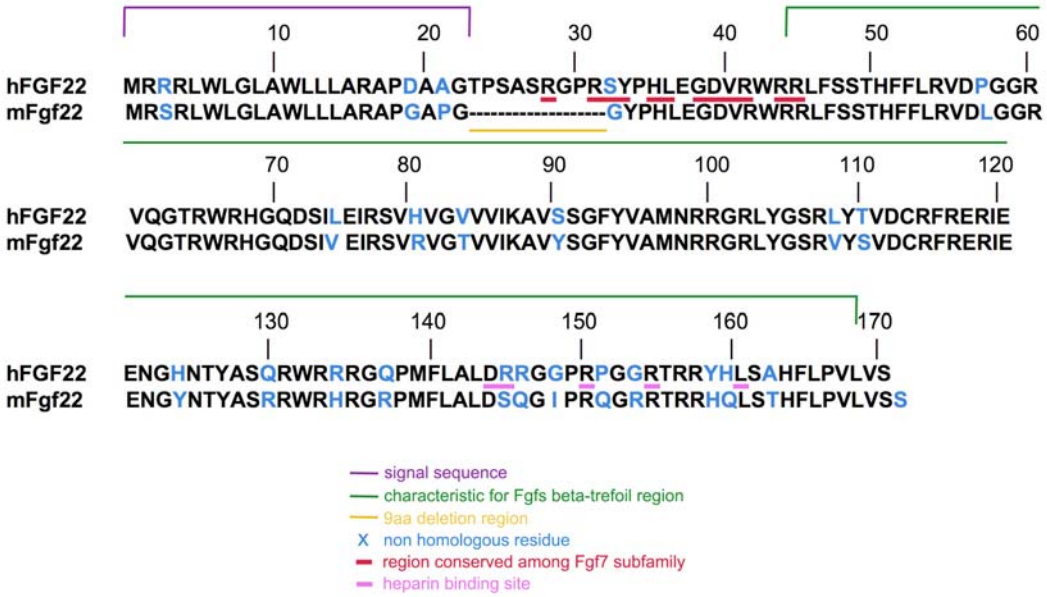

Figure 3.2 Amino acid sequence comparison of human and mouse FGF22.

Although much is known about the *Fgf22* expression pattern, bizarrely it is not clear whether FGF22 is a secreted protein. On one hand FGF22 has an hydrophobic amino terminus of about 20 amino acids, which is a typical signal sequence, so it is thought to be secreted (Fig 3.2) (Nakatake et al., 2001). On the other hand, the protein lacks a consensus sequence for N-terminal glycosylation, which is in contrast to FGF7 and FGF10 and is a feature of most secreted FGFs (Beyer et al., 2003). Also, in transiently transfected COS-1 cells (monkey kidney origin, fibroblast-like) with an HA-tagged *Fgf22* construct, FGF22 could not be detected in conditioned medium, even after a 50-fold concentration of the supernatant and addition of heparin to the culture medium (Beyer et al., 2003). Contrastingly, cells transfected with *Fgf7* and *Fgf10* expression constructs readily secreted those growth factors into the culture medium (Beyer et al., 2003). Others reported that FGF22, with a putative N-terminal signal peptide, remains attached to the cell surface rather than being secreted (Itoh and Ornitz, 2004). However, there was an account of a stably transfected BHK (baby hamster kidney) cell line

secreting FGF22 into culture medium (Zhang et al., 2006). It is also speculated that FGF22 remains bound to 34 kDa fibroblast growth factor binding protein 1 (FGFBP1), which is a molecule described as typically associated with cell membrane proteoglycans. Thus, following secretion, FGF22 could quickly be immobilised by FGFBP1, only to be released at a later time, or aided by FGFBP1 in its interaction with FGFR2b (Beer et al., 2005).

Subcellular localisation of FGF22 protein is also not clear and seems to depend on the cell type. In MCF-7 cells (human breast adenocarcinoma), FGF22 appears to be localised predominantly to large nuclear bodies, characteristic of the nucleolar localization seen with some other FGFs, such as FGF1, FGF2 and FGF3. However, in COS-1 cells, FGF22 was reticular and perinuclear, as expected for association with the ER/Golgi network and similar to the subcellular localization of FGF7 (Beyer et al., 2003).

By investigating an *Fgf22* total knockout mouse model I wanted to contribute to a better understanding of the diversity in FGF signalling and function, especially in skin development and homeostasis.

3.2 Results

3.2.1 Generation of *Fgf22* knockout mice

To generate mutant mice lacking *Fgf22*, an homologous recombination approach was taken, whereby key elements of the *Fgf22* genomic sequence were replaced by a Neomycin selection cassette.

The *Fgf22* targeting construct was designed and prepared by Dr Richard Grose, such that homologous recombination eliminated the entire coding region of the *Fgf22* gene (exons 1, 2 and 3). This coding region was replaced by a Neomycin resistance gene flanked by loxP sites cloned between approximately 5kb and 1.2kb of upstream and downstream homologous genomic DNA sequence, respectively, from the murine *Fgf22* locus (Fig 3.3). The homologous arms were generated by PCR amplification from genomic DNA isolated from 129/ola embryonic stem (ES) cells. After ES cell transfection and positive antibiotic selection, two G418-resistant clones were identified as homologous recombinants by Southern blot analysis after EcoRI digestion (Fig 3.4), using a probe external to the homologous sequence to confirm correct targeting.

The two mutant clones were injected separately into C57Bl6/J blastocysts. Male chimaeric animals of at least 70% 129ola contribution (as judged by coat colour) were mated with C57Bl6/J females to obtain germline transmission. The heterozygous offspring of these mice were then mated to produce homozygous mutants, which occurred at the expected Mendelian frequency of 25%.

To identify the *Fgf22* knockout mice, PCR genotyping was performed on ear snip or tail snip DNA with primers for the wild type (wt) allele generating a 286bp product and null (ko) allele a 130bp product (Fig 3.5).

In order to verify that the targeted homologous recombination resulted in abrogation of *Fgf22* mRNA expression, total RNA was isolated from mouse brain, known to express *Fgf22* at a detectable level. Following cDNA synthesis, PCR was performed using primers spanning exon1 and exon3 of the *Fgf22* coding sequence. As expected, relative to control wild type mouse brain, *Fgf22* mRNA expression was reduced in heterozygous brains and completely absent in knockouts (Fig 3.6).

To check levels of *Fgf22* mRNA expression in wild type mice, Real Time RT-PCR was performed. RNA was obtained from the oesophagus, a novel site of *Fgf22* expression discovered during my characterisation of *Fgf22* knockout mice. Real Time RT-PCR assay demonstrated a statistically significant difference ($P<0.05$) in relative *Fgf22* mRNA expression levels between wild type male and female tissue with females expressing notably less of the growth factor (Fig 3.7).

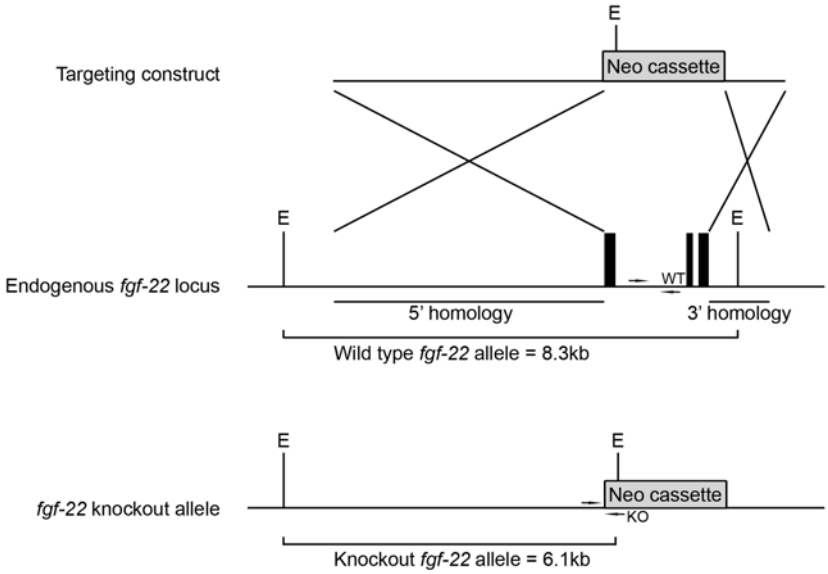

Figure 3.3 Targeting strategy for the *Fgf22* knockout mouse. The structures of the wild type allele and the disrupted allele are shown. In the wild type allele, exons 1 to 3 are represented by black boxes. E indicates EcoRI restriction enzyme recognition sites. The primers used for routine genotyping are represented by arrows.

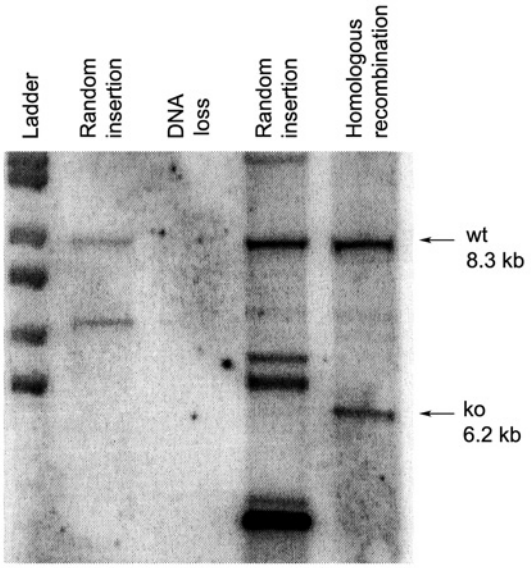

Figure 3.4 *Fgf22* Southern Blot. Total DNA extracted from ES cells was digested with EcoRI restriction enzyme and separated by electrophoresis on a 0.8% Agarose/TBE gel according to size. The DNA was blotted onto nylon membrane and hybridised overnight with a radioactively-labelled probe. The membrane was washed and exposed to a storage phosphor screen overnight. Clear bands at 8.3kb and 6.2 kb (arrows) corresponding to the predicted size of the wild type and knockout fragment respectively can be seen in the last lane. A total of 192 ES clones was analysed and 2 scored positive for homologous recombination and displayed identical hybridisation patterns (data not shown).

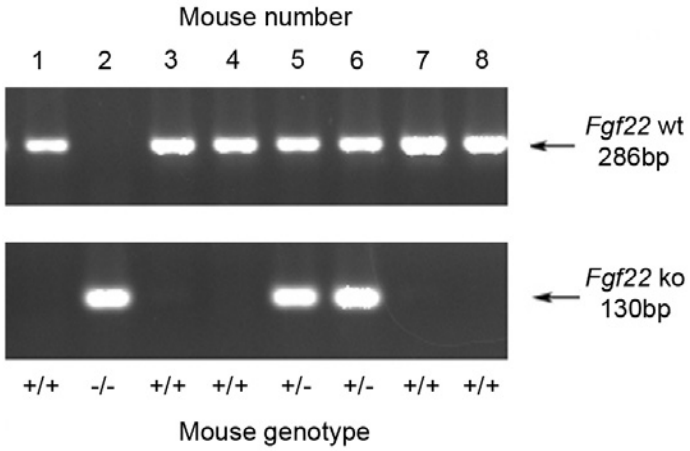

Figure 3.5 Genotyping mice. PCR analysis of genomic DNA isolated from ear snips of 3 weeks old pups from an heterozygous breeding pair. Genotyping results determined the presence or absence of null (ko) and wild type (wt) alleles at the *Fgf22* locus. WT (+/+) samples showed a single *Fgf22* wt band at 286bp (mice nos. 1, 3, 4, 7 and 8), *Fgf22* ko (-/-) displayed a single ko allele at 130bp (mouse no. 2) and heterozygous (+/-) samples amplified both wt and ko alleles (mice nos. 5 and 6).

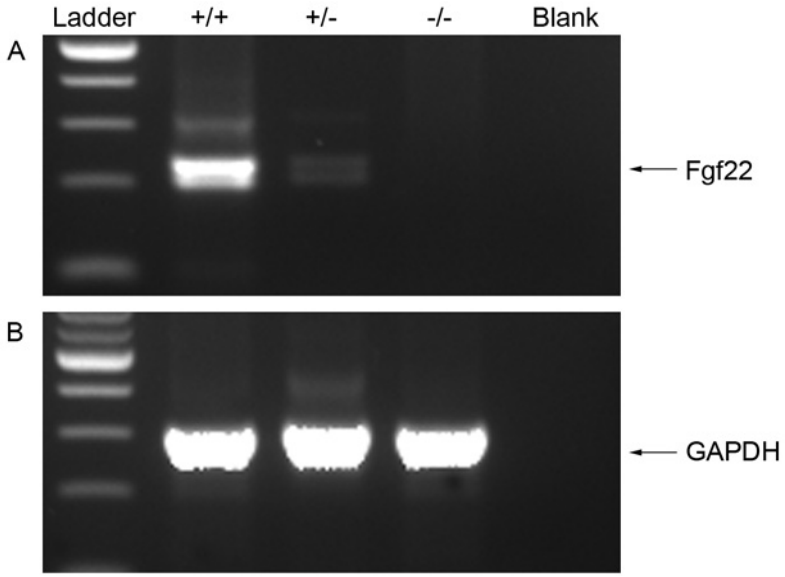

Figure 3.6 Confirmation of gene deletion. A) RT-PCR analysis of cDNA generated with random hexamers from RNA isolated from mouse brain. Results show the presence/absence of *Fgf22* gene expression. Wild type (+/+) samples display a *Fgf22* band at 286bp, *Fgf22*-heterozygous samples (+/-) display same size band whereas *Fgf22* knockout (-/-) lack the presence of a correct size band. B) *GAPDH* primers display a single band at 297bp and were used as a control for RNA quality and concentration. Blank represents PCR reaction mix without cDNA. Experiment was carried out on 3 *Fgf22* wild type, 3 *Fgf22* heterozygous and 3 *Fgf22 knockout* male mice.

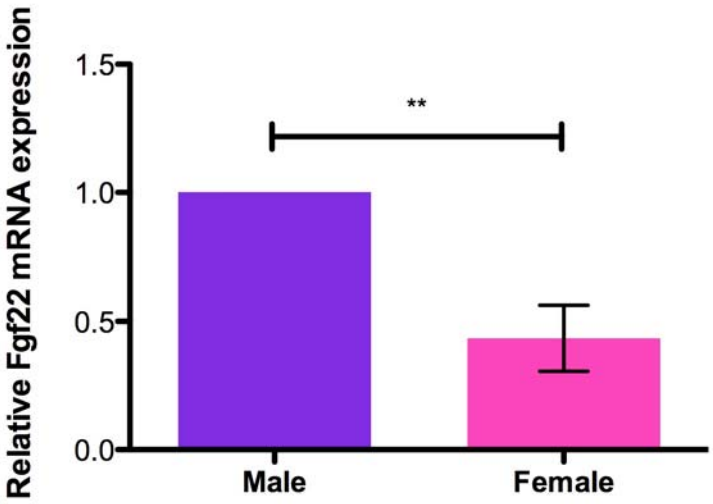

Figure 3.7 Comparison of *Fgf22* mRNA expression level in male and female wild type mice. mRNA levels of *Fgf22* were determined by Real Time RT-PCR analysis performed on cDNA generated from mouse oesophagus RNA. There was a statistically significant difference ($P<0.05$) in relative levels of the growth factor expression, with *GAPDH* used as normalising control, when male and female tissue was compared. Experiments were carried out on 6 female and 6 male mice (n=6) and error bars represent standard error among the samples.

3.2.2 Characterisation of *Fgf22* knockout mice

Fgf22 knockout animals, born according to predicted Mendelian ratios, were viable and fertile. Knockout mice did not display any obvious gross abnormalities.

Since FGF22 is a member of the FGF7 subfamily of FGF ligands, I examined expression of *Fgfs 7* and *10* in knockout mice. Relative mRNA levels of *Fgf7* were not altered and, *Fgf10* levels were reduced in knockout male animals, when examined by Real Time RT-PCR (Fig 3.8).

As FGF22 is both a ligand for FGFR2b and is expressed in the skin, I first performed a detailed analysis of those epidermal structures known to be altered in mice lacking *Fgfr2b* in the epidermis. There were no evident differences in pelage growth or sebaceous gland morphology between knockout and wild type mice. All the major hair types (zigzag, guard and awl) were present in knockout mouse skin and these hairs did not demonstrate any morphological differences when compared with those of wild type littermates (Fig 3.9). Whole-mount staining of the sebaceous glands in adult tail skin did not reveal any discernible differences between knockout and wild type mice (Fig 3.10). H&E stained sections of back and tail skin from wild type and knockout mice also appeared identical when examined histologically, in terms of epidermal, dermal and adipose thickness as well as hair follicle frequency (Fig 3.11).

Since there were no obvious defects in the unchallenged skin of *Fgf22* knockout mice, I investigated their capacity to respond to skin injury and carcinogenic insult, both of which have been shown to depend at least in part on FGF signalling. Wound healing studies, where mice were subject to 3 mm

diameter full thickness punch biopsy wounds, showed that mice lacking *Fgf22* in the skin were able to heal acute wounds just as efficiently as wild type mice, although 5 days after wounding knockout male wounds appeared to have healed faster (Fig 3.12A and 3.13A), with more efficient re-epithelialisation (Fig 3.13B) and a high rate of proliferation of cells involved in the process at this time-point (Fig 3.12B and 3.15). However, at all the other time-points during wound healing, morphometric analysis showed very similar values for both male and female *Fgf22* wild type and knockout animals (Fig 3.13 and 3.14). In addition, Sirius red staining of 14 and 21 day wounds demonstrated similar collagen fibre remodelling in healing wounds for male mice of both genotypes (Fig 3.16).

By means of Real Time RT-PCR, fluctuations in FGF expression over the course of the wound healing process were followed (Fig 3.17). The relative levels of *FGF22* mRNA expression increased during the course of wound closure, peaking at 14 days after wounding in wild type mice, when the wound already was healed. Interestingly, levels of *Fgf7* mRNA expression mirrored the expression levels of *Fgfr1b* receptor whereas *Fgf10* levels corresponded to those of its main receptor *Fgfr2b*. Moreover relative levels of *Fgf7* and *Fgfr1b* were consistently high, while relative levels of *Fgf10* and *Fgfr2b* were low. Nevertheless, in general, the expression levels of FGFRs and their ligands involved in wound healing process did not differ significantly between wild type and knockout mice.

Concomitant with the wound healing study, conditions for the *in vitro* culture of primary keratinocytes were optimised. Isolated cells from wild type and knockout mice (Fig 3.18) were used for a simple 2D scratch wound assay. This *in vitro* assay complemented the *in vivo* study, proving that *Fgf22* knockout keratinocytes were perfectly able to migrate towards the wound gap in order to

close it and there was no difference in the time of migration between the knockout and wild type animals (Fig 3.19).

Finally, I challenged the mice with a classical two-step skin carcinogenesis assay using DMBA and TPA. These experiments were performed on female mice, since they involved long-term observation and multiple mice could be kept together. When cohorts of *Fgf22* knockout female mice were subjected to two-step (DMBA/TPA) skin carcinogenesis treatment, they developed considerably less papillomas than wild type mice. *Fgf22* wild type and knockout mice subjected to TPA treatment alone never developed papillomas (Fig 3.20).

The only noticeable dissimilarity observed between unchallenged control and knockout animals concerned their body weight, with older *Fgf22* knockout mice appearing much leaner than age matched wild type mice (Fig 3.21A). At 10 weeks of age, *Fgf22* knockout male mice fed on a regular mouse chow diet showed a significant reduction in body weight when compared with wild type male mice (Fig 3.21B). When a group of 66 mice in total (males and females) was followed over a 21-week period, the difference in male mouse weight was much more evident than in female mice, nevertheless female knockout mice weight also was reduced (Fig 3.22). Differences in the pattern of the growth curve became observable around the time of weaning (3-4 weeks).

To investigate further the origin of this weight difference, *Fgf22* expression was checked by RT-PCR in all the parts of the digestive system. Thus I discovered that the growth factor of interest was expressed at low levels in almost all the parts of the intestinal tract and at high levels in the oesophagus and stomach (Fig 3.23). The findings were validated by checking 3 more female and male mice of both genotypes. As expected the *Fgf22* specific band was missing in

all knockout animal oesophagus RNA samples (Fig 3.24). Next, the morphology of knockout and wild type tissue sections was compared. No obvious differences in tissue appearance were observed. Moreover, a series of immunohistochemical staining (anti-p63, -K14 and -Loricrin) did not reveal any changes in expression pattern (Fig 3.25). Subsequently, the expression of *Fgf22* in the forestomach and stomach was checked (Fig 3.26A), tissue morphology was examined (Fig 3.26B and C) and sections stained with antibodies specific to discrete stomach cell populations; anti-ATP4B for parietal cells (Fig 3.27), anti-Pepsinogen for chief cells (Fig 3.28) and anti-TFF1 antibody for pit cells (Fig 3.29). As previously, there were no dissimilarities observed between *Fgf22* wild type and knockout tissue sections.
I also checked serum leptin levels in *Fgf22* wild type and knockout male mice by ELISA, but levels were not statistically different between the genotypes (Fig 3.30).

During the process of *Fgf22* knockout mouse characterisation, I found that *Fgf22* was expressed in the eye (Fig 3.31). Once more, tissue morphology was checked (Fig 3.32) and at first glance there was no difference between the genotypes. Nevertheless, further investigation into the retina layers (Fig 3.33A) revealed changes in their thickness in knockout male mice (Fig 3.33B).

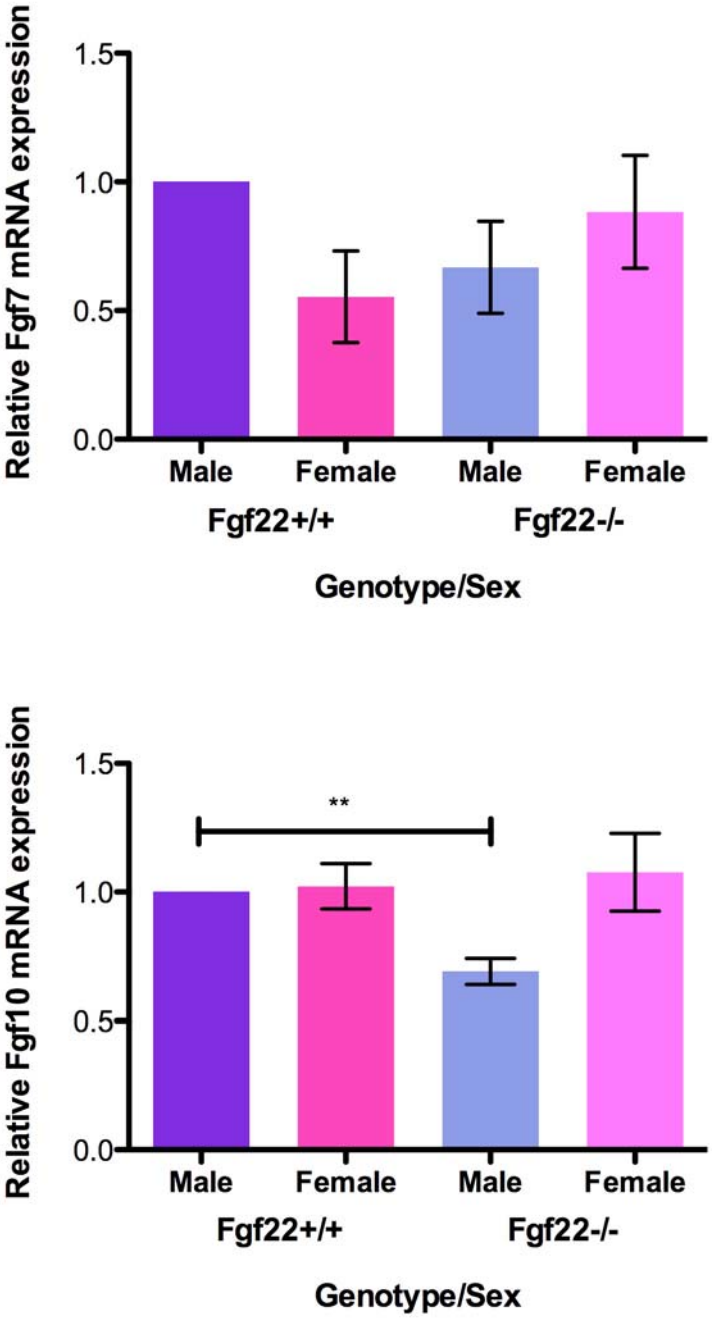

Figure 3.8 Evaluation of *Fgf7* and *Fgf10* mRNA expression levels in *Fgf22* wild type and knockout mice. Real Time RT-PCR analysis of cDNA generated from mouse oesophagus. The assay showed lack of significant effect on relative levels of *Fgf7* mRNA in mouse tissue after *Fgf22* deletion, although levels of *Fgf10* mRNA were significantly ($P<0.05$) reduced in male oesophagus. *GAPDH* primers were used for the normalising control. Experiments were carried out on 6 female and 6 male mice and error bars represent standard error among the samples.

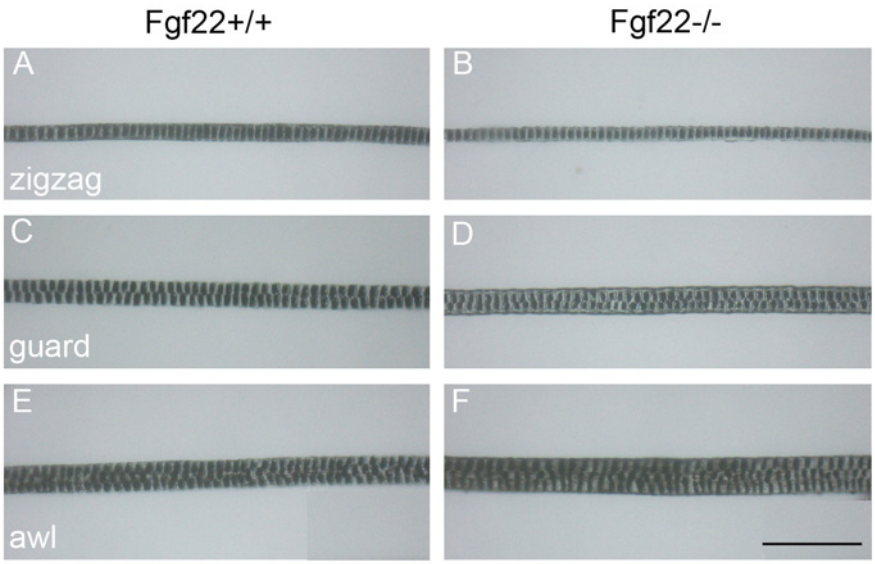

Figure 3.9 Comparison of pelage hair structure. All major hair shaft types (zigzag, guard and awl) were present in both wild type and knockout animals. The morphology of different hair types showed no difference between *Fgf22* wild type (A, C and E) and knockout (B, D and F) mice as shown by light microscopic analysis. Hairs were plucked from five 8-week old *Fgf22* wild type mice (n=100 hairs) and compared with hairs of *Fgf22* knockout mice (n=100 hairs). Scale bar (200 µm) identical for all pictures.

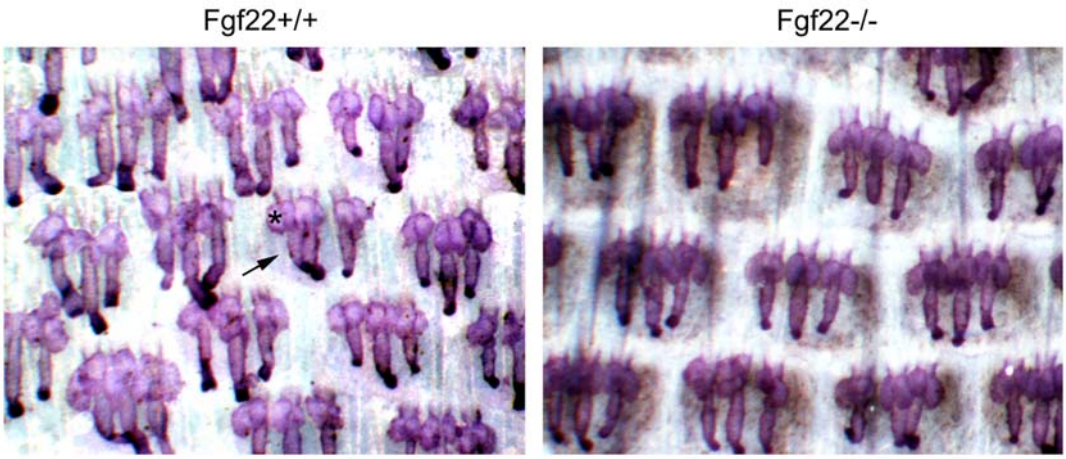

Figure 3.10 Normal sebaceous gland morphology. Tail epidermis whole-mount preparations from two and a half month old mice, stained with Mayer's haemalum, revealed no difference between *Fgf22* wild type and knockout mice in terms of sebaceous gland number and morphology. Comparison was carried out on 5 *Fgf22* wild type and 5 *Fgf22* knockout mice. (hair follicle is indicated by arrow and sebaceous gland by asterisk).

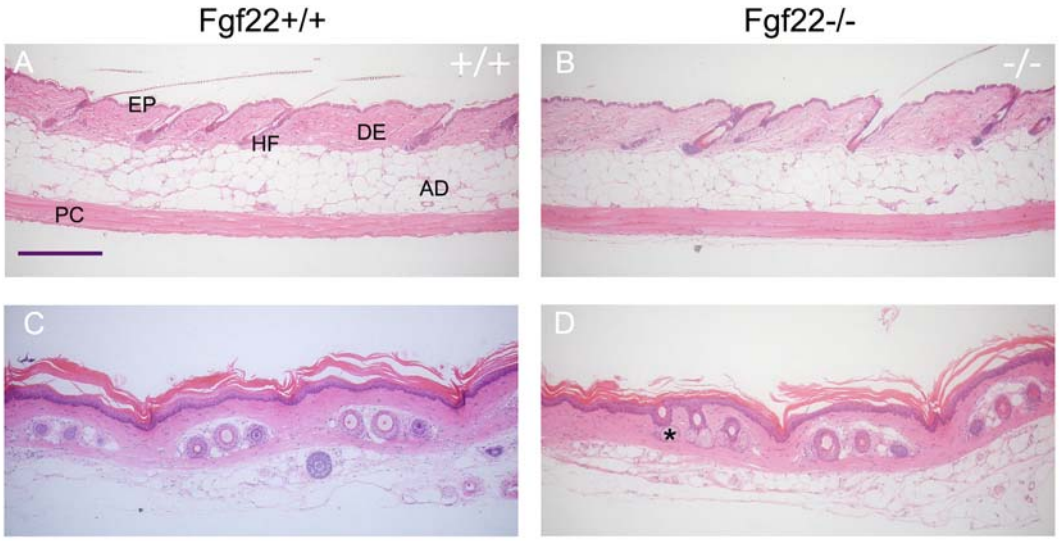

Figure 3.11 Skin structure. Histological analysis of H&E stained back (A, B) and tail (C, D) skin sections from 5 four month old *Fgf22* knockout (B and D) and age-matched 5 wild type (A and C) controls. No difference in skin thickness or morphology, neither in back skin (A and B) nor in tail skin (C and D), was observed. (EP epidermis, DE dermis, AD adipose tissue, PC *panniculus carnosus*, HF hair follicle, * sebaceous gland). Scale bar (200 µm).

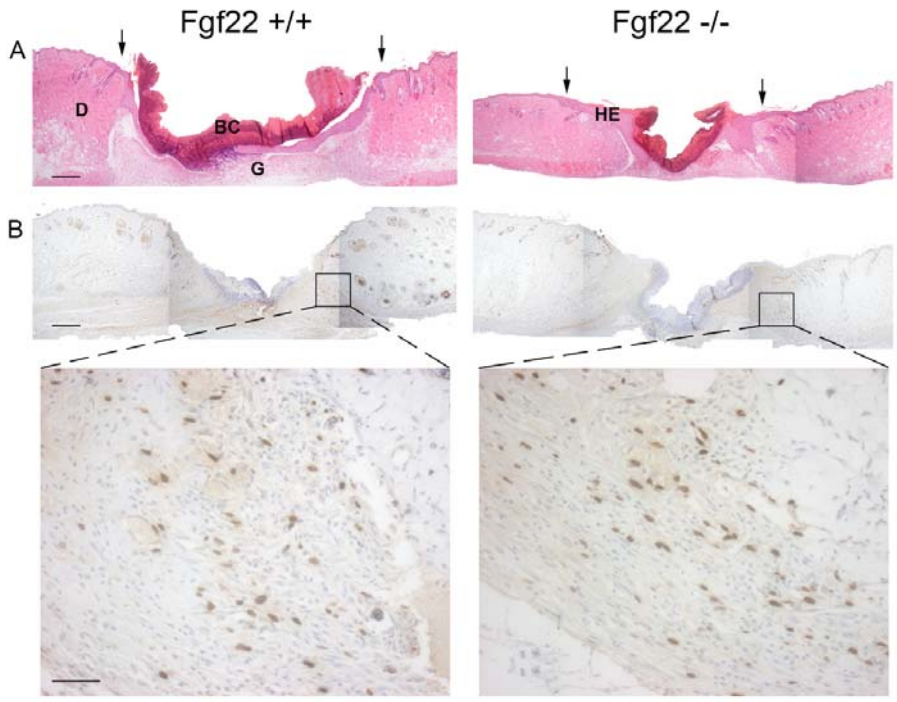

Figure 3.12 Wound healing in *Fgf22* wild type and knockout male mice. A) Paraffin-embedded, acetic ethanol fixed tissue sections of 3mm punch biopsy wounds 5 days after wounding were stained with Haematoxylin and eosin. The morphology of wounds from 3 *Fgf22* wild type and 3 knockout mice appeared very variable, but the re-epithelialised epidermis was usually thicker in knockout wounds. B) Tissue sections were immunostained for 5-bromo-2-deoxyuridine (BrdU)-positive cells (brown) at the wound site. (HE hyperproliferative epidermis, D dermis, G granulation tissue, BC blod clot. Wound margins are indicated by arrows). Scale bar (200 µm) in A) and B) top panel; (50 µm) in B) bottom panel.

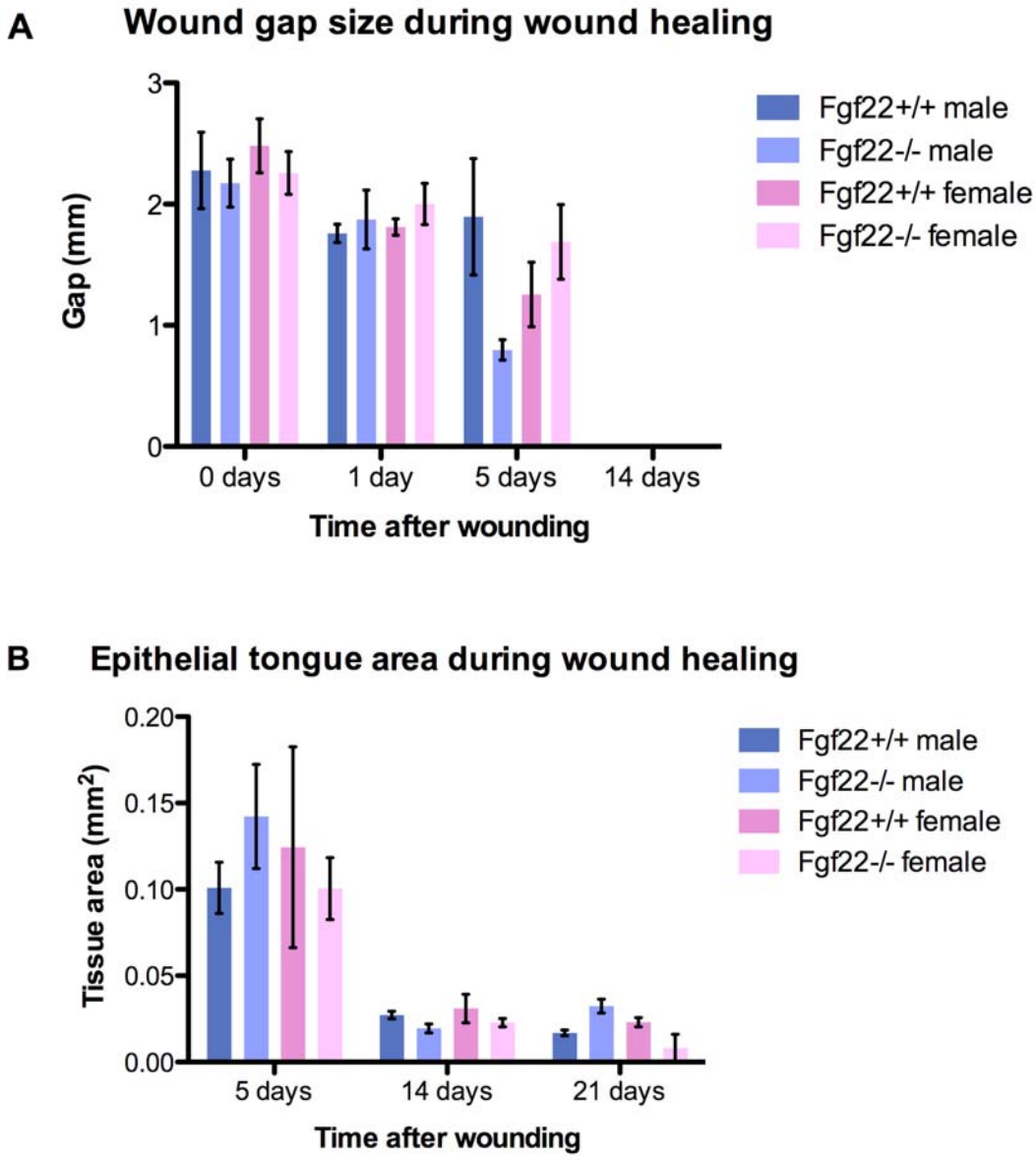

Figure 3.13 Morphometric analysis of wound repair. Morphometric measurements of wounds were performed on Haematoxylin and eosin stained paraffin sections from three independent wounds for each genotype and each time point. A) The wound gap was calculated as the distance between two margins of the inward growing epithelium and was measured three times for each wound section. B) Tissue sections for each time point were also analysed to determine the area of epithelial tongue. Error bars represent SEM.

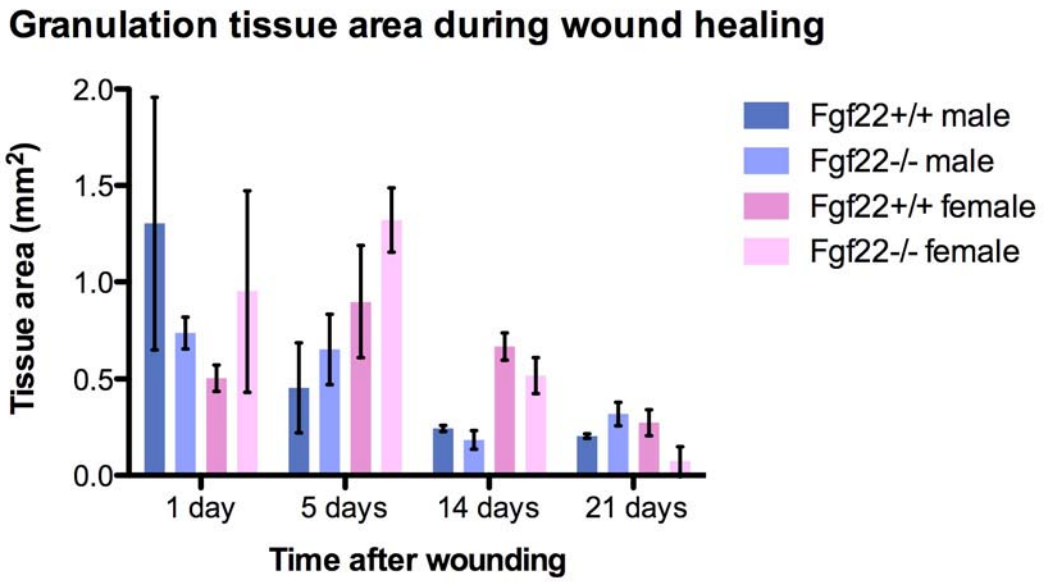

Figure 3.14 Granulation tissue area during wound healing. Graph represents mean values of the area of granulation tissue at all the time points checked after wounding. Two sections per wound, three mice per genotype were measured. Error bars represent SEM.

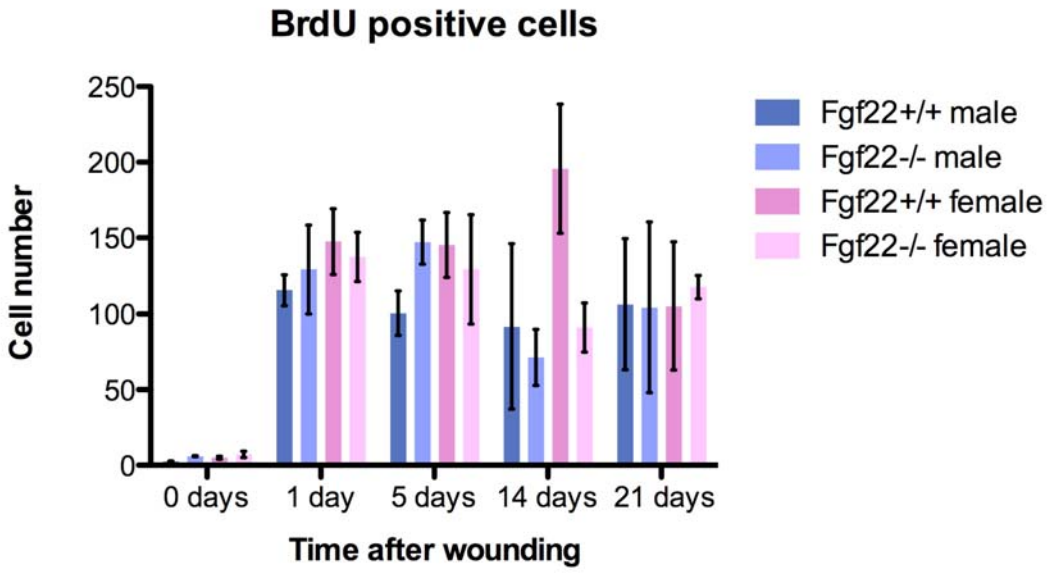

Figure 3.15 BrdU positive cell count. Mice were injected with BrdU one hour prior to culling. Number of proliferating cells was calculated from immunostained sections shown in figure 3.12B - sections from the entire wound were photographed and combined; the total number of BrdU positive cells per total wound were counted. Plots show mean of three independent wounds per genotype per time point where two slides per wound were counted. Error bars represent SEM.

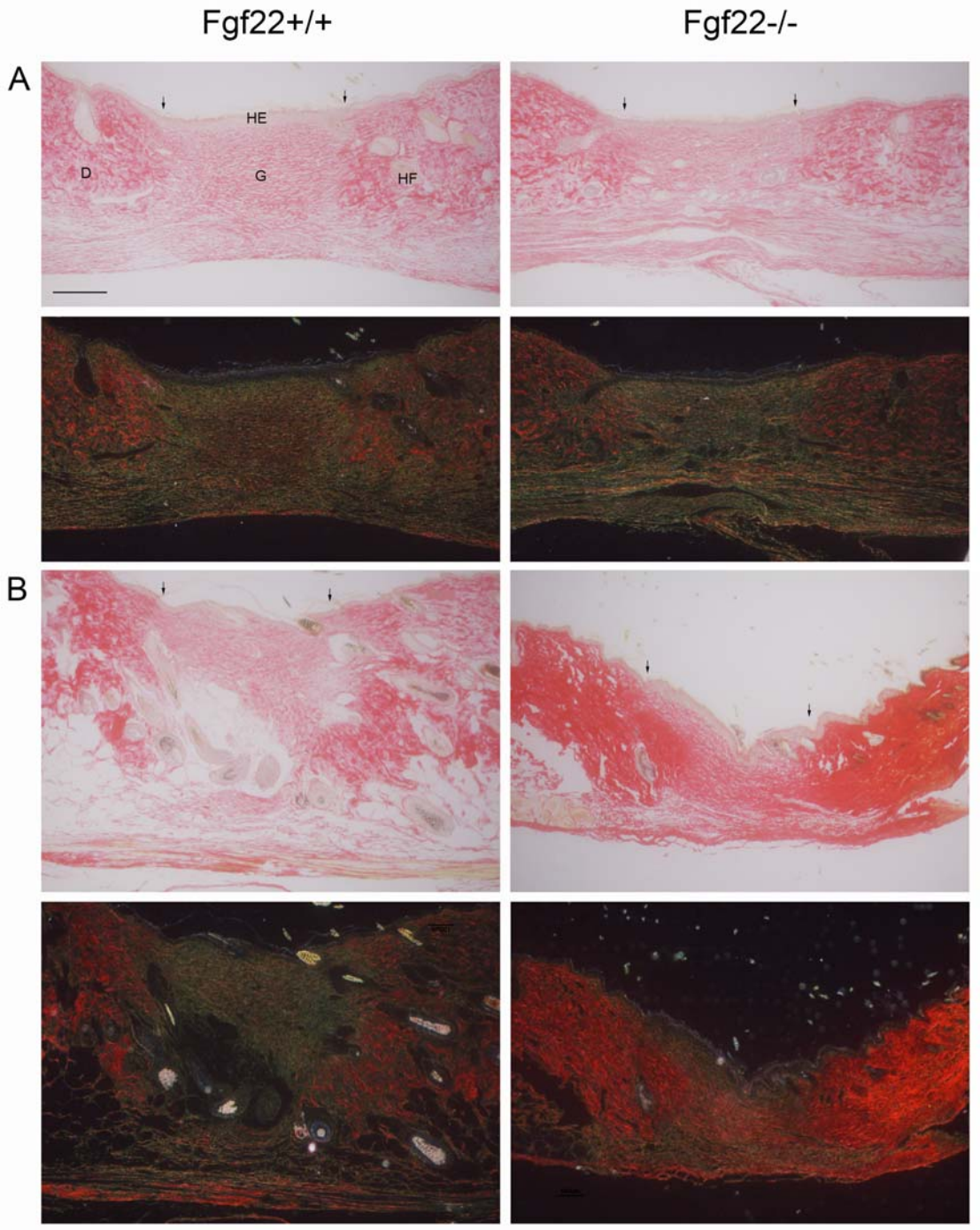

Figure 3.16 Sirius red staining of *Fgf22* wild type and knockout male mice wounds at day A) 14 and B) 21 post-wounding. At day 14 after wounding, epithelial regeneration was completed. Wounds were fully healed with a dense and mature multilayered epithelium. At both time points, granulation tissue showed organised, parallel bundles of collagen fibres. In both A) and B) top and bottom

panels represent the same section in bright field and dark field, respectively, stained with Sirius red. By means of histochemical reaction with collagen molecules, Sirius red enhances the normal birefringence of collagen types I, II, III and IV. Under polarised light, the colour of stained collagen varies as a function of the structural and biochemical properties of the collagen fibres. The spectrum of colours includes green, yellow, orange and red in a progressive way according to the packing of collagen molecules. (HE=hyperproliferative epidermis, D=dermis, G=granulation tissue, HF=hair follicle; wound margins are indicated by arrows). Scale bar (200 µm).

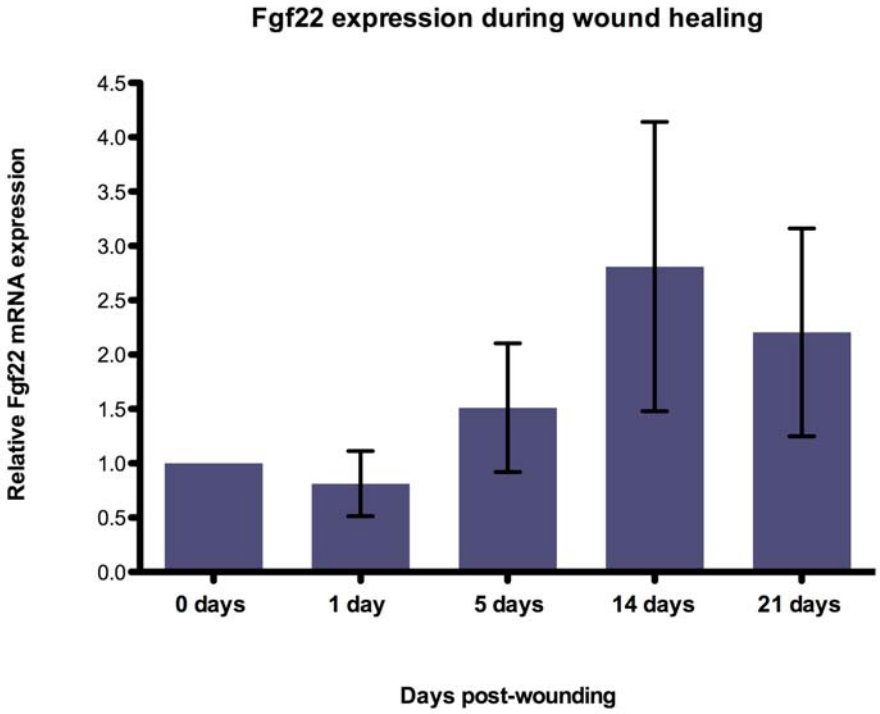
Fgf22 expression during wound healing
Relative Fgf22 mRNA expression
4.5
4.0
3.5
3.0
2.5
2.0
1.5
1.0
0.5
0.0
0 days
1 day
5 days
14 days
21 days
Days post-wounding

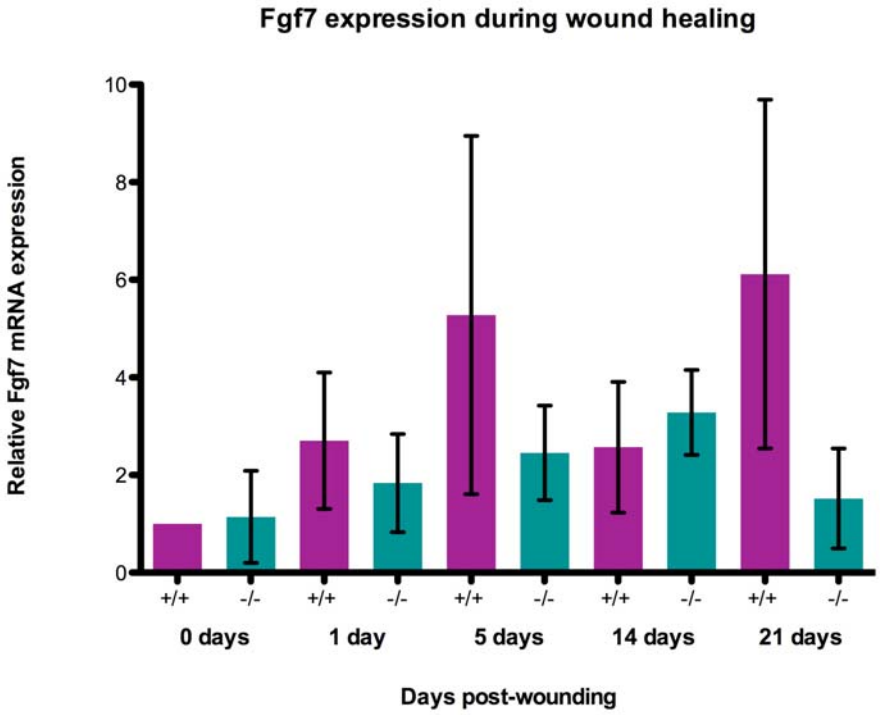
Fgf7 expression during wound healing
Relative Fgf7 mRNA expression
10
8
6
4
2
0
+/+
-/-
+/+
-/-
+/+
-/-
+/+
-/-
+/+
-/-
0 days
1 day
5 days
14 days
21 days
Days post-wounding

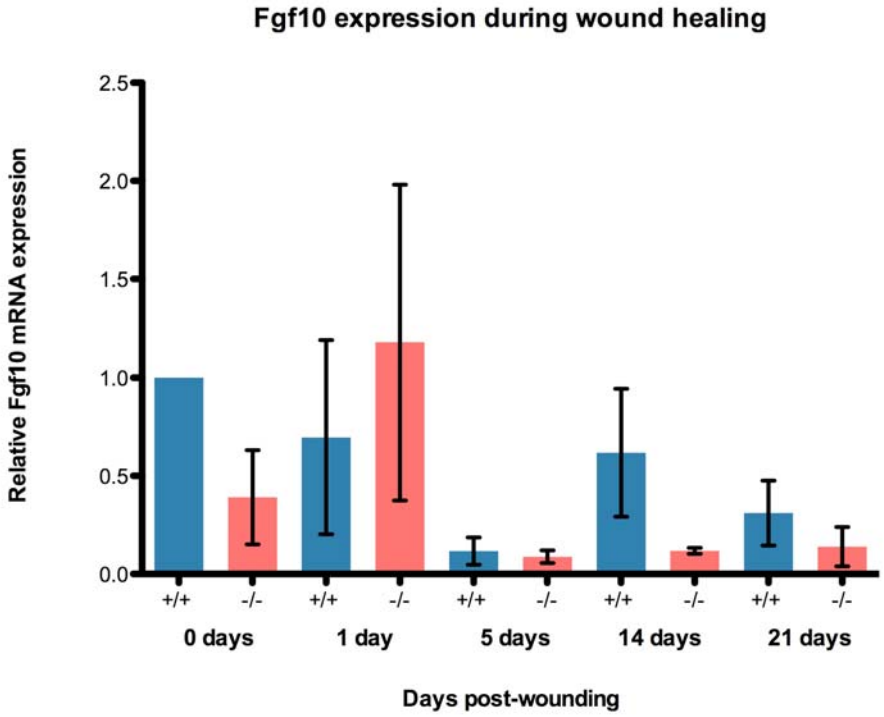
Fgf10 expression during wound healing
Relative Fgf10 mRNA expression
2.5
2.0
1.5
1.0
0.5
0.0
+/+
-/-
0 days
1 day
5 days
14 days
21 days
Days post-wounding

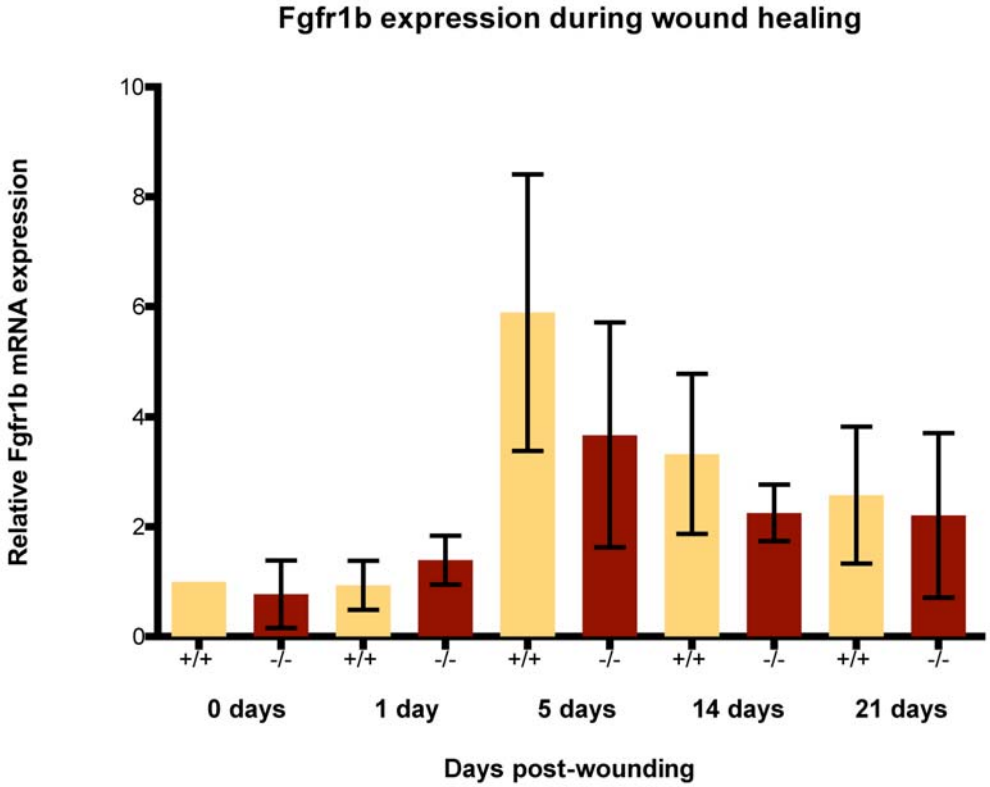
Fgfr1b expression during wound healing
Relative Fgfr1b mRNA expression
10
8
6
4
2
0
+/+
-/-
0 days
1 day
5 days
14 days
21 days
Days post-wounding

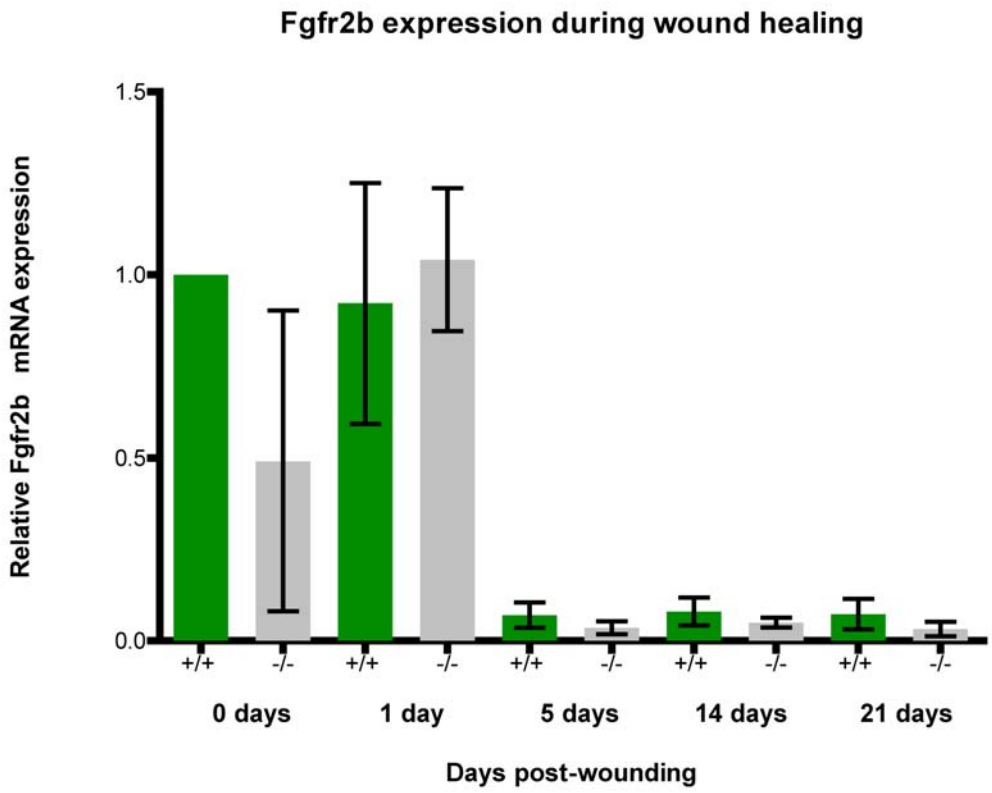

Figure 3.17 Real Time RT-PCR based comparison of *Fgf22, Fgf7, Fgf10, Fgfr1b* and *Fgfr2b* expression in *Fgf22* wild type and knockout male mice during wound healing. Total RNA was extracted from wound tissue and 265ng of RNA was subjected to Real Time RT-PCR analysis. Values were normalised to the corresponding values of the *GAPDH* housekeeping gene for individual samples. Plots represent mean of three wound samples for each genotype. Error bars represent SEM.

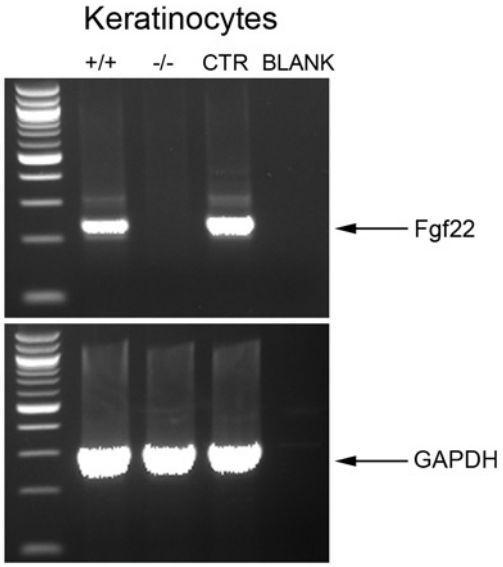

Figure 3.18 Primary cell culture. Primary keratinocytes were isolated from tail skin of *Fgf22* wild type and knockout mice aged 2 months. Keratinocytes were cultured *in vitro* for up to 3 passages, then RNA was extracted from the cell monolayer and RT-PCR analysis was performed. *GAPDH* primers were used as a control for RNA quality and concentration and oesophagus cDNA was used as a positive control. Blank was a PCR without cDNA.

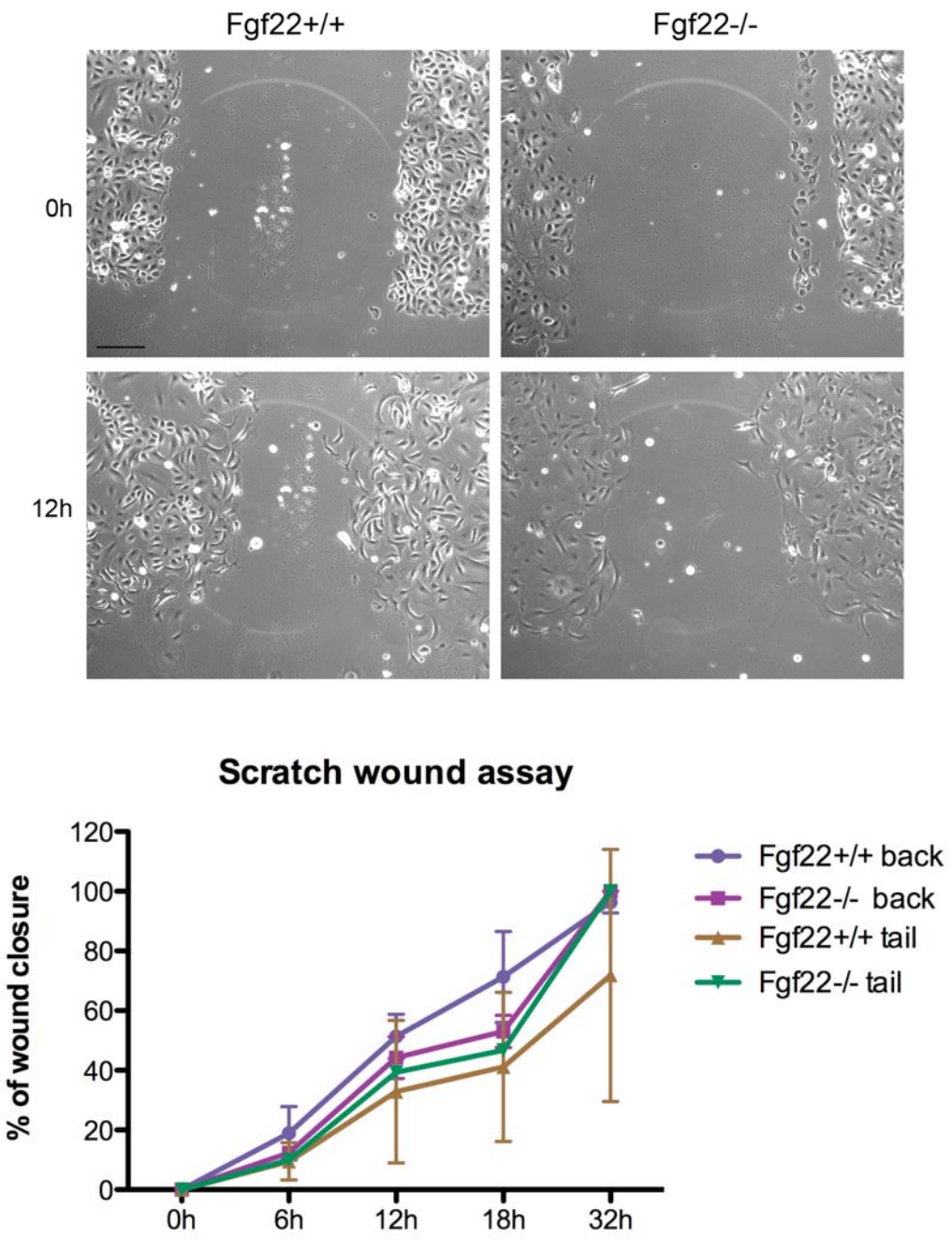

Figure 3.19 Scratch wound assay. *In vitro* wound closure was investigated in primary keratinocytes isolated from *Fgf22* wild type and knockout male back skin and tail skin. A) Photographs show the migration of wild type and knockout primary keratinocytes to wounded regions of the monolayer culture. B) Closure of the wounds was monitored, photographed and measured at 6, 12, 18 and 32 hours after wounding. Error bars represent SEM. Scale bar (200 μm).

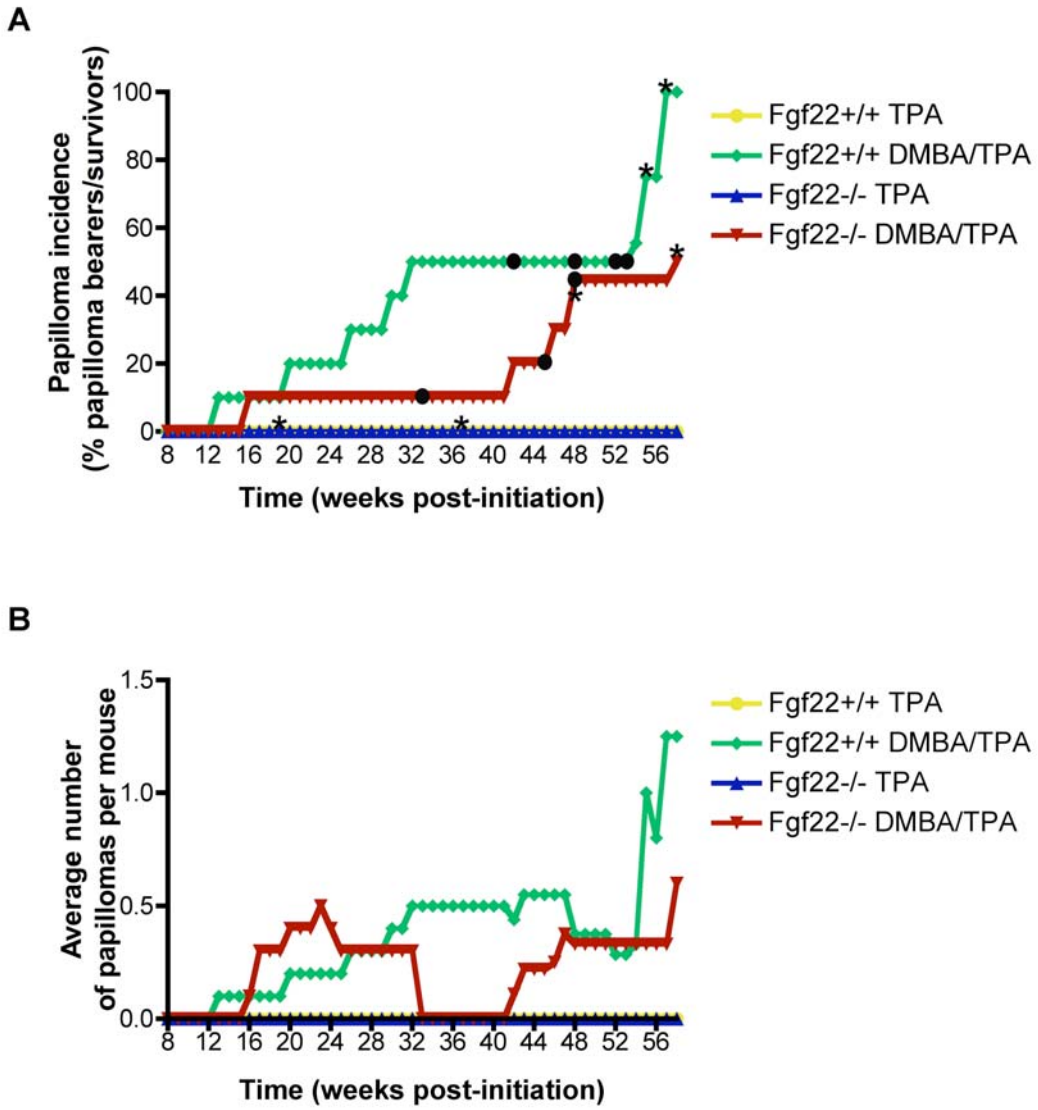

Figure 3.20 DMBA-induced tumorigenesis study. Cohorts of female mice (n=10) were subjected to classical two-step skin carcinogenesis treatment. Mice were treated with DMBA or solvent Acetone alone at 8 weeks of age and then all treated weekly with TPA for 15 weeks. A) At 58 weeks post initiation, when the experiment was terminated, 100% of DMBA treated wild type mice had developed papillomas while only 50% of knockout treated mice had papillomas. Control TPA treated mice of both genotypes never developed any neoplastic skin lesions. Circles represent mice killed due to papillomas exceeding size specified in the

Project licence. Stars represent mice deaths due to unrelated to experiment reasons. B) Average number of papillomas per mouse at the indicated times after the start of DMBA/TPA treatment. Maximum number of papillomas on a knockout female was 5, whereas wild type DMBA treated females never developed more than 2 papillomas per mouse**.**

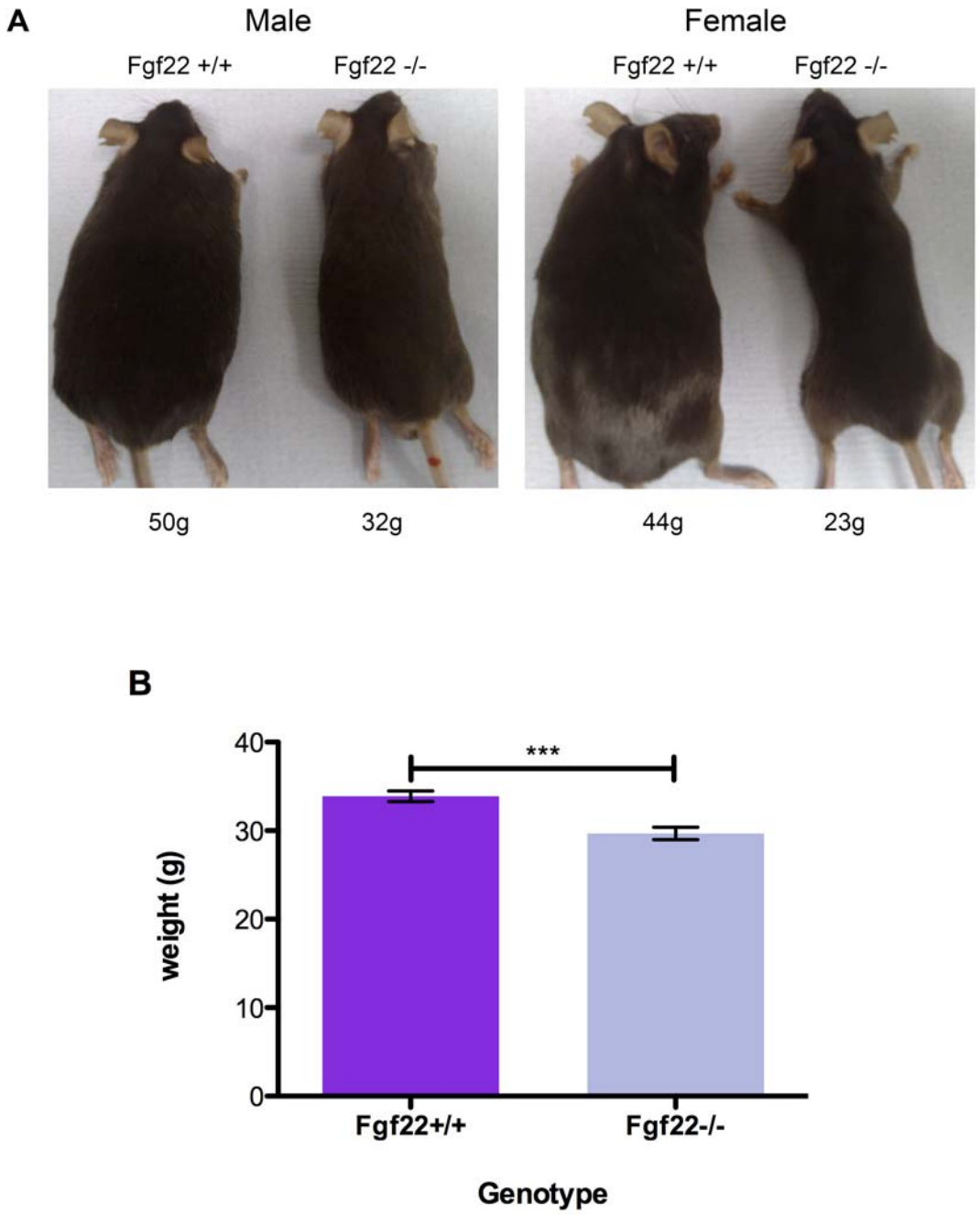

Figure 3.21 *Fgf22* knockout mice exhibit a weight loss phenotype. A) Representative photographs of 6 months old *Fgf22* wild type and knockout animals fed regular mouse chow diet. Below the photograph, corresponding mice weights are indicated. B) Mouse body weights measured at 10 weeks of age, having been fed an *ad libidum* diet of standard mouse chow. Mean body weights

are shown for wild type (33.9g; n=25) and Fgf22 knockout (29.7 g; n=18) mice. A 12% statistically significant body weight reduction in knockout males versus wild type males was observed ($P<0.0001$). Error bars represent SEM.

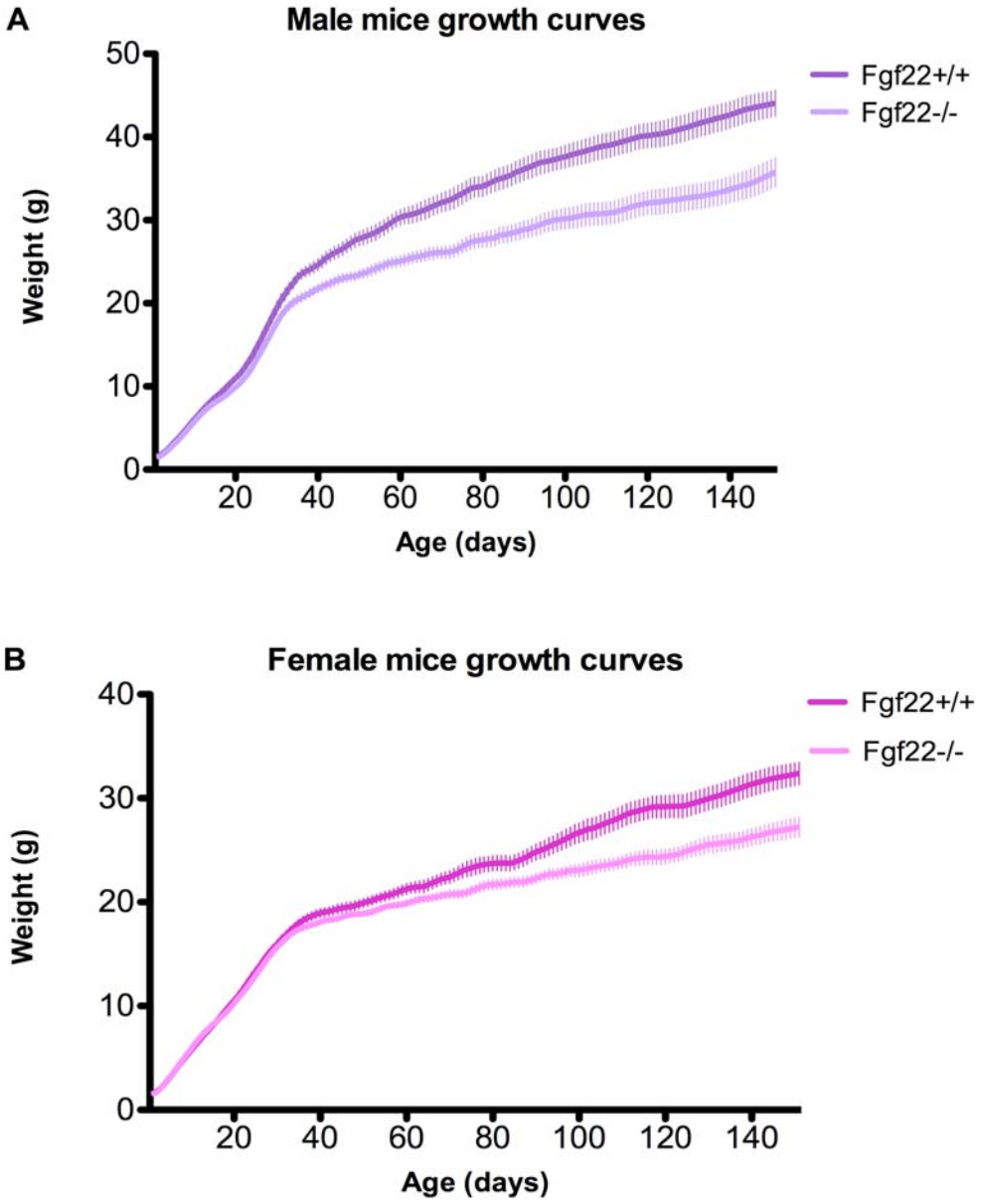

Figure 3.22 Alterations in pattern of growth curve in *Fgf22* knockout mice. A) Growth curves for male *Fgf22* wild type and knockout mice. B) Growth curves for female *Fgf22* wild type and knockout mice. Mice were fed on a regular chow diet and their weight was recorded from birth until 150 days (21 weeks) of age. In total, 13 *Fgf22* wild type male and 18 female mice, comparing to 12 *Fgf22* knockout male and 20 female mice were weighed twice a week. Each data point is the mean ± SEM for minimum of three animals.

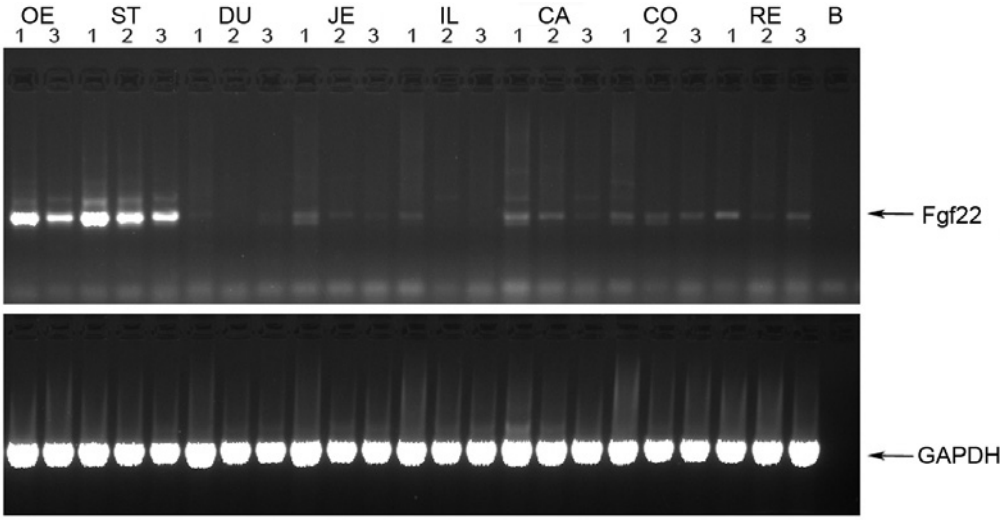

Figure 3.23 *Fgf22* mRNA expression in the digestive tract. RT-PCR analysis of cDNA from three 4.5 months old wild type male mice. Results showed the presence/absence of *Fgf22* gene expression in different regions of the digestive system. Samples from the oesophagus and stomach displayed an intense *Fgf22* band at 226bp. Less intense bands were observed in jejunum, caecum, colon and rectum samples. *GAPDH* primers displayed a single band at 297bp and were used as a control for RNA quality and concentration. Blank PCR without cDNA. (OE=oesophagus, ST=stomach, DU=duodenum, JE=jejunum, IL=ileum, CA=caecum, CO=colon, RE=rectum, B=blank).

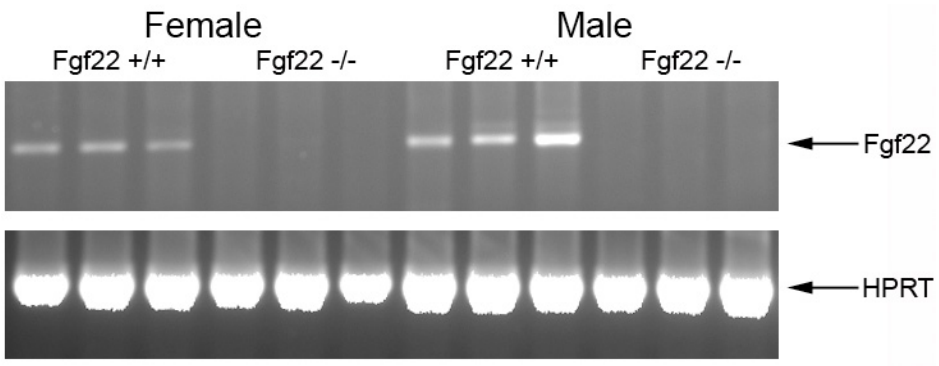

Figure 3.24 *Fgf22* expression in the oesophagus. RT-PCR was carried out using total RNA isolated from mouse oesophagus to asses *Fgf22* gene expression in female and male, wild type and knockout animals (3 mice per group). As expected the *Fgf22* specific band was absent in samples from knockout animals. *HPRT* primers were used as loading and RNA quality controls.

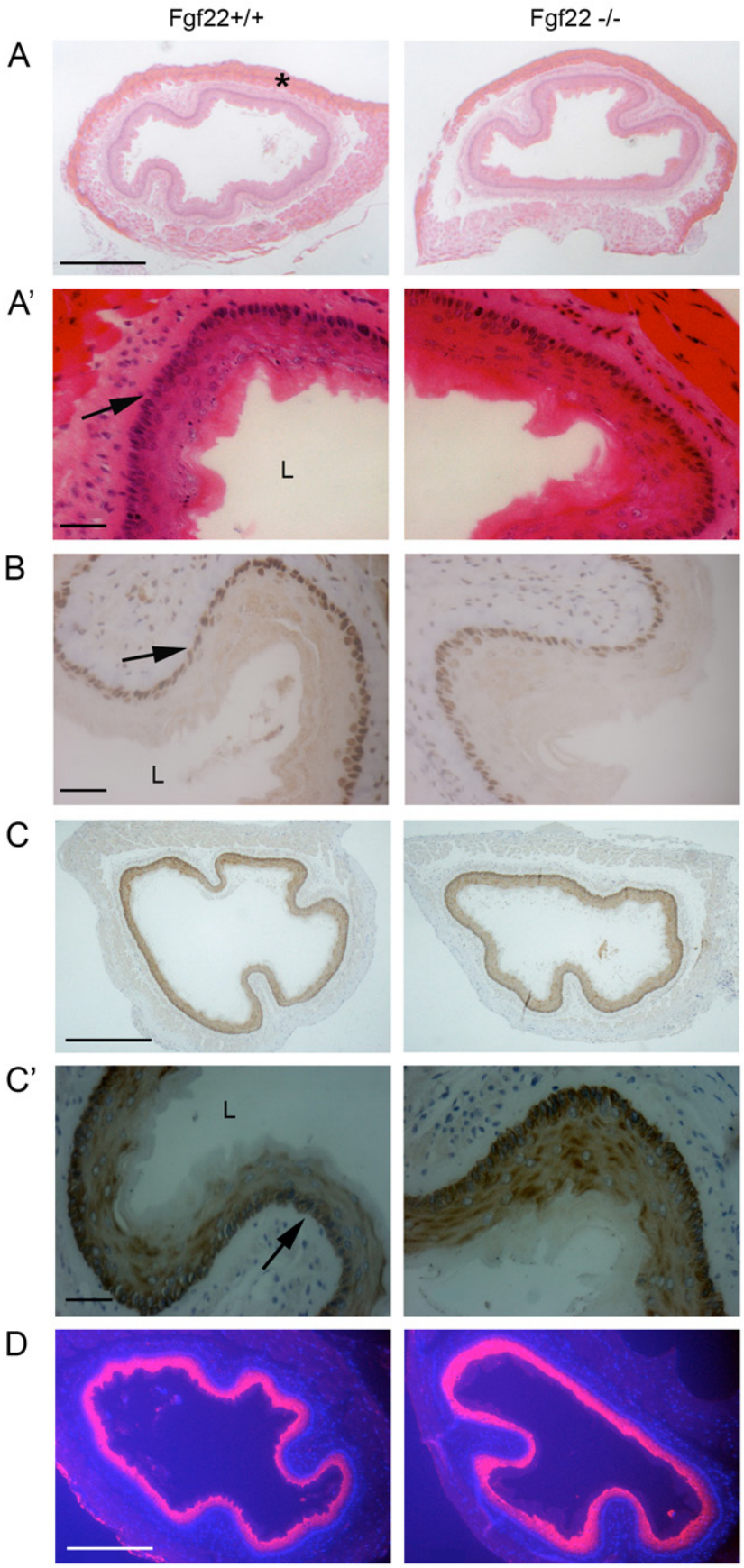
Fgf22+/+
Fgf22 -/-
A
*
A'
L
B
L
C
C'
L
D

Figure 3.25 Histological analysis of oesophageal tissue. Tissue morphology of 4 µm sections of oesophagus prepared from 2 month old animals was compared and revealed no differences between wild type and knockout animals (n=6) when stained with A) Haematoxylin and eosin (H&E). B) p63 immunohistochemical staining did not show any alterations in the nuclear staining pattern. Immunostaining for differentiation markers C) K14 and D) Loricrin showed no changes in the epithelial differentiation process of the investigated tissue. (*= muscle, L=lumen of oesophagus, → =basal layer of epithelial cells). Scale bars (200 µm) (A, C, D) and (20 µm) (A', B', D).

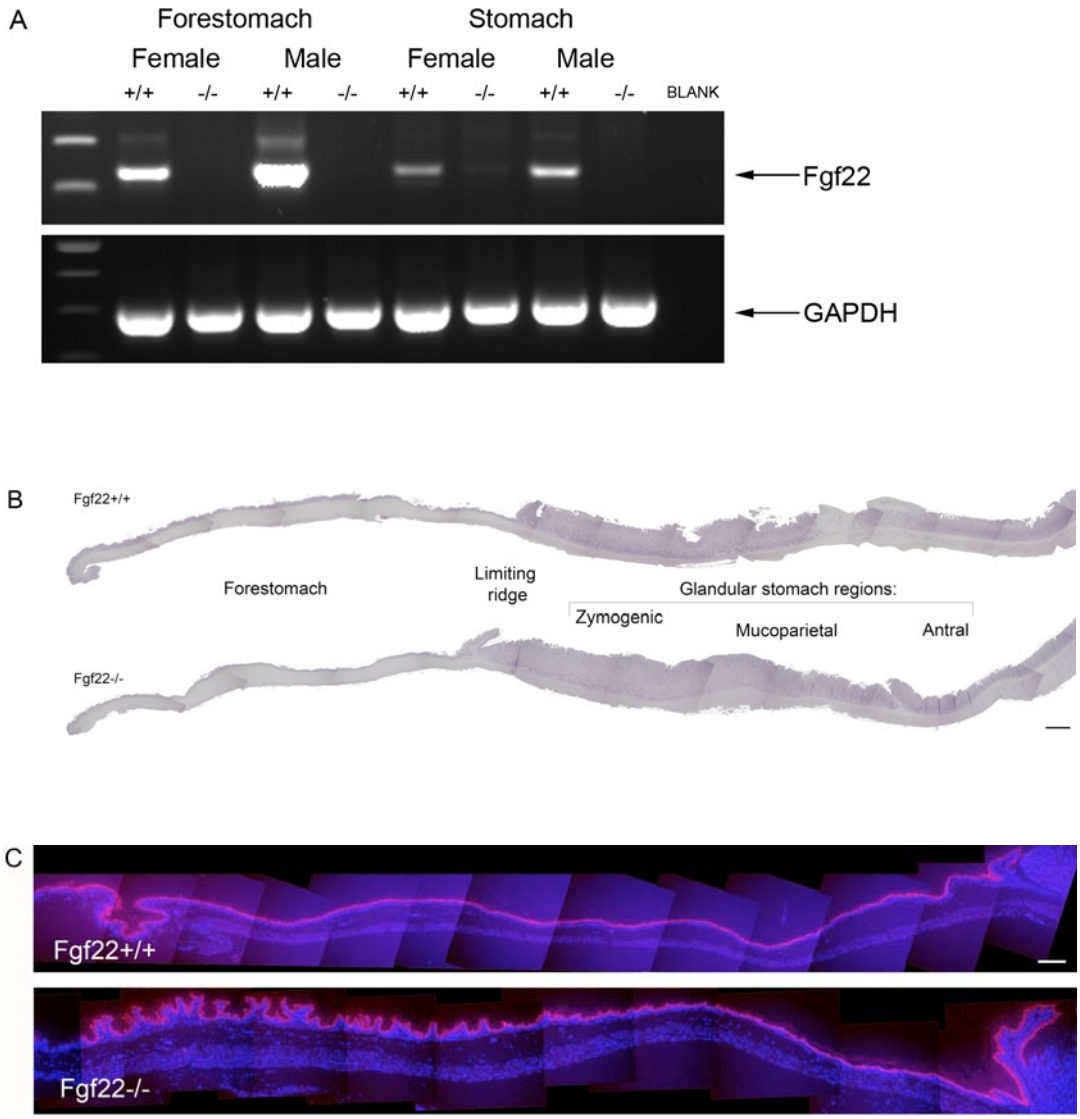

Figure 3.26 *Fgf22* and stomach. A) *Fgf22* was expressed in the forestomach and stomach of wild type but not knockout mice. Blank PCR without cDNA. B) H&E staining of 5 *Fgf22* wild type and 5 knockout mice stomachs. The forestomach is lined with a stratified squamous epithelium, whereas the glandular stomach epithelium can be subdivided into zymogenic, mucoparietal and antral regions depending upon cell lineages populating their gastric units. Scale bar (1 mm). C) Expression of the epithelial differentiation marker, Loricrin in the forestomach did not show any obvious alterations in the differentiation process in 5 wild type and 5 knockout animals. Scale bar (200 μm).

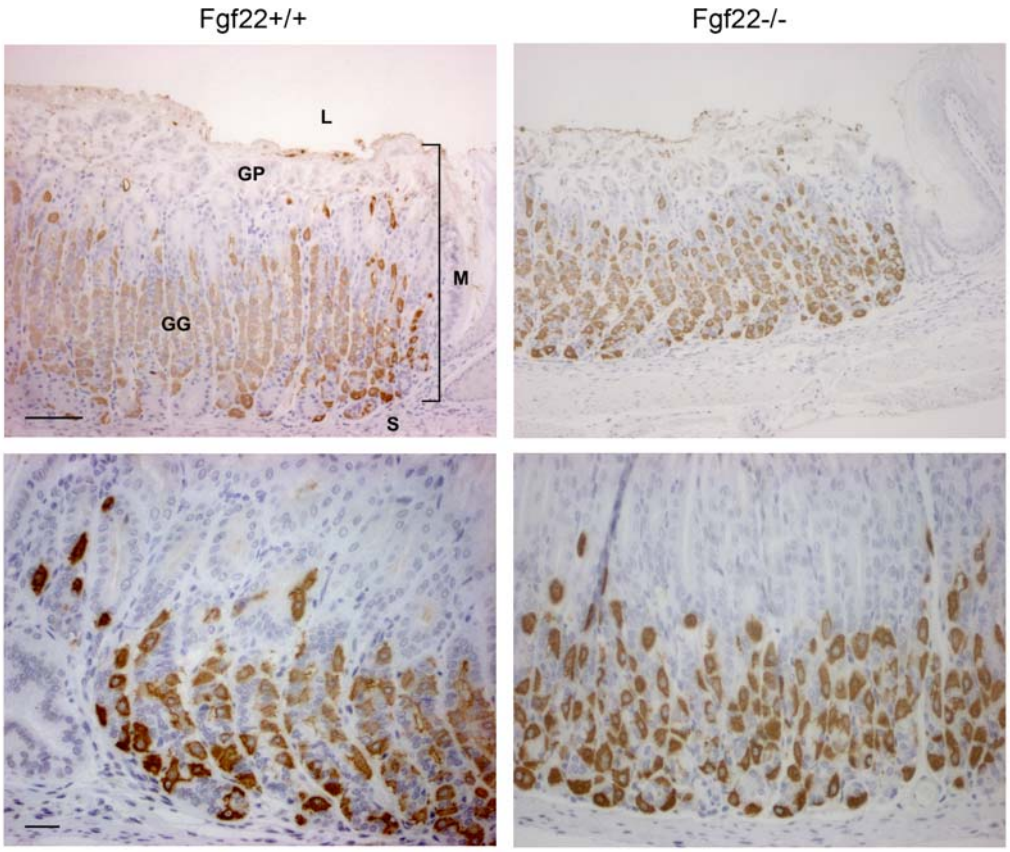

Figure 3.27 Stomach - parietal cells. Paraffin sections (4 µm) from 5 *Fgf22* wild type and 5 knockout stomachs were stained with an antibody specific to ATP4B protein, staining acid secreting parietal cells (brown). Parietal cells are large, triangular cells with very eosinophillic cytoplasm, large nucleus and a narrow apical part that points towards the pit. There were no noticeable differences in the staining pattern between wild type and knockout mice stomach sections. (L=lumen of stomach, M=mucosa, S=submucosa, GP=gastric pit, GG=gastric gland). Scale bar (100 µm) top panel, (50 µm) bottom panel.

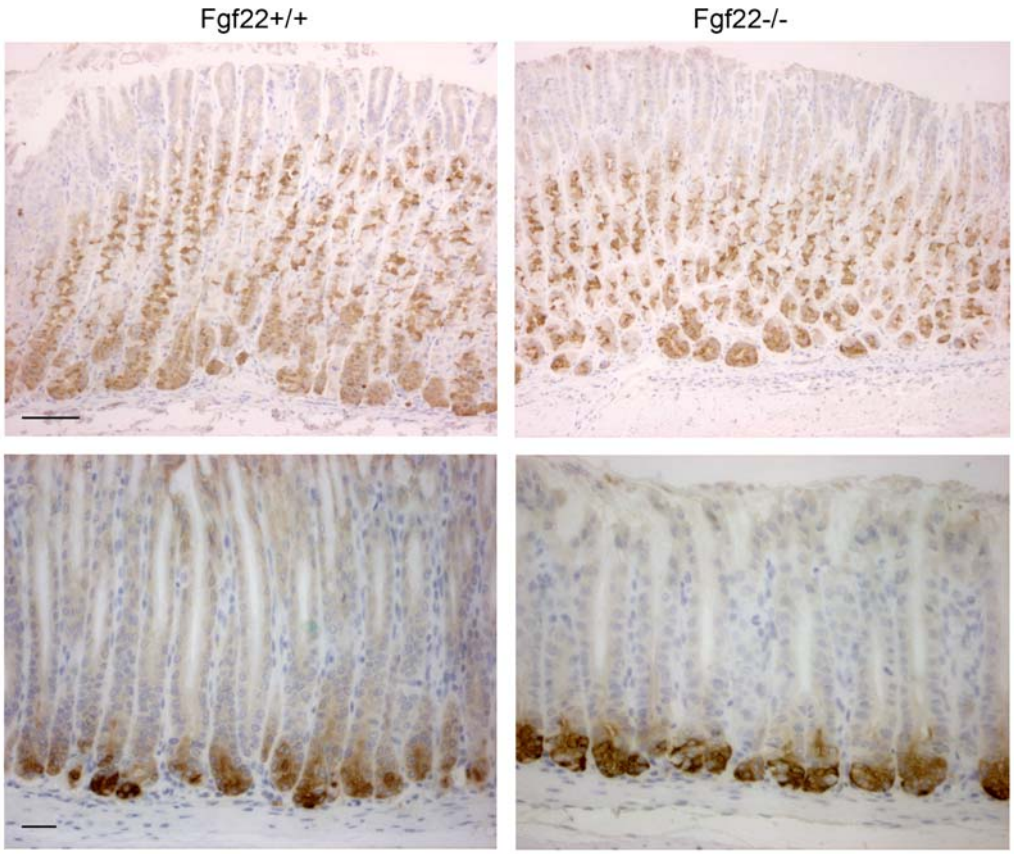

Figure 3.28 Stomach - chief cells. Stomach sections of 5 *Fgf22* wild type and 5 knockout mice were immunostained with anti-Pepsinogen antibody to highlight the digestive enzyme secreting cells (brown staining). Chief cells are small, cuboidal, basophilic cells with the highest in number at the base of the gland (bottom panel). No differences in the staining pattern were observed. Scale bar (100 µm) top panel, (50 µm) bottom panel.

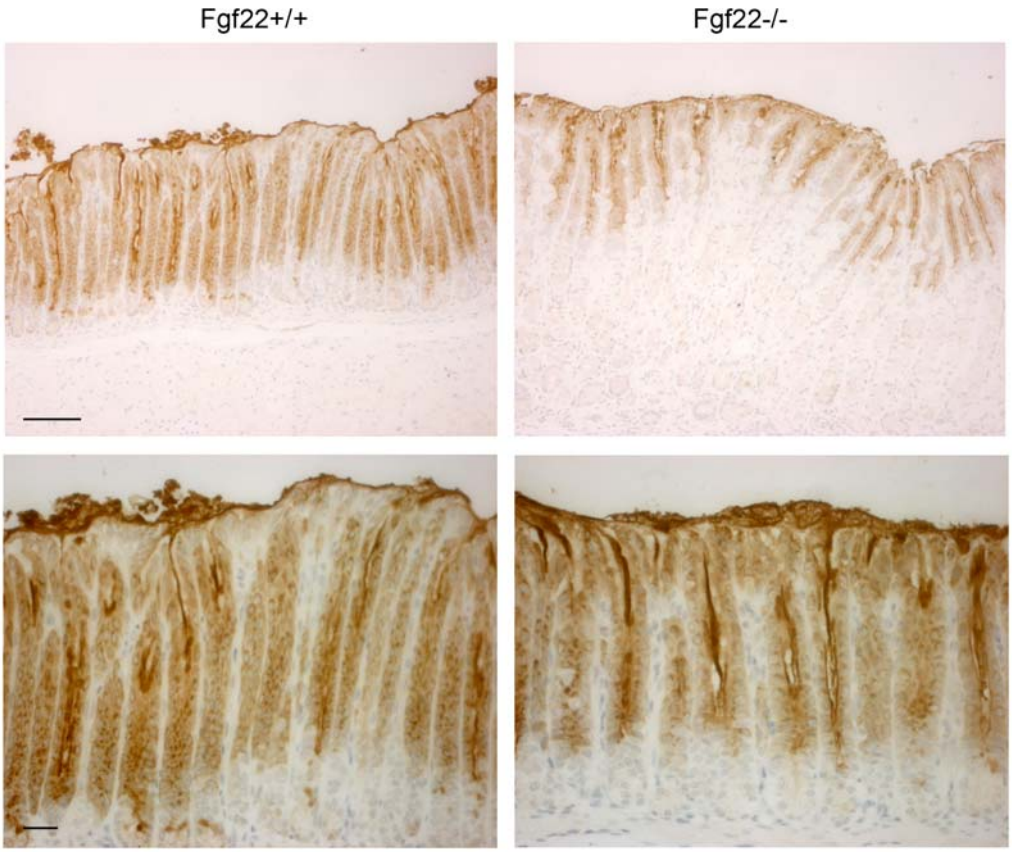

Figure 3.29 Stomach - pit cells. *Fgf22* wild type (n=5) and knockout (n=5) stomach sections were stained with anti-trefoil factor 1 (TFF1) antibody. TFF1 is a stable secreted protein expressed in gastrointestinal surface mucosa of the gastric pits and in the overlying mucus. Pit cells are epithelial cells found in the gastric epithelium in the central (corpus) region of the stomach. They secrete an alkaline mucus that protects the epithelium against shear stress and acid. No changes in staining pattern between the samples were observed. Scale bar (100 µm) top panel, (50 µm) bottom panel.

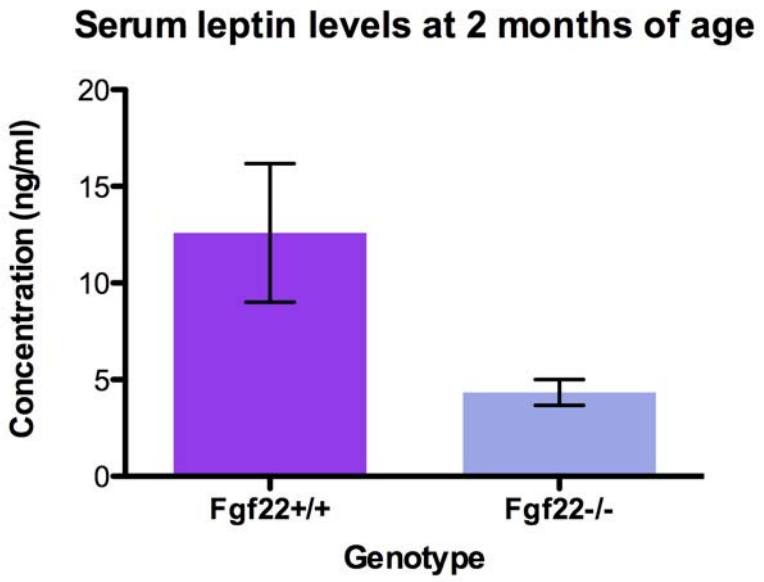

Figure 3.30 Serum leptin levels of *Fgf22* wild type and knockout male mice. Serum leptin concentration was determined by colorimetric sandwich enzyme-linked immunosorbent assay (ELISA) from mice at 2 months of age. Age matched wild type male mice had higher serum leptin levels than knockout males but the difference was not statistically significant (n=4). Error bars represent standard error among the samples.

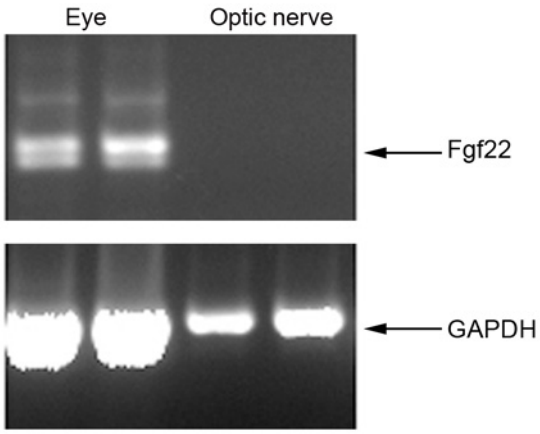

Figure 3.31 *Fgf22* gene expression in the eye. When examined by RT-PCR, *Fgf22* expression was detected in RNA isolated from the whole eye but the expression was undetectable in the optic nerve. *GAPDH* was used as the internal control.

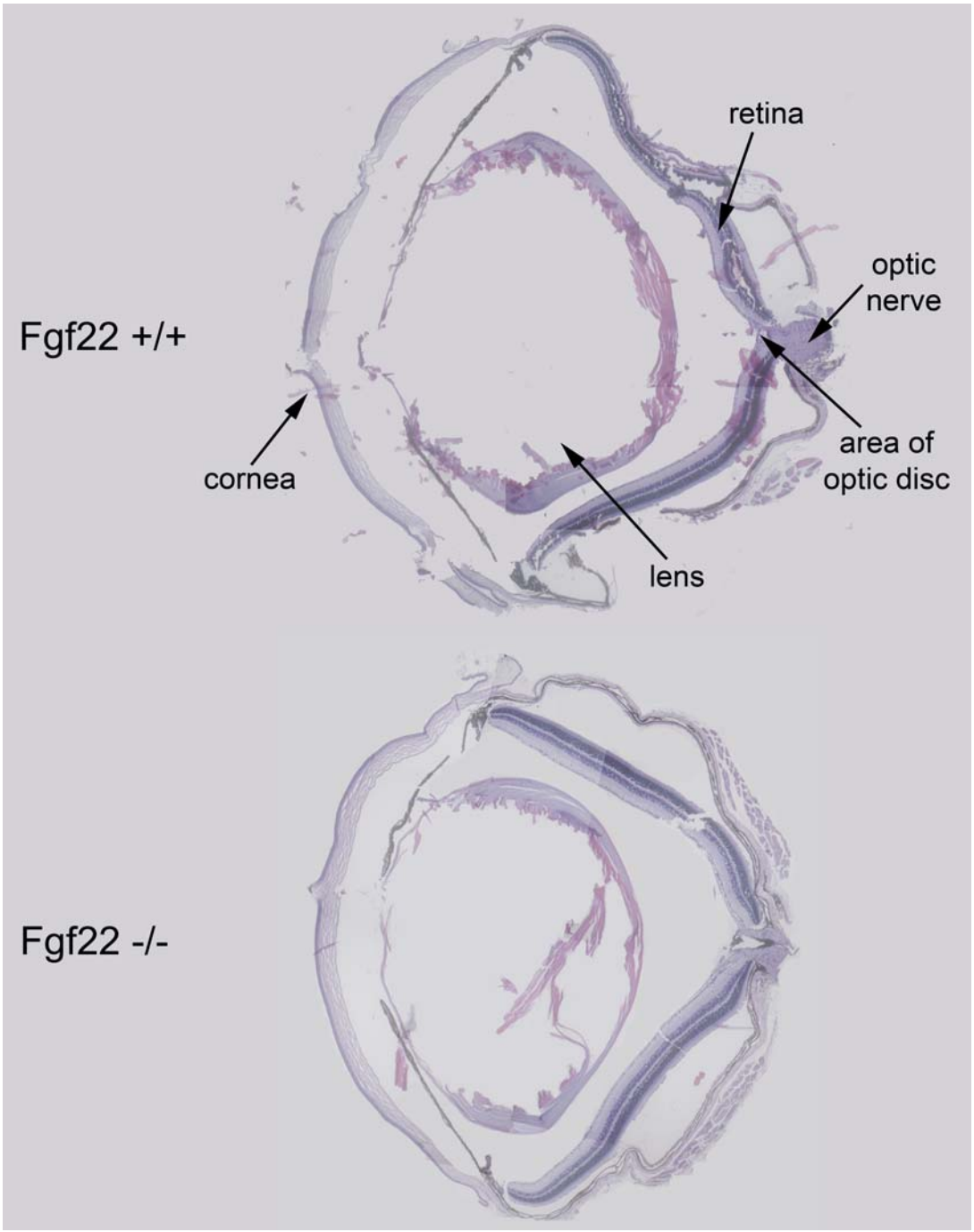

Figure 3.32 Histology of the eye. Picture shows H&E stained transverse section of *Fgf22* wild type mouse eye with marked in all the main tissue elements. When compared with H&E stained sections from the eye of *Fgf22* knockout mice no obvious differences were found. The lens tissue is missing as a result of fixation and sectioning artefact, but the retinal layers were relatively well preserved.

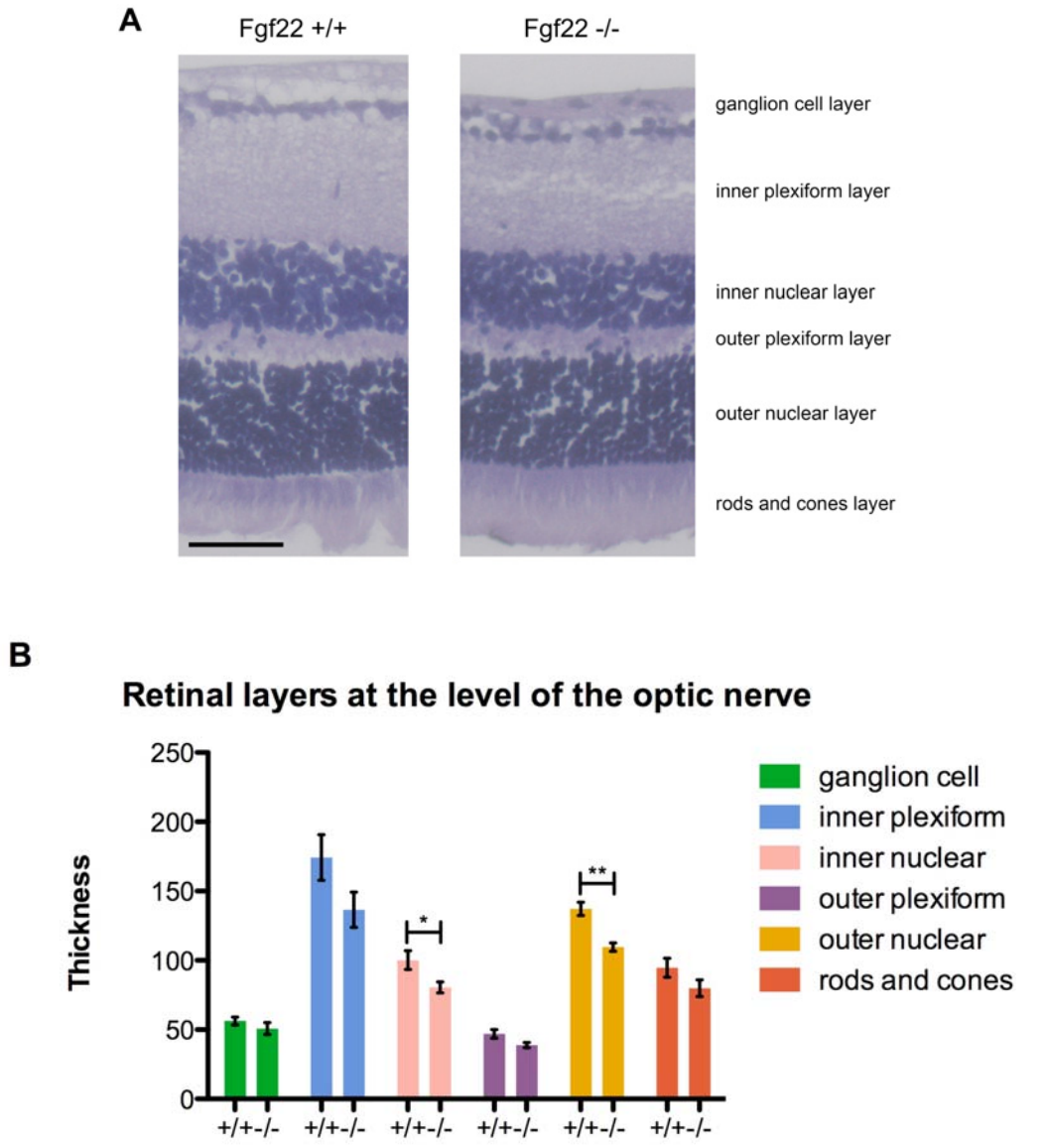

Figure 3.33 Thickness of the retinal layers. A) Layers of the retina. The retina is a multi-layered, light sensitive sensory tissue that lines the back of the eye. Picture shown is an H&E stained retina of *Fgf22* wild type mouse with all the layers marked. Scale bar (50 µm). B) Thickness of all the retinal layers was measured in eye sections from 2 months old *Fgf22* wild type and knockout male mice (n=3 for each genotype). H&E stained transverse eye sections from the left and right eye were measured at eight points at close distance to the optic nerve. Identical measurements were performed on sections above the optic nerve, at the optic

nerve level and below the optic nerve level. Error bars represent SEM. The same trend for retinal layer thinning was observed at all measured levels in knockout mice but the differences were statistically significant ($P<0.05$ and $P<0.001$) only at the level of the optic nerve.

3.3 Discussion

Numerous studies on FGF7, FGF10 and their receptors have shown the importance of this subfamily of FGFs for normal embryonic development and adult tissue homeostasis. Little is known though, about the role and importance of FGF22 in those processes.

During the first year of my PhD, I focused on investigating the function of FGF22 using an *in vitro* cell culture approach (results not shown). I obtained a stably transfected BHK cell line reported to express and secrete FGF22 (Zhang et al., 2006). Firstly, I confirmed *Fgf22* expression by RT-PCR and Western blot in transfected cells. However, despite repeated efforts, including concentrating conditioned medium and adding various concentrations of heparin, I was not able to detect secreted FGF22. As a positive control, I performed transient transfections with a construct encoding FGF7, which was readily secreted by COS cells, but not by both BHK and HC11 transfected cells, suggesting that there was a problem with the secretion of recombinant proteins in these cells. HC11 is a mammary epithelial cell line in which, in contrast to BHK cells, FGFR2b is expressed, as confirmed by restriction digestion of RT-PCR products, so there is a question of instant uptake of the growth factor into an autocrine loop system. Afterwards I wanted to use cell migration and proliferation as a read out assay of FGF22 signalling. Scratch wound assays on HC11 cell monolayer treated with conditioned medium from FGF22 expressing cells showed no difference in cell proliferation and migration comparing to control cells. From the above I concluded that FGF22 is not a secreted protein, at least in these cell lines.

In spite of the fact that *Fgf22* was reported to be expressed at different stages of mouse embryonic development (Beyer et al., 2003), disruption of *Fgf22*

did not result in embryonic lethality in our knockout mouse model. Mice lacking the entire coding sequence of the growth factor developed normally and, when born, did not display any obvious abnormalities, demonstrating that FGF22 is not essential for embryonic development.

Genotype distributions at birth matched expected Mendelian ratios and *Fgf22* knockout mice were indistinguishable from their wild type and heterozygous littermates. To investigate any requirement for *Fgf22* for both male and female fertility, a number of matings between knockout animals were performed. These revealed that both knockout males and females were fertile and that litter size and average number of pups did not vary from those observed in wild type matings. The time interval between the setting up of mating pairs and birth of the first litter was comparable between wild type and knockout mice, suggesting normal mating behaviour.

Previous studies have shown that *Fgf22* is expressed in the brain and that it is essential for the development of functional presynaptic structures (Umemori et al., 2004). RT-PCR analysis indeed demonstrated that the *Fgf22* transcript was present in the brain of an adult wild type mouse but not in the *Fgf22* knockout mouse (Fig 3.6). Interestingly, lack of FGF22 in the brain did not seem to affect mouse development or behaviour in any obvious way. It has been shown before, that *Fgf22* is expressed in cerebellar granule cells at the same time that they are being innervated by mossy fibres from FGFR2b expressing vestibular and pontine neurons (Umemori et al., 2004). All three major FGFR2b ligands - FGF7, 10 and 22 were shown to have presynaptic organising abilities. However, FGF22 was expressed at much higher levels in the cerebellum than either FGF7 or FGF10, so it seemed likely that it is the main presynaptic organising molecule, at least in this part of the brain. The cerebellum is a critical centre of motor control, responsible

for precise timing of coordinated, smooth movements of the skeletal muscular system. If *Fgf22* deletion would cause any defects in the construction of synapses in this part of the brain we could expect balance and coordination problems in our mice, which never occurred.

Furthermore, our collaborator Hisashi Umemori from University of Michigan USA bought a commercially generated *Fgf22* knockout line (not available to us as licencing costs $26,000) and confirmed our findings, with mice showing no overt phenotype under normal husbandry conditions. Nevertheless, his group studying *Fgf22* knockout mice have preliminary data that *Fgf22* and *Fgf7* are highly expressed by CA3 pyramidal neurons in the hippocampus and both FGFs are presynaptic organisers in CA3. However, FGF22 promotes excitatory presynaptic differentiation and FGF7 promotes inhibitory presynaptic differentiation in the hippocampus. The balance between excitatory and inhibitory inputs on a neuron controls its neural excitability. When the ultrastructure of synapses in CA3 was examined by electron microscopy, the number of synapses formed was similar between *Fgf22* knockout and wild type mice but the distribution of synaptic vesicles at excitatory synapses was more diffuse in knockout mice (Terauchi, A., Javed, D. Regulation of excitatory and inhibitory synapse formation by FGF22 and FGF7. 2008 Neuroscience Meeting Planner, Washington, DC: Society for Neuroscience, 2008. Online). Interestingly, knockout mice for STAM1 (signal transducing adapter molecule), also present in synaptic regions, are characterised by gradual disappearance of hippocampal CA3 pyramidal neurons with age and display age dependent growth retardation detectable by 2 weeks of age (Yamada et al., 2001). The neurological abnormality in STAM1 knockout mice was first suspected on the basis of observation of unusual leg-clasping reflex apart from normal coordination of movement, something never noticed in *Fgf22* knockout mice. Nevertheless, given our collaboration with Dr Umemori, a specialist

neurobiologist, coupled with our lack of expertise in neurobiology, I did not pursue this site of *Fgf22* expression further.

Interestingly, an observation of statistically significant sex-related difference in basal *Fgf22* mRNA expression levels was made. Wild type male mice expressed much higher levels of *Fgf22* mRNA compared with female mice when assayed by quantitative RT-PCR (Fig 3.7). That was an unexpected finding but not an uncommon one, since a large extent of sexual dimorphism in gene expression has been observed before (Yang et al., 2006). In fact when liver, brain, adipose and muscle tissue were studied for differentially expressed genes between males and females, thousands of genes were identified, suggesting a widespread sexually dimorphic gene expression in mice. The degree of sexual dimorphism of actively expressed genes in various tissues ranged from 14% in brain to 70% in liver (Yang et al., 2006). Since most common diseases exhibit some degree of sex bias, a systematic understanding of the mechanisms underlying physiological differences between sexes is of great importance. Moreover, such an understanding in, for example, cancer biology could be useful in explaining gender differences in drug metabolism and toxicity. It also brings to attention the fact that there is evidence that women have been less enrolled in clinical trials and that a gender-specific analysis usually is not included in the evaluation of results. Gender differences in pharmacology have to be considered in order to improve drug safety efficacy and to optimise medical therapy both in men and women.

Since the FGF subfamily members have similar receptor-binding properties and overlapping patterns of expression, functional redundancy is very likely. Due to that, I wanted to verify that normal development and fertility of *Fgf22* knockout mice was not a result of *Fgf7/Fgf10* compensation (Fig 3.8). Relative levels of *Fgf7* in wild type and knockout mice were variable but not significantly different.

Moreover, levels of *Fgf10* were significantly decreased in knockout male mice compared to wild type mice, which potentially excludes the possibility of functional compensation unless FGF22 counteracts the signalling of FGF10 – in which case down-regulation of FGF10 would compensate for down-regulation of FGF22.

Given that previous reports described *Fgf22* expression in the inner root sheath of the hair follicle (Nakatake et al., 2001) and a clear hair phenotype in *Fgfr2b* null skin (Grose et al., 2007), the possibility of a hair phenotype in knockout mice was anticipated. Nevertheless, knockout mice possessed all three major hair types in identical proportions to wild type littermates (Fig 3.9). Also, sebaceous glands did not display any differences between knockout and wild type animals (Fig 3.10), which was somewhat disappointing since skin specific deletion of *Fgfr2b* resulted in severe sebaceous gland atrophy (Grose et al., 2007).

Fgf22 expression was described in normal and wounded skin in two independent studies (Beyer et al., 2003). The sites and timing of *Fgf22* expression led us to hypothesise that this growth factor may play a role in helping to control tissue homeostasis, perhaps by damping down FGFR2b signalling and ensuring that over-proliferation of keratinocytes does not occur. In theory, *Fgf22* knockout mice could suffer from uncontrolled keratinocyte proliferation, like in psoriasis (McKay and Leigh, 1995), or abnormal wound healing with papillomas forming at the injury sites (Rappolee et al., 1988). However, the unchallenged skin of *Fgf22* knockout mice looked normal in terms of histology, layer thickness and organisation (Fig 3.11). I therefore analysed the capacity of *Fgf22* null mouse skin to respond to a challenge stimulus. Mice were subject either to wounding (Fig 3.12) or to classical two-step skin carcinogenesis (Fig 3.20), since both of these interventions cause an increase in keratinocyte proliferation, either transiently in the case of wound repair or more permanently in the case of carcinogenesis.

These studies allowed me to question whether FGF22 was capable of driving keratinocyte differentiation and/or inhibiting their proliferation.

The wound healing study revealed that gross healing (Fig 3.12), as well as more detailed histological analysis (Fig 3.13 - 3.16), was not significantly different in knockout mice when compared with wild type mice, implying that mice lacking *Fgf22* in the skin were able to heal acute wounds just as efficiently as wild type mice. This apparent redundancy in the FGF-FGFR axis during repair is not without precedent, with mice lacking *Fgf7, Fgfr1b* or *Fgfr2b* showing no obvious wound healing phenotype despite expression of these molecules during the repair process (Guo et al., 1996). Polarised light microscopy of Sirius red stained sections from 14 and 21 day wounds indicated no differences in collagen fibre organisation and maturation at the wound site, moreover wounds of wild type and knockout mice at 21 days, when the experiment was terminated, were indistinguishable (Fig 3.16). From the above picture it appeared that FGF22 is dispensable for the wound healing process, which was unexpected, since FGF22 is highly expressed in the hyperproliferative wound epithelium (Beyer et al., 2003). Moreover, the relative levels of *Fgf22* mRNA expression assayed by Real Time RT-PCR peaked at 14 days after wounding in wild type mice (Fig 3.17), when the wound was already healed, consistent with already published data. Furthermore, expression levels of *Fgf7* and *10, Fgfr1b* and *Fgfr2b* all of which are expressed during the wound healing process (Werner et al., 1992, Tagashira et al., 1997, Zhang et al., 2004, Werner et al., 1994) did not differ significantly between wild type and knockout mice (Fig 3.17). Additional evidence for wound healing not requiring FGF22 came from the lack of difference in time required for *in vitro* wound closure by primary keratinocytes isolated from wild type and knockout mice (Fig 3.19).

Classical two-step skin carcinogenesis revealed that only 50% of DMBA treated knockout mice developed papillomas compared to 100% of treated wild type mice over the 58 weeks period of experiment duration (Fig 3.20). Moreover, the onset of papilloma formation was hugely delayed (by 27 weeks) in knockout mice, as well as tumour multiplicity being reduced in knockout mice. That was unexpected, considering the above hypothesis, coupled with the fact that data from our lab show mice lacking *Fgfr2b* in the epidermis have increased cancer susceptibility, develop spontaneous papillomas and demonstrate dramatic tumorigenesis following DMBA treatment. Results obtained from the carcinogenesis experiment demonstrate that tumour suppressive role of the FGFR2b does not act via FGF22, as *Fgf22* knockout mice exhibit resistance to DMBA induced tumorigenesis. That suggests a possibility that *Fgf22* confers sensitivity to chemically induced skin carcinogenesis. Moreover, it might even antagonise the *Fgfr2b* role in this process. Speculative counteraction of ligand-receptor arrangement would involve even more potent *Fgfr2b* tumour protective action given *Fgf22* deletion. One way of investigating this exciting hypothesis would be generating *Fgf22* over-expressing mouse model and checking its phenotypical answer to chemically induced skin carcinogenesis.

The only noticeable difference between unchallenged *Fgf22* knockout and wild type mice was in body weight (Fig 3.21). Adult male knockout mice appeared much leaner when compared with age-matched wild type male mice, and detailed study of weight gain over time confirmed these findings (Fig 3.22). The difference in weight gain was first observable around the time of weaning (3 weeks of age) and became increasingly apparent when mice reached puberty at 5-6 weeks of age. Interestingly, both adult male and female wild type mice on the C57BL/6J background generally reached higher body mass than the record found in the literature for this inbred mouse strain. According to the Jackson Laboratory, at 16

weeks of age, C57BL/6J mouse maximum body weight for a male was 30.1 grams and 21.9 grams for female. In my study, by this age wild type C57BL/6J male mice reached 39.3 grams and female 28.7 grams and increased further upon aging. Nevertheless, it is well known that even mice raised with the same diet, in the same types of cages, with the same husbandry procedures can have a remarkable range of body size and composition (Reed et al., 2007). Body weight is usually considered as a typical polygenic characteristic, meaning that a large number of genes are assumed to influence it, with each having a very small effect. However the number, location and effect of individual genes contributing to variation is mostly unknown. We can speculate whether *Fgf22* is a novel gene affecting body weight. Body weight is a composite trait resulting from fat and non-fat, lean tissue. Most light mice have very little fat whereas heavy mice are almost half fat by weight (Reed et al., 2007). Some genes might affect fat or lean tissue whereas other genes might affect both. Interestingly, FGF10 has been reported to play an important role in adipogenesis since development of white adipose tissue was reduced in *Fgf10* knockout mice (Sakaue et al., 2002). Further studies are required to determine whether *Fgf22* gene deletion causes reduction of fat mass or increase in lean mass. There are a number of possible mechanisms that can produce weight loss; for example behavioural or hormonal differences, a subtle tooth or digestive tract phenotype or stimulated thermogenesis. The cause of weight loss in *Fgf22* knockout mice is not likely a result of imbalance in appetite controlling hormones since serum leptin levels, an important mediator of feeding behaviour and energy homeostasis, in two months old knockout male mice were not different from those in wild type mice (Fig 3.30).

Also, no obvious macroscopic problems with food absorption and digestion were noticed when the whole gastrointestinal tract of wild type and knockout mice was dissected and compared. Nevertheless, *Fgf22* expression was checked by

RT-PCR in all the parts of the digestive system and the growth factor was discovered to be expressed at low levels in almost all the parts of the intestinal tract, with particularly high levels of expression in the oesophagus and stomach (Fig 3.23). Subsequently, the morphology of knockout oesophagus and stomach sections was examined but no obvious differences in tissue appearance were observed (Fig 3.25 and 3.26). Moreover, a series of immunohistochemical staining (anti-p63, -K14 and -Loricrin, -ATP4B, -Pepsinogen and -TFF1) for the major characteristic cell types of the digestive tract, did not reveal any changes in protein expression pattern of cell differentiation (Fig 3.27-3.29). Thus, in spite of my studies to date, the underlying reason for weight loss in *Fgf22* knockout mice remains unclear.

During the process of *Fgf22* knockout mouse characterisation, I found that *Fgf22* was expressed in the eye (Fig 3.31). Once more, tissue morphology was checked and this time it revealed changes in retinal layer thickness in knockout male mice (Fig 3.33). Selective thinning of inner retinal layers is common in type 1 diabetic patients (van Dijk et al., 2009). In diabetic retinopathy, high sugar and blood pressure levels cause blood flow to increase, which slowly damages blood vessels supporting the retina. Thus I can speculate that *Fgf22* knockout mice are diabetic, or, since it is thought that early diabetic retinopathy includes a neurodegenerative component (Lieth et al., 2000), that lack of *Fgf22* expression in the brain is the root cause.

It is clear that further experiments are required in order to fully understand the physiological role of *Fgf22*. Preliminary results obtained during the course of my PhD project are valuable in context of narrowing the number of investigative possibilities and hopefully pointing future research in the right direction.

3.4 Future directions

Undoubtedly the powerful technology of gene targeting in embryonic stem cells has enabled the simple generation of mice lacking a specific gene. However, in a significant proportion of such knockout mice, even within the FGF family, either no or only very subtle phenotypes could be detected. Advancements in the field of mouse phenotyping and use of extensive experimental pathology tests on each knockout mouse show that abnormal phenotypes were sometimes detected in physiological areas where they were not initially anticipated, or only manifested under certain conditions, emphasising the need for careful phenotypic investigation (Barbaric et al., 2007). This is exactly the case for *Fgf22* knockout mice, in which the weight loss phenotype was entirely unexpected. However, it is possible that the *Fgf22* knockout mouse has another phenotype, but the tests I used to characterise it were not sufficiently sensitive or perhaps different classes of tests should be carried out. Conceivably, crossing *Fgf22* knockout mice with other FGF deficient lines to generate double or triple knockout mice would reveal further functions of the gene. Also, backcrossing *Fgf22* knockout mice to a different background could prove a means to uncover a distinctive phenotype since, for example, *Keratin 8* knockout mice have very differing phenotypes depending on the genetic background. On a C57BL/6J background, *Keratin 8* knockout mice died due to internal bleeding (Baribault et al., 1993), whereas on a FVB/N background they were viable but displayed colorectal hyperplasia (Baribault et al., 1994). It is also well known, that breeding strategies have produced mice strains with skin epithelium highly susceptible or resistant to tumour development or else with particular sensitivity to develop benign (squamous papillomas) and malignant (squamous carcinomas) tumours. For example a mixed background of 129ola and C57Bl6/J mouse strain is relatively tumour resistant while FVB/N mice are moderately susceptible to papilloma

formation, but the benign tumours are unusually prone to undergo malignant conversion (Woodworth et al., 2004). Another unwelcome possibility is simply that the *Fgf22* gene is truly not important for development and tissue homeostasis.

Given more time, I would have liked to have continued further characterisation of metabolic differences in *Fgf22* knockout mice. A series of experiments can be performed in order to do that including; monitored food intake, before and after fast, over a set period of time, mice fed high fat diet or put on a pair-fed experiment where wild type and knockout mice are restricted to eat the same amount of food and their weight gain is recorded. Most useful would be putting wild type and knockout mice into special metabolic cages. Given time I would have liked also to do a glucose and insulin tolerance test on those mice. Glucose tolerance test determines how quickly glucose is cleared from the blood after its administration, and it would be used to check for diabetes and insulin resistance in *Fgf22* knockout mice. An insulin tolerance test, in which insulin is given intravenously, is intended to induce hypoglycemia, in response to which adrenocorticotropic hormone (ACTH) and growth hormone (GH) are released as a part of the stress mechanism. ACTH elevation causes the adrenal cortex to release cortisol, which is responsible for keeping stable sugar blood levels, physiological blood pressure and right fluid balance. Normally, both cortisol and GH serve as counter-regulatory hormones, opposing the action of insulin, acting against the hypoglycemia (Greenwood et al., 1966). Insulin tolerance test is routinely used for assessing the integrity of the hypothalamo-pituitary-adrenal axis.

CHAPTER 4

FIBROBLAST GROWTH FACTOR RECEPTOR 2

CHAPTER 4: Fibroblast growth factor receptor 2

4.1 Introduction

4.1.1 The role of FGFR in carcinogenesis

As discussed earlier, as a general rule, FGFRs encoding exon IIIb (FGFR IIIb) are expressed on epithelial cells while the FGFRs encoding exon IIIc (FGFR IIIc) are expressed on mesenchymal cells (Mohammadi et al., 2005). By contrast, the cognate ligands for the IIIb isoform are often expressed by mesenchymal cells, while ligands for IIIc are expressed by epithelial cells. This establishes a paracrine mechanism of signalling between epithelia and mesenchyme that is critical to normal development and tissue homeostasis. Deregulation of this precise mechanism of FGF signalling often is implicated in initiation or development of multiple cancer types, through directly driving cancer cell proliferation and survival, and also by supporting tumour angiogenesis. As our knowledge progresses we can now, in the tumorigenesis field, distinguish two contrasting effects of FGF receptor biology; tumour suppressive and oncogenic, with the segregation into one of the groups being dependent on receptor isoform, tissue and temporal specificity (Grose and Dickson, 2005).

4.1.2 FGFR2 as a tumour suppressor

Skin

Recently, a novel role for *Fgfr2b* has been discovered. Genetically engineered mice lacking *Fgfr2b* in the skin epidermis were characterised by a thin and silky coat, sebaceous gland atrophy, increased macrophage infiltration to the

dermis and epidermal thickening accompanied by basal-layer dysplasia and parakeratosis. Of even greater interest was the fact that about 10% of mutant mice developed spontaneous papillomas with age and also showed great sensitivity to chemical carcinogenic insult by rapidly developing papillomas, some of which progressed to squamous cell carcinomas (Grose et al., 2007). For the first time, the epithelial isoform of the *Fgfr2* receptor was shown to play a tumour suppressive role in the skin. Those interesting findings now need to be translated to human skin, where they will determine whether there is a tumour suppressive role of FGFR2b in man.

Most recently, it has been reported that 10% of melanoma tumours and cell lines harbour mutations in the *FGFR2* gene. These novel mutations include three truncating mutations and 20 missense mutations occurring at evolutionarily conserved residues common not only in *FGFR2* orthologues, but among all four *FGFRs*. Such mutations result in receptor loss of function through several distinct mechanisms, including loss of ligand binding affinity, impaired receptor dimerisation, destabilisation of the extracellular domains, and reduced kinase activity (Gartside et al., 2009).

Bladder

FGFR2b expression is reported to be decreased in about 30% of primary bladder tumours and 50% of bladder cancer cell lines. Down-regulation of this receptor in the bladder epithelium is associated with a poor prognosis (Diez de Medina et al., 1997). FGFR2b has an inhibitory function in bladder cancers, blocking cell growth both *in vitro* and *in vivo*. Receptor inactivation is an important step in human bladder tumour progression. Interestingly, FGFR1 is not present in the normal urothelium, but is expressed in many bladder carcinoma and cell lines,

suggesting that FGFR1 on the other hand may accelerate tumour progression (Ricol et al., 1999). Furthermore, gain-of-function mutations in *FGFR3* are the most commonly observed mutations in bladder cancer (Cappellen et al., 1999).

Prostate

Similar findings were reported in prostate cancer where, in both mouse and human, decreased expression of FGFR2 results in over-expression of FGFR1, which in turn drives cancer progression (Jin et al., 2003). FGFR1 is normally not expressed in prostate epithelium, but it becomes up-regulated in about 40% of poorly differentiated prostate adenocarcinomas (Kwabi-Addo et al., 2004). Moreover it has been shown in a rat model that, when non-malignant epithelial cells, expressing FGFR2b, were mixed with stromal cells, they resulted in non-malignant tumours (Yan et al., 1993). However, when the stromal cells were absent, epithelial cells underwent a splicing switch, from the IIIb to IIIc isoform, and up-regulated FGF2 expression potentially initiating an autocrine loop (Yan et al., 1993). The transcription factor Homeobox C6 (HOXC6) has been shown to directly up-regulate expression of FGFR2 but, curiously, HOXC6 is over-expressed in prostate cancers and this increased epithelial expression correlates with cancer progression. Most probably, *FGFR2* in this case is silenced by hypermethylation, which prevents receptor activation when HOXC6 is over-expressed (McCabe et al., 2008).

Salivary gland

Salivary adenocarcinomas represent another type of tumour where FGFR2, or rather its absence, plays a major role. Normal salivary gland epithelial cells and benign salivary gland tumours exclusively express FGFR2. During the

malignant transformation of salivary gland epithelial cells, the expression of FGFR2 is abolished, whereas expression of FGFR1c and FGFR4 are up-regulated (Tanaka et al., 1997).

Thyroid

FGFR2b mRNA is detectable in normal thyroid but not in thyroid carcinoma cell lines, whereas *FGFR2c* mRNA is not detectable in either. Alongside this, *FGFR1* expression is up-regulated in thyroid cancer and it is postulated to act in a tumour-promoting manner (Thompson et al., 1998). Co-expression of FGFR1 and elevated levels of FGF1 and FGF2 expression in thyroid cancer potentially drive the cancer progression by an autocrine signalling loop (Eggo et al., 1995). These findings suggest that, in thyroid cancer, loss of expression of the tumour suppressive FGFR2 plays an important role. The mechanism of down-regulation recently has been identified to occur through CpG methylation in the 5' region of the *FGFR2* gene (Kondo et al., 2007).

4.1.3 *FGFR2* as an oncogene

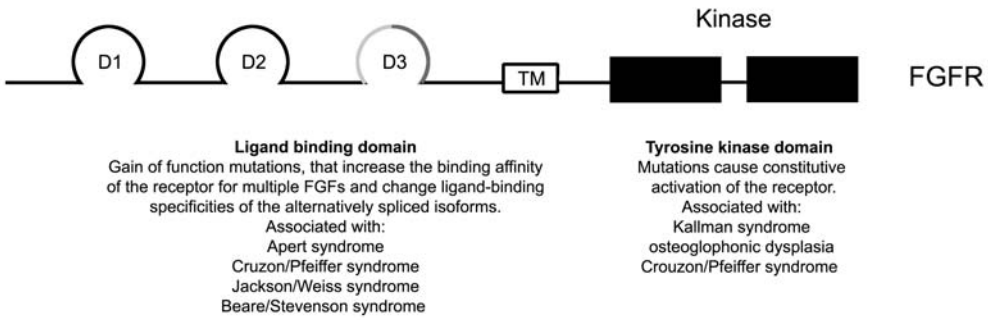

Figure 4.1 Common sites of *FGFR* mutations and the skeletal abnormalities caused by such. D1-3 represent the three extracellular IgG like domains and TM represents the transmembrane region.

Uterus

Recently, there has been strong evidence emerging for *FGFR2* involvement in endometrial and breast cancer. Despite *FGFR2* being highly expressed in normal human endometrial epithelium (endometrium), increased *FGFR2* expression in endometrial adenocarcinomas has been associated with tumour progression, and gain of function mutations in *FGFR2* were identified in 16% of endometrial cancers (Pollock et al., 2007). In this study 11 different *FGFR2* mutations were identified in 30% of the endometrial cell lines and in 10% of the primary uterine tumours investigated. Remarkably, the majority of somatic mutations identified were identical to germline activating mutations in *FGFR2* and *FGFR3* that cause Apert syndrome, Beare-Stevenson syndrome,

hypochondroplasia, achondroplasia and severe achondroplasia with developmental delay and acanthosis nigricans (SADDAN syndrome) (Fig 4.1) (Hajihosseini, 2008). The two most common somatic mutations identified were S252W and N550K, plus another four novel mutations, three of which are also likely to result in receptor gain-of-function (Pollock et al., 2007). Mutations in the extracellular domain of FGFR2 lead to ligand independent dimerisation of the receptor via an inter-molecular cysteine di-sulphide bridge. In a different study on 40 primary endometrial carcinoma tumour DNA samples, mutations were present in 12% of them, plus additional instances were found in lung squamous cell carcinoma and cervical carcinoma (Dutt et al., 2008). The same group also performed some cell culture studies and found that the small-molecule inhibitor PD173074 diminishes survival and anchorage-independent growth of endometrial cancer cell lines expressing activating *FGFR2* mutations (Dutt et al., 2008).

It seems that the *FGFR2* gene lies within a region of significant linkage to endometriosis on chromosome 10q, causing the possibility that variation in *FGFR2* could contribute to the genetic risk of the disease. Nevertheless, after an in-depth genome-wide association study, no evidence was found for association between endometriosis and the key (rs2981582 and rs1219648) *FGFR2* SNPs (Zhao et al., 2008).

Breast

FGFR2 is amplified and over-expressed in 5–10% of breast tumours (Adnane et al., 1991). Two recent genome-wide association studies of breast cancer have identified association of common genetic variants in the *FGFR2* gene with this disease (Easton et al., 2007). In both studies, the most significantly associated SNPs were identified in intron 2 of *FGFR2*. For example, the SNP at

rs2981582 lying within intron 2 of *FGFR2,* was reported to be associated with an increased risk of breast cancer. These susceptibility alleles are very common; approximately 14% of the UK population and 19% of UK breast cancer cases are homozygous for the minor allele at rs2981582. On the other hand, the increased risks associated with these alleles are relatively small - on the basis of UK population rates, the estimated breast cancer risk by age 70 years associated with rs2981582 ranges somewhere between 5.5% and 10.5% (Easton *et al*., 2007). These results were confirmed in another study that has also found SNPs in intron 2 of *FGFR2* (Hunter et al., 2007). Interestingly, the SNP only appears to appreciably increase the risk of developing oestrogen receptor (ER) positive breast cancer (Garcia-Closas et al., 2008), with only a minor impact on ER negative breast cancer. It is still not clear precisely how the SNP confers this increased risk of breast cancer. The probable explanation is that the SNP up-regulates the *FGFR2* gene expression by altering the binding sites of the transcription factors Oct-1/Runx2 (Meyer et al., 2008). Binding sites for ER and Oct often cluster together, suggesting a model where ER and OCT cooperate in regulating *FGFR2* expression. The potential role of ER in determining the functional effects of this SNP may explain the restriction of risk attributed this SNP to ER positive breast cancer.

Stomach

Many stomach carcinoma cell lines express elevated levels of FGFR2, suggesting that, in these cancers, FGFR2 may accelerate tumour progression (Kunii et al., 2008). In fact *FGFR2* is amplified in approximately 10% of gastric cancer, and the amplification appears to be more frequent in undifferentiated or diffuse subtype of gastric cancer, as opposed to the well-differentiated intestinal subtype. This amplification results in a highly over-expressed and constitutively

phosphorylated receptor (Kunii et al., 2008). Over-expression of FGFR2 has thus been correlated with poor prognosis in gastric cancer. Also, some activating mutations in the IIIc isoform of the receptor have been described in human gastric cancer (Jang et al., 2001). Those mutations are identical to germ line mutations predisposing to skeletal dysplasia.

Similarly, two somatic mutations of *FGFR2* were found in a squamous cell lung cancer at an identical position to germ line mutations that also cause Pfeiffer syndrome (Davies et al., 2005).

Pancreas

In normal human pancreas, FGFR2 is expressed in the endocrine islet cells and in the ductal cells. In pancreatic cancer, and pancreatic cancer cell lines, FGFR2 and FGF7 co-expression has been observed (Ishiwata et al., 1998). This indicated a potential FGF7-dependent autocrine loop driving pancreatic cancer growth, as it has been reported previously that *in vivo* injection of FGF7 led to enhanced pancreatic ductal cell proliferation (Yi et al., 1994). In fact increased expression of FGFR2 and FGF7 was detected in ~41% and 34% of examined human pancreatic cancer samples, and their co-expression was detected in ~25% of the samples. There also was a significant correlation between the presence of FGF7, or the co-expression of FGFR2 and FGF7, and poor prognosis. Interestingly FGFR2 expression alone in pancreatic cancer cells was not associated with a poor prognosis (Cho et al., 2007).

FGFR2 as a tumour suppressor	FGFR2 as an oncogene
Skin Tumour protective role against squamous cell carcinomas (Grose et al., 2007). Receptor loss of function mutations in melanoma (Gartside et al., 2009).	Uterine adenocarcinomas Upregulated expression associated with tumour progression plus receptor gain of function mutations (Pollock et al., 2007).
Bladder tumours Decreased expression associated with a poor prognosis (Diez de Medina et al., 1997).	Breast tumours Receptor amplified and overexpressed in 5–10% of tumours (Adnane et al., 1991). SNPs associated with increase risk of breast cancer (Easton et al., 2007).
Prostate cancer Decreased expression of tumour protective receptor results in overexpression of FGFR1, which drives cancer progression (Jin et al., 2003).	Gastric cancer Overexpression of receptor correlated with poor prognosis (Kunii et al., 2008). Activating mutations in the IIIc isoform of the receptor identified (Jang et al., 2001).
Salivary gland tumours Abolished expression of the receptor drives malignant transformation via FGFR1c and FGFR4 activation (Zhang et al., 2001).	Lung cancer Activating mutations found in squamous cell cancer (Davies et al., 2005).
Thyroid carcinoma Loss of FGFR2b transcript and upregulation of FGFR1 expression in thyroid carcinoma (Thompson et al., 1998).	Pancreatic cancer Observed FGFR2 and FGF7 co-expression driving cancer growth and associated with poor prognosis (Ishiwata et al., 1998).

Table 7 FGFR2 status and cancer.

4.1.4 FGFR2 germline mutations

Mutations in human *FGFRs* have been shown to occur in three members of the *FGFR* gene family (Passos-Bueno et al., 1999). Mutations in *FGFR1*, *FGFR2* and *FGFR3* have been demonstrated in craniosynostosis syndromes, and mutations of *FGFR3* are found in a variety of skeletal dysplasias. *FGFR2* activating mutations cause craniosynostosis syndromes including Crouzon, Jackson-Weiss, Pfeiffer, Apert, and Beare-Stevenson syndromes (Fig 4.1).

Affected children show premature fusion of sutures that separate the calvarial and facial bones that results in abnormal skull shape, usually recognised as a tall forehead, widely spaced and prominent eyes, and mid-face hypoplasia. These may be accompanied by limb as well as sporadic visceral and neural abnormalities (Hajihosseini, 2008). So far, 95 individual *FGFR2* mutations have been recognised in craniosynostosis syndromes and some of them have also been found in different types of cancer (Table 8). The aforementioned receptor mutations have been identified primarily in the extracellular region, involved in ligand binding, and the transmembrane domain, but also in the intracellular tyrosine kinase domain involved in signalling. For example, Ser252Trp and Pro253Arg mutations in the ectodomain of FGFR2 cause Apert's syndrome by enhancing ligand binding affinity and promoting binding of inappropriate ligands (Ibrahimi et al., 2001), thus gain of function mutations in FGFR2c allow binding of ligands normally specific for FGFR2b. Nevertheless, the most common mutation is a missense mutation and most often it is a substitution of a cysteine for another amino acid, altering the disulphide bonds formed in ligand binding domain (Ingersoll et al., 2001). Mutations in the kinase domain of FGFR2 that cause craniosynostosis constitutively activate the receptor by disengaging an autoinhibitory molecular brake at the hinge region of the domain (Chen et al., 2007). On the other hand, kinase domain loss of function mutations in *FGFR2* and *FGFR3* have been identified in autosomal dominant lacrimo-ariculo-dento-digital (LADD) syndrome (Rohmann et al., 2006).

Mutation:	Germline	Somatic
S252W	Apert syndrome (Wilkie et al., 1995)	uterine cancer (Pollock et al., 2007)
S267P	Crouzon syndrome (Oldridge et al., 1995)	gastric cancer (Jang et al., 2001)
W290C	Pfeiffer syndrome (Tartaglia et al., 1997)	squamous lung cancer (Davies et al., 2005)
S372C	Beare-Stevenson cutis gyrata syndrome (Przylepa et al., 1996)	uterine cancer (Pollock et al., 2007)
Y375C	Beare-Stevenson cutis gyrata syndrome (Przylepa et al., 1996)	uterine cancer (Pollock et al., 2007)

Table 8 An example of identical *FGFR2* germline mutations identified in craniosynostosis syndromes and somatic mutations in uterine, gastric and lung cancer. Mutations clustered around the hinge region and the third Ig-like domain of FGFR2.

4.1.5 Potential therapeutic approaches

It is very promising that oral administration of AZD2171 or Ki23057 inhibited *in vivo* proliferation of cancer cells with aberrant FGFR2 signalling activation in rodents (Katoh, 2009). It is not known if similar FGFR2 inhibitors would cause the same effect in humans with malignancies associated with activating *FGFR2* mutations or *FGFR2* gene amplification. FGFR2 inhibitors have the potential to disrupt several beneficial homeostatic processes, including cytoprotective mechanisms against environmental insults, such as UV irradiation, X-ray irradiation, chronic infection, and tobacco smoke. Future studies will determine whether the benefits of FGFR2 inhibitors outweigh their risks (Katoh, 2009)

In light of these established data concerning FGFR2, I wanted to broaden understanding of the role of this protein in the complex biology of cancer development and progression.

4.2 Results

Given that the tumour suppressive role for *Fgfr2b* in mouse skin (Grose et al., 2007) was discovered in our lab, I wanted to check whether the receptor can play a similar role in human skin. In collaboration with Karin Purdie and Catherine Harwood (ICMS, Barts and The London), I have begun to investigate FGFR2b in human skin using histochemical, molecular and cell biological approaches.

4.2.1 *FGFR2* genomic sequence in SCC keratinocyte cell lines

As a first approach to investigate *FGFR2* in human skin cancer, I obtained six cell lines derived from squamous skin carcinoma patients (see above). After extracting genomic DNA, I attempted to amplify each of the 18 exons of *FGFR2* using PCR, thus enabling possible detection of any deletions as well as providing DNA for subsequent sequence analysis. Initial findings suggested lack of one exon in all six SCC cell lines isolated from patient tumours. Exon 11 was detectable in DNA isolated from an hTERT immortalised normal human keratinocyte, NTERT, but not in the SCC cell lines (Fig 4.2). Performing gradient temperature PCR, I established the optimal annealing temperature (66.6°C) for generating the exon 11 specific product and, despite the initial findings, subsequent PCR amplified the band of interest in all samples, although the amplification was highly dependent on DNA quality (Fig 4.3). “Old” DNA samples, obtained at the same time as the cell lines, yielded an extremely weak band when resolved on a 2% Agarose/TBE gel, whereas “new” freshly prepared DNA samples gave a clear single band of the expected size.

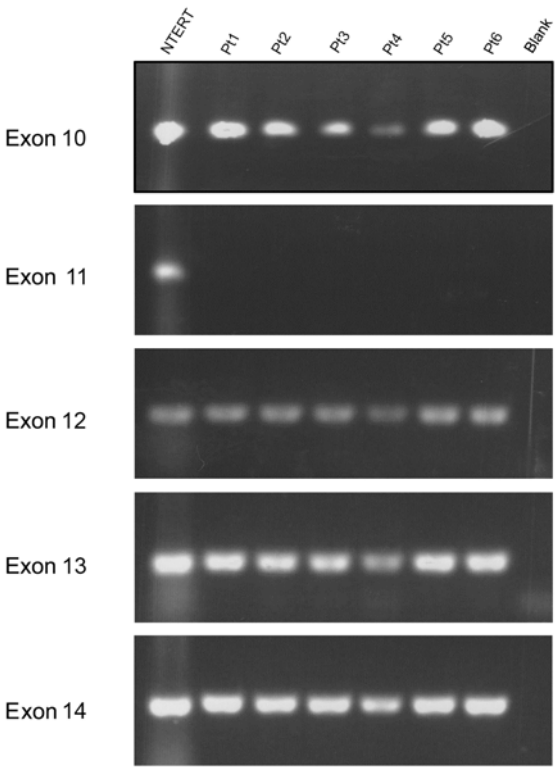

Figure 4.2 Human *FGFR2* PCR analysis. PCR analysis of genomic DNA isolated from 6 primary human SCC cell lines (Pt1-6), generated from patient tumours, and control normal human keratinocytes transduced with hTERT (NTERT cells). The results reveal the absence of the exon 11 of *FGFR2* in all 6 SCC samples.

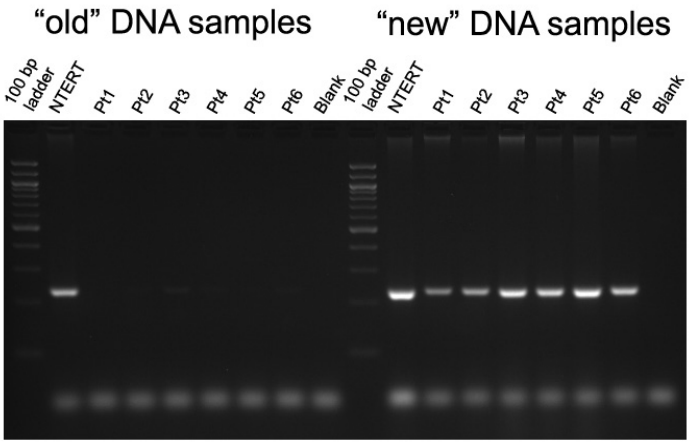

Figure 4.3 Human *FGFR2* exon 11 analysis. PCR analysis of exon 11, as described above, was repeated with a higher annealing temperature (66.6°C), which was established after performing a PCR gradient of temperatures for old DNA samples – left panel, and new DNA samples – right panel. Results show that exon 11 of *FGFR2* is present in all 6 SCC samples but that the quality of input DNA affects its detection.

4.2.2 *FGFR2* mutation screening

A single nucleotide change (point mutation) in the coding region of a gene can have profound biochemical and physiological consequences on an organism. Well characterised examples of such changes are the germline gain of function mutations in *FGFR1, 2* and *3* causing craniosynostosis and chondrodysplasia syndromes (Wilkie, 2005). Mutations in the *FGFR2* gene were also reported in breast, endometrial and gastric/colorectal cancers (Stephens et al., 2005). Guided by these reports, I decided to screen the *FGFR2* coding sequence for mutations in skin cancer. A PCR based assay was used to identify mutations in genomic DNA isolated from SCC cell lines. Initially I concentrated on screening exons that already were known to carry mutations in the above pathologies – exons 7, 10, 13 and 15. The first attempt to perform direct sequencing of a PCR product was aborted due to the imprecise electropherograms obtained and thus the very low probability of detecting heterozygous mutation. Instead I cloned the PCR product using TOPO® vector and then sequenced the cloned PCR products from four positive clones per exon (Fig 4.4). In the process of sequence analysis, eleven mutations were identified, one of which had been reported previously (Fig 4.5). Five identified mutations were localised in exon 7, encoding the IIIa part of the D3 extracellular domain, one mutation in exon 10, encoding the transmembrane domain of the receptor, and a further three in the kinase domains (Fig 4.5). These results were encouraging, as it is well known that within exon 7 several different regions are recognised as hot spots for germline activating mutations (Kan et al., 2002). All identified changes were single base pair substitutions resulting in missense mutations, with the exception of two synonymous mutations that did not affect the amino acid sequence and one single nucleotide deletion causing change of reading frame. Four independent mutations were identified in the patient 2 (Pt2) cell line and three in patient 5 (Pt5). In both cases, the cell lines were derived from

moderately differentiated tumours. Three out of eleven found mutations were confirmed by specific restriction enzyme digestion (Fig 4.6).

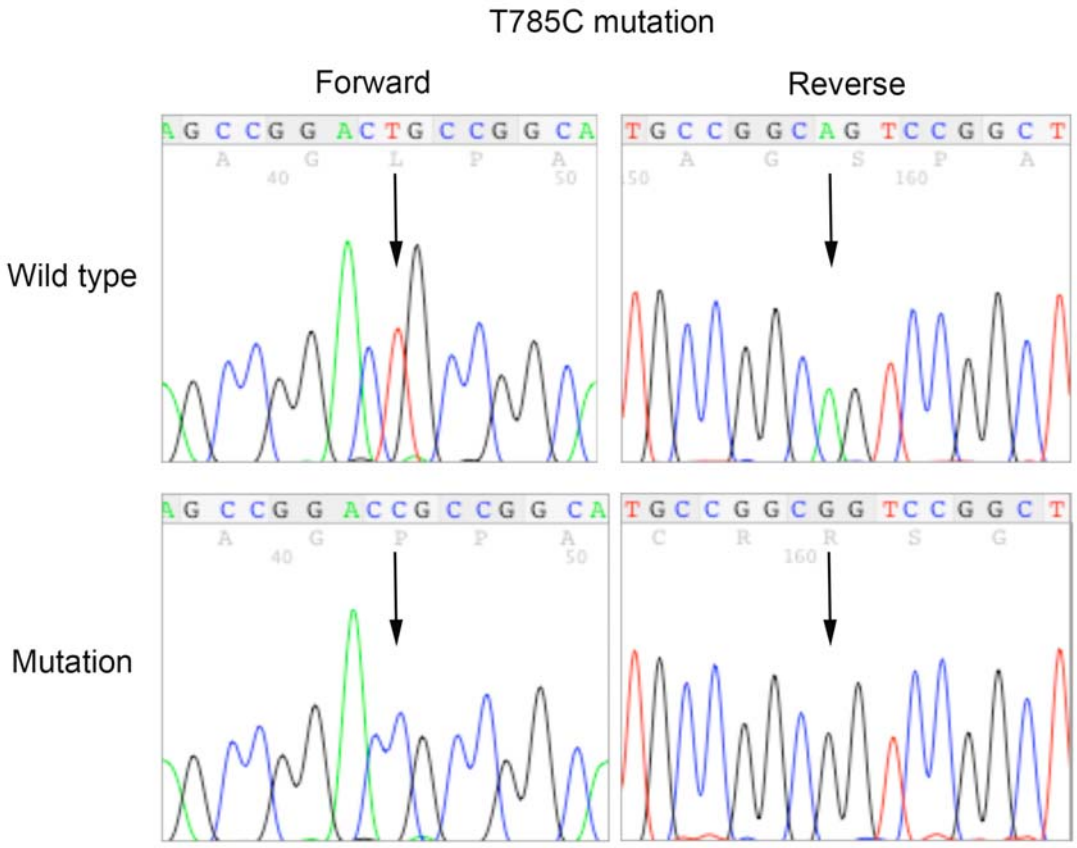

Wild type	Mutation	Position
AAGGTTTACAGTGATG	AAGGTTCACAGTGATG	T841C
AACGGCAGTAAATACG	AACGGCAGCAAATACG	T897C
CGGCAGTAAATACGGG	CGGCAGTAGATACGGG	A899G
GGCAGTAAATACGGGC	GGCAGTAAGTACGGGC	A900G
AAGAACACGACCAAGA	AAGAACGCGACCAAGA	A1210G
ACGTATCCCCCTGCGG	ACGTACCCCCCTGCGG	T1268C
CGCTGGTGAGGATAAC	CGCTGGTGCGGATAAC	A1339C
TCCTATGACATTAAC	TCCTATGGCATTAAC	A1769G
GCAGCCAGAAATGT	GCAGCCAGAAATGT	A1895G
GATGAAAATAGCAGA	TCCTATG_CATTAAC	1923_1925delA

Figure 4.4 Somatic mutations identified in the human *FGFR2* sequence. An example of sequence electropherograms of mutation (arrowheads) found in

human skin squamous cell carcinoma cell line and the corresponding normal sequence. Genomic DNA was isolated from 6 SCC cell lines from patient tumours. *FGFR2* exons from each cell line were amplified by PCR and cloned into TOPO vector. Four clones per sample were identified by PCR and the reaction product was sequenced. All identified mutations are shown in the table.

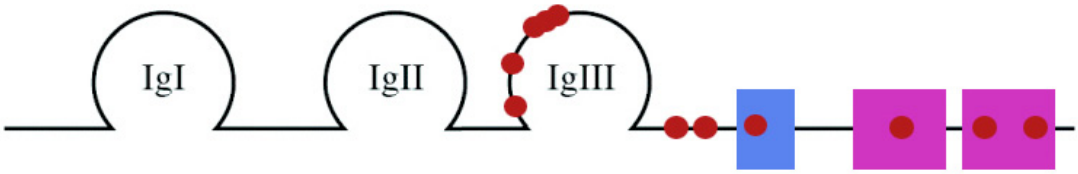

Figure 4.5 A schematic representation of *FGFR2* and the locations of identified mutations. FGFR schematic structure of three Ig-like domains (Ig I–III), a transmembrane domain (blue box) and a split tyrosine kinase domain (pink boxes). Red circles indicate areas where point mutations have been identified. The table below gives more detail of identified mutations in human SCC cell lines (numbering relative to NM_022970.0 and NP_075259.2). *Crouzon syndrome, **Pfeiffer syndrome.

Case	FGR2b nucleotide	FGFR2b codon	Previous reports
Pt1	T785C	L262P	no, but P263L yes in CS*
Pt5	T841C	Y281H	yes, but Y281C in CS*
Pt2	T897C	S299S	no
Pt4	A899G	K300R	no, but Y301C yes in CS*
Pt6	A900G	K300R	no, but Y301C yes in CS*
Pt2	A900G	K300K	no, but Y301C yes in CS*
Pt2	A1210G	T404A	no
Pt1	T1268C	I423T	no
Pt5	A1339C	R447R	no
Pt2	A1769G	D590G	no
Pt5	A1895G	N632S	no
Pt6	1923_1925delA	I641del+change of reading frame	no, but K641R yes in PS**

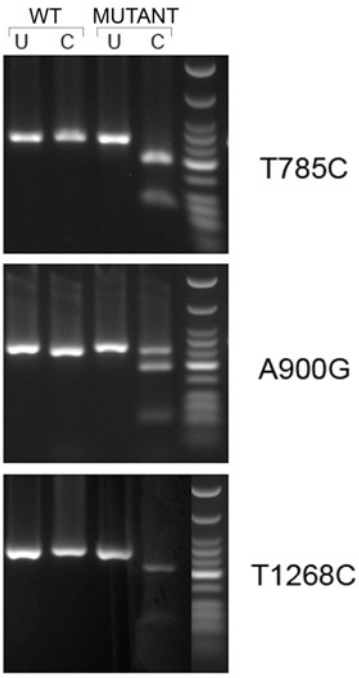

Mutation	Restriction enzyme	Cutting site	Products size in wild type sample	Product size in mutated sample
T785C	AvaII	g/gwcc	271bp	74bp and 197bp
A900G	RsaI	gt/ac	15bp and 256bp	15bp, 63bp and 193bp
T1268C	AvaII	g/gwcc	291bp	71bp and 220bp

Figure 4.6 Mutation-specific restriction enzyme digestion. PCR products were obtained from TOPO vector clones. The identified mutations were analysed by specific restriction enzyme digest. The digested PCR products, (U) uncut and (C) cut with appropriate enzyme, were analysed by 2% Agarose gels and the DNA was visualised by staining with ethidium bromide. Restriction enzymes, cutting sites and the expected fragments sizes for the wild type and mutant alleles are shown in the table.

4.2.3 SCC cell lines express the FGFR2IIIb splice isoform

A switch in splice variant of FGFR2 causes dramatic differences in ligand binding specificity, thereby affecting receptor signalling. Thus, the choice of splice isoform expressed might be of great importance in cancer development and progression. To determine whether the mechanism of isoform switching is relevant in skin cancer I wanted to know which FGFR2 splice variant was present in a panel of SCC cell lines.

In the first step, cDNA corresponding to the receptor sequence was amplified by RT-PCR. Primers for the reaction were designed to span the third Ig-like extracellular domain and the transmembrane domain of the receptor (cartoon in Fig 4.7) and amplify a 290 bp product, in the case of FGFR2IIIb isoform, and 287 bp, for the IIIc isoform. Since such a small difference in the product size could not be resolved by Agarose gel electrophoresis, products were digested with specific restriction enzymes to detect the alternative isoforms. Digestion of the FGFR2 PCR product with AvaI resulted in cleavage products of 182 and 108 bp, indicating the presence of the IIIb isoform. Contrastingly, digestion with HincII resulted in products of 119, 115 and 53 bp, indicating the presence of the IIIc isoform. Unfortunately, the digestion of RT-PCR products did not reproducibly distinguish the splice isoform of the FGFR2 expressed by SCC keratinocytes cell lines. Depending whether the primers used for PCR, were based on human or mouse sequence (which share 70% homology), specific yet contradictory results were obtained. To find out whether cell line passage number influenced the results, I went back to the stock of lowest passage number cells but that did not clarify the issue. Therefore, I checked whether the results were dependent on the level of confluence to which the cells were grown prior to RNA extraction. The experiment was repeated with a control human keratinocyte cell line (HaCaT) and

two SCC cell lines (Pt1 and Pt2) grown to 1%, 50%, 80% and 110% of confluency, only to reprise the previous confusing results (Fig. 4.8 A and B). The results indicated that the expressed splice variant depended only on the choice of primers used for RT-PCR analysis. Finally, sequencing of the PCR product obtained with mouse specific primers revealed that a mouse *Fgfr2c* sequence was amplified in this reaction, suggesting that the human keratinocyte cell lines were contaminated with murine fibroblasts. Furthermore, when cells were grown to overconfluence, patches of elongated, fibroblastic cells were observed in the culture dish (Fig 4.9). In the mean time though, some organotypic experiments were performed with the abovementioned cell lines and normal human keratinocytes (HaCaT) grown on top of collagen layer enriched with dermal fibroblasts. In organotypic culture experiments I wanted to assess cancer invasion and progression. The morphology of SCC compared to HaCaT cells in the co-culture appeared to be very different. Normal keratinocytes were organised into continuous and compact layers, which resembled differentiated epidermis, whereas SCC cells were enlarged, had many vacuoles and were scattered with very little cell-cell contact (Fig 4.10). Again, altered cell appearance may be due to fibroblast contamination. Since I learned about this contamination the organotypic culture experiments were abandoned. Had I had more time available I could have used single cell cloning to re-derive a pure epithelial cell population prior to re-embarking on these experiments.

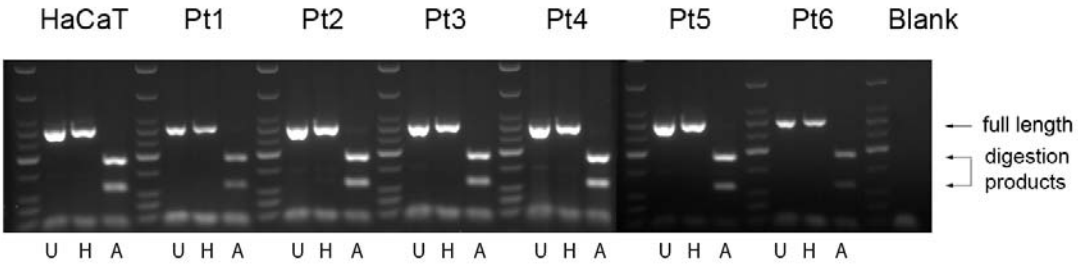

Figure 4.7 Identification of *FGFR2* splice isoform expressed in HaCaT and SCC cell lines. RT-PCR was performed on HaCaT and SCC cell line cDNA with human sequence specific primers spanning the third Ig-like loop of the extracellular domain and the transmembrane domain. The forward primer is located in the IIIa domain and the reverse primer in TM domain, as illustrated in the cartoon below. PCR products were then digested with HincII (H) and AvaI (A) restriction enzymes, which recognise IIIc and IIIb splicing isoforms respectively. Digestion reaction products were run on a 2% Agarose/TBE gel alongside full length, undigested PCR product (U). Results indicate that all tested SCC cell lines expressed epithelial specific IIIb isoform of FGFR2.

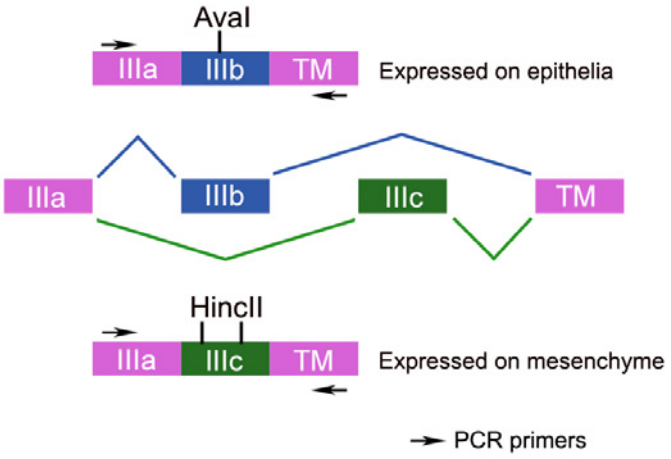

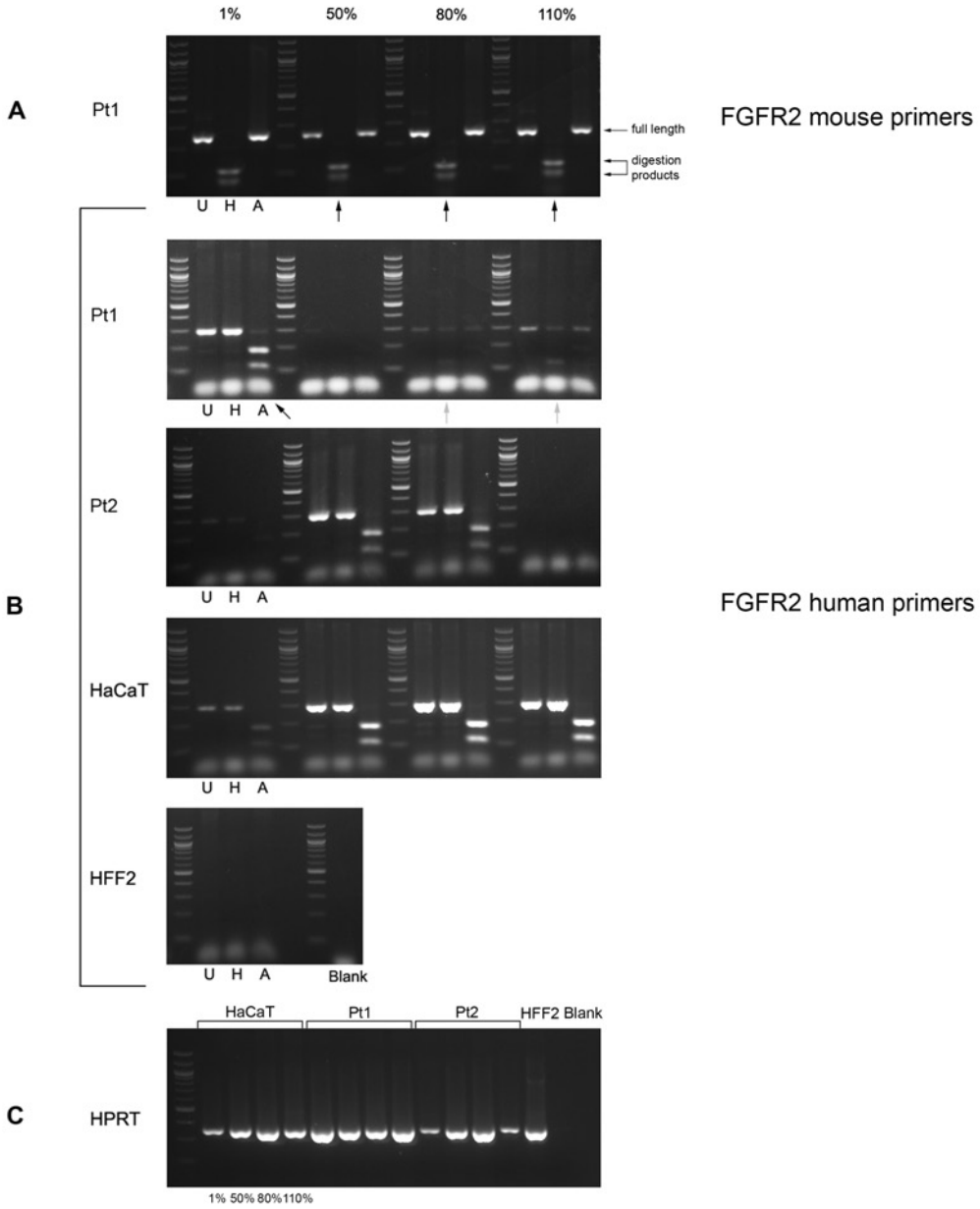

Figure 4.8 Identification of *FGFR2* splice isoform expressed in HaCaT, Pt1 and Pt2 SCC and HFF2 cell lines, dependent on cell confluence. RT-PCR was performed on HaCaT cells and two SCC cell lines grown to 1%, 50%, 80% and 110% confluence. Human Foreskin Fibroblast cell line (HFF2) cDNA was used as a control for *FGFR2* expression. Used primers spanning the IIIa and TM domain were specific to *FGFR2* A) mouse sequence B) human sequence. Contradictory

results were obtained in the case of Pt1 cells, where cells expressed either the IIIc isoform (arrows in A) or the IIIb isoform (black arrow in B) of FGFR2. (B) At low confluence, Pt1 cells expressed the IIIb isoform, whereas at high confluence the IIIc isoform was expressed (grey arrows). (C) *HPRT* primers were used as a control for RNA quality and concentration. (U) undigested PCR products were run alongside PCR products digested with HincII (H) and AvaI (A) restriction enzymes. Blank PCR without cDNA.

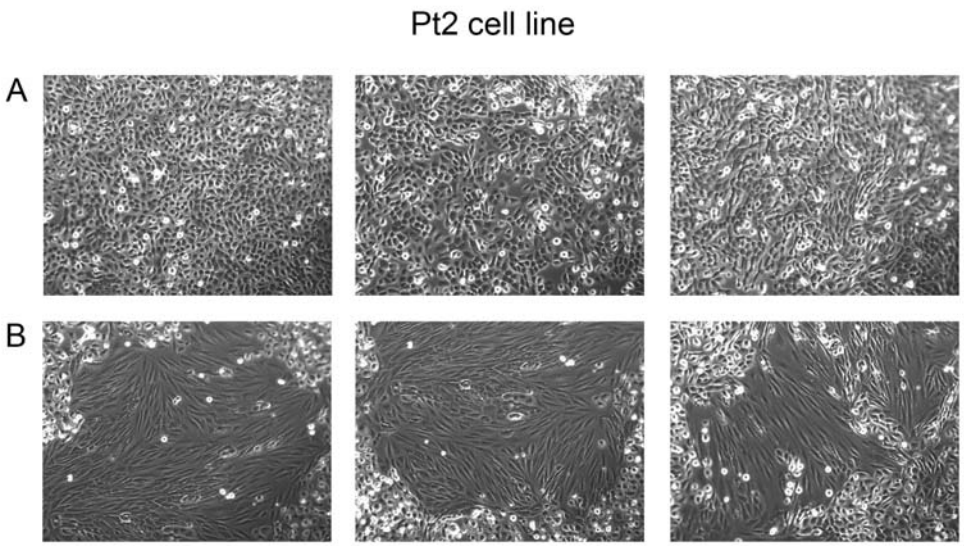

Figure 4.9 Pt2 cell line. A) Pt2 cells grown to confluence show dense cobblestone appearance by phase contrast microscopy. B) In the same culture dish, areas of elongated, fibroblastic cells were observed.

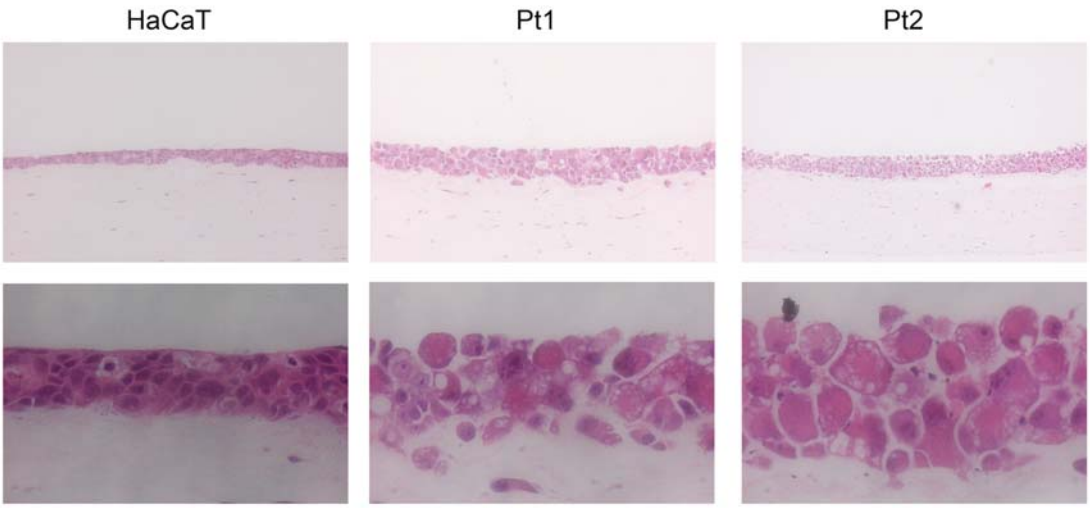

Figure 4.10 Organotypic culture of skin equivalent. Normal human keratinocytes (HaCaT) and human SCC keratinocytes (1×10^6) were plated on top of the stroma consisting of collagen and human fibroblasts (5×10^5), as shown in the scheme below, and co-cultured for 6 days. Images shown are of 6 day cultures, fixed, sectioned and stained with H&E.

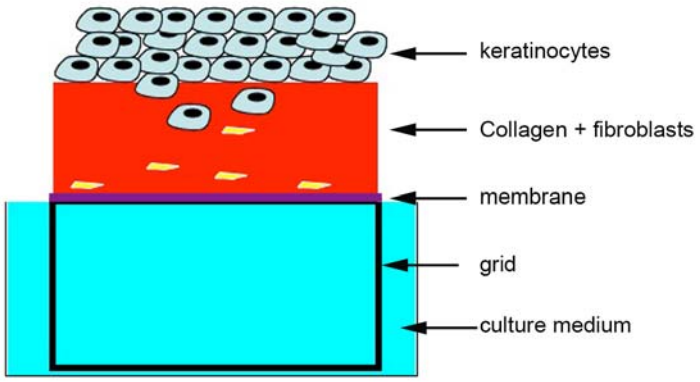

4.2.4 FGFR2 expression in normal human skin and human squamous cell carcinoma

Immunostaining of normal human skin sections showed a strong cell membrane staining for FGFR2 in the epithelium (Fig. 4.11 A, B, D). FGFR2 staining was also visible in normal skin fibroblasts, since the anti-FGFR2 antibody was targeted against a C-terminal epitope and thus recognised both epithelial IIIb and mesenchymal IIIc receptor isoforms. However, immunoreactivity of FGFR2 was more intense in the epidermis compared with dermis. In contrast to normal skin, FGFR2 is seen throughout the nucleus and cytoplasm in SCC sections (Fig 4.11 C, E).

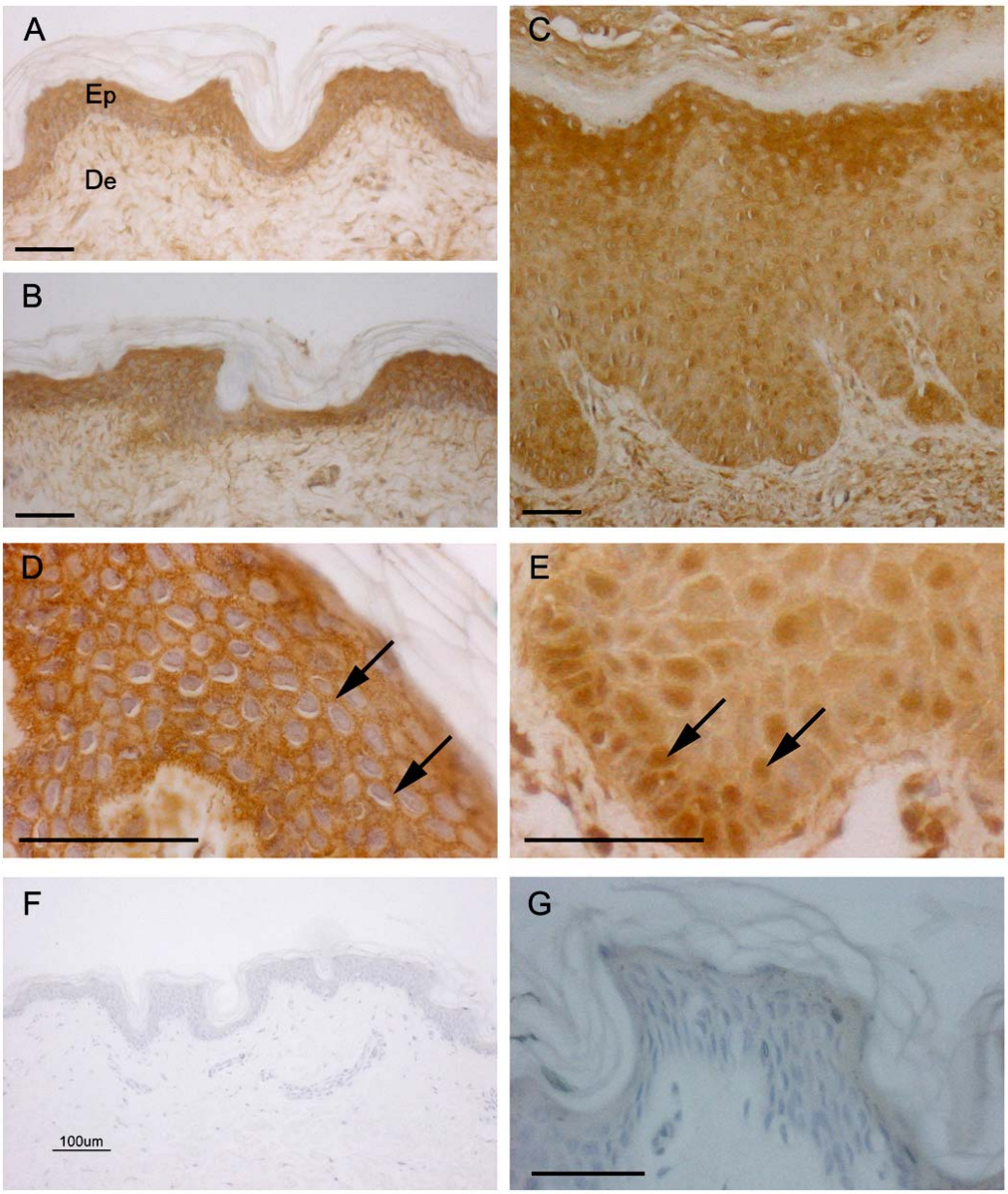

Figure 4.11 Anti-FGFR2 immunostaining. Immunostaining was performed on sections from normal human skin (A, B, D and F) and human SCC (C, E and G). Skin sections show expression of FGFR2 in both epidermis (Ep) and dermis (De). In normal skin sections, the epidermal staining is localised to the cell surface (arrows in D). However, in SCC this pattern is absent, with staining seen throughout the nucleus and cytoplasm (arrows in E). Negative controls using the

same staining protocol but with an isotype specific control antibody show no positive staining (F and G). Scale bars (50 μm) in all but F (100 μm).

4.3 Discussion

FGFR2 appears to play a paradoxical role in cancer, depending on the tissue type and pathology. While some studies have suggested that increased expression of FGFR2b raises breast cancer risk, data from our lab and others suggest that it also can act protectively, particularly in mouse skin (Grose et al., 2007). One of the aspects of my project was to verify whether it plays a similar role in human skin, by investigating SCC cell lines isolated from patient tumours.

Firstly, the genomic organisation of *FGFR2* was examined in a search for obvious alterations. Initially, an exciting result was obtained with exon 11 PCR product missing in all DNA samples from SCC cell lines (Fig 4.2). Exon 11 encodes the juxtamembrane domain of FGFR2, which is a docking site for the main downstream signalling molecule FRS2 (Eswarakumar et al., 2005). Lack of this docking site could, potentially, block the two main signalling pathways of FGFR2 activation and abolish its tumour suppressive character. Unfortunately that result later turned out to be an artefact caused by using old DNA as a template (Fig 4.3). The quality of DNA is dependent on extraction and storage conditions. Some DNA samples' are highly fragmented or damaged by preservation procedures, while others are better preserved and will give different results in a PCR-based assay. Several methods are commonly used to assess DNA quality like gel electrophoresis, Southern blot or gene-specific PCR. Although these methods provide information on the degree of DNA fragmentation, not all can predict the samples ability to support PCR (Siwoski et al., 2002). If researchers do not pre-screen samples for DNA quality, but rather directly measure the status of a gene, screening it for mutations by single or multiplex PCR, the obtained results might not be reliable.

Secondly, the above PCR products were cloned and screened for mutations in the coding sequence of the gene (Fig 4.4). It is well documented that mutations in ligand binding domain (D3) of FGFR2 and FGFR3 arise in patients with gastric and colorectal cancers (Jang et al., 2001), endometrial cancers (Pollock et al., 2007) and melanomas (Gartside et al., 2009). Furthermore, activating mutations of *FGFR3* occur at a high frequency in bladder carcinoma and at a low frequency in B-cell lymphoma and cervical carcinoma (Chaffer et al., 2007). My screening resulted in identification of eleven different point mutations, localised in the ligand binding domain and the transmembrane domain of FGFR2 (Fig 4.5). One of those mutations, Y281C, was previously reported in Crouzon syndrome - a genetic disorder causing craniofacial synostosis (Kan et al., 2002). The fact that this mutation was discovered in a developmental disorder and not cancer was not discouraging. In endometrial cancer, twelve different mutations were identified in *FGFR2*, seven of which were the same as those associated with craniosynostosis and chondrodysplasia syndromes (Pollock et al., 2007). On the other hand, over 20 novel mutations having a great impact on FGFR2 receptor functionality were identified recently in melanoma tumours (Gartside et al., 2009). One of the novel mutations, that I identified in SCC samples, which did not affect the reading frame (K300R – A900G), was present in two independent cell lines, which was very encouraging. Even though one study suggested that there was no association between *FGFR2* mutation and patient survival in endometrial cancer (Zhao et al., 2008), the prevalence of these mutations provides a rationale for using FGFR inhibitors as an adjuvant therapy to treat cancer patients.

Another potentially interesting result obtained concerns the splicing isoform of FGFR2 expressed by SCC cell lines. Despite problems with murine fibroblast contamination, there was a definite change in splice isoform of FGFR2 depending on cell confluence (Fig 4.8). However, it might just be that the observed incidence

of exon switching is due to fibroblast cell contamination. It has been reported before that when SVK14 human keratinocyte cells, seeded at low density, were cultured in the presence of exogenous FGF1 or FGF2, a partial IIIb to IIIc switch of FGFR2 was observed, while cells cultured at low density in standard medium expressed only IIIb transcripts. In contrast, when the cells were at confluency before addition of FGF1 or FGF2, this switch in isoform expression was not seen (Scotet and Houssaint, 1998). A very similar result of IIIb to IIIc switch, complemented by morphological changes characteristic for EMT (epithelial mesenchymal transition), was recorded for the NBT-II carcinoma cell line stimulated with FGF1 (Savagner et al., 1994). It is possible therefore, in my experiments, that contaminating mouse fibroblasts stimulated human keratinocyte SCC cells by secreting FGFs to switch the FGFR2 splice isoform. As described before, the change in FGFR2 variant expression modifies cellular response to growth factors. Unfortunately, also because of contamination, my organotypic co-culture experiments did not provide any new information into understanding of SCC pathogenesis.

Discovery of murine fibroblast contamination was very disappointing but, on the other hand, it was fortunate that the contamination was discovered quite early on in the process of SCC cell line characterisation. That is the opposite to, for example, the human thyroid endothelial cell case. The European Collection of Cell Cultures (ECACC) after multiplex analysis of the mentioned TEC61 cell line, described by Patel et al. in American Journal of Physiology, 2003 (Patel et al., 2003), proved that the cell line was in fact identical to the JEG3 cell line. The JEG3 cell line was derived from a human choriocarcinoma, and the cell-conditioned medium from this line was used to support the growth of the putative endothelial cell line. No early-passage cells exist, so it is not possible to determine when cross-contamination occurred. Since the overall premise and conclusions of

the paper could no longer be assured, the authors had to retract the paper in June 2009.

In fact, estimates of the incidence of research papers flawed by the use of misidentified and cross-contaminated cell cultures approximate 15-20% (Nardone, 2007). But, there are even more worrying news as, for example, Liscovitch and Ravid reported that DNA fingerprinting analysis revealed that the NCI/ADR-RES cell line is actually an ovarian tumor cell line, OVCAR-8, rather than a breast cancer cell line. NCI/ADR-RES is included in the National Cancer Institute (NCI) panel of 60 cell lines distributed for evaluation of potential anti-cancer drugs (Liscovitch and Ravid, 2007). The same authors estimate that about 300 papers have been published with the incorrect identification. The importance of absolute certainty regarding cell line authenticity in biomedical research, cannot be stressed strongly enough.

According to the classical theory of signal transduction, the role of a membrane-associated growth factor receptor is to transmit signal from the extracellular environment to the cytoplasm, where other cytoplasmic proteins and kinases serve as second messengers propagating the signal downstream to the nucleus. However, nowadays it is well known that this is not the only scenario of signal transduction. For example, it was established that cell surface FGFR1 redistributes to a cytoplasmic-perinuclear location after cell stimulation by exogenous ligand (Prudovsky et al., 1994). FGFR1 is also able to traffic to the nucleus, where its majority is found in a patchy distribution within the nuclear matrix, at which point it remains functional (Stachowiak et al., 1996). Nevertheless the question of nuclear FGFR1 function remains unanswered, even though there are numerous suggestions that receptor role is associated with specific regions of nuclear matrix. It has been speculated that nuclear growth factor receptors may

act as weak transcription factors, topoisomerases and/or nuclear kinases. Another function of nuclear FGFRs may be phosphorylation of nuclear substrates, as the forced nuclear translocation of FGFRs leads to an increase in the phosphorylation of nuclear proteins, and some activities of the nuclear receptor are abolished by deactivation of the kinase domain (Schmahl et al., 2004). Observed FGFR2 nucleus translocation (Fig 4.11) is presumably stimulated by demand for increased gene transcription, granting advanced keratinocyte proliferation associated with SCC progression.

4.4 Future directions

Given more time, I would have liked to have continue my mutation screening to identify more *FGFR2* mutations in human skin SCC samples, hoping to be able to find a link between the frequency and location of their occurrence and the nature of skin cancer. Thus far, the Human Gene Mutation Database (HGMD) reports 95 independent mutations in the *FGFR2* gene, but there is nothing to suggest that this list is exhaustive. Through my studies, I hoped to be able to add to this catalogue of mutations and to determine the potential roles of those mutations associated with skin cancer. Unfortunately the model for my research was far from perfect, as the SCC cell lines used for DNA sequencing turned out to be contaminated with mouse fibroblasts. Although all the identified mutations were true human gene mutations, not homologous with mouse gene sequence, the SCC cell lines did not provide a good model for any kind of functional assays. A good cell-based assay for the pathogenesis study of SCC would involve pure human SCC keratinocytes, which can be characterised by cell viability, death, clonogenicity and migration or invasion measurements. None of those would bring informative results if keratinocyte growth was stimulated via growth factors secreted by fibroblasts.

In the future it will be important to confirm that the identified mutations are of somatic origin and are not germline mutations. I hope that these preliminary results are exciting enough to start a high throughput sequencing experiment with a large number of human skin SCC samples.

I would also like to continue work on the change of expression of the FGFR2 splicing isoform. I would like to check whether it is dependent purely on cell confluency or, perhaps, on the presence of fibroblast contamination. In order

to do that I could single cell clone, as mentioned already, or I could try to eliminate fibroblast contamination by differential trypsinisation, when the culture is exposed to sterile Hank's Buffered Salt Solution containing 0.05% trypsin. The junctions formed between the epithelial cells limit access of trypsin, thus the nonepithelial fibroblasts detach from the plate first and can be carefully removed. This procedure, when repeated several times at 5-7 days intervals, is reported to enrich the purity of epithelial cell culture. With the use of antibodies directed against epithelial markers, magnetic-activated cell sorting or immunofluorescence cell sorting (FACS) also can be used to remove fibroblast contamination.

The observed differences in immunostaining of skin tumours might have their explanation in FGFR2 splice isoform switch, but while *In situ* hybridisation studies with exon specific probes would give useful data, until reliable isoform specific antibodies are available this will be hard to determine.

CHAPTER 5

FINAL DISCUSSION

CHAPTER 5: Final discussion

Deregulation of fibroblast growth factor receptor signalling pathways increasingly has been recognised to play an important role in the pathobiology of many malignancies. Communication between epithelia and mesenchyme/stroma, critical for organogenesis and carcinogenesis, is mediated by those pathways. The effects of disrupted signalling are wide ranging and involve enhanced proliferation, resistance to cell death, increased motility and invasiveness, increased angiogenesis, enhanced metastasis and resistance to chemotherapy and radiation (Kwabi-Addo et al., 2004). However, the underlying mechanism of how aberrant FGF signalling leads to tumour formation and progression is far from clear.

The justification supporting further research into cancer biology is clear. There are more than 100 different types of cancer and on average 293,000 newly diagnosed cancer cases each year in the UK (from 2004–06), with around 147,000 cases among males and 146,000 among females. The three most common cancers are prostate, lung and colorectal for males, and breast, lung and colorectal for females. There were, on average, 154,000 deaths from cancer each year in the UK (from 2004–06), with around 80,000 deaths among males and 74,000 among females (Office for National Statistics, Cancer incidence and mortality Statistical Bulletin - August 2009). That is equivalent to the population of Peterborough in England disappearing every year.

In the 35 years since the first FGF was discovered, the FGF family has expanded to 22 ligands that signal through tyrosine kinase receptors (Ornitz, 2000). The list of *Fgf* and *Fgfr* knockout mice is almost complete and, coupled with data from many other animal model systems, it provides essential knowledge of

the wide spectrum of physiological roles played by those growth factors in development, disease and repair. For instance, studies on chick embryos determined that FGFs are essential for limb bud outgrowth and patterning (Martin, 1998) as well as neural induction (Streit et al., 2000), whereas the effect of FGFs on mesoderm formation was first demonstrated and most extensively studied in *Xenopus* (Isaacs, 1997). Invertebrate model organisms, such as *Drosophila melanogaster* and *Caenorhabditis elegans,* turned out to be relatively simple and genetically tractable systems for studying various aspects of FGF signalling. The only known Fgf in *Drosophila* - *branchless* is involved, as its name implies, in branching morphogenesis and its receptor, *breathless*, is expressed in the developing tracheal system (Reichman-Fried et al., 1994). A second Fgfr in *Drosophila, heartless,* is necessary for heart formation and mesodermal cell migration (Shishido et al., 1997), while *egl-15*, encoding the only Fgf receptor in *C. elegans*, plays a crucial role in gonad development (Huang and Stern, 2005). By contrast, the Fgf family in zebrafish, a widely used vertebrate model for studying morphogenesis and metabolism, comprises twenty-seven Fgf family members (Itoh, 2007).

The main focus of my PhD was to investigate the role of FGF22 in development and tissue homeostasis, using a knockout mouse model, and thus contribute to a fuller understanding of the broad field of FGF biology. To date, only *Fgf20* and *Fgf22* knockout mice still remain undescribed in the literature but, despite this almost complete coverage, it is very likely that additional roles for already described FGFs will be identified in the future, as more physiological challenges are performed in knockout mouse models.

Summary of my principal results:

FGF22 is not essential for normal embryogenesis.

FGF22 is not required for normal postnatal development.

FGF22 is not necessary for skin homeostasis and repair.

Fgf22 knockout mice exhibit resistance to chemical carcinogenesis.

Fgf22 knockout mice display a significant weight loss phenotype.

Fgf22 knockout mice show thinning of retinal layers in the eye.

FGF22 is expressed throughout the digestive tract, in particular in the oesophagus and stomach.

These key observations support the conclusion that FGF22 is not essential for embryonic and postnatal development, contrary to previous expectations. Moreover, despite its up-regulation in the hair follicle (Nakatake et al., 2001) and in the healed wound epidermis (Beyer et al., 2003), FGF22 is not required for normal hair development, neither is it essential for efficient wound healing. Furthermore, FGF22 clearly is not a critical modulator of presynaptic organisation in developing brain (Umemori et al., 2004), since knockout mice develop normally and do not display any distinctive behavioural defects. However, FGF22 does appear to play a potential oncogenic role in skin tumorigenesis - an entirely unexpected phenotype given its postulated negative role during epithelial repair (Beyer et al., 2003).

An additional surprising finding was that FGF22 appears to be involved in control of body weight. Discovery of *Fgf22* expression through the digestive tract further increased my interest in this area. Although it is well established that FGFR2b signalling is essential for digestive tract development (Burns et al., 2004), the involvement of its ligand FGF22 in the system was unforeseen. It is recognised that absence of embryonic expression of *Fgfr2b* or *Fgf10* results in intestinal atresia (Fairbanks et al., 2004). Likewise, foetuses lacking *Fgfr2b* or *Fgf10* develop smaller stomachs than wild type littermates, with a disproportionately severe reduction in the development of the glandular stomach (Spencer-Dene et al., 2006). Building on these foundations, the pattern of *Fgf22* expression in the gastro-intestinal tract is illustrated for the first time. Despite relatively high expression levels in the oesophagus and stomach, the role for *Fgf22* within the digestive system remains unclear, since knockout mice do not demonstrate any phenotype in the unchallenged state. All the same, the pattern of *Fgf22* expression is intriguing in the context of regulation of food intake.

The key feature of the system regulating food intake is that most, if not all, of the peptides that influence satiation are made in the digestive tract and are also synthesised in the brain (Woods and D'Alessio, 2008). Likewise, *Fgf22* is expressed in both compartments and its abrogation causes weight loss. In these circumstances, one can hypothesise that *Fgf22* affects satiation by stimulating food intake. There is only one other known gastro-intestinal hormone of similar function: ghrelin, a product of specific endocrine cells in the stomach and duodeum that relays a message to its receptors localised in the hypothalamus (Woods and D'Alessio, 2008). The above findings open a completely new aspect of studying the potential involvement of *Fgf22* in control of body weight and feeding behaviour.

Providing greater understanding into the role of FGF and FGFR interactions involved in normal and pathological conditions was a goal of my studies. Thus, in a parallel arm of my project, I wanted to investigate the tumour suppressive character of *Fgfr2* in the skin, focusing on translating earlier mouse findings (Grose et al., 2007) into a human model. This investigation was based on characterising SCC cell lines, isolated from patient tumours, in terms of their expression of *FGFR2* and any associated genetic mutations.

Summary of my principal results:

Frequent *FGFR2* mutations are detected in SCC cell lines.

FGFR2 splicing is dependent on cell confluency.

FGFR2 shows a specific change in expression pattern in SCC.

The *FGFR2* mutations in SCC cell lines that I identified were localised in the ligand binding and transmembrane domains of the receptor. However, the character of novel mutations was not determined. Further analysis, including mapping of identified mutations onto the known crystal structures of FGFR2 followed by *in vitro* and *in vivo* studies would be required to pursue this project. However, one can speculate that novel mutations are loss-of-function mutations, as essentially that would be consistent with previous findings of the tumour suppressive character of *Fgfr2* in murine skin (Grose et al., 2007). Moreover, these type of mutations recently have been reported in human melanoma, where *FGFR2* is thought to lose its activity through several distinct mechanisms, including loss of ligand binding affinity, impaired receptor dimerisation, destabilisation of the extracellular domains and reduced kinase activity (Gartside

et al., 2009). Hypothetically, these mutations can also affect *FGFR2* splicing, causing inappropriate FGFR2c isoform expression in the epidermis, which is in keeping with *in vitro* findings. Consequently that can cause, stimulated via an autocrine signalling loop, rapid and uncontrolled keratinocyte proliferation. On the other hand, if the identified mutations are of activating character then the receptor can drive malignant cell growth in an exclusively ligand independent manner.

Recent studies have established that *Fgfr2b* and *Fgfr1b* are essential for maintenance of skin homeostasis and epidermal barrier function. *Fgfr2b/Fgfr1b* receptor double knockout mice show a defective skin barrier and develop epidermal hyperthickening with age, as a result of chronic inflammation (Sabine Werner - personal communication). Given that *Fgf22* knockout mice do not phenocopy those changes, *Fgf22* clearly is not essential for normal skin physiology. Nevertheless, there is an obvious discrepancy in phenotypes that we must consider. *Fgfr2b* null mice show great sensitivity to chemically induced carcinogenesis whereas, contrastingly, *Fgf22* knockout mice are more resistant to carcinogenesis insult than wild type littermates. It is intriguing that, in these particular circumstances, the ligand and its receptor appear to have antagonising effects, with a putative tumour suppressive receptor appearing to be activated by an oncogenic ligand. It is not a groundbreaking theory, since it is recognised that at least several members of the FGF family have oncogenic potential and are implicated in different cancers such as leukaemia and Kaposi's sarcoma (Delli Bovi et al., 1987).

Fgf22 expression in the hair follicle in normal skin is most likely involved in regulation of FGFR signalling, but redundancy in the system prevents occurrence of an overt phenotype in knockout mouse. During wound healing, in contrast to FGF7 and FGF10, which appear to drive the healing process, FGF22 expression

is up-regulated towards the end of repair (Beyer et al., 2003). Thus my hypothesis was that it acts as a negative regulator of FGFR2 signalling, either by decreasing proliferation or increasing differentiation. However, since *Fgf22* knockout mice do not present a wound healing phenotype, it is possible simply that natural decrease in expression of pro-mitogenic ligands is sufficient to turn off the epithelial healing process. Therefore once again there is redundancy within the system.

Figure 5.1 Graph representing changes in *Fgfs* expression during *in vivo* wound healing.

Decreased sensitivity to chemically induced carcinogenesis in *Fgf22* knockout mice implies that basal expression of *Fgf22* is conferring sensitivity to skin carcinogenesis. If we assume the presence of the above control mechanism, then lack of FGF22 may cause increased signalling via FGF7 and FGF10. It is well documented that FGF7 and FGF10 hold a potent cytoprotective signal for keratinocytes, and FGF7 is already in use in the clinic for oral mucositis.

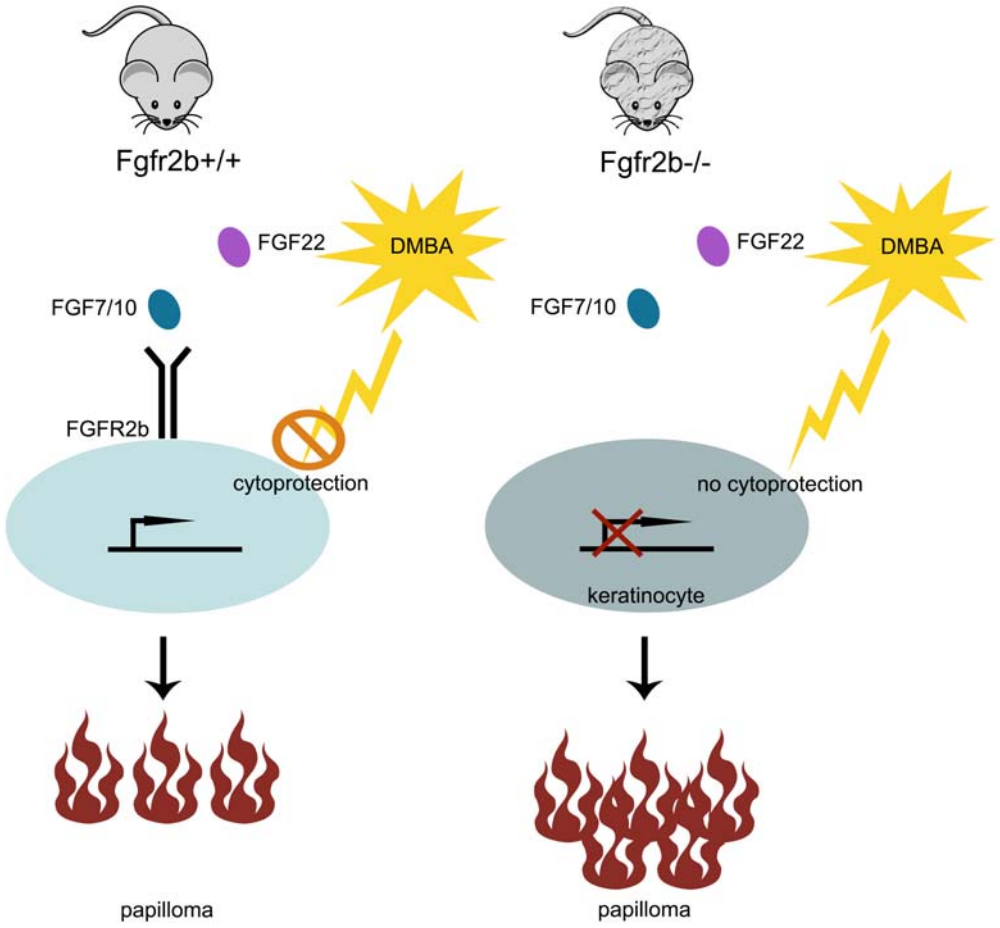

Figure 5.2 Cartoon illustrating a potential mechanistic insight into the phenotype seen in *Fgfr2b* knockout mice. Lack of downstream cytoprotective signalling mediated via FGF7 promotes a more pro-tumorigenic phenotype.

FGF7 has the potential to regulate genes that are mediators of the cytoprotective effect, like *peroxiredoxin VI* or *Nrf2* (Braun et al., 2004). Peroxiredoxin VI is a cytoplasmic enzyme that detoxifies hydrogen peroxide and organic peroxides, whereas Nrf2 is a transcription factor responsible for the activation of various cytoprotective genes, which encode ROS-detoxifying enzymes and other anti-oxidative proteins (Braun et al., 2004). In *Fgfr2b* knockout

mice this cytoprotective mechanism is inactive due to lack of signalling receptor, which is a likely contribution to the huge numbers of papillomas forming in response to chemically induced carcinogenesis. In *Fgf22* knockout mice on the other hand, FGF7 does not have to compete with FGF22 for receptor binding which allows strong FGF7 signalling yielding increased cytoprotective effect and, in consequence, reduced papilloma formation.

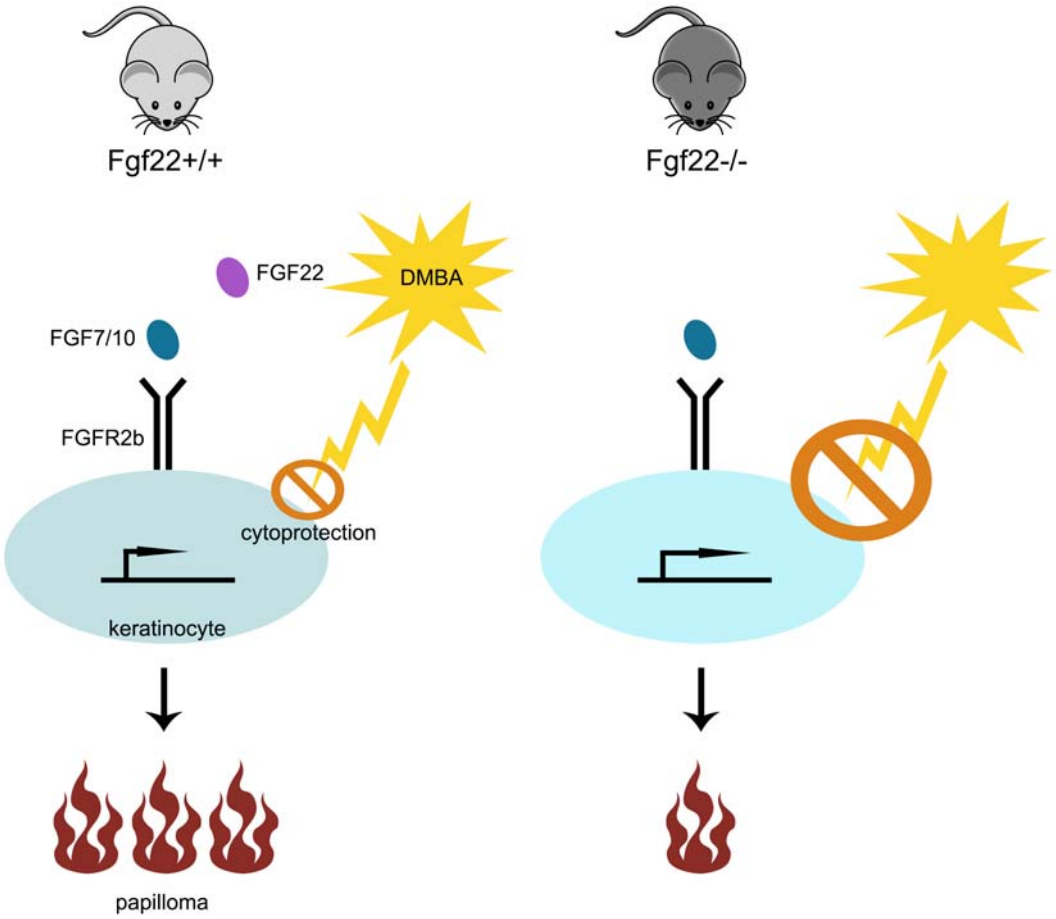

Figure 5.2 Cartoon illustrating difference in response of *Fgf22* wild type and knockout mice to chemically induced tumorigenesis.

Taken together outlined above results provide first insight into the unanticipated character of *Fgf22 in vivo* using knockout mouse model and function of FGFR2 in human skin. Data obtained during my PhD project provide a unifying framework for future research.

APPENDIX

EXPERIMENTAL PATHOLOGY LABORATORY

EPL PATHOLOGY REPORT

CANCER RESEARCH UK

Report Generated: 26/01/09

EPL NUMBER: 32
User Monika Jarosz

LINE: Fgf22

SPECIMEN:

GENOTYPE:

COLLECTED:

DISSECTED:

DOB:

DOD:

SEX:

TISSUE WEIGHT: N/A

TOTAL No. OF BLOCKS:

TOTAL SLIDES (H&E):

TOTAL SLIDES (UNSTAINED):

TOTAL SLIDES (IHC):

TOTALSLIDES (ISH):

TOTAL SLIDES (SPECIALS):

TOTAL SLIDES (OTHER):

FULL POST MORTEM

6 Male mice:

3 x Fgf22 wild type male & 3 x Fgf22 knockout male mice

Fgf22 WT A (age: 2.4 months, weight: 30 grams)
Fgf22 WT B (age: 2.4 months, weight: 29 grams)
Fgf22 WT C (age: 6.7 months, weight: 45 grams)

Fgf22 KO 1L(age: 2.3 months, weight: 29 grams); (missing pit as very small and damaged when removed)
Fgf22 KO 1R - (age: 6.4 months, weight: 26 grams)
Fgf22 KO NM - (age: 2.3 months, weight: 27 grams)

EXPERIMENTAL PATHOLOGY LABORATORY

EPL PATHOLOGY REPORT
MICROSCOPIC ANALYSIS

Contact:
Experimental Pathology Lab
Cancer Research UK
44 Lincoln's Inn Fields
London
WC2A 3BX

Tel: 0207 269 3621

Fgf22 WTB

1. Normal skin and subcutaneous tissue
2. Normal distal urethra normal seminal vesicles normal anterior prostate normal dorsal prostate normal urinary bladder normal preputial glands normal epididymis normal testes with active spermatogenesis
3. normal spleen
4. normal colonic mucosa
5. normal caecum normal small intestine normal proximal small intestine
6. normal pancreas
7. normal mesenteric lymph node
8. normal kidney normal adrenal glands
9. normal stomach normal duodenum with normal Brunners glands
10. normal liver
11. normal lungs normal esophagus normal trachea normal thyroid gland
12. normal lacrimal gland
13. normal heart
14. normal thymus gland
15. normal salivary gland
16. normal eye structure normal Harderian gland
17. normal brain normal midbrain normal cerebellum
18. normal pituitary gland with all three elements present
19. normal anterior head normal middle ear
20. normal vertebral body normal haemopoietic marrow

Fgf22 KO NM

1. normal skin and normal subcutaneous tissue
2. normal distal urethra normal seminal vesicles normal anterior prostate normal urinary bladder normal dorsal prostate normal bulbourethral gland normal testis with active spermatogenesis normal epididymis normal preputial gland
3. normal spleen
4. normal colonic mucosa
5. normal caecum normal terminal ileum normal proximal small intestine
6. pancreas with prominent eosinophilic cell change in acinar cells. Otherwise normal structure (incidental finding)
7. normal mesenteric lymph node
8. normal kidneys normal adrenal glands
9. normal stomach normal duodenum with normal Brunners glands
10. normal liver
11. normal lung normal esophagus normal trachea normal thyroid gland
12. normal lacrimal gland
13. normal heart
14. normal thymus gland
15. normal salivary glands
16. normal eye structure normal Harderian gland
17. normal brain normal midbrain normal cerebellum
18. normal pituitary gland
19. normal anterior head normal tooth development normal middle ear
20. normal vertebral body normal haemopoietic marrow

EXPERIMENTAL PATHOLOGY LABORATORY

EPL PATHOLOGY REPORT

Fgf22 KO 1R

1. normal skin and normal subcutaneous tissue with some reactive lymph nodes
2. normal distal urethra normal seminal vesicle normal anterior prostate normal dorsal prostate normal urinary bladder normal testis with active spermatogenesis normal preputial glands
3. spleen with slight prominence of the marginal zone but probably within normal limits
4. normal colonic mucosa
5. normal caecum normal distal small intestine normal proximal small intestine
6. normal pancreas with normal islets
7. normal mesenteric lymph node
8. normal kidneys normal adrenal gland
9. normal stomach normal duodenum with normal Brunners glands
10. normal liver
11. normal lung normal esophagus trachea not visualised
12. normal salivary gland
13. normal heart
14. normal thymus gland
15. normal salivary gland
16. normal eye structure normal Harderian gland
17. normal brain normal midbrain normal cerebellum
18. normal pituitary gland
19. normal anterior head normal tooth development normal middle ear
20. normal vertebral body normal haemopoietic marrow

Special Techniques:

Fgf22 KO 1L

1. normal skin and normal subcutaneous tissue with a reactive lymph node
2. normal distal urethra normal seminal vesicles normal anterior prostate normal dorsal prostate normal epididymis normal testes with active spermatogenesis normal preputial gland
3. normal spleen
4. normal colonic mucosa
5. normal caecum normal distal small intestine normal proximal small intestine
6. normal pancreas normal islets
7. mesenteric flat with no lymph node identified
8. normal kidneys normal adrenal glands
9. normal stomach normal duodenum with normal Brunners glands
10. normal liver and normal gallbladder
11. normal lung normal esophagus trachea not visualised
12. normal lacrimal gland
13. normal heart
14. normal thymus gland
15. normal salivary gland
16. normal eye structure normal Harderian gland
17. normal brain and normal cerebellum

18,19, 20 no slides present

Future Experiments Required:

EXPERIMENTAL PATHOLOGY LABORATORY

EPL PATHOLOGY REPORT

Fgf22 WTA

1. normal skin and subcutaneous tissue
2. normal distal urethra normal seminal vesicles normal anterior prostate normal dorsal prostate normal urinary bladder normal preputial glands normal epididymis normal testes with active spermatogenesis
3. normal spleen
4. normal colonic mucosa
5. normal caecum normal small intestine normal proximal small intestine
6. normal pancreas
7. normal mesenteric lymph node
8. normal kidney normal adrenal glands
9. normal stomach normal duodenum with normal Brunners glands
10. normal liver
11. normal lungs normal esophagus normal trachea normal thyroid gland
12. normal lacrimal gland
13. normal heart
14. normal thymus gland
15. normal salivary gland
16. normal eye structure normal Harderian gland
17. normal brain normal midbrain normal cerebellum
18. normal pituitary gland with all three elements present
19. normal anterior head normal middle ear
20. normal vertebral body normal haemopoietic marrow

Special Techniques:

Fgf22 WTC

1. normal skin and subcutaneous tissue
2. normal distal urethra normal seminal vesicles normal anterior prostate normal dorsal prostate normal urinary bladder normal preputial glands normal epididymis normal testes with active spermatogenesis
3. normal spleen
4. normal colonic mucosa
5. normal caecum normal small intestine normal proximal small intestine
6. normal pancreas
7. normal mesenteric lymph node
8. normal kidney normal adrenal glands
9. normal stomach normal duodenum with normal Brunners glands
10. normal liver
11. normal lungs normal esophagus normal trachea normal thyroid gland
12. normal lacrimal gland
13. normal heart
14. normal thymus gland
15. normal salivary gland
16. no slides present
17. normal brain normal midbrain normal cerebellum
18. normal pituitary gland with all three elements present
19. normal anterior head normal middle ear
20. normal vertebral body normal hematopoietic marrow

Future Experiments Required:

Comments:

USER: Monika Jarosz **LINE**: Fgf22

EPL No.: 32/09 Report completed: 09.02.09 Previous report:

The EMBO Journal (2007) 26, 1268–1278 | © 2007 European Molecular Biology Organization | All Rights Reserved 0261-4189/07
www.embojournal.org

THE EMBO JOURNAL

The role of fibroblast growth factor receptor 2b in skin homeostasis and cancer development

Richard Grose[1,*], Vera Fantl[2], Sabine Werner[3], Athina-Myrto Chioni[1], Monika Jarosz[1], Robert Rudling[4], Barbara Cross[4], Ian R Hart[1] and Clive Dickson[2]

[1]Centre for Tumour Biology, Institute of Cancer, Bart's & The London, Queen Mary's School of Medicine & Dentistry, London, UK, [2]Cancer Research UK London Research Institute, London, UK, [3]Department of Biology, Institute of Cell Biology, ETH Zürich, Zürich, Switzerland and [4]Biological Services, Cancer Research UK London Research Institute, Clare Hall Laboratories, Herts, UK

The epithelial isoform of fibroblast growth factor receptor 2 (Fgfr2b) is essential for embryogenesis, and Fgfr2b-null mice die at birth. Using Cre-Lox transgenics to delete Fgfr2b in cells expressing keratin 5, we show that mice lacking epidermal Fgfr2b survive into adulthood but display striking abnormalities in hair and sebaceous gland development. Epidermal hyperthickening develops with age, and 10% of mutant mice develop spontaneous papillomas, demonstrating the role of Fgfr2b in post-natal skin development and in adult skin homeostasis. Mice lacking epithelial Fgfr2b show great sensitivity to chemical carcinogenic insult, displaying several oncogenic *ha-ras* mutations with dramatic development of papillomas and squamous cell carcinomas. Mutant mice have increased inflammation in the skin, with increased numbers of macrophages and γδT cells with abnormal morphology. Mutant skin shows several changes in gene expression, including enhanced expression of the pro-inflammatory cytokine interleukin 18 and decreased expression of Serpin a3b, a potential tumor suppressor. Thus we describe a novel role of Fgfr2b and provide the first evidence of a tyrosine kinase receptor playing a tumor suppressive role in the skin.

The EMBO Journal (2007) **26,** 1268–1278. doi:10.1038/sj.emboj.7601583; Published online 15 February 2007
Subject Categories: signal transduction; molecular biology of disease
Keywords: cancer; epidermis; Fgf; inflammation; sebaceous gland

Introduction

Reciprocal intercellular signalling between epithelium and mesenchyme is a fundamental process in the induction and patterning of many organs. Fibroblast growth factors (Fgfs) participate in this process by instructing cells to proliferate, survive, migrate or differentiate. In mammals, there are 22 Fgf family members that signal via one or more receptor tyrosine kinases encoded by four Fgf receptor genes (Fgfr1–4), which are expressed as alternatively spliced variants (Ornitz and Itoh, 2001). Germline knockout of the IIIb exon of the Fgfr2 gene results in mice that die at birth from multiple developmental defects, identifying Fgfr2b as a critical mediator of organogenesis (De Moerlooze *et al*, 2000; Revest *et al*, 2001). Similar results were obtained by overexpressing a soluble dominant-negative version of the Fgfr2b isoform (Celli *et al*, 1998), and studies in which Fgf-10 was knocked out showed this to be the key ligand for Fgfr2b during development (Min *et al*, 1998; Sekine *et al*, 1999).

A role of Fgfr2b in post-natal skin development was established by studying full-thickness skin grafts from late-stage Fgfr2b-null and wild-type fetuses, grown on the back of nude mice. When the first wave of hair morphogenesis was complete, after 21 days, histological analysis showed Fgfr2b signalling was crucial for normal epidermal growth and development as well as for subsequent hair follicle morphogenesis (Petiot *et al*, 2003). However, the grafting approach was not suitable for following long-term skin homeostasis. Thus, for this study, we adopted a Cre-Lox strategy to knock out Fgfr2b in the epidermis.

The expression of Cre recombinase under the control of the bovine keratin 5 (K5) promoter mediates extremely efficient excision of floxed target genes in the epidermis (Brakebusch *et al*, 2000) when inherited paternally (Ramirez *et al*, 2004). This approach is different from germline deletion, in that the skin develops normally during embryogenesis, as Cre is not active until embryonic day 15.5 (Ramirez *et al*, 2004), with Fgfr2b not being excised until late in fetal development. Therefore, our studies address the role of Fgfr2b in post-natal epidermal homeostasis rather than in skin development.

Various mouse models have been used to study Fgfr2b signalling in adult skin. Mice expressing a membrane-bound, dominant-negative Fgfr2b, lacking tyrosine kinase activity, under the control of the keratin 14 promoter, displayed epidermal atrophy, hair follicle abnormalities and dermal hyperthickening with severely delayed re-epithelialization of excisional wounds (Werner *et al*, 1994). Expression of Fgf-7, which binds to Fgfr2b exclusively, has been modulated by germline knockout (Guo *et al*, 1996) and by keratinocyte-specific overexpression, again under the control of the keratin 14 promoter (Guo *et al*, 1993). The only phenotype in the skin of Fgf-7 knockout mice was matting of the fur in aging male mice (Guo *et al*, 1996), whereas Fgf-7 overexpression resulted in neonatal epidermal hyperthickening, followed by progressive epidermal thinning and loss of adipose tissue as the mice aged (Guo *et al*, 1993).

None of the above studies address the role of Fgfr2b specifically; the dominant-negative receptor is able to out-

*Corresponding author. Centre for Tumour Biology, Institute of Cancer, Bart's & The London, Queen Mary's School of Medicine & Dentistry, John Vane Science Centre, Charterhouse Square, London EC1M 6BQ, UK. Tel.: +44 20 7014 0415; Fax: +44 20 7014 0401; E-mail: r.p.grose@qmul.ac.uk

Received: 27 June 2006; accepted: 9 January 2007; published online: 15 February 2007

compete any receptor that shares ligands with Fgfr2b, for example Fgfr1b, and the Fgf-7 ligand knockout fails to address the possibility of compensation by an alternative ligand, such as Fgf-10. Thus, we wished to address the role of Fgfr2b in the skin, both in terms of post-natal development and in terms of tissue homeostasis.

The FGFRs are not involved solely in the regulation of normal skin development. There is a growing body of evidence implicating FGFRs as causative and suppressive factors in cancer (Grose and Dickson, 2005), with activating mutations in FGFR2 having been described in human gastric cancer (Jang *et al*, 2001). FGFR2b has been suggested to act as a tumor suppressor in the urothelium, with decreased expression of FGFR2b correlating with poor prognosis in transitional cell carcinoma (Diez de Medina *et al*, 1997; Ricol *et al*, 1999). Further studies revealed that this tumor-suppressive effect was not dependent on the tyrosine kinase activity of FGFR2b, but suggested that the C-terminus of the receptor was modulating IGF-II signalling (Bernard-Pierrot *et al*, 2004). Thus, in the absence of FGFR2b, IGFII was overexpressed, resulting in increased tumor cell proliferation and decreased apoptosis. In human salivary adenocarcinoma, FGFR2b acts to induce differentiation and apoptosis of cancer cells (Zhang *et al*, 2001), whereas in prostate carcinoma, in both mouse and human, decreased expression of FGFR2 results in overexpression of FGFR1, which in turn drives cancer progression (Jin *et al*, 2003; Yasumoto *et al*, 2004). Our study provides the first evidence of a protective role of Fgfr2b in cancer development in the skin.

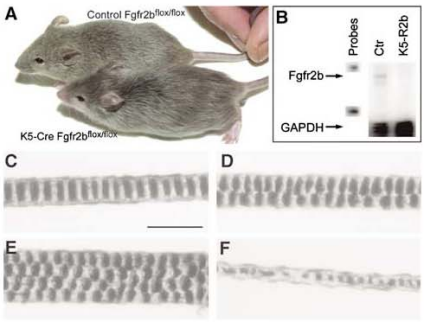

Figure 1 Skin-specific deletion of Fgfr2b leads to defective hair formation. (**A**) Five-week-old male littermates. Both mice are homozygous for the floxed Fgfr2b allele—the lower mouse also carries the K5 Cre transgene. Mice lacking Fgfr2b in the epidermis are normal size compared with wild-type siblings, but show clear coat differences, with their fur appearing sleek and silky compared with wild types. (**B**) RNase protection assay. Expression of Fgfr2b mRNA in skin from 8-week-old control and K5-R2b-null littermates. Levels of GAPDH mRNA were assayed in the same samples to serve as a control of both loading levels and RNA quality. Each hybridization probe (1000 c.p.m.) was loaded in the lanes labelled 'probes' and used as size markers. Arrows indicate the protected fragments for Fgfr2b and control (GAPDH) mRNA. (**C–F**) Pelage hair structure. Light microscopy of the three main hair subtypes from control mice: (C) Zigzag, (D) Guard and (E) Awl hairs. (F) Disorganized zigzag hair from a K5-R2b-null mouse. Scale bar, 20 μm.

Results

Defective pelage growth in K5-R2b-null mice

K5-R2b-null (Fgfr2b$^{flox/flox}$; K5-Cre positive) mice could be distinguished phenotypically as soon as their pelage hair begins to grow, a few days after birth, with their coat appearing thin and silky compared with control (Fgfr2b$^{flox/flox}$; K5-Cre-negative) littermates. This difference in appearance persisted throughout adulthood, as illustrated in the comparison of two 5-week-old male littermates (Figure 1A). No difference in overall growth, behavior or fertility was observed, although K5-R2b-null mice developed abnormally long claws compared with control littermates (data not shown). RNase protection assays with a riboprobe specific for the IIIb variant of Fgfr2 and a glyceraldehyde-3-phosphate dehydrogenase (GAPDH) riboprobe as a control confirmed that Fgfr2b mRNA was no longer expressed in the skin of 8-week-old K5-R2b-null mice (Figure 1B). Although Fgf receptors are expressed at low levels, a band corresponding to the protected fragment for Fgfr2b was clearly discernible in control samples and not in skin samples from K5-R2b mice (Figure 1B).

Light microscopy of hairs plucked from five 8-week-old wild-type mice ($n = 100$ hairs) revealed all the usual hair subtypes present in the correct ratios; 70% Zigzag (Figure 1C), 2% Guard (Figure 1D) and 28% Awl/Auchene (Figure 1E). Hairs were classified by virtue of their length and classical patterns of air spaces within the hair (Sundberg and Hogan, 1994). In contrast, hairs from mice lacking Fgfr2b in the skin ($n = 100$ hairs) showed a grossly disorganized zigzag structure (Figure 1F), as well as being of a thinner diameter (ranging from 5 to 7 μm when measured midway along the hair shaft, compared with 9 to 12 μm in control zigzag hairs).

Hair follicle abnormalities and cutaneous inflammation in the absence of Fgfr2b

Defects in hair follicle cycling were apparent, with immunostaining confirming the asynchronous nature of the first morphogenetic wave in K5-R2b-null mice. Longitudinal sections through back skin of 16 days post partum (d.p.p.) mice stained for keratin 6 permitted clear visualization of hair follicles and revealed no misexpression of keratin 6 in the interfollicular epidermis (Supplementary Figure 1A and B). Whereas the follicles of wild-type mice all were situated within the dermis in the resting phase (telogen) by 16 d.p.p. (Figure 2A), many follicles in knockout mice at the same stage still extended down beneath the dermis, with some reaching to the muscle layer at the base of the adipose tissue (mean number of follicles below dermis = 3.2 ± 2.6 (s.d.) per microscopic field (×20); average of 10 fields from sections from three mice). Additionally, follicles of K5-R2b-null mice often appeared disorganized in structure, with more than one follicle coalescing to emerge at the same site in the epidermis (Supplementary Figure 1B). As with mice lacking Fgfr2b in the germ line (Petiot *et al*, 2003), no defects were observed in the expression of markers of epidermal differentiation (data not shown).

Concomitant with the hair defects, an increased level of macrophage recruitment was observed in K5-R2b-null skin. F4/80 immunostaining for macrophages and monocytes in control 16 d.p.p. skin revealed some resident tissue macrophages present in the dermis (Supplementary Figure 1C), but

similar staining of K5-R2b-null skin revealed markedly increased macrophage recruitment to both the dermis and the adipose tissue (Supplementary Figure 1D and E).

Sebaceous glands develop in the skin of K5-R2b-null mice, but subsequently atrophy

Male mice lacking Fgf-7 were reported as having greasy, matted fur (Guo *et al*, 1996). As the coats of K5-R2b-null mice have a silky appearance that might be attributable to an oily coat, we investigated sebaceous gland development in these mice. Whereas the relatively small sebaceous glands that develop on pelage follicles appeared unaffected in mutant mice (data not shown), whole-mount staining of tail skin epidermis revealed dramatic differences in mutant mice. By 6 d.p.p., the tail hair follicles are already midway through the first anagen growth phase, and nascent sebaceous glands can be seen as rudimentary buds near the top of the follicle in both control and K5-R2b-null mice (Supplementary Figure 2). From day 6 onwards, the differences in the rate of sebaceous gland growth between the two genotypes became more evident, with K5-R2b glands barely increasing in size after 2 weeks of age, whereas control glands continued to grow (Supplementary Figure 2).

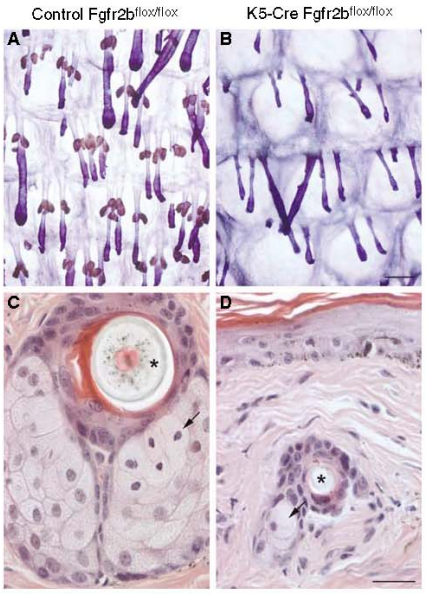

Figure 2 Sebaceous gland atrophy in K5-R2b-null mice. By 3 months of age, epidermal whole-mount peroxidase staining (sebaceous glands appear brown) combined with Mayer's hemalum counterstain revealed that sebaceous glands in the tail of K5-R2b-null mice were virtually absent (compare (**A**) with (**B**)). This absence was confirmed by scanning through H&E-stained serial transverse sections of tail skin, looking for sebocytes (arrows in (C) and (D); asterisks indicate transversely sectioned hair shafts). (**C**) and (**D**) represent sections showing the largest proportion of sebaceous tissue encountered in serial transverse sections from tails of wild-type and K5-R2b-null mice, respectively. Scale bar, 200 μm.

By virtue of their high endogenous peroxidase activity, mature sebocytes are readily apparent in epidermal whole-mount preparations (Figure 2A). By 3 months of age, in contrast to the abundance of sebaceous glands in control tail skin, in the null mice, there was a virtual absence of sebaceous glands (Figure 2B). This was confirmed by scanning through hematoxylin and eosin (H&E)-stained serial transverse sections of tail skin. In sections from control mice that show the largest concentration of sebocytes, the sebaceous glands fill the entire field of view (Figure 2C). This was never the case for null mice, where no more than two or three sebocytes were ever observed (Figure 2D).

Epidermal hyperthickening and dysplasia develop with age in the absence of Fgfr2b

As K5-R2b-null mice aged, the hair phenotype became more extreme, such that by 18 months of age, both males and females had extremely sparse pelage hair. H&E staining of longitudinal sections through back skin harvested from control (Figure 3A and A′) and K5-R2b (Figure 3B and B′) mice highlighted the sparse hair follicles in the mutant mice. Somewhat surprisingly, the interfollicular epidermis of K5-R2b-null mice was thicker than that of control mice. Interfollicular epidermis of control mice is extremely thin and although the dermis becomes tougher with age, ordinarily remains little more than one-cell thick (Figure 3A′). In mice lacking epidermal Fgfr2b, not only was the epidermis thicker but also there was an apparent parakeratosis, where keratinocyte nuclei that normally would be lost as the cells commit to terminal differentiation were retained within the epidermis (Figure 3B′). Such differences were even more apparent in the tail, where differences in skin phenotypes are more marked by virtue of its multilayered structure and higher proliferative index. Transverse sections from wild-type tail skin displayed a clearly defined basal layer of keratinocytes, with nuclei obviously becoming less abundant toward the keratinized surface of the skin (Figure 3C). By comparison, the basal layer of keratinocytes in Fgfr2b-null tail skin showed regions of dysplasia while the differentiation process in the epidermis was compromised, with clear evidence of parakeratosis (Figure 3D).

Defects in the skin were not restricted to elderly mice alone. Thorough macroscopic examination of our mouse colony revealed that K5-R2b-null virgin female mice exhibited a clear hyperproliferative defect in the nipples. Nipples of wild-type 8-month-old virgin female mice were barely discernible by the naked eye (Supplementary Figure 3A). In contrast, those of mice lacking Fgfr2b in the epidermis were very prominent (Supplementary Figure 3B). Transverse sections through the nipples of control (Supplementary Figure 3C) and K5-R2b-null mice (Supplementary Figure 3D) revealed epithelial hyperplasia and the frequent occurrence of keratin-filled cysts in the mutant mice.

Spontaneous papilloma formation in the absence of Fgfr2b

Despite being bred onto a mixed background of 129ola and C57Bl6/J strains, which are relatively tumor resistant (Woodworth *et al*, 2004), 10% of K5-R2b mice older than 8 months developed spontaneous papillomas ($n=6$ from 60

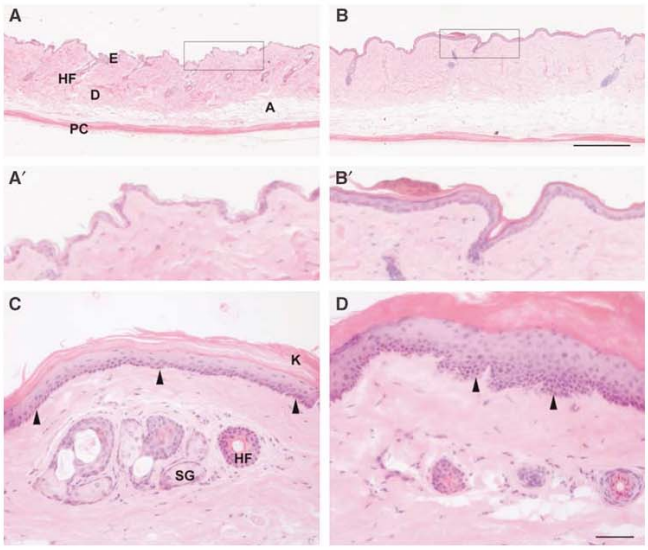

Figure 3 Epidermal hyperthickening in the absence of Fgfr2b. Transverse sections through back and tail skin of 18-month-old mice were stained with H&E. Back skin of control (**A** and **A′**) and K5-R2b-null mice (**B** and **B′**). In wild-type tail skin (**C**), the basal layer of keratinocytes is clearly visible as a distinct line of nuclei at the dermo-epidermal junction (arrowheads) and anuclear, keratinized squames can be seen sloughing from the surface. By comparison, Fgfr2b-null tail skin (**D**) shows regions of dysplasia (arrowheads) and parakeratosis. A, adipose layer; D, dermis; E, epidermis; HF, hair follicle; K, keratinized squames; PC, *panniculus carnosus*; SG, sebaceous gland. Scale bars, 200 μm (A, B) and 50 μm (C, D).

mice; one papilloma per mouse). These papillomas exhibited classical exophytic morphology, with a stalk of relatively normal skin leading to a hyperthickened, keratinized papilloma packed with inflammatory cells (Figure 4A). These papillomas also showed upregulation of keratin 6, not normally expressed in the interfollicular epidermis, which is a classical marker of activated keratinocytes (Figure 4B). 5-Bromo-2′-deoxyuridine (BrdU) staining for proliferating cells highlighted the hyperproliferative nature of the papilloma keratinocytes and also revealed that proliferation was not restricted to the basal layer (Figure 4C). Interestingly, the papillomas tended to arise in regions of mechanical stress, such as around the face and in the perianal region.

Heightened sensitivity to skin carcinogenesis in mice lacking Fgfr2b in the skin

Having observed the occurrence of spontaneous papillomas and other epidermal defects, we hypothesized that Fgfr2b might be fulfilling a tumor-suppressive role in the skin. Therefore, we assessed the sensitivity of K5-R2b-null mice to classical two-step skin carcinogenesis protocols using DMBA initiation followed by TPA tumor promotion. In an initial study, using only female mice (n = minimum of eight per group) and a twice weekly TPA treatment regime, mice lacking Fgfr2b in the epidermis developed their first papillomas within 8 weeks of DMBA treatment (Figure 5A). This was 3 months earlier than the first papilloma that appeared in K5-R2b-null mice treated with TPA alone. In contrast, control mice treated with DMBA/TPA did not develop papillomas until 34 weeks post-initiation, by which time 100% of the knockout mice had developed papillomas or even carcinomas. Control mice subject to TPA treatment alone never developed papillomas.

To confirm the validity of these dramatic findings, the study was repeated with both male and female mice (average $n = 5$). The protocol was adjusted slightly, with the mice receiving once weekly applications of 7.4 μg TPA rather than the twice weekly application of 3.7 μg TPA. Once again, the results were clearcut; even in cases where control mice treated with DMBA developed papillomas, the number of papillomas per mouse was never above two, whereas knockout mice were recorded as developing up to 26 per animal (Figure 5B). Thus, both sets of data show an unequivocally enhanced sensitivity to DMBA-induced skin carcinogenesis in K5-R2b-null mice.

Enhanced progression of skin lesions to squamous cell carcinoma in K5-R2b-null mice

Mutant mice also exhibited changes that suggested that Fgfr2b might play an important role in blocking the progression of benign papillomatous lesions to benign keratoacanthomas (Figure 6A), and more invasive squamous cell carcinomas (Figure 6B). In the present study, on a C57Bl6/

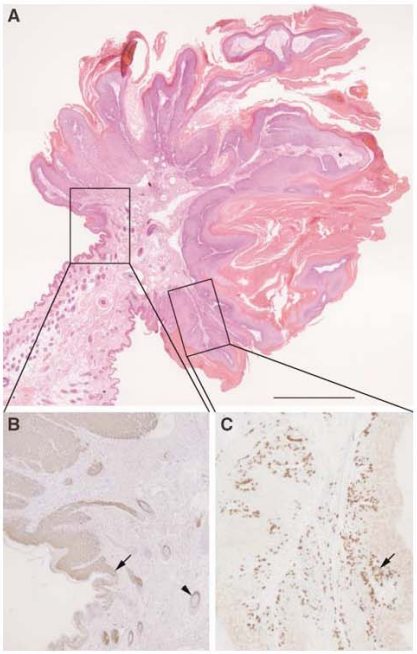

Figure 4 Spontaneous papilloma formation in the absence of Fgfr2b. (**A**) H&E staining reveals classical exophytic morphology of spontaneous papillomas, with a stalk of relatively normal skin leading to a hyperthickened, keratinized papilloma packed with inflammatory cells. Higher magnification views of the boxed areas in (A) show that papilloma keratinocytes express keratin 6 (brown immunostaining in (**B**)), normally restricted to hair follicles (arrowhead), from the margin, where the papilloma begins (arrow). BrdU staining for proliferating cells (**C**) in both basal and suprabasal layers (arrow). Scale bar, 200 μm.

Jx129ola background, no lesion on a DMBA-treated control mouse progressed to squamous cell carcinoma ($n=3$ papillomas from 10 mice >6 months old). Although the mice used in this study were on a mixed background, our observations are in line with published data, which suggest that papillomas do not convert on a C57Bl6/J background (Woodworth *et al*, 2004). In contrast, K5-R2b-null mice treated with DMBA developed squamous cell carcinomas ($n=6$ squamous cell carcinomas from 57 papillomas on 12 mice >6 months old; maximum of two carcinomas per mouse).

Mutations in codon 61 of ha-ras

DNA obtained from frozen skin, papillomas and tumors excised from mice was analyzed by restriction fragment length polymorphism (RFLP) for *ha-ras* codon 61 mutations. No mutations were detected in 20 uninvolved skin samples taken from K5-R2b mice. Three of the four previously reported *ha-ras* mutations (Jaworski *et al*, 2005) were detected in this study (Figure 6C). One tumor arising spontaneously on a K5-R2b-null mouse showed G61L conversion in the absence of DMBA treatment. This activating mutation was found in a further five tumors taken from K5-R2b-null mice treated with DMBA/TPA. Of further mutations in this group, one mouse had two tumors, with each bearing a different activating mutation, G61L and G61K respectively; a tumor from a different mouse harbored the G61K mutation; the G61H mutation was found in two papillomas from another; and, of the additional seven papillomas analyzed from the treated K5-R2b-null mice, all showed G61L mutation although the mutant band was often quite weak, indicating dilution of the sample with non-mutated cells. These comprised either inflammatory cells or non-mutated keratinocytes from the margins of the lesion. Two papillomas arising spontaneously in the K5-R2b mice treated only with TPA showed no detectable *ha-ras* mutations and, surprisingly, this also was the case for the only two papillomas analyzed from DMBA/TPA-treated control mice. This may reflect a large contribution of non-mutated cells in samples taken from these relatively small lesions masking any mutant polymerase chain reaction (PCR) product.

Differential gene expression in knockout and wild-type skin

To gain further insight into the potential mechanism underlying the enhanced sensitivity of Fgfr2b-null skin to cancer development, we performed gene expression profiling on RNA isolated from back skin samples from 1-year-old control and mutant mice, using the Illumina Sentrix MouseRef-8® microarray platform. Using a two-fold change in expression level as a cutoff, we detected elevated expression levels of several differentiation-specific genes in mutant skin, which most likely reflect the epidermal hyperthickening (data not shown). We also saw elevated expression of the pro-inflammatory cytokine interleukin (IL)-18 (Supplementary Figure 4). Several genes also showed reduced expression in mutant skin, among them Serpin a3b, a member of the serine protease inhibitor family that was reduced dramatically (Supplementary Figure 4). Differential expression levels were confirmed by semiquantitative RT–PCR, using RNA samples taken from 3- and 6-month-old control and mutant mice. These included full-thickness back and tail skin, as well as RNA isolated from only the epidermis of tail skin. For all samples, we confirmed that the starting cDNAs were of equivalent concentration and quality by amplifying the housekeeping gene hypoxanthine-guanine phosphoribosyltransferase (HPRT). Only products from cycles 30 and 35 are illustrated, but these clearly show the differences between control and mutant tissues, and that the increase in IL-18 expression is seen both in total skin and epidermis of mutant mice (Supplementary Figure 4). This indicates that IL-18 is likely to be expressed by mutant keratinocytes themselves, rather than the levels just reflecting increased inflammatory infiltrate.

Alongside these studies, we also examined gene expression in tumors and papillomas of control (papillomas only) and knockout mice, to look for differences in expression of Fgf ligands and receptors as well as known Fgf target genes (auf dem Keller *et al*, 2006). However, no significant differences were found in the expression levels of any of the above, or in expression of Igf or Egf ligand or receptor families (data not shown).

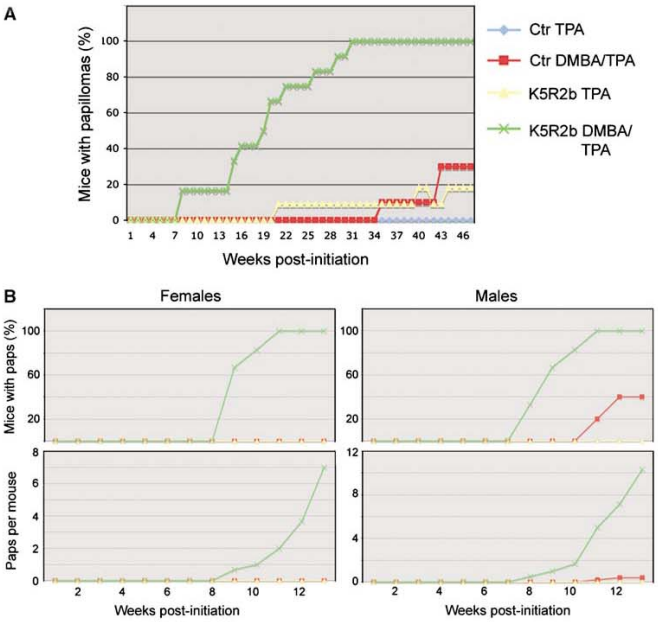

Figure 5 Enhanced sensitivity to skin carcinogenesis in K5-R2b-null mice. Cohorts of female mice were subjected to classical two-step skin carcinogenesis treatment. (**A**) Female mice were treated with DMBA or solvent acetone alone at 8 weeks of age and then all treated twice weekly with TPA for 15 weeks. In a repeat study (**B**), the protocol was adjusted slightly, such that male and female mice were treated, giving a total of eight groups (key same as for (A)). The treatment regime differed only in that the mice received once weekly applications of a double dose of TPA.

Altered γδT-cell features in Fgfr2b-null skin

Previous work has shown that γδT cells resident within the epidermis, also known as dendritic epidermal T-cells, are key sources of Fgfs 7 and 10 during wound repair (Jameson *et al*, 2002), and also that mice lacking γδT cells show enhanced sensitivity to the two-step model of skin carcinogenesis, as used in our study (Girardi *et al*, 2001). Therefore, we analyzed the γδT cells resident within the skin of 1-year-old control and K5-R2b-null mice, using immunofluorescent staining of epidermal whole mounts to assess both cell number and morphology. The most appropriate tissue for this purpose is the epidermis of the ear, as it can be dissociated from the dermis in a manner similar to tail epidermis, but is much thinner and the γδT cells can more readily be visualized by immmunostaining. By using ImageJ software to analyze single-channel greyscale confocal images that reflected γδT-cell staining, it was possible to quantitate automatically the number of cells per image and also measure their perimeter. We observed significantly more γδT cells within the epidermis of mutant skin when compared with control skin (38% increase, $P<0.01$ using the Mann–Whitney test; compare Figure 7A and B, quantitated in Figure 7C) and also saw a significant increase in γδT-cell perimeter in mutant skin (33% increase, $P<0.001$ using the Mann–Whitney test; quantitated in Figure 7D), reflecting a difference in cell morphology, with cells in the mutant skin exhibiting a more dendritic appearance.

Discussion

Our mice, lacking Fgfr2b only in keratinized epithelia, provide the first opportunity to study the specific functions of Fgfr2b in adult skin. Previous studies that have sought to investigate the role of Fgfr2b in the skin have been hampered either by interference with signalling via other receptors that share common ligands in mice overexpressing dominant-negative Fgfr2b in the epidermis (Werner *et al*, 1994), ligand redundancy in the case of Fgf-7 knockout mice (Guo *et al*, 1996), or perinatal lethality, and a consequent reliance on skin grafting, in Fgfr2b knockout mice (Petiot *et al*, 2003).

Defects in skin development in the absence of Fgfr2b

Our initial findings recapitulate those data obtained from Fgfr2b knockout studies where late-stage embryonic skin was grafted onto nude mouse recipients (Petiot *et al*, 2003). These experiments showed that although keratinocytes could undergo terminal differentiation in the absence of Fgfr2b, they failed to form morphologically normal pelage hairs, and the hair follicles that formed failed to orientate properly, resulting in a chaotic first wave of hair morphogenesis

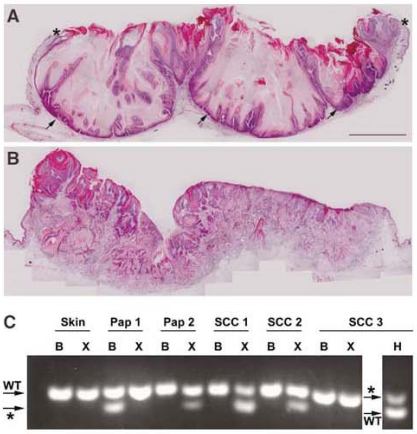

Figure 6 Progression of skin carcinogenesis lesions to squamous cell carcinoma. Transverse sections through lesions from K5-R2b-null mice highlight keratoacanthoma (**A**) and squamous cell carcinoma (**B**). Although keratoacanthomas no longer exhibit the exophytic growth of papillomas, with their margins covered with normal skin (asterisks in (A)), they are still non-invasive, with a clearly defined basal layer of keratinocytes (arrows in (A)). In contrast, the lesions that progress to squamous cell carcinoma (B) show no clearly defined basal surface, but rather a mass of invasive keratinocyte projections and a strong recruitment of inflammatory cells. (**C**) RFLP analysis of mutations in codon 61 of *ha-ras*. PCR products derived from skin, papilloma (Pap) or squamous cell carcinoma (SCC) digested with *Bsp*HI (B), *Xba*I (X) and *Hpy*118II (H) were separated on 4% agarose gels. Bands diagnostic of the wild-type (WT) and mutant (*) alleles are indicated (arrows).

(Petiot *et al*, 2003). The defects that we observed in K5-R2b-null mice are similar in terms of failed hair patterning, but are less dramatic in terms of follicle orientation. This is entirely consistent with our strategy of using the expression of Cre recombinase under the control of the bovine keratin 5 promoter to delete Fgfr2b, as Cre is not active in the epidermis until around E15.5, with target gene deletion not being attained until late in fetal development (Ramirez *et al*, 2004), well after follicle patterning has been established. Throughout fetal development, the skin of K5-R2b-null mice, therefore, develops as wild type and, despite there being no detectable Fgfr2b message in neonatal skin of K5-R2b-null mice (data not shown), defects in skin development do not become apparent until the mice are approximately 1 week old. Recent transgenic studies overexpressing dominant-negative Fgfr2b, under the control of the FoxN1 promoter, also have recapitulated the hair patterning defects seen in Fgfr2b-null mice, identifying Igfbp5 as a key modulator of Fgf signalling in the developing hair follicle (Schlake, 2005).

Having confirmed the validity and efficacy of our approach, our study provides the first evidence of the role of Fgfr2b in sebaceous gland development. Fgfr2b is expressed throughout the epidermis, hair follicles and sebaceous glands (Danilenko *et al*, 1995), and we have observed that the continued presence of Fgfr2b in the skin is a necessary prerequisite for the long-term survival of sebocytes. Whether this is due to a requirement for Fgfr2b to be expressed on sebocytes, or whether keratinocytes produce some kind of survival signal as a consequence of ligand–receptor interaction is the subject of ongoing investigations.

Fgfr2b as a tumor suppressor in the skin

The epidermal hyperthickening that developed as K5-R2b-null mice aged was somewhat surprising, given that Fgfr2-null embryos have thin skin relative to wild-type littermates (Petiot *et al*, 2003), and a hypertrophic phenotype is not what might be expected when a growth factor receptor is deleted. This led us to investigate whether Fgfr2b might function as a suppressor of growth in the adult.

Fgfr2b has been implicated as a tumor suppressor in the urothelium, with decreased expression correlating with worse prognosis in transitional cell carcinoma (Diez de Medina *et al*, 1997; Ricol *et al*, 1999). Given that xenografting studies suggest that this tumor-suppressive effect is due to the C-terminus of Fgfr2b modulating IGF-II signalling (Bernard-Pierrot *et al*, 2004), the increased tumor cell proliferation and decreased apoptosis seen might well result from elevated IGF-II levels. Assuming similar mechanisms were operative in human disease, they could result in increased aggressiveness of tumors and account for poorer survival of patients with transitional cell carcinoma of the bladder (Diez de Medina *et al*, 1997; Ricol *et al*, 1999). However, we saw no changes in the expression of either the ligands Igf-I and Igf -II or their receptors (data not shown), suggesting that this is not the case for our model.

FGFR2 also has been implicated as a tumor suppressor in other cancers. Thus, in human salivary adenocarcinoma, it appears to act to induce differentiation and alter apoptosis of cancer cells (Zhang *et al*, 2001). In prostate carcinoma, both murine and human, decreased expression of FGFR2 has resulted in overexpression of FGFR1, which is thought to drive uncontrolled proliferation and subsequent tumorigenesis (Jin *et al*, 2003; Yasumoto *et al*, 2004). We found no change in Fgfr1 expression in either K5-R2b mutant skin or in neoplastic lesions from carcinogen-treated mice. FGFR2 may well exert its protective effect via different mechanisms dependent on the tissue type, and indeed may not always act as a tumor suppressor. For example, activating mutations in FGFR2 have been described in human gastric cancer (Jang *et al*, 2001), but our study provides the first evidence of a protective role of Fgfr2b in the skin.

The precise mechanism underlying this protective effect is not yet clear. Fgf-7, signalling via Fgfr2b, has been shown to upregulate a wide array of downstream target genes in keratinocytes (Steiling and Werner, 2003). Among these genes, the Nrf2 transcription factor has been implicated as being an essential regulator of tumor prevention, both acting to detoxify carcinogens and to prevent oxidative damage. Thus, mice expressing a dominant-negative Nrf2 transgene in the epidermis exhibited strikingly enhanced skin tumor development in response to two-stage skin carcinogenesis treatment (auf dem Keller *et al*, 2006). However, Nrf2 expression was unaffected in K5-R2b-null mice, and no differences in the expression levels of known Nrf2 targets (auf dem Keller *et al*, 2006) were detected in our microarray experiments, suggesting that this mechanism is not responsible for the observed phenotype.

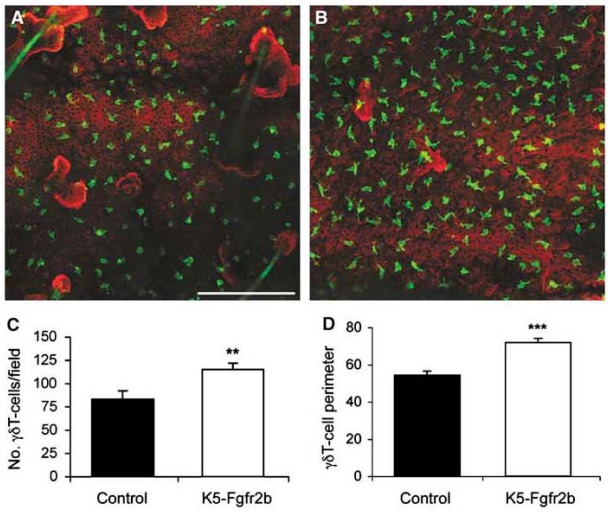

Figure 7 γδT-cell abnormalities in K5-R2b-null epidermis. Whole-mount preparations of ear epidermis from control (**A**) and K5-R2b-null (**B**) mice stained with antibodies to γδT cells (green) and keratin 14 (red) highlight the increased γδT-cell density in mutant epidermis (quantitated in (**C**)). In addition to being present in increased numbers, γδT cells in mutant epidermis display an altered morphology, adopting a more dendritic appearance, reflected by a significantly increased cell perimeter (quantitated in (**D**)). Scale bar in (A), 50 μm. $^{**}P<0.01$; $^{***}P<0.001$ using the Mann–Whitney test.

The absence of Fgfr2b may affect other protective pathways, as we see a large frequency of lesions in K5-R2b-null mice in response to carcinogenic insult, and an unusual range of mutations at the *ha-ras* codon 61 locus. Classically, topical DMBA treatment elicits a CAA to CTA (G61L) mutation in keratinocytes (Quintanilla *et al*, 1991), but RFLP analysis identified three independent mutations in lesions of K5-R2b-null mice. This suggests that enhanced genomic instability in the absence of Fgfr2b might underlie the phenotype we observe. This hypothesis is further supported by the finding that FGFR2b-null mice develop papillomas in response to TPA treatment without a preceding carcinogenic insult.

At the level of gene expression, two genes of particular interest showed differential expression between control and mutant skin. IL-18, expression of which is upregulated in RNA samples isolated from mutant skin and epidermis, has been shown to be upregulated both in inflammatory cells and keratinocytes in neoplastic skin lesions (Park *et al*, 2001; Yamanaka *et al*, 2006). Thus, upregulation might reflect the increased inflammatory infiltrate in the skin, but the epidermal expression suggests keratinocyte upregulation with subsequent recruitment of inflammatory cells. In contrast, expression of the serine proteinase inhibitor Serpin a3b was markedly reduced in mutant skin and epidermal samples. Very little is known about this molecule, but the related protein Maspin has been shown to act as an epithelial tumor suppressor, and other members of the family have been reported to modulate the activity of the urokinase pathway, a pathway that can drive invasion and metastasis (Lockett *et al*, 2006). Future studies will address the functions of these and other potential Fgfr2b-dependent genes in the skin.

Recent data supporting the role of inflammatory responses in driving tumor progression (Balkwill, 2004; Balkwill and Coussens, 2004) might suggest that the increased macrophage infiltration observed in K5-R2b-null animals could be acting as a promoting factor. Possibly the lack of sebocytes in such animals leads to drier and more scaly skin, which, together with the enhanced IL-18 expression, causes the accumulation of infiltrating macrophage/monocytes. However, the level of infiltration of these cells, although substantial, may not solely be responsible for the observed changes in response to carcinogen treatment. As indicated, the mice were bred on a carcinogen-resistant background, yet the high frequency of papilloma formation coupled with the conversion to carcinoma was so dramatic as to cause us to wonder whether the level of inflammation *per se* was the only driving factor.

Previous studies have shown γδT cells, inflammatory cells resident within the epidermis, to play important roles in the skin. As key sources of the Fgfr2b ligands Fgf-7 and Fgf-10, knockout studies showed γδT cells to be crucial for wound re-epithelialization (Jameson *et al*, 2002). Interestingly, their absence also correlated with enhanced sensitivity to chemical carcinogenesis in the skin (Girardi *et al*, 2001). Thus, one of their key functions in the skin is to act as sentinels, detecting abnormal keratinocytes, such as those damaged by wounding or by carcinogens. Looking at γδT cells in the epidermis of control and mutant mice, we found significantly increased numbers in the ears of year old

null mice. At first sight, this finding seemed paradoxical given the findings already reported on an inverse correlation between γδT-cell levels and carcinogen sensitivity (Girardi *et al*, 2001). However, the morphology of the cells in mutant skin differed from that in control skin, perhaps reflecting a different state of activation. Activated γδT cells at a wound margin were shown to adopt a more rounded morphology relative to that more distant from the edge (Jameson *et al*, 2002). Thus, even though there are more γδT cells present in the skin of K5-R2b-null mice, it may be that they are unable to communicate properly with the keratinocytes, resulting in less cell activation and a failure to detect malignant keratinocytes. This possible mechanism is the subject of ongoing investigations. Also, our data thus far only describe differences in ear epidermis, as this is the best site to visualize γδT cells, and it will be important to establish that similar changes occur in back skin.

Although the precise basis for the observed effects on tumor development and progression is yet to be fully understood, our findings provide a potential mechanistic insight into the phenotype we see in K5-R2b-null mice, suggesting that the nature of the inflammatory reaction tips toward a more pro-tumorigenic phenotype. Whatever the basis, the effect of Fgfr2b loss in the skin remains sufficiently severe to suggest that Fgfr2b is a major player in regulating normal skin homeostasis in response to carcinogenic insult and thus represents a potential target for therapeutic intervention or for cancer prevention.

Materials and methods

K5-R2b-null mice

Mice lacking Fgfr2b in the epidermis (K5-R2b null) were generated as follows: female mice were bred to homozygosity for a floxed allele ($Fgfr2b^{flox/flox}$), with loxP sites inserted into the introns flanking the IIIb exon of the Fgfr2 gene (De Moerlooze *et al*, 2000). These were crossed with male mice carrying one copy of the *Cre* recombinase transgene under the control of the keratin 5 promoter (Ramirez *et al*, 2004). The K5-Cre transgene has been shown previously to give high-efficacy excision of a floxed target gene (Brakebusch *et al*, 2000). Provided that the *cre* allele is transmitted paternally, only epithelia derived from keratin 5-expressing cells are targeted for deletion. Maternal transmission results in ubiquitous excision of the floxed sequence caused by Cre expression in the maternal germ line (Ramirez *et al*, 2004). Mice were maintained on a mixed C57Bl6/J × 129ola background for all studies. Littermate controls ($Fgfr2b^{flox/flox}$ Cre negative) were maintained alongside K5-R2b-null mice under identical husbandry conditions.

RNA isolation and RNase protection assay

RNA isolation (Chomczynski and Sacchi, 1987) and RNase protection assays (on 20 μg total RNA samples) (Werner *et al*, 1992) were performed as described. As a loading control, 1 μg of each RNA sample was resolved through a 1% agarose gel and stained with ethidium bromide (data not shown). In addition to an antisense RNA probe recognising Fgfr2b, the RNA samples also were hybridized with a probe for the housekeeping gene GAPDH (Zhang *et al*, 2004).

Preparation of skin sections

Back skin was harvested onto a nitrocellulose membrane (Amersham, UK) and fixed overnight in 1% acetic acid/95% ethanol at 4°C, rinsed in 100% ethanol and processed for paraffin wax embedding. Longitudinal sections (4 μm) were cut along the line of the pelage hair follicles, parallel to the dorsal midline. Tail skin was removed from the bone and laid flat on a nitrocellulose membrane as above and, after wax embedding, transverse sections (4 μm) were cut perpendicular to the line of the hair follicles.

Immunohistochemistry

Wax sections (4 μm) were incubated with the appropriate primary antibody: macrophages/monocytes—1:125 dilution of a rat monoclonal antibody targeted to F4/80 (Serotec, Oxford, UK); keratin 6—1:2000 dilution of a rabbit polyclonal anti-K6 antibody (Covance, Denver, CO, USA), and incubated with biotinylated donkey anti-rat IgG or anti-rabbit IgG (Dianova GMBH, Hamburg, Germany). The VectaStain avidin–biotin–peroxidase complex kit was then used according to the manufacturer's instructions, before peroxidase detection with a diaminobenzidine-peroxidase substrate kit (both from Vector Laboratories, Burlingame, CA, USA). Sections were counterstained with Mayer's hemalum. Macrophage/monocyte infiltration was quantified by counting F4/80-positive cells in $2 \times 0.3\,mm^2$ fields from immunostained back skin sections ($n = 4$ mice for each genotype).

Immunofluorescent γδT-cell staining

Ears were cut from mice (12 months old, $n = 3$ mice per genotype) and the skin peeled away from the cartilage using forceps. Skin preparations were incubated in PBS + 20 mM EDTA for 4 h at room temperature, and then the epidermis was removed with forceps and washed in PBS before fixation in ice-cold acetone for 20 min at −20°C. After rinsing in PBS, epidermal sheets were blocked for 1 h in 2% BSA in PBS at room temperature and then primary antibodies (keratin 14—1:10 000 dilution of a rabbit polyclonal anti-keratin 14 antibody (Covance, Harrogate, UK); γδT cells—1:100 dilution of GL3, an FITC-conjugated hamster anti-γδT-cell receptor monoclonal antibody (BD Biosciences, Oxford, UK)) were added directly to the blocking solution and incubated overnight at 4°C. The following morning, sheets were washed with PBS and incubated for 90 min at room temperature with a 1:100 dilution of Cy-3-conjugated donkey anti-rabbit secondary antibody (Upstate, Hampshire, UK), washed in PBS and mounted on silane-coated slides in Vectashield mounting medium + DAPI (Vector Labs, Burlingame, CA). Images were acquired on a Zeiss Axiovert 200M Confocal Microscope using the LSM510 Meta software (Zeiss, Welwyn Garden City, UK) and analyzed using ImageJ software (Rasband and Image, 1997–2004).

BrdU labelling

BrdU labelling was performed as described (Werner *et al*, 1994). Sections (4 μm) were incubated with a peroxidase-conjugated monoclonal antibody directed against BrdU (Roche Diagnostics, Rotkreuz, Switzerland) and stained with a diaminobenzidine-peroxidase substrate kit as above.

Tail epidermis whole mounts

Epidermal whole mounts were prepared as described (Braun *et al*, 2003) and fixed overnight in 1% acetic acid/95% ethanol at 4°C. After rinsing in 100% ethanol, they were rehydrated through a graded alcohol series to water and transferred to PBS. For Supplementary Figure 2, the specimens were counterstained for 10 s in a 1:4 dilution of Mayer's hemalum/water and mounted in 30% glycerol in PBS. For Figure 2, whole mounts were processed using the VectaStain peroxidase detection kit as described above for immunohistochemistry, dehydrated through alcohols into xylene and mounted in organic mounting medium.

Expression analysis

Total RNA was isolated from skin and papillomas of 1-year-old control and mutant mice, and squamous cell carcinoma from mutant mice only (using TriReagent according to the manufacturer's instructions; Sigma, Poole, UK). Total RNA (250 ng) was fluorescently labelled and samples hybridized to an Illumina Sentrix MouseRef-8® microarray chip according to the manufacturer's protocols (Illumina, San Diego, CA) and a two-fold change in expression level used as a cutoff. Differential expression levels were confirmed by semiquantitative RT–PCR, using RNA samples taken from 12-week-old control and mutant mice. These included full thickness back and tail skin, as well as RNA isolated from only the epidermis of tail skin. For all samples, we ran PCR reactions for 20, 25, 30 and 35 cycles to ensure we were comparing linear amplification products and confirmed that the starting cDNAs were of equivalent concentration and quality by amplifying the housekeeping gene HPRT. Primer details are as follows: IL-18 (forward: acaacttttggccgacttcac; reverse: atcttcctttttggcaagcaa; $T_M = 60°C$; product 388 bp), Serpin a3b (forward: tgctcagatggcacactagg; reverse: tcttcatcccggaagtatgg; $T_M = 60°C$; product 707 bp), HPRT (forward:

Table I *Ha-ras* RFLP analysis

	Diagnostic restriction sites in *Ha-ras* PCR product			
	*Hpy*118III **tCNN**ga	*Taq*I tCGA	*Xba*I **tCTA**ga	*Bsp*HI **tCAT**ga
WT sequence				
CAA (Gln)	1	1	—	—
Mutant sequences				
AAA (Lys)	—	1	—	—
CGA (Arg)	1	2	—	—
CTA (Leu)	1	1	1	—
CAT (His)	1	1	—	1

cctgctggattacattaaagcgctg; reverse: gtcaagggcatatccaacaacaaac; $T_M = 60°C$; product 351 bp).

Skin carcinogenesis

Cohorts of female control and K5-R2b-null mice were subjected to two-step skin carcinogenesis protocols. In the first experiment, female mice (n = minimum of eight per group) were shaved at 7 weeks of age before treatment with topically applied DMBA (Sigma, UK; 25 μg in 200 μl acetone), or acetone alone, 1 week later. From 9 weeks old, all mice were treated twice weekly with TPA (Sigma, UK; 3.7 μg in 200 μl acetone) for 15 weeks. In a repeat study, the protocol was adapted such that both male and female mice were treated, giving a total of eight groups. The treatment regime differed only in that instead of twice weekly application of 3.7 μg TPA, the mice received 15 once weekly applications of 7.4 μg TPA in 200 μl acetone, in accordance with altered animal licence permission. The group sizes were as follows: females, Ctr TPA $n = 5$, Ctr DMBA/TPA $n = 5$, K5R2b TPA $n = 5$, K5R2b DMBA/TPA $n = 6$; males, Ctr TPA $n = 5$, Ctr DMBA/TPA $n = 5$, K5R2b TPA $n = 3$, K5R2b DMBA/TPA $n = 3$. Mice were monitored on a daily basis and papilloma/tumor counts recorded weekly for up to 46 weeks post-initiation, at which stage the experiment was terminated. If mice appeared sick or the tumor burden reached a predefined limit, they were killed and examined post-mortem. Skin lesions and macroscopically normal skin were harvested and either fixed overnight in 10% buffered formalin, snap frozen in liquid nitrogen or embedded in OCT for frozen sectioning. All experiments with animals were carried out under Home Office licence and according to Institutional guidelines.

Ha-ras mutational analysis

Small pieces (1–2 mm^2) of frozen tissues were digested with proteinase K overnight. After heat inactivation, 1 μl of the resultant mixture was amplified by PCR using standard methods to give a 166-bp fragment. Forward and reverse primers were GGGAGACA TGTCTACTGGACATC and TAGCCATAGGTGGCTCACCT, respectively. Skin, papillomas and tumors were analyzed for mutations at *ha-ras* codon 61 by RFLP analysis (Jaworski *et al*, 2005). Restriction enzymes used were *Hpy*118III, *Taq*I, *Xba*I and *Bsp*HI (New England Biolabs). For further details, see Table I.

Supplementary data

Supplementary data are available at *The EMBO Journal* Online (http://www.embojournal.org).

Acknowledgements

We thank Professor José Jorcano for keratin-5 Cre transgenic mice, Dr Jessica Strid and Professor Adrian Hayday for advice on γδT-cell biology, Pooja Seedah and George Elia for excellent technical assistance, Dr Charles Mein and Nadiya Mahmud for help with microarray analysis, Dr Gareth Thomas for histopathological advice and Dr Simon Hughes for advice on RFLP analysis. This work was supported by Cancer Research UK (RG, VF, IH and CD), The Royal Society (RG), The Wellcome Trust (RG and A-MC), Bart's and The London Charitable Foundation (MJ) and the Swiss National Science Foundation (grant no. 3100Ao-109340/1 to SW).

References

auf dem Keller U, Huber M, Beyer TA, Kumin A, Siemes C, Braun S, Bugnon P, Mitropoulos V, Johnson DA, Johnson JA, Hohl D, Werner S (2006) Nrf transcription factors in keratinocytes are essential for skin tumor prevention but not for wound healing. *Mol Cell Biol* **26:** 3773–3784

Balkwill F (2004) Cancer and the chemokine network. *Nat Rev Cancer* **4:** 540–550

Balkwill F, Coussens LM (2004) Cancer: an inflammatory link. *Nature* **431:** 405–406

Bernard-Pierrot I, Ricol D, Cassidy A, Graham A, Elvin P, Caillault A, Lair S, Broet P, Thiery JP, Radvanyi F (2004) Inhibition of human bladder tumour cell growth by fibroblast growth factor receptor 2b is independent of its kinase activity. Involvement of the carboxy-terminal region of the receptor. *Oncogene* **23:** 9201–9211

Brakebusch C, Grose R, Quondamatteo F, Ramirez A, Jorcano JL, Pirro A, Svensson M, Herken R, Sasaki T, Timpl R, Werner S, Fassler R (2000) Skin and hair follicle integrity is crucially dependent on beta 1 integrin expression on keratinocytes. *EMBO J* **19:** 3990–4003

Braun KM, Niemann C, Jensen UB, Sundberg JP, Silva-Vargas V, Watt FM (2003) Manipulation of stem cell proliferation and lineage commitment: visualisation of label-retaining cells in whole mounts of mouse epidermis. *Development* **130:** 5241–5255

Celli G, LaRochelle WJ, Mackem S, Sharp R, Merlino G (1998) Soluble dominant-negative receptor uncovers essential roles for fibroblast growth factors in multi-organ induction and patterning. *EMBO J* **17:** 1642–1655

Chomczynski P, Sacchi N (1987) Single-step method of RNA isolation by acid guanidinium thiocyanate–phenol–chloroform extraction. *Anal Biochem* **162:** 156–159

Danilenko DM, Ring BD, Yanagihara D, Benson W, Wiemann B, Starnes CO, Pierce GF (1995) Keratinocyte growth factor is an important endogenous mediator of hair follicle growth, development, and differentiation. Normalization of the nu/nu follicular differentiation defect and amelioration of chemotherapy-induced alopecia. *Am J Pathol* **147:** 145–154

De Moerlooze L, Spencer-Dene B, Revest J, Hajihosseini M, Rosewell I, Dickson C (2000) An important role for the IIIb isoform of fibroblast growth factor receptor 2 (FGFR2) in mesenchymal–epithelial signalling during mouse organogenesis. *Development* **127:** 483–492

Diez de Medina SG, Chopin D, El Marjou A, Delouvee A, LaRochelle WJ, Hoznek A, Abbou C, Aaronson SA, Thiery JP, Radvanyi F (1997) Decreased expression of keratinocyte growth factor receptor in a subset of human transitional cell bladder carcinomas. *Oncogene* **14:** 323–330

Girardi M, Oppenheim DE, Steele CR, Lewis JM, Glusac E, Filler R, Hobby P, Sutton B, Tigelaar RE, Hayday AC (2001) Regulation of cutaneous malignancy by gammadelta T cells. *Science* **294:** 605–609

Grose R, Dickson C (2005) Fibroblast growth factor signaling in tumorigenesis. *Cytokine Growth Factor Rev* **16:** 179–186

Guo L, Degenstein L, Fuchs E (1996) Keratinocyte growth factor is required for hair development but not for wound healing. *Genes Dev* **10:** 165–175

Guo L, Yu QC, Fuchs E (1993) Targeting expression of keratinocyte growth factor to keratinocytes elicits striking changes in epithelial differentiation in transgenic mice. *EMBO J* **12:** 973–986

Jameson J, Ugarte K, Chen N, Yachi P, Fuchs E, Boismenu R, Havran WL (2002) A role for skin gammadelta T cells in wound repair. *Science* **296:** 747–749

Jang JH, Shin KH, Park JG (2001) Mutations in fibroblast growth factor receptor 2 and fibroblast growth factor receptor 3 genes associated with human gastric and colorectal cancers. *Cancer Res* **61:** 3541–3543

Jaworski M, Buchmann A, Bauer P, Riess O, Schwarz M (2005) B-raf and Ha-ras mutations in chemically induced mouse liver tumors. *Oncogene* **24:** 1290–1295

Jin C, McKeehan K, Guo W, Jauma S, Ittmann MM, Foster B, Greenberg NM, McKeehan WL, Wang F (2003) Cooperation between ectopic FGFR1 and depression of FGFR2 in induction of prostatic intraepithelial neoplasia in the mouse prostate. *Cancer Res* **63:** 8784–8790

Lockett J, Yin S, Li X, Meng Y, Sheng S (2006) Tumor suppressive maspin and epithelial homeostasis. *J Cell Biochem* **97:** 651–960

Min H, Danilenko DM, Scully SA, Bolon B, Ring BD, Tarpley JE, DeRose M, Simonet WS (1998) Fgf-10 is required for both limb and lung development and exhibits striking functional similarity to *Drosophila* branchless. *Genes Dev* **12:** 3156–3161

Ornitz DM, Itoh N (2001) Fibroblast growth factors. *Genome Biol* **2:** REVIEWS3005

Park H, Byun D, Kim TS, Kim YI, Kang JS, Hahm ES, Kim SH, Lee WJ, Song HK, Yoon DY, Kang CJ, Lee C, Houh D, Kim H, Cho B, Kim Y, Yang YH, Min KH, Cho DH (2001) Enhanced IL-18 expression in common skin tumors. *Immunol Lett* **79:** 215–219

Petiot A, Conti FJ, Grose R, Revest JM, Hodivala-Dilke KM, Dickson C (2003) A crucial role for Fgfr2-IIIb signalling in epidermal development and hair follicle patterning. *Development* **130:** 5493–5501

Quintanilla M, Haddow S, Jonas D, Jaffe D, Bowden GT, Balmain A (1991) Comparison of ras activation during epidermal carcinogenesis *in vitro* and *in vivo*. *Carcinogenesis* **12:** 1875–1881

Ramirez A, Page A, Gandarillas A, Zanet J, Pibre S, Vidal M, Tusell L, Genesca A, Whitaker DA, Melton DW, Jorcano JL (2004) A keratin K5Cre transgenic line appropriate for tissue-specific or generalized Cre-mediated recombination. *Genesis* **39:** 52–57

Rasband WS, Image J (1997–2004) Bethesda, Maryland, USA: National Institutes of Health, http://rsb.info.nih.gov/ij/

Revest JM, Spencer-Dene B, Kerr K, De Moerlooze L, Rosewell I, Dickson C (2001) Fibroblast growth factor receptor 2-IIIb acts upstream of Shh and Fgf4 and is required for limb bud maintenance but not for the induction of Fgf8, Fgf10, Msx1, or Bmp4. *Dev Biol* **231:** 47–62

Ricol D, Cappellen D, El Marjou A, Gil-Diez-de-Medina S, Girault JM, Yoshida T, Ferry G, Tucker G, Poupon MF, Chopin D, Thiery JP, Radvanyi F (1999) Tumour suppressive properties of fibroblast growth factor receptor 2-IIIb in human bladder cancer. *Oncogene* **18:** 7234–7243

Schlake T (2005) FGF signals specifically regulate the structure of hair shaft medulla via IGF-binding protein 5. *Development* **132:** 2981–2990

Sekine K, Ohuchi H, Fujiwara M, Yamasaki M, Yoshizawa T, Sato T, Yagishita N, Matsui D, Koga Y, Itoh N, Kato S (1999) Fgf10 is essential for limb and lung formation. *Nat Genet* **21:** 138–141

Steiling H, Werner S (2003) Fibroblast growth factors: key players in epithelial morphogenesis, repair and cytoprotection. *Curr Opin Biotechnol* **14:** 533–537

Sundberg JP, Hogan ME (1994) Hair types and subtypes in the laboratory mouse.In *Handbook of Mouse Mutations with Skin and Hair Abnormalities: Animal Models and Biomedical Tools*,Sundberg JP (ed) pp 57–68. Bar Harbor, MI: CRC Press

Werner S, Peters KG, Longaker MT, Fuller-Pace F, Banda MJ, Williams LT (1992) Large induction of keratinocyte growth factor expression in the dermis during wound healing. *Proc Natl Acad Sci USA* **89:** 6896–6900

Werner S, Smola H, Liao X, Longaker MT, Krieg T, Hofschneider PH, Williams LT (1994) The function of KGF in morphogenesis of epithelium and reepithelialization of wounds. *Science* **266:** 819–822

Woodworth CD, Michael E, Smith L, Vijayachandra K, Glick A, Hennings H, Yuspa SH (2004) Strain-dependent differences in malignant conversion of mouse skin tumors is an inherent property of the epidermal keratinocyte. *Carcinogenesis* **25:** 1771–1778

Yamanaka K, Clark R, Dowgiert R, Hurwitz D, Shibata M, Rich BE, Hirahara K, Jones DA, Eapen S, Mizutani H, Kupper TS (2006) Expression of interleukin-18 and caspase-1 in cutaneous T-cell lymphoma. *Clin Cancer Res* **12:** 376–382

Yasumoto H, Matsubara A, Mutaguchi K, Usui T, McKeehan WL (2004) Restoration of fibroblast growth factor receptor2 suppresses growth and tumorigenicity of malignant human prostate carcinoma PC-3 cells. *Prostate* **61:** 236–242

Zhang H, Dessimoz J, Beyer TA, Krampert M, Williams LT, Werner S, Grose R (2004) Fibroblast growth factor receptor 1-IIIb is dispensable for skin morphogenesis and wound healing. *Eur J Cell Biol* **83:** 3–11

Zhang Y, Wang H, Toratani S, Sato JD, Kan M, McKeehan WL, Okamoto T (2001) Growth inhibition by keratinocyte growth factor receptor of human salivary adenocarcinoma cells through induction of differentiation and apoptosis. *Proc Natl Acad Sci USA* **98:** 11336–11340

Bibliography:

ADNANE, J., GAUDRAY, P., DIONNE, C. A., CRUMLEY, G., JAYE, M., SCHLESSINGER, J., JEANTEUR, P., BIRNBAUM, D. & THEILLET, C. (1991) BEK and FLG, two receptors to members of the FGF family, are amplified in subsets of human breast cancers. *Oncogene,* 6**,** 659-63.

AIGNER, A., MALERCZYK, C., HOUGHTLING, R. & WELLSTEIN, A. (2000) Tissue distribution and retinoid-mediated downregulation of an FGF-binding protein (FGF-BP) in the rat. *Growth Factors,* 18**,** 51-62.

ARMAND, A. S., LAZIZ, I. & CHANOINE, C. (2006) FGF6 in myogenesis. *Biochim Biophys Acta,* 1763**,** 773-8.

BADMAN, M. K., KOESTER, A., FLIER, J. S., KHARITONENKOV, A. & MARATOS-FLIER, E. (2009) Fibroblast growth factor 21-deficient mice demonstrate impaired adaptation to ketosis. *Endocrinology,* 150**,** 4931-40.

BARBARIC, I., MILLER, G. & DEAR, T. N. (2007) Appearances can be deceiving: phenotypes of knockout mice. *Brief Funct Genomic Proteomic,* 6**,** 91-103.

BARIBAULT, H., PENNER, J., IOZZO, R. V. & WILSON-HEINER, M. (1994) Colorectal hyperplasia and inflammation in keratin 8-deficient FVB/N mice. *Genes Dev,* 8**,** 2964-73.

BARIBAULT, H., PRICE, J., MIYAI, K. & OSHIMA, R. G. (1993) Mid-gestational lethality in mice lacking keratin 8. *Genes Dev,* 7**,** 1191-202.

BEENKEN, A. & MOHAMMADI, M. (2009) The FGF family: biology, pathophysiology and therapy. *Nat Rev Drug Discov,* 8**,** 235-53.

BEER, H. D., BITTNER, M., NIKLAUS, G., MUNDING, C., MAX, N., GOPPELT, A. & WERNER, S. (2005) The fibroblast growth factor binding protein is a novel interaction partner of FGF-7, FGF-10 and FGF-22 and regulates FGF activity: implications for epithelial repair. *Oncogene,* 24**,** 5269-77.

BELLUS, G. A., HEFFERON, T. W., ORTIZ DE LUNA, R. I., HECHT, J. T., HORTON, W. A., MACHADO, M., KAITILA, I., MCINTOSH, I. & FRANCOMANO, C. A. (1995) Achondroplasia is defined by recurrent G380R mutations of FGFR3. *Am J Hum Genet,* 56**,** 368-73.

BERKING, C., TAKEMOTO, R., BINDER, R. L., HARTMAN, S. M., RUITER, D. J., GALLAGHER, P. M., LESSIN, S. R. & HERLYN, M. (2002) Photocarcinogenesis in human adult skin grafts. *Carcinogenesis,* 23**,** 181-7.

BERNDT, T. J., CRAIG, T. A., MCCORMICK, D. J., LANSKE, B., SITARA, D., RAZZAQUE, M. S., PRAGNELL, M., BOWE, A. E., O'BRIEN, S. P., SCHIAVI, S. C. & KUMAR, R. (2007) Biological activity of FGF-23 fragments. *Pflugers Arch,* 454**,** 615-23.

BEYER, T. A., WERNER, S., DICKSON, C. & GROSE, R. (2003) Fibroblast growth factor 22 and its potential role during skin development and repair. *Exp Cell Res,* 287**,** 228-36.

BOTTCHER, R. T. & NIEHRS, C. (2005) Fibroblast growth factor signaling during early vertebrate development. *Endocr Rev,* 26**,** 63-77.

BRAUN, S., AUF DEM KELLER, U., STEILING, H. & WERNER, S. (2004) Fibroblast growth factors in epithelial repair and cytoprotection. *Philos Trans R Soc Lond B Biol Sci,* 359**,** 753-7.

BURNS, R. C., FAIRBANKS, T. J., SALA, F., DE LANGHE, S., MAILLEUX, A., THIERY, J. P., DICKSON, C., ITOH, N., WARBURTON, D., ANDERSON, K. D. & BELLUSCI, S. (2004) Requirement for fibroblast growth factor 10 or fibroblast growth factor receptor 2-IIIb signaling for cecal development in mouse. *Dev Biol,* 265**,** 61-74.

CAPPELLEN, D., DE OLIVEIRA, C., RICOL, D., DE MEDINA, S., BOURDIN, J., SASTRE-GARAU, X., CHOPIN, D., THIERY, J. P. & RADVANYI, F. (1999) Frequent activating mutations of FGFR3 in human bladder and cervix carcinomas. *Nat Genet,* 23**,** 18-20.

CHAFFER, C. L., DOPHEIDE, B., SAVAGNER, P., THOMPSON, E. W. & WILLIAMS, E. D. (2007) Aberrant fibroblast growth factor receptor signaling in bladder and other cancers. *Differentiation,* 75**,** 831-42.

CHEN, H., MA, J., LI, W., ELISEENKOVA, A. V., XU, C., NEUBERT, T. A., MILLER, W. T. & MOHAMMADI, M. (2007) A molecular brake in the kinase hinge region regulates the activity of receptor tyrosine kinases. *Mol Cell,* 27**,** 717-30.

CHEN, L. & DENG, C. X. (2005) Roles of FGF signaling in skeletal development and human genetic diseases. *Front Biosci,* 10**,** 1961-76.

CHEN, Y., CHOU, K., FUCHS, E., HAVRAN, W. L. & BOISMENU, R. (2002) Protection of the intestinal mucosa by intraepithelial gamma delta T cells. *Proc Natl Acad Sci U S A,* 99**,** 14338-43.

CHESI, M., NARDINI, E., BRENTS, L. A., SCHROCK, E., RIED, T., KUEHL, W. M. & BERGSAGEL, P. L. (1997) Frequent translocation t(4;14)(p16.3;q32.3) in multiple myeloma is associated with increased expression and activating mutations of fibroblast growth factor receptor 3. *Nat Genet,* 16**,** 260-4.

CHO, K., ISHIWATA, T., UCHIDA, E., NAKAZAWA, N., KORC, M., NAITO, Z. & TAJIRI, T. (2007) Enhanced expression of keratinocyte growth factor and its receptor correlates with venous invasion in pancreatic cancer. *Am J Pathol,* 170**,** 1964-74.

CHOMCZYNSKI, P. & SACCHI, N. (1987) Single-step method of RNA isolation by acid guanidinium thiocyanate-phenol-chloroform extraction. *Anal Biochem,* 162**,** 156-9.

CHOW, L. Q. & ECKHARDT, S. G. (2007) Sunitinib: from rational design to clinical efficacy. *J Clin Oncol,* 25**,** 884-96.

COLVIN, J. S., BOHNE, B. A., HARDING, G. W., MCEWEN, D. G. & ORNITZ, D. M. (1996) Skeletal overgrowth and deafness in mice lacking fibroblast growth factor receptor 3. *Nat Genet,* 12**,** 390-7.

COLVIN, J. S., GREEN, R. P., SCHMAHL, J., CAPEL, B. & ORNITZ, D. M. (2001a) Male-to-female sex reversal in mice lacking fibroblast growth factor 9. *Cell,* 104**,** 875-89.

COLVIN, J. S., WHITE, A. C., PRATT, S. J. & ORNITZ, D. M. (2001b) Lung hypoplasia and neonatal death in Fgf9-null mice identify this gene as an essential regulator of lung mesenchyme. *Development,* 128**,** 2095-106.

COUMOUL, X. & DENG, C. X. (2003) Roles of FGF receptors in mammalian development and congenital diseases. *Birth Defects Res C Embryo Today,* 69**,** 286-304.

DAILEY, L., AMBROSETTI, D., MANSUKHANI, A. & BASILICO, C. (2005) Mechanisms underlying differential responses to FGF signaling. *Cytokine Growth Factor Rev,* 16**,** 233-47.

DANILENKO, D. M., RING, B. D., YANAGIHARA, D., BENSON, W., WIEMANN, B., STARNES, C. O. & PIERCE, G. F. (1995) Keratinocyte growth factor is an important endogenous mediator of hair follicle growth, development, and differentiation. Normalization of the nu/nu follicular differentiation defect and amelioration of chemotherapy-induced alopecia. *Am J Pathol,* 147**,** 145-54.

DAVIES, H., HUNTER, C., SMITH, R., STEPHENS, P., GREENMAN, C., BIGNELL, G., TEAGUE, J., BUTLER, A., EDKINS, S., STEVENS, C., PARKER, A., O'MEARA, S., AVIS, T., BARTHORPE, S., BRACKENBURY, L., BUCK, G., CLEMENTS, J., COLE, J., DICKS, E., EDWARDS, K., FORBES, S., GORTON, M., GRAY, K., HALLIDAY, K., HARRISON, R., HILLS, K., HINTON, J., JONES, D., KOSMIDOU, V., LAMAN, R., LUGG, R., MENZIES, A., PERRY, J., PETTY, R., RAINE, K., SHEPHERD, R., SMALL, A., SOLOMON, H., STEPHENS, Y., TOFTS, C., VARIAN, J., WEBB, A., WEST, S., WIDAA, S., YATES, A., BRASSEUR, F., COOPER, C. S., FLANAGAN, A. M., GREEN, A., KNOWLES, M., LEUNG, S. Y., LOOIJENGA, L. H., MALKOWICZ, B., PIEROTTI, M. A., TEH, B. T., YUEN, S. T., LAKHANI, S. R., EASTON, D. F., WEBER, B. L., GOLDSTRAW, P., NICHOLSON, A. G., WOOSTER, R., STRATTON, M. R. & FUTREAL, P. A. (2005) Somatic mutations of the protein kinase gene family in human lung cancer. *Cancer Res,* 65**,** 7591-5.

DE MOERLOOZE, L., SPENCER-DENE, B., REVEST, J. M., HAJIHOSSEINI, M., ROSEWELL, I. & DICKSON, C. (2000) An important role for the IIIb isoform of fibroblast growth factor receptor 2 (FGFR2) in mesenchymal-epithelial signalling during mouse organogenesis. *Development,* 127**,** 483-92.

DELLI BOVI, P., CURATOLA, A. M., KERN, F. G., GRECO, A., ITTMANN, M. & BASILICO, C. (1987) An oncogene isolated by transfection of Kaposi's sarcoma DNA encodes a growth factor that is a member of the FGF family. *Cell,* 50**,** 729-37.

DENG, C., WYNSHAW-BORIS, A., ZHOU, F., KUO, A. & LEDER, P. (1996) Fibroblast growth factor receptor 3 is a negative regulator of bone growth. *Cell,* 84**,** 911-21.

DENG, C. X., WYNSHAW-BORIS, A., SHEN, M. M., DAUGHERTY, C., ORNITZ, D. M. & LEDER, P. (1994) Murine FGFR-1 is required for early postimplantation growth and axial organization. *Genes Dev,* 8**,** 3045-57.

DIEZ DE MEDINA, S. G., CHOPIN, D., EL MARJOU, A., DELOUVEE, A., LAROCHELLE, W. J., HOZNEK, A., ABBOU, C., AARONSON, S. A., THIERY, J. P. & RADVANYI, F. (1997) Decreased expression of keratinocyte growth factor receptor in a subset of human transitional cell bladder carcinomas. *Oncogene,* 14**,** 323-30.

DONO, R., TEXIDO, G., DUSSEL, R., EHMKE, H. & ZELLER, R. (1998) Impaired cerebral cortex development and blood pressure regulation in FGF-2-deficient mice. *EMBO J,* 17**,** 4213-25.

DRAKE, L. A., CEILLEY, R. I., CORNELISON, R. L., DOBES, W. A., DORNER, W., GOLTZ, R. W., LEWIS, C. W., SALASCHE, S. J., TURNER, M. L., GRAHAM, G. F. & ET AL. (1992) Guidelines of care for basal cell carcinoma. The American Academy of Dermatology Committee on Guidelines of Care. *J Am Acad Dermatol,* 26**,** 117-20.

DROGEMULLER, C., RUFENACHT, S., WICHERT, B. & LEEB, T. (2007) Mutations within the FGF5 gene are associated with hair length in cats. *Anim Genet,* 38**,** 218-21.

DUAN, D. S., WERNER, S. & WILLIAMS, L. T. (1992) A naturally occurring secreted form of fibroblast growth factor (FGF) receptor 1 binds basic FGF in preference over acidic FGF. *J Biol Chem,* 267**,** 16076-80.

DUTT, A., SALVESEN, H. B., CHEN, T. H., RAMOS, A. H., ONOFRIO, R. C., HATTON, C., NICOLETTI, R., WINCKLER, W., GREWAL, R., HANNA, M., WYHS, N., ZIAUGRA, L., RICHTER, D. J., TROVIK, J., ENGELSEN, I. B., STEFANSSON, I. M., FENNELL, T., CIBULSKIS, K., ZODY, M. C., AKSLEN, L. A., GABRIEL, S., WONG, K. K., SELLERS, W. R., MEYERSON, M. & GREULICH, H. (2008) Drug-sensitive FGFR2 mutations in endometrial carcinoma. *Proc Natl Acad Sci U S A,* 105**,** 8713-7.

EASTON, D. F., POOLEY, K. A., DUNNING, A. M., PHAROAH, P. D., THOMPSON, D., BALLINGER, D. G., STRUEWING, J. P., MORRISON, J., FIELD, H., LUBEN, R., WAREHAM, N., AHMED, S., HEALEY, C. S., BOWMAN, R., MEYER, K. B., HAIMAN, C. A., et al. (2007) Genome-wide association study identifies novel breast cancer susceptibility loci. *Nature,* 447**,** 1087-93.

EGGO, M. C., HOPKINS, J. M., FRANKLYN, J. A., JOHNSON, G. D., SANDERS, D. S. & SHEPPARD, M. C. (1995) Expression of fibroblast growth factors in thyroid cancer. *J Clin Endocrinol Metab,* 80**,** 1006-11.

ESWARAKUMAR, V. P., LAX, I. & SCHLESSINGER, J. (2005) Cellular signaling by fibroblast growth factor receptors. *Cytokine Growth Factor Rev,* 16**,** 139-49.

ESWARAKUMAR, V. P., MONSONEGO-ORNAN, E., PINES, M., ANTONOPOULOU, I., MORRISS-KAY, G. M. & LONAI, P. (2002) The IIIc

alternative of Fgfr2 is a positive regulator of bone formation. *Development,* 129**,** 3783-93.

ESWARAKUMAR, V. P. & SCHLESSINGER, J. (2007) Skeletal overgrowth is mediated by deficiency in a specific isoform of fibroblast growth factor receptor 3. *Proc Natl Acad Sci U S A,* 104**,** 3937-42.

FAIRBANKS, T. J., KANARD, R. C., DE LANGHE, S. P., SALA, F. G., DEL MORAL, P. M., WARBURTON, D., ANDERSON, K. D., BELLUSCI, S. & BURNS, R. C. (2004) A genetic mechanism for cecal atresia: the role of the Fgf10 signaling pathway. *J Surg Res,* 120**,** 201-9.

FALARDEAU, J., CHUNG, W. C., BEENKEN, A., RAIVIO, T., PLUMMER, L., SIDIS, Y., JACOBSON-DICKMAN, E. E., ELISEENKOVA, A. V., MA, J., DWYER, A., QUINTON, R., NA, S., HALL, J. E., HUOT, C., ALOIS, N., PEARCE, S. H., COLE, L. W., HUGHES, V., MOHAMMADI, M., TSAI, P. & PITTELOUD, N. (2008) Decreased FGF8 signaling causes deficiency of gonadotropin-releasing hormone in humans and mice. *J Clin Invest,* 118**,** 2822-31.

FELDMAN, B., POUEYMIROU, W., PAPAIOANNOU, V. E., DECHIARA, T. M. & GOLDFARB, M. (1995) Requirement of FGF-4 for postimplantation mouse development. *Science,* 267**,** 246-9.

FENG, S., WANG, F., MATSUBARA, A., KAN, M. & MCKEEHAN, W. L. (1997) Fibroblast growth factor receptor 2 limits and receptor 1 accelerates tumorigenicity of prostate epithelial cells. *Cancer Res,* 57**,** 5369-78.

FIRNBERG, N. & NEUBUSER, A. (2002) FGF signaling regulates expression of Tbx2, Erm, Pea3, and Pax3 in the early nasal region. *Dev Biol,* 247**,** 237-50.

FLOSS, T., ARNOLD, H. H. & BRAUN, T. (1997) A role for FGF-6 in skeletal muscle regeneration. *Genes Dev,* 11**,** 2040-51.

FORE, J. (2006) A review of skin and the effects of aging on skin structure and function. *Ostomy Wound Manage,* 52**,** 24-35; quiz 36-7.

FREINKEL, W. D. (Ed.) (2001) *The biology of the skin.*, The Parthenon Publishing Group.

FU, L., JOHN, L. M., ADAMS, S. H., YU, X. X., TOMLINSON, E., RENZ, M., WILLIAMS, P. M., SORIANO, R., CORPUZ, R., MOFFAT, B., VANDLEN, R., SIMMONS, L., FOSTER, J., STEPHAN, J. P., TSAI, S. P. & STEWART, T. A. (2004) Fibroblast growth factor 19 increases metabolic rate and reverses dietary and leptin-deficient diabetes. *Endocrinology,* 145**,** 2594-603.

GALIANO, R. D., MICHAELS, J. T., DOBRYANSKY, M., LEVINE, J. P. & GURTNER, G. C. (2004) Quantitative and reproducible murine model of excisional wound healing. *Wound Repair Regen,* 12**,** 485-92.

GARCIA-CLOSAS, M., HALL, P., NEVANLINNA, H., POOLEY, K., MORRISON, J., RICHESSON, D. A., BOJESEN, S. E., NORDESTGAARD, B. G., AXELSSON, C. K., ARIAS, J. I., MILNE, R. L., RIBAS, G., GONZALEZ-

NEIRA, A., et al. (2008) Heterogeneity of breast cancer associations with five susceptibility loci by clinical and pathological characteristics. *PLoS Genet,* 4**,** e1000054.

GARTSIDE, M. G., CHEN, H., IBRAHIMI, O. A., BYRON, S. A., CURTIS, A. V., WELLENS, C. L., BENGSTON, A., YUDT, L. M., ELISEENKOVA, A. V., MA, J., CURTIN, J. A., HYDER, P., HARPER, U. L., RIEDESEL, E., MANN, G. J., TRENT, J. M., BASTIAN, B. C., MELTZER, P. S., MOHAMMADI, M. & POLLOCK, P. M. (2009) Loss-of-function fibroblast growth factor receptor-2 mutations in melanoma. *Mol Cancer Res,* 7**,** 41-54.

GIRI, D., ROPIQUET, F. & ITTMANN, M. (1999) Alterations in expression of basic fibroblast growth factor (FGF) 2 and its receptor FGFR-1 in human prostate cancer. *Clin Cancer Res,* 5**,** 1063-71.

GOSPODAROWICZ, D. (1974) Localisation of a fibroblast growth factor and its effect alone and with hydrocortisone on 3T3 cell growth. *Nature,* 249**,** 123-7.

GOSPODAROWICZ, D. & CHENG, J. (1986) Heparin protects basic and acidic FGF from inactivation. *J Cell Physiol,* 128**,** 475-84.

GREEN, C. L. & KHAVARI, P. A. (2004) Targets for molecular therapy of skin cancer. *Semin Cancer Biol,* 14**,** 63-9.

GREENWOOD, F. C., LANDON, J. & STAMP, T. C. (1966) The plasma sugar, free fatty acid, cortisol, and growth hormone response to insulin. I. In control subjects. *J Clin Invest,* 45**,** 429-36.

GROSE, R. & DICKSON, C. (2005) Fibroblast growth factor signaling in tumorigenesis. *Cytokine Growth Factor Rev,* 16**,** 179-86.

GROSE, R., FANTL, V., WERNER, S., CHIONI, A. M., JAROSZ, M., RUDLING, R., CROSS, B., HART, I. R. & DICKSON, C. (2007) The role of fibroblast growth factor receptor 2b in skin homeostasis and cancer development. *EMBO J,* 26**,** 1268-78.

GUO, L., DEGENSTEIN, L. & FUCHS, E. (1996) Keratinocyte growth factor is required for hair development but not for wound healing. *Genes Dev,* 10**,** 165-75.

GUO, L., YU, Q. C. & FUCHS, E. (1993) Targeting expression of keratinocyte growth factor to keratinocytes elicits striking changes in epithelial differentiation in transgenic mice. *EMBO J,* 12**,** 973-86.

HAFNER, C., VOGT, T. & HARTMANN, A. (2006) FGFR3 mutations in benign skin tumors. *Cell Cycle,* 5**,** 2723-8.

HAJIHOSSEINI, M. K. (2008) Fibroblast growth factor signaling in cranial suture development and pathogenesis. *Front Oral Biol,* 12**,** 160-77.

HANAHAN, D. & WEINBERG, R. A. (2000) The hallmarks of cancer. *Cell,* 100**,** 57-70.

HEBERT, J. M., ROSENQUIST, T., GOTZ, J. & MARTIN, G. R. (1994) FGF5 as a regulator of the hair growth cycle: evidence from targeted and spontaneous mutations. *Cell,* 78**,** 1017-25.

HOLOWACZ, T. & SOKOL, S. (1999) FGF is required for posterior neural patterning but not for neural induction. *Dev Biol,* 205**,** 296-308.

HOUSLEY, D. J. & VENTA, P. J. (2006) The long and the short of it: evidence that FGF5 is a major determinant of canine 'hair'-itability. *Anim Genet,* 37**,** 309-15.

HUANG, P. & STERN, M. J. (2005) FGF signaling in flies and worms: more and more relevant to vertebrate biology. *Cytokine Growth Factor Rev,* 16**,** 151-8.

HUNTER, D. J., KRAFT, P., JACOBS, K. B., COX, D. G., YEAGER, M., HANKINSON, S. E., WACHOLDER, S., WANG, Z., WELCH, R., HUTCHINSON, A., WANG, J., YU, K., CHATTERJEE, N., ORR, N., WILLETT, W. C., COLDITZ, G. A., ZIEGLER, R. G., BERG, C. D., BUYS, S. S., MCCARTY, C. A., FEIGELSON, H. S., CALLE, E. E., THUN, M. J., HAYES, R. B., TUCKER, M., GERHARD, D. S., FRAUMENI, J. F., JR., HOOVER, R. N., THOMAS, G. & CHANOCK, S. J. (2007) A genome-wide association study identifies alleles in FGFR2 associated with risk of sporadic postmenopausal breast cancer. *Nat Genet,* 39**,** 870-4.

IBRAHIMI, O. A., ELISEENKOVA, A. V., PLOTNIKOV, A. N., YU, K., ORNITZ, D. M. & MOHAMMADI, M. (2001) Structural basis for fibroblast growth factor receptor 2 activation in Apert syndrome. *Proc Natl Acad Sci U S A,* 98**,** 7182-7.

IINO, M., EHAMA, R., NAKAZAWA, Y., IWABUCHI, T., OGO, M., TAJIMA, M. & ARASE, S. (2007) Adenosine stimulates fibroblast growth factor-7 gene expression via adenosine A2b receptor signaling in dermal papilla cells. *J Invest Dermatol,* 127**,** 1318-25.

INAGAKI, T., CHOI, M., MOSCHETTA, A., PENG, L., CUMMINS, C. L., MCDONALD, J. G., LUO, G., JONES, S. A., GOODWIN, B., RICHARDSON, J. A., GERARD, R. D., REPA, J. J., MANGELSDORF, D. J. & KLIEWER, S. A. (2005) Fibroblast growth factor 15 functions as an enterohepatic signal to regulate bile acid homeostasis. *Cell Metab,* 2**,** 217-25.

INGERSOLL, R. G., PAZNEKAS, W. A., TRAN, A. K., SCOTT, A. F., JIANG, G. & JABS, E. W. (2001) Fibroblast growth factor receptor 2 (FGFR2): genomic sequence and variations. *Cytogenet Cell Genet,* 94**,** 121-6.

ISAACS, H. V. (1997) New perspectives on the role of the fibroblast growth factor family in amphibian development. *Cell Mol Life Sci,* 53**,** 350-61.

ISHIWATA, T., FRIESS, H., BUCHLER, M. W., LOPEZ, M. E. & KORC, M. (1998) Characterization of keratinocyte growth factor and receptor expression in human pancreatic cancer. *Am J Pathol,* 153**,** 213-22.

ITOH, N. (2007) The Fgf families in humans, mice, and zebrafish: their evolutional processes and roles in development, metabolism, and disease. *Biol Pharm Bull,* 30**,** 1819-25.

ITOH, N. & ORNITZ, D. M. (2004) Evolution of the Fgf and Fgfr gene families. *Trends Genet,* 20**,** 563-9.

JAMESON, J., UGARTE, K., CHEN, N., YACHI, P., FUCHS, E., BOISMENU, R. & HAVRAN, W. L. (2002) A role for skin gammadelta T cells in wound repair. *Science,* 296**,** 747-9.

JANG, J. H., SHIN, K. H. & PARK, J. G. (2001) Mutations in fibroblast growth factor receptor 2 and fibroblast growth factor receptor 3 genes associated with human gastric and colorectal cancers. *Cancer Res,* 61**,** 3541-3.

JANSEN, H. G. & SANYAL, S. (1984) Development and degeneration of retina in rds mutant mice: electron microscopy. *J Comp Neurol,* 224**,** 71-84.

JIN, C., MCKEEHAN, K., GUO, W., JAUMA, S., ITTMANN, M. M., FOSTER, B., GREENBERG, N. M., MCKEEHAN, W. L. & WANG, F. (2003) Cooperation between ectopic FGFR1 and depression of FGFR2 in induction of prostatic intraepithelial neoplasia in the mouse prostate. *Cancer Res,* 63**,** 8784-90.

JOHNSON, T. M., ROWE, D. E., NELSON, B. R. & SWANSON, N. A. (1992) Squamous cell carcinoma of the skin (excluding lip and oral mucosa). *J Am Acad Dermatol,* 26**,** 467-84.

JONES, P. & SIMONS, B. D. (2008) Epidermal homeostasis: do committed progenitors work while stem cells sleep? *Nat Rev Mol Cell Biol,* 9**,** 82-8.

KAN, S. H., ELANKO, N., JOHNSON, D., CORNEJO-ROLDAN, L., COOK, J., REICH, E. W., TOMKINS, S., VERLOES, A., TWIGG, S. R., RANNAN-ELIYA, S., MCDONALD-MCGINN, D. M., ZACKAI, E. H., WALL, S. A., MUENKE, M. & WILKIE, A. O. (2002) Genomic screening of fibroblast growth-factor receptor 2 reveals a wide spectrum of mutations in patients with syndromic craniosynostosis. *Am J Hum Genet,* 70**,** 472-86.

KATO, S. & SEKINE, K. (1999) FGF-FGFR signaling in vertebrate organogenesis. *Cell Mol Biol (Noisy-le-grand),* 45**,** 631-8.

KATOH, M. (2009) FGFR2 abnormalities underlie a spectrum of bone, skin, and cancer pathologies. *J Invest Dermatol,* 129**,** 1861-7.

KHARITONENKOV, A., SHIYANOVA, T. L., KOESTER, A., FORD, A. M., MICANOVIC, R., GALBREATH, E. J., SANDUSKY, G. E., HAMMOND, L. J., MOYERS, J. S., OWENS, R. A., GROMADA, J., BROZINICK, J. T., HAWKINS, E. D., WROBLEWSKI, V. J., LI, D. S., MEHRBOD, F., JASKUNAS, S. R. & SHANAFELT, A. B. (2005) FGF-21 as a novel metabolic regulator. *J Clin Invest,* 115**,** 1627-35.

KLIEWER, S. A. & MANGELSDORF, D. J. (2010) Fibroblast growth factor 21: from pharmacology to physiology. *Am J Clin Nutr,* 91**,** 254S-257S.

KOMI-KURAMOCHI, A., KAWANO, M., ODA, Y., ASADA, M., SUZUKI, M., OKI, J. & IMAMURA, T. (2005) Expression of fibroblast growth factors and their

receptors during full-thickness skin wound healing in young and aged mice. *J Endocrinol,* 186**,** 273-89.

KONDO, T., ZHENG, L., LIU, W., KUREBAYASHI, J., ASA, S. L. & EZZAT, S. (2007) Epigenetically controlled fibroblast growth factor receptor 2 signaling imposes on the RAS/BRAF/mitogen-activated protein kinase pathway to modulate thyroid cancer progression. *Cancer Res,* 67**,** 5461-70.

KUNII, K., DAVIS, L., GORENSTEIN, J., HATCH, H., YASHIRO, M., DI BACCO, A., ELBI, C. & LUTTERBACH, B. (2008) FGFR2-amplified gastric cancer cell lines require FGFR2 and Erbb3 signaling for growth and survival. *Cancer Res,* 68**,** 2340-8.

KWABI-ADDO, B., OZEN, M. & ITTMANN, M. (2004) The role of fibroblast growth factors and their receptors in prostate cancer. *Endocr Relat Cancer,* 11**,** 709-24.

LANGMAN, J. (2006) *Langman's Medical Embryology*.

LAZARUS, J. E., HEGDE, A., ANDRADE, A. C., NILSSON, O. & BARON, J. (2007) Fibroblast growth factor expression in the postnatal growth plate. *Bone,* 40**,** 577-86.

LI, A. J., OZAWA, K., TSUBOYAMA, H. & IMAMURA, T. (1999) Distribution of fibroblast growth factor-5 in rat hypothalamus, and its possible role as a regulator of feeding behaviour. *Eur J Neurosci,* 11**,** 1362-8.

LIETH, E., GARDNER, T. W., BARBER, A. J. & ANTONETTI, D. A. (2000) Retinal neurodegeneration: early pathology in diabetes. *Clin Experiment Ophthalmol,* 28**,** 3-8.

LISCOVITCH, M. & RAVID, D. (2007) A case study in misidentification of cancer cell lines: MCF-7/AdrR cells (re-designated NCI/ADR-RES) are derived from OVCAR-8 human ovarian carcinoma cells. *Cancer Lett,* 245**,** 350-2.

LIU, A. & JOYNER, A. L. (2001) Early anterior/posterior patterning of the midbrain and cerebellum. *Annu Rev Neurosci,* 24**,** 869-96.

LIU, Z., XU, J., COLVIN, J. S. & ORNITZ, D. M. (2002) Coordination of chondrogenesis and osteogenesis by fibroblast growth factor 18. *Genes Dev,* 16**,** 859-69.

LIVAK, K. J. & SCHMITTGEN, T. D. (2001) Analysis of relative gene expression data using real-time quantitative PCR and the 2(-Delta Delta C(T)) Method. *Methods,* 25**,** 402-8.

LU, S. Y., SHEIKH, F., SHEPPARD, P. C., FRESNOZA, A., DUCKWORTH, M. L., DETILLIEUX, K. A. & CATTINI, P. A. (2008) FGF-16 is required for embryonic heart development. *Biochem Biophys Res Commun,* 373**,** 270-4.

MARTIN, G. R. (1998) The roles of FGFs in the early development of vertebrate limbs. *Genes Dev,* 12**,** 1571-86.

MCCABE, C. D., SPYROPOULOS, D. D., MARTIN, D. & MORENO, C. S. (2008) Genome-wide analysis of the homeobox C6 transcriptional network in prostate cancer. *Cancer Res,* 68**,** 1988-96.

MCKAY, I. A. & LEIGH, I. M. (1995) Altered keratinocyte growth and differentiation in psoriasis. *Clin Dermatol,* 13**,** 105-14.

MEYER, K. B., MAIA, A. T., O'REILLY, M., TESCHENDORFF, A. E., CHIN, S. F., CALDAS, C. & PONDER, B. A. (2008) Allele-specific up-regulation of FGFR2 increases susceptibility to breast cancer. *PLoS Biol,* 6**,** e108.

MEYERS, E. N., LEWANDOSKI, M. & MARTIN, G. R. (1998) An Fgf8 mutant allelic series generated by Cre- and Flp-mediated recombination. *Nat Genet,* 18**,** 136-41.

MILLER, D. L., ORTEGA, S., BASHAYAN, O., BASCH, R. & BASILICO, C. (2000) Compensation by fibroblast growth factor 1 (FGF1) does not account for the mild phenotypic defects observed in FGF2 null mice. *Mol Cell Biol,* 20**,** 2260-8.

MILUNSKY, J. M., ZHAO, G., MAHER, T. A., COLBY, R. & EVERMAN, D. B. (2006) LADD syndrome is caused by FGF10 mutations. *Clin Genet,* 69**,** 349-54.

MIN, H., DANILENKO, D. M., SCULLY, S. A., BOLON, B., RING, B. D., TARPLEY, J. E., DEROSE, M. & SIMONET, W. S. (1998) Fgf-10 is required for both limb and lung development and exhibits striking functional similarity to Drosophila branchless. *Genes Dev,* 12**,** 3156-61.

MOHAMMADI, M., OLSEN, S. K. & IBRAHIMI, O. A. (2005) Structural basis for fibroblast growth factor receptor activation. *Cytokine Growth Factor Rev,* 16**,** 107-37.

MOHAMMADI, M., SCHLESSINGER, J. & HUBBARD, S. R. (1996) Structure of the FGF receptor tyrosine kinase domain reveals a novel autoinhibitory mechanism. *Cell,* 86**,** 577-87.

MOON, A. M. (2006) Mouse models for investigating the developmental basis of human birth defects. *Pediatr Res,* 59**,** 749-55.

MUENKE, M., SCHELL, U., HEHR, A., ROBIN, N. H., LOSKEN, H. W., SCHINZEL, A., PULLEYN, L. J., RUTLAND, P., REARDON, W., MALCOLM, S. & ET AL. (1994) A common mutation in the fibroblast growth factor receptor 1 gene in Pfeiffer syndrome. *Nat Genet,* 8**,** 269-74.

NAKATAKE, Y., HOSHIKAWA, M., ASAKI, T., KASSAI, Y. & ITOH, N. (2001) Identification of a novel fibroblast growth factor, FGF-22, preferentially expressed in the inner root sheath of the hair follicle. *Biochim Biophys Acta,* 1517**,** 460-3.

NARDONE, R. M. (2007) Eradication of cross-contaminated cell lines: a call for action. *Cell Biol Toxicol,* 23**,** 367-72.

NISHIMURA, T., NAKATAKE, Y., KONISHI, M. & ITOH, N. (2000) Identification of a novel FGF, FGF-21, preferentially expressed in the liver. *Biochim Biophys Acta,* 1492**,** 203-6.

NISHIMURA, T., UTSUNOMIYA, Y., HOSHIKAWA, M., OHUCHI, H. & ITOH, N. (1999) Structure and expression of a novel human FGF, FGF-19, expressed in the fetal brain. *Biochim Biophys Acta,* 1444**,** 148-51.

NUTT, S. L., DINGWELL, K. S., HOLT, C. E. & AMAYA, E. (2001) Xenopus Sprouty2 inhibits FGF-mediated gastrulation movements but does not affect mesoderm induction and patterning. *Genes Dev,* 15**,** 1152-66.

O'LEARY, D. D., CHOU, S. J. & SAHARA, S. (2007) Area patterning of the mammalian cortex. *Neuron,* 56**,** 252-69.

OHBAYASHI, N., SHIBAYAMA, M., KUROTAKI, Y., IMANISHI, M., FUJIMORI, T., ITOH, N. & TAKADA, S. (2002) FGF18 is required for normal cell proliferation and differentiation during osteogenesis and chondrogenesis. *Genes Dev,* 16**,** 870-9.

OHMACHI, S., MIKAMI, T., KONISHI, M., MIYAKE, A. & ITOH, N. (2003) Preferential neurotrophic activity of fibroblast growth factor-20 for dopaminergic neurons through fibroblast growth factor receptor-1c. *J Neurosci Res,* 72**,** 436-43.

OLDRIDGE, M., WILKIE, A. O., SLANEY, S. F., POOLE, M. D., PULLEYN, L. J., RUTLAND, P., HOCKLEY, A. D., WAKE, M. J., GOLDIN, J. H., WINTER, R. M. & ET AL. (1995) Mutations in the third immunoglobulin domain of the fibroblast growth factor receptor-2 gene in Crouzon syndrome. *Hum Mol Genet,* 4**,** 1077-82.

OLSEN, S. K., IBRAHIMI, O. A., RAUCCI, A., ZHANG, F., ELISEENKOVA, A. V., YAYON, A., BASILICO, C., LINHARDT, R. J., SCHLESSINGER, J. & MOHAMMADI, M. (2004) Insights into the molecular basis for fibroblast growth factor receptor autoinhibition and ligand-binding promiscuity. *Proc Natl Acad Sci U S A,* 101**,** 935-40.

ORNITZ, D. M. (2000) FGFs, heparan sulfate and FGFRs: complex interactions essential for development. *Bioessays,* 22**,** 108-12.

ORNITZ, D. M. & ITOH, N. (2001) Fibroblast growth factors. *Genome Biol,* 2**,** REVIEWS3005.

ORNITZ, D. M., XU, J., COLVIN, J. S., MCEWEN, D. G., MACARTHUR, C. A., COULIER, F., GAO, G. & GOLDFARB, M. (1996) Receptor specificity of the fibroblast growth factor family. *J Biol Chem,* 271**,** 15292-7.

PARTANEN, J., PURI, M. C., SCHWARTZ, L., FISCHER, K. D., BERNSTEIN, A. & ROSSANT, J. (1996) Cell autonomous functions of the receptor tyrosine kinase TIE in a late phase of angiogenic capillary growth and endothelial cell survival during murine development. *Development,* 122**,** 3013-21.

PASSOS-BUENO, M. R., WILCOX, W. R., JABS, E. W., SERTIE, A. L., ALONSO, L. G. & KITOH, H. (1999) Clinical spectrum of fibroblast growth factor receptor mutations. *Hum Mutat,* 14**,** 115-25.

PATEL, V. A., LOGAN, A., WATKINSON, J. C., UZ-ZAMAN, S., SHEPPARD, M. C., RAMSDEN, J. D. & EGGO, M. C. (2003) Isolation and characterization of human thyroid endothelial cells. *Am J Physiol Endocrinol Metab,* 284**,** E168-76.

PELLEGRINI, L., BURKE, D. F., VON DELFT, F., MULLOY, B. & BLUNDELL, T. L. (2000) Crystal structure of fibroblast growth factor receptor ectodomain bound to ligand and heparin. *Nature,* 407**,** 1029-34.

PETIOT, A., CONTI, F. J., GROSE, R., REVEST, J. M., HODIVALA-DILKE, K. M. & DICKSON, C. (2003) A crucial role for Fgfr2-IIIb signalling in epidermal development and hair follicle patterning. *Development,* 130**,** 5493-501.

PLIKUS, M. V. & CHUONG, C. M. (2008) Complex hair cycle domain patterns and regenerative hair waves in living rodents. *J Invest Dermatol,* 128**,** 1071-80.

POLLOCK, P. M., GARTSIDE, M. G., DEJEZA, L. C., POWELL, M. A., MALLON, M. A., DAVIES, H., MOHAMMADI, M., FUTREAL, P. A., STRATTON, M. R., TRENT, J. M. & GOODFELLOW, P. J. (2007) Frequent activating FGFR2 mutations in endometrial carcinomas parallel germline mutations associated with craniosynostosis and skeletal dysplasia syndromes. *Oncogene,* 26**,** 7158-62.

PRUDOVSKY, I., SAVION, N., ZHAN, X., FRIESEL, R., XU, J., HOU, J., MCKEEHAN, W. L. & MACIAG, T. (1994) Intact and functional fibroblast growth factor (FGF) receptor-1 trafficks near the nucleus in response to FGF-1. *J Biol Chem,* 269**,** 31720-4.

PRZYLEPA, K. A., PAZNEKAS, W., ZHANG, M., GOLABI, M., BIAS, W., BAMSHAD, M. J., CAREY, J. C., HALL, B. D., STEVENSON, R., ORLOW, S., COHEN, M. M., JR. & JABS, E. W. (1996) Fibroblast growth factor receptor 2 mutations in Beare-Stevenson cutis gyrata syndrome. *Nat Genet,* 13**,** 492-4.

QIAO, J., UZZO, R., OBARA-ISHIHARA, T., DEGENSTEIN, L., FUCHS, E. & HERZLINGER, D. (1999) FGF-7 modulates ureteric bud growth and nephron number in the developing kidney. *Development,* 126**,** 547-54.

RAMIREZ, A., PAGE, A., GANDARILLAS, A., ZANET, J., PIBRE, S., VIDAL, M., TUSELL, L., GENESCA, A., WHITAKER, D. A., MELTON, D. W. & JORCANO, J. L. (2004) A keratin K5Cre transgenic line appropriate for tissue-specific or generalized Cre-mediated recombination. *Genesis,* 39**,** 52-7.

RAND, V., HUANG, J., STOCKWELL, T., FERRIERA, S., BUZKO, O., LEVY, S., BUSAM, D., LI, K., EDWARDS, J. B., EBERHART, C., MURPHY, K. M., TSIAMOURI, A., BEESON, K., SIMPSON, A. J., VENTER, J. C., RIGGINS, G. J. & STRAUSBERG, R. L. (2005) Sequence survey of receptor tyrosine kinases reveals mutations in glioblastomas. *Proc Natl Acad Sci U S A,* 102**,** 14344-9.

RAPPOLEE, D. A., MARK, D., BANDA, M. J. & WERB, Z. (1988) Wound macrophages express TGF-alpha and other growth factors in vivo: analysis by mRNA phenotyping. *Science,* 241**,** 708-12.

REED, D. R., BACHMANOV, A. A. & TORDOFF, M. G. (2007) Forty mouse strain survey of body composition. *Physiol Behav,* 91**,** 593-600.

REICHMAN-FRIED, M., DICKSON, B., HAFEN, E. & SHILO, B. Z. (1994) Elucidation of the role of breathless, a Drosophila FGF receptor homolog, in tracheal cell migration. *Genes Dev,* 8**,** 428-39.

REVEST, J. M., SPENCER-DENE, B., KERR, K., DE MOERLOOZE, L., ROSEWELL, I. & DICKSON, C. (2001) Fibroblast growth factor receptor 2-IIIb acts upstream of Shh and Fgf4 and is required for limb bud maintenance but not for the induction of Fgf8, Fgf10, Msx1, or Bmp4. *Dev Biol,* 231**,** 47-62.

RICOL, D., CAPPELLEN, D., EL MARJOU, A., GIL-DIEZ-DE-MEDINA, S., GIRAULT, J. M., YOSHIDA, T., FERRY, G., TUCKER, G., POUPON, M. F., CHOPIN, D., THIERY, J. P. & RADVANYI, F. (1999) Tumour suppressive properties of fibroblast growth factor receptor 2-IIIb in human bladder cancer. *Oncogene,* 18**,** 7234-43.

ROHMANN, E., BRUNNER, H. G., KAYSERILI, H., UYGUNER, O., NURNBERG, G., LEW, E. D., DOBBIE, A., ESWARAKUMAR, V. P., UZUMCU, A., ULUBIL-EMEROGLU, M., LEROY, J. G., LI, Y., BECKER, C., LEHNERDT, K., CREMERS, C. W., YUKSEL-APAK, M., NURNBERG, P., KUBISCH, C., SCHLESSINGER, J., VAN BOKHOVEN, H. & WOLLNIK, B. (2006) Mutations in different components of FGF signaling in LADD syndrome. *Nat Genet,* 38**,** 414-7.

RON, D., BOTTARO, D. P., FINCH, P. W., MORRIS, D., RUBIN, J. S. & AARONSON, S. A. (1993) Expression of biologically active recombinant keratinocyte growth factor. Structure/function analysis of amino-terminal truncation mutants. *J Biol Chem,* 268**,** 2984-8.

ROSENQUIST, T. A. & MARTIN, G. R. (1996) Fibroblast growth factor signalling in the hair growth cycle: expression of the fibroblast growth factor receptor and ligand genes in the murine hair follicle. *Dev Dyn,* 205**,** 379-86.

RUBIN, J. S., OSADA, H., FINCH, P. W., TAYLOR, W. G., RUDIKOFF, S. & AARONSON, S. A. (1989) Purification and characterization of a newly identified growth factor specific for epithelial cells. *Proc Natl Acad Sci U S A,* 86**,** 802-6.

RUEHL-FEHLERT, C., KITTEL, B., MORAWIETZ, G., DESLEX, P., KEENAN, C., MAHRT, C. R., NOLTE, T., ROBINSON, M., STUART, B. P. & DESCHL, U. (2003) Revised guides for organ sampling and trimming in rats and mice--part 1. *Exp Toxicol Pathol,* 55**,** 91-106.

SAITO, H., KUSANO, K., KINOSAKI, M., ITO, H., HIRATA, M., SEGAWA, H., MIYAMOTO, K. & FUKUSHIMA, N. (2003) Human fibroblast growth factor-23 mutants suppress Na+-dependent phosphate co-transport activity and 1alpha,25-dihydroxyvitamin D3 production. *J Biol Chem,* 278**,** 2206-11.

SAKAUE, H., KONISHI, M., OGAWA, W., ASAKI, T., MORI, T., YAMASAKI, M., TAKATA, M., UENO, H., KATO, S., KASUGA, M. & ITOH, N. (2002) Requirement of fibroblast growth factor 10 in development of white adipose tissue. *Genes Dev,* 16**,** 908-12.

SAKSELA, O. & RIFKIN, D. B. (1990) Release of basic fibroblast growth factor-heparan sulfate complexes from endothelial cells by plasminogen activator-mediated proteolytic activity. *J Cell Biol,* 110**,** 767-75.

SAVAGNER, P., VALLES, A. M., JOUANNEAU, J., YAMADA, K. M. & THIERY, J. P. (1994) Alternative splicing in fibroblast growth factor receptor 2 is associated with induced epithelial-mesenchymal transition in rat bladder carcinoma cells. *Mol Biol Cell,* 5**,** 851-62.

SCHAFER, M. & WERNER, S. (2007) Transcriptional control of wound repair. *Annu Rev Cell Dev Biol,* 23**,** 69-92.

SCHLAKE, T. (2005) FGF signals specifically regulate the structure of hair shaft medulla via IGF-binding protein 5. *Development,* 132**,** 2981-90.

SCHLESSINGER, J. (2000) Cell signaling by receptor tyrosine kinases. *Cell,* 103**,** 211-25.

SCHMAHL, J., KIM, Y., COLVIN, J. S., ORNITZ, D. M. & CAPEL, B. (2004) Fgf9 induces proliferation and nuclear localization of FGFR2 in Sertoli precursors during male sex determination. *Development,* 131**,** 3627-36.

SCHON, M. P., BLUME-PEYTAVI, U., SCHON, M. & ORFANOS, C. E. (1995) The human hair follicle: glycoprotein-related antigenic profile of distinct keratinocyte populations in vivo and their alterations in vitro. *Arch Dermatol Res,* 287**,** 591-8.

SCOTET, E. & HOUSSAINT, E. (1998) Exon III splicing switch of fibroblast growth factor (FGF) receptor-2 and -3 can be induced by FGF-1 or FGF-2. *Oncogene,* 17**,** 67-76.

SEKINE, K., OHUCHI, H., FUJIWARA, M., YAMASAKI, M., YOSHIZAWA, T., SATO, T., YAGISHITA, N., MATSUI, D., KOGA, Y., ITOH, N. & KATO, S. (1999) Fgf10 is essential for limb and lung formation. *Nat Genet,* 21**,** 138-41.

SHIMADA, T., KAKITANI, M., YAMAZAKI, Y., HASEGAWA, H., TAKEUCHI, Y., FUJITA, T., FUKUMOTO, S., TOMIZUKA, K. & YAMASHITA, T. (2004) Targeted ablation of Fgf23 demonstrates an essential physiological role of FGF23 in phosphate and vitamin D metabolism. *J Clin Invest,* 113**,** 561-8.

SHISHIDO, E., ONO, N., KOJIMA, T. & SAIGO, K. (1997) Requirements of DFR1/Heartless, a mesoderm-specific Drosophila FGF-receptor, for the formation of heart, visceral and somatic muscles, and ensheathing of longitudinal axon tracts in CNS. *Development,* 124**,** 2119-28.

SITARA, D., RAZZAQUE, M. S., HESSE, M., YOGANATHAN, S., TAGUCHI, T., ERBEN, R. G., JUPPNER, H. & LANSKE, B. (2004) Homozygous ablation of fibroblast growth factor-23 results in hyperphosphatemia and impaired skeletogenesis, and reverses hypophosphatemia in Phex-deficient mice. *Matrix Biol,* 23**,** 421-32.

SIWOSKI, A., ISHKANIAN, A., GARNIS, C., ZHANG, L., ROSIN, M. & LAM, W. L. (2002) An efficient method for the assessment of DNA quality of archival microdissected specimens. *Mod Pathol,* 15**,** 889-92.

SMITH, J. C., PRICE, B. M., GREEN, J. B., WEIGEL, D. & HERRMANN, B. G. (1991) Expression of a Xenopus homolog of Brachyury (T) is an immediate-early response to mesoderm induction. *Cell,* 67**,** 79-87.

SOUTHERN, E. M. (1975) Detection of specific sequences among DNA fragments separated by gel electrophoresis. *J Mol Biol,* 98**,** 503-17.

SPENCER-DENE, B., SALA, F. G., BELLUSCI, S., GSCHMEISSNER, S., STAMP, G. & DICKSON, C. (2006) Stomach development is dependent on fibroblast growth factor 10/fibroblast growth factor receptor 2b-mediated signaling. *Gastroenterology,* 130**,** 1233-44.

SPIELBERGER, R., STIFF, P., BENSINGER, W., GENTILE, T., WEISDORF, D., KEWALRAMANI, T., SHEA, T., YANOVICH, S., HANSEN, K., NOGA, S., MCCARTY, J., LEMAISTRE, C. F., SUNG, E. C., BLAZAR, B. R., ELHARDT, D., CHEN, M. G. & EMMANOUILIDES, C. (2004) Palifermin for oral mucositis after intensive therapy for hematologic cancers. *N Engl J Med,* 351**,** 2590-8.

STACHOWIAK, M. K., MAHER, P. A., JOY, A., MORDECHAI, E. & STACHOWIAK, E. K. (1996) Nuclear accumulation of fibroblast growth factor receptors is regulated by multiple signals in adrenal medullary cells. *Mol Biol Cell,* 7**,** 1299-317.

STARK, H. J., SZABOWSKI, A., FUSENIG, N. E. & MAAS-SZABOWSKI, N. (2004) Organotypic cocultures as skin equivalents: A complex and sophisticated in vitro system. *Biol Proced Online,* 6**,** 55-60.

STEPHENS, P., EDKINS, S., DAVIES, H., GREENMAN, C., COX, C., HUNTER, C., BIGNELL, G., TEAGUE, J., SMITH, R., STEVENS, C., O'MEARA, S., PARKER, A., TARPEY, P., AVIS, T., BARTHORPE, A., BRACKENBURY, L., BUCK, G., BUTLER, A., CLEMENTS (2005) A screen of the complete protein kinase gene family identifies diverse patterns of somatic mutations in human breast cancer. *Nat Genet,* 37**,** 590-2.

STREIT, A., BERLINER, A. J., PAPANAYOTOU, C., SIRULNIK, A. & STERN, C. D. (2000) Initiation of neural induction by FGF signalling before gastrulation. *Nature,* 406**,** 74-8.

STREIT, S., BANGE, J., FICHTNER, A., IHRLER, S., ISSING, W. & ULLRICH, A. (2004) Involvement of the FGFR4 Arg388 allele in head and neck squamous cell carcinoma. *Int J Cancer,* 111**,** 213-7.

SUGI, Y., ITO, N., SZEBENYI, G., MYERS, K., FALLON, J. F., MIKAWA, T. & MARKWALD, R. R. (2003) Fibroblast growth factor (FGF)-4 can induce proliferation of cardiac cushion mesenchymal cells during early valve leaflet formation. *Dev Biol,* 258**,** 252-63.

SUN, X., MARIANI, F. V. & MARTIN, G. R. (2002) Functions of FGF signalling from the apical ectodermal ridge in limb development. *Nature,* 418**,** 501-8.

SUZUKI, K., YAMANISHI, K., MORI, O., KAMIKAWA, M., ANDERSEN, B., KATO, S., TOYODA, T. & YAMADA, G. (2000) Defective terminal differentiation and hypoplasia of the epidermis in mice lacking the Fgf10 gene. *FEBS Lett,* 481**,** 53-6.

SZEBENYI, G. & FALLON, J. F. (1999) Fibroblast growth factors as multifunctional signaling factors. *Int Rev Cytol,* 185**,** 45-106.

TAGASHIRA, S., HARADA, H., KATSUMATA, T., ITOH, N. & NAKATSUKA, M. (1997) Cloning of mouse FGF10 and up-regulation of its gene expression during wound healing. *Gene,* 197**,** 399-404.

TAKEUCHI, K., NAKAZAWA, M. & MIZUKOSHI, S. (2008) Systemic administration of nilvadipine delays photoreceptor degeneration of heterozygous retinal degeneration slow (rds) mouse. *Exp Eye Res,* 86**,** 60-9.

TANIGUCHI, F., HARADA, T., YOSHIDA, S., IWABE, T., ONOHARA, Y., TANIKAWA, M. & TERAKAWA, N. (1998) Paracrine effects of bFGF and KGF on the process of mouse blastocyst implantation. *Mol Reprod Dev,* 50**,** 54-62.

TAO, H., SHIMIZU, M., KUSUMOTO, R., ONO, K., NOJI, S. & OHUCHI, H. (2005) A dual role of FGF10 in proliferation and coordinated migration of epithelial leading edge cells during mouse eyelid development. *Development,* 132**,** 3217-30.

TARTAGLIA, M., VALERI, S., VELARDI, F., DI ROCCO, C. & BATTAGLIA, P. A. (1997) Trp290Cys mutation in exon IIIa of the fibroblast growth factor receptor 2 (FGFR2) gene is associated with Pfeiffer syndrome. *Hum Genet,* 99**,** 602-6.

TEKIN, M., HISMI, B. O., FITOZ, S., OZDAG, H., CENGIZ, F. B., SIRMACI, A., ASLAN, I., INCEOGLU, B., YUKSEL-KONUK, E. B., YILMAZ, S. T., YASUN, O. & AKAR, N. (2007) Homozygous mutations in fibroblast growth factor 3 are associated with a new form of syndromic deafness characterized by inner ear agenesis, microtia, and microdontia. *Am J Hum Genet,* 80**,** 338-44.

THOMPSON, S. D., FRANKLYN, J. A., WATKINSON, J. C., VERHAEG, J. M., SHEPPARD, M. C. & EGGO, M. C. (1998) Fibroblast growth factors 1 and 2 and fibroblast growth factor receptor 1 are elevated in thyroid hyperplasia. *J Clin Endocrinol Metab,* 83**,** 1336-41.

TOMLINSON, E., FU, L., JOHN, L., HULTGREN, B., HUANG, X., RENZ, M., STEPHAN, J. P., TSAI, S. P., POWELL-BRAXTON, L., FRENCH, D. & STEWART, T. A. (2002) Transgenic mice expressing human fibroblast growth factor-19 display increased metabolic rate and decreased adiposity. *Endocrinology,* 143**,** 1741-7.

TORII, S., KUSAKABE, M., YAMAMOTO, T., MAEKAWA, M. & NISHIDA, E. (2004) Sef is a spatial regulator for Ras/MAP kinase signaling. *Dev Cell,* 7**,** 33-44.

TSANG, M., FRIESEL, R., KUDOH, T. & DAWID, I. B. (2002) Identification of Sef, a novel modulator of FGF signalling. *Nat Cell Biol,* 4**,** 165-9.

TURNER, N. & GROSE, R. (2010) Fibroblast growth factor signalling: from development to cancer. *Nat Rev Cancer,* 10**,** 116-29.

UMEMORI, H., LINHOFF, M. W., ORNITZ, D. M. & SANES, J. R. (2004) FGF22 and its close relatives are presynaptic organizing molecules in the mammalian brain. *Cell,* 118**,** 257-70.

VAN DIJK, H. W., KOK, P. H., GARVIN, M., SONKA, M., DEVRIES, J. H., MICHELS, R. P., VAN VELTHOVEN, M. E., SCHLINGEMANN, R. O., VERBRAAK, F. D. & ABRAMOFF, M. D. (2009) Selective loss of inner retinal layer thickness in type 1 diabetic patients with minimal diabetic retinopathy. *Invest Ophthalmol Vis Sci,* 50**,** 3404-9.

WANG, J., STOCKTON, D. W. & ITTMANN, M. (2004) The fibroblast growth factor receptor-4 Arg388 allele is associated with prostate cancer initiation and progression. *Clin Cancer Res,* 10**,** 6169-78.

WERNER, S. (1998) Keratinocyte growth factor: a unique player in epithelial repair processes. *Cytokine Growth Factor Rev,* 9**,** 153-65.

WERNER, S. & GROSE, R. (2003) Regulation of wound healing by growth factors and cytokines. *Physiol Rev,* 83**,** 835-70.

WERNER, S., PETERS, K. G., LONGAKER, M. T., FULLER-PACE, F., BANDA, M. J. & WILLIAMS, L. T. (1992) Large induction of keratinocyte growth factor expression in the dermis during wound healing. *Proc Natl Acad Sci U S A,* 89**,** 6896-900.

WERNER, S., SMOLA, H., LIAO, X., LONGAKER, M. T., KRIEG, T., HOFSCHNEIDER, P. H. & WILLIAMS, L. T. (1994) The function of KGF in morphogenesis of epithelium and reepithelialization of wounds. *Science,* 266**,** 819-22.

WILKIE, A. O. (2005) Bad bones, absent smell, selfish testes: the pleiotropic consequences of human FGF receptor mutations. *Cytokine Growth Factor Rev,* 16**,** 187-203.

WILKIE, A. O., SLANEY, S. F., OLDRIDGE, M., POOLE, M. D., ASHWORTH, G. J., HOCKLEY, A. D., HAYWARD, R. D., DAVID, D. J., PULLEYN, L. J., RUTLAND, P. & ET AL. (1995) Apert syndrome results from localized mutations of FGFR2 and is allelic with Crouzon syndrome. *Nat Genet,* 9**,** 165-72.

WOODS, S. C. & D'ALESSIO, D. A. (2008) Central control of body weight and appetite. *J Clin Endocrinol Metab,* 93**,** S37-50.

WOODWORTH, C. D., MICHAEL, E., SMITH, L., VIJAYACHANDRA, K., GLICK, A., HENNINGS, H. & YUSPA, S. H. (2004) Strain-dependent differences in malignant conversion of mouse skin tumors is an inherent property of the epidermal keratinocyte. *Carcinogenesis,* 25**,** 1771-8.

XU, J., LIU, Z. & ORNITZ, D. M. (2000) Temporal and spatial gradients of Fgf8 and Fgf17 regulate proliferation and differentiation of midline cerebellar structures. *Development,* 127**,** 1833-43.

XU, X., WEINSTEIN, M., LI, C., NASKI, M., COHEN, R. I., ORNITZ, D. M., LEDER, P. & DENG, C. (1998) Fibroblast growth factor receptor 2

(FGFR2)-mediated reciprocal regulation loop between FGF8 and FGF10 is essential for limb induction. *Development,* 125**,** 753-65.

YAGUCHI, Y., YU, T., AHMED, M. U., BERRY, M., MASON, I. & BASSON, M. A. (2009) Fibroblast growth factor (FGF) gene expression in the developing cerebellum suggests multiple roles for FGF signaling during cerebellar morphogenesis and development. *Dev Dyn,* 238**,** 2058-72.

YAMADA, M., TAKESHITA, T., MIURA, S., MURATA, K., KIMURA, Y., ISHII, N., NOSE, M., SAKAGAMI, H., KONDO, H., TASHIRO, F., MIYAZAKI, J. I., SASAKI, H. & SUGAMURA, K. (2001) Loss of hippocampal CA3 pyramidal neurons in mice lacking STAM1. *Mol Cell Biol,* 21**,** 3807-19.

YAMASHITA, T., YOSHIOKA, M. & ITOH, N. (2000) Identification of a novel fibroblast growth factor, FGF-23, preferentially expressed in the ventrolateral thalamic nucleus of the brain. *Biochem Biophys Res Commun,* 277**,** 494-8.

YAN, G., FUKABORI, Y., MCBRIDE, G., NIKOLAROPOLOUS, S. & MCKEEHAN, W. L. (1993) Exon switching and activation of stromal and embryonic fibroblast growth factor (FGF)-FGF receptor genes in prostate epithelial cells accompany stromal independence and malignancy. *Mol Cell Biol,* 13**,** 4513-22.

YANG, X., SCHADT, E. E., WANG, S., WANG, H., ARNOLD, A. P., INGRAM-DRAKE, L., DRAKE, T. A. & LUSIS, A. J. (2006) Tissue-specific expression and regulation of sexually dimorphic genes in mice. *Genome Res,* 16**,** 995-1004.

YI, E. S., YIN, S., HARCLERODE, D. L., BEDOYA, A., BIKHAZI, N. B., HOUSLEY, R. M., AUKERMAN, S. L., MORRIS, C. F., PIERCE, G. F. & ULICH, T. R. (1994) Keratinocyte growth factor induces pancreatic ductal epithelial proliferation. *Am J Pathol,* 145**,** 80-5.

YIN, L., DU, X., LI, C., XU, X., CHEN, Z., SU, N., ZHAO, L., QI, H., LI, F., XUE, J., YANG, J., JIN, M., DENG, C. & CHEN, L. (2008) A Pro253Arg mutation in fibroblast growth factor receptor 2 (Fgfr2) causes skeleton malformation mimicking human Apert syndrome by affecting both chondrogenesis and osteogenesis. *Bone,* 42**,** 631-43.

YU, C., WANG, F., KAN, M., JIN, C., JONES, R. B., WEINSTEIN, M., DENG, C. X. & MCKEEHAN, W. L. (2000) Elevated cholesterol metabolism and bile acid synthesis in mice lacking membrane tyrosine kinase receptor FGFR4. *J Biol Chem,* 275**,** 15482-9.

ZHANG, H., DESSIMOZ, J., BEYER, T. A., KRAMPERT, M., WILLIAMS, L. T., WERNER, S. & GROSE, R. (2004) Fibroblast growth factor receptor 1-IIIb is dispensable for skin morphogenesis and wound healing. *Eur J Cell Biol,* 83**,** 3-11.

ZHANG, T., GUAN, H. & YANG, K. (2010) Keratinocyte growth factor promotes preadipocyte proliferation via an autocrine mechanism. *J Cell Biochem*.

ZHANG, X., IBRAHIMI, O. A., OLSEN, S. K., UMEMORI, H., MOHAMMADI, M. & ORNITZ, D. M. (2006) Receptor specificity of the fibroblast growth factor

family. The complete mammalian FGF family. *J Biol Chem,* 281**,** 15694-700.

ZHANG, Y., WANG, H., TORATANI, S., SATO, J. D., KAN, M., MCKEEHAN, W. L. & OKAMOTO, T. (2001) Growth inhibition by keratinocyte growth factor receptor of human salivary adenocarcinoma cells through induction of differentiation and apoptosis. *Proc Natl Acad Sci U S A,* 98**,** 11336-40.

ZHAO, Z. Z., POLLOCK, P. M., THOMAS, S., TRELOAR, S. A., NYHOLT, D. R. & MONTGOMERY, G. W. (2008) Common variation in the fibroblast growth factor receptor 2 gene is not associated with endometriosis risk. *Hum Reprod,* 23**,** 1661-8.

ZHONG, W., WANG, Q. T., SUN, T., WANG, F., LIU, J., LEACH, R., JOHNSON, A., PUSCHECK, E. E. & RAPPOLEE, D. A. (2006) FGF ligand family mRNA expression profile for mouse preimplantation embryos, early gestation human placenta, and mouse trophoblast stem cells. *Mol Reprod Dev,* 73**,** 540-50.

ZHOU, M., SUTLIFF, R. L., PAUL, R. J., LORENZ, J. N., HOYING, J. B., HAUDENSCHILD, C. C., YIN, M., COFFIN, J. D., KONG, L., KRANIAS, E. G., LUO, W., BOIVIN, G. P., DUFFY, J. J., PAWLOWSKI, S. A. & DOETSCHMAN, T. (1998) Fibroblast growth factor 2 control of vascular tone. *Nat Med,* 4**,** 201-7.